The Dissertation Committee for Tianyu Gao Certifies that this is the approved version of the following Dissertation:

Absorber Modeling and Design in Amine Scrubbing for Carbon Capture

Committee:

Gary T. Rochelle, Supervisor

Michael Baldea

Roger T. Bonnecaze

Betty K. Pun

Absorber Modeling and Design in Amine Scrubbing for Carbon Capture

by

Tianyu Gao

Dissertation

Presented to the Faculty of the Graduate School of

The University of Texas at Austin

in Partial Fulfillment

of the Requirements

for the Degree of

Doctor of Philosophy

The University of Texas at Austin

August 2021

Dedication

To my family

Acknowledgements

I would like to first thank Dr. Rochelle. His positive attitude towards life and family and passion to research greatly affects me and the time working with him is the greatest learning experience I ever had. His knowledge, critical thinking, and creativity set a great example for me and inspire me to learn, to solve problems, and to make contributions. All the time he spent on me, the graduate students, and even the undergraduate students made him a real educator. The pandemic has been extremely challenging to everyone but being able to work with him greatly encouraged me through all the difficulties.

I also want to thank my committee members: Dr. Baldea, Dr. Bonnecaze and Dr. Pun. They provided important feedback to my work and many thought-provoking questions. I also appreciate to work with Dr. Eric Chen and Dr. Fred Closmann. They are valuable resource for the Texas Carbon Management program and has been greatly helpful with their knowledge and experience. Maeve Cooney has been a great support in the report writing and administrative issues. My thanks also go to Dr. Abhoyjit Bhown, Dr. Yang Du, George Booras, and Adam Berger and the CCS team on EPRI. I enjoyed working with these experienced engineers and learnt a lot about CCS in a broader sense and about the industry.

I have spent a great time working with the Texas Carbon Engineers and it has been a pleasure to have them with me on the journey. I would like to thank Dr. Yue Zhang for mentoring me during her fifth year. She guided me into the absorber modeling and set a great example for me. I also want to thank Dr. Di Song, Dr. Ye Yuan, Dr. Kent Fischer, Dr. Fei Liu, Yuying Wu, Ching-Ting Liu, Korede Akinpelumi, Joe Selinger, Athreya Suresh, Miguel Abreu, Benjamin Drewry, Chih-I Chen, and Ariel Platz for the great

conversations on research and life. I was lucky to share my time at UT with the exceptional group of people. My thanks also go to the peers Yutong Liu, Xin Yang, Wen Liu, and Qining Chen. Their companion brought laugh and positive altitude through the journey.

I gratefully acknowledge the support of our sponsors in the Texas Carbon Management Program, $CCSI^2$ project, and CCP4. Without their finical support and technical advice, our work would not be possible. As a student, it is a valuable experience to interact with the leaders from both academia and industry.

Finally, I would like to thank my family for their love and support. My parents have always been a warm harbor, supporting me cross the sea. Last but not least, to my wife Yuqi, you have supported me with your love through my academic journey. The past six years would not have been more memorable without you. Words cannot express my love to you and I am so lucky to share my rest life with you.

Abstract

Absorber Modeling and Design in Amine Scrubbing for Carbon Capture

Tianyu Gao, Ph.D.

The University of Texas at Austin, 2021

Supervisor: Gary T. Rochelle

Absorber design is associated with the most important trade-off between capital and operating cost for CO_2 capture by amine scrubbing process. A rate-based absorber model using aqueous piperazine (PZ) has been developed prior to this work. The model is built from bench-scale or small pilot-scale experiments using "bottom-up" strategies and can be improved by larger scale pilot plant experiments.

Three pilot plant campaigns were designed and conducted in this work for model validation and improvement. By identifying the systematic bias of solvent equilibrium and applying one adjustable parameter on PZ concentration (8% for NCCC 2019 and SRP 2018, 3% for NCCC 2018), the model can predict the absorber number of transfer units (NTU) and temperature profile with good accuracy. The packing performance model was also validated using experiments running with less packing area that are away from mass transfer pinch.

With pilot plant experiments and process modeling, the absorber design using pump-around absorber with hot flue gas inlet was demonstrated as a superior configuration for flue gas with 4% CO_2. The pump-around increases the liquid flow and provides

effective cooling to the absorber. This configuration was used to design the first-of-its-kind commercial scale absorber in west Texas. The design requires only 25 ft packing, eliminates direct contact cooler and trim cooler to reduce capital cost, and uses 0.2 lean loading, low pump-around temperature (30 °C), and high pump-around rate to improve the performance and to reduce the operating cost.

The hybrid and crossflow absorbers were proposed and simulated as an intensification of the pump-around absorber. The hybrid absorber can be as effective as the pump-around absorber but is constrained by intercooling temperature and water balance. The crossflow absorber features small size and high velocity and is favored when the capital cost is relatively high.

Achieving higher removal using amine scrubbing was studied using both PZ and MEA solvent, and the optimal CO_2 removal was found above 90% (95% for coal and 93% for gas). Zero emission of power plant was feasible using amine scrubbing with an overall cost of 50.4 $/tonne and should be considered before deploying other direct air capture technologies.

Table of Contents

List of Tables

List of Figures

Chapter 1: Introduction

1.1 Carbon Capture and Amine Scrubbing

According to the Intergovernmental Panel on Climate Change (IPCC), human activities have caused about 1 °C of global warming above pre-industrial levels and it is likely to reach 1.5 °C between 2030 and 2052 if it continues to increase at the current rate (IPCC, 2018). The human influence is "extremely likely" to be the dominant reason for the global warming (IPCC, 2013) and the largest influence has been the greenhouse gas (GHG) emission. The chances of limiting warming to 1.5 °C requires immediate actions to achieve zero CO_2 emission in less than 15 years. To achieve this aggressive goal, implementing carbon capture and utilization (CCS) will be a critical pathway.

In response to the urgent requirement of reducing CO_2 emission, research and development has been focusing on post combustion carbon capture for large point sources such as coal-fired and natural gas-fired power plant. In US, electricity production accounted for 25% of CO_2 emissions in 2019 and it is the second largest share of greenhouse gas emissions (EPA, 2020).

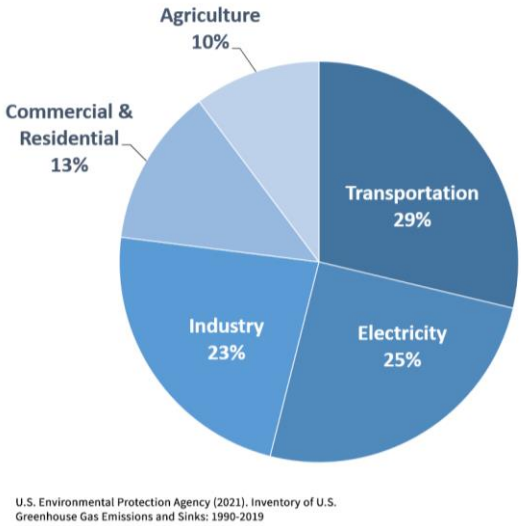

Figure 1.1: Total US GHG emissions by economic sector in 2019 (EPA).

Amine scrubbing is currently the most mature and robust technology for post-combustion carbon capture (PCCC) because of its long history in industrial applications such as natural gas sweetening, and the flexibility of retrofitting existed power plants. Recent development in technologies, environmental policies, and financial incentives have pushed amine scrubbing to demonstration in medium and large scale plants. The Boundary Dam plant in Canada captures CO_2 from a 110 MW coal-fired power plant (Preston et al., 2018) and the Petra Nova plant near Houston treats a 240 MW slipstream from a coal-fired plant (Kennedy, 2020). These projects demonstrate the feasibility and reliable operation of amine scrubbing at commercial scale and thus are very important initial steps for the deployment of the technology.

Along with large scale demonstration projects, research continues to focus on the development of new amine solvent, process design and optimization, solvent management and construction material selection. The Piperazine Advanced Stripper^{TM} (PZAS) has been demonstrated as the benchmark for 2nd generation amine scrubbing because of its fast

reaction rate, low energy consumption, low thermal and oxidative degradation, and low amine emission.

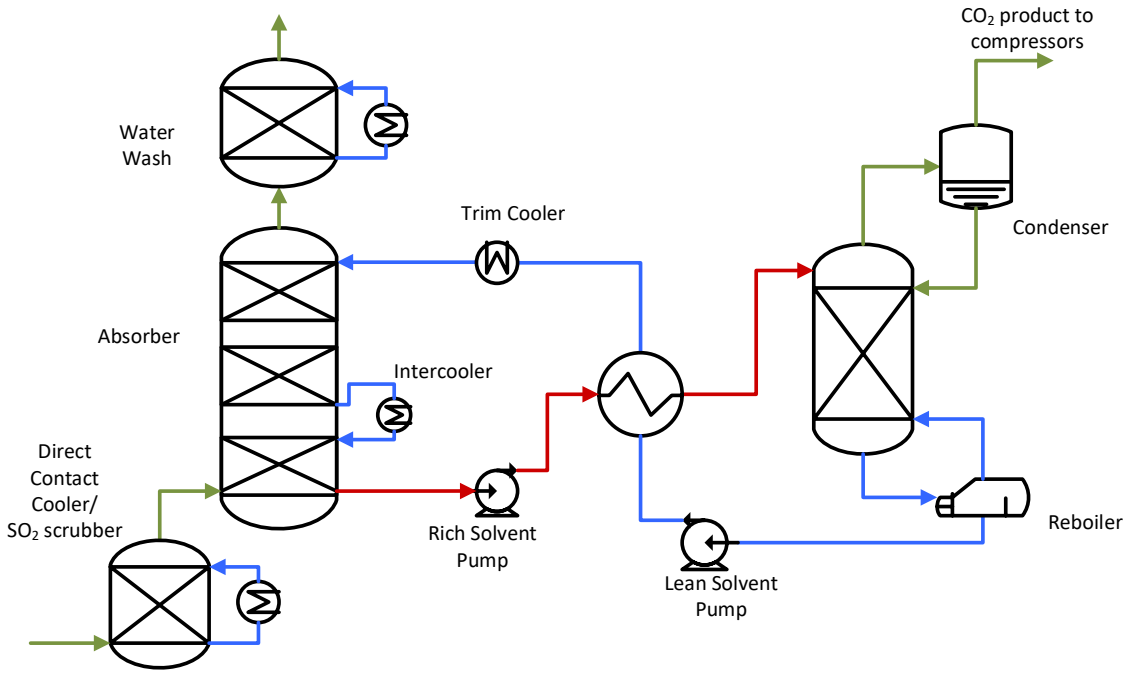

Figure 1.2: Simplified flowsheet of absorption-stripping process

Figure 1.2 shows a simplified flowsheet of absorption-stripping for CO_2 capture. Flue gas from coal-fired or natural gas-fired boiler or other industrial sources containing 4-20% CO_2 is sent to the absorber after pretreatment. The absorber column filled with packing provides mass transfer area for the countercurrent contacting between flue gas and amine solvent. The absorber operates at low temperature and is sometimes intercooled to remove the heat of absorption, improve driving force, and enhance the performance. The CO_2 stripped gas then flows through a packed water wash section for amine emission and water balance control. By recycling water in the water wash, entrained amine and aerosol are removed, and the water concentration in the vented gas is controlled by the water wash temperature and flowrate. The CO_2 rich solvent is then sent to the stripper for regeneration

and preheated by the returning lean solvent. Steam is usually required for the regeneration. The high-pressure CO_2 product is then cooled and sent to compression. The hot lean solvent first exchanges the sensible heat with cold rich solvent and then cooled by a trim cooler before returning to the absorber.

This work mainly focuses on the modeling, design, and development of the absorber using 5 m PZ as a case study. Research in absorber modeling, design, and optimization is significant for two reasons: the complexity of rigorous rate-based modeling and the economic significance of absorber optimization. An accurate absorber model requires good representations of the physical properties, equilibrium, and kinetics of the solvent. The CO_2 absorption process is rate-controlled by both chemical reaction and the physical mass transfer. Therefore, the conventional equilibrium method is insufficient. Furthermore, the absorption is coupled with the temperature rise because of the heat of absorption. The temperature profile in the absorber usually shows a bulge in the column, which reduces the driving force and leads to mass transfer pinches. Modeling the temperature effect in the absorber is crucial for understanding the limiting mechanism, proposing mitigation for the temperature bulge, and improving the performance.

From the perspective of economics, the absorber is usually the largest equipment in an amine scrubbing plant and can take up to 30-50% of the total purchase equipment cost (PEC) of the capture system. The design of the absorber balances the most important tradeoff between the capital cost and the energy cost: a large absorber column leads to greater capital cost but it provides more mass transfer area, requires less solvent circulation, and results in a better energy performance. The absorber design and optimization built upon process modeling and project economics are essential to reduce the cost for CO_2 capture.

With the increasingly urgent requirement to reduce CO_2 emissions, absorber modeling also lays the foundation to study the possibilities of higher removal and carbon

neutrality using amine scrubbing. Removing 99.6% of the CO_2 from coal-fired flue gas or 99% from gas turbine flue gas means net zero emission from the power plants. Such high removal cases become increasingly important because of the interest in zero emissions and negative emissions. Absorber design and optimization for high removal make amine scrubbing more flexible and applicable to achieve carbon neutral and gives amine scrubbing advantages over other competing technologies such as membrane separation.

Prior research in absorber modeling focuses on model development using bottom-up strategies based on bench-scale experiments and modeling performance for 90% removal. The Texas Carbon Engineers (researchers in the Texas Carbon Management Program) have done extensive work on concentrated piperazine (PZ) and its blend for solvent development. Large amounts of experimental data with good quality on solvent physical properties (Freeman, 2011), thermodynamics (Cullinane, 2005; Hilliard, 2008), and kinetics (Frailie, 2014; Plaza, 2011) were collected. Based on these experiments, a rigorous PZ model—the "Independence" model-- was developed by Frailie in Aspen Plus®. The solvent model, together with the rate-based method developed by Freguia and Plaza to model the mass transfer enhanced by chemical reactions, lays the foundation of the rigorous modeling of absorber performance.

In parallel with solvent development, absorber performance with concentrated PZ has been studied in the pilot plant at the University of Texas Separation Research Program (UT-SRP). From 2008 to 2018, different absorber configurations with concentrated PZ (8 *m* and 5 *m*) were tested over 8 pilot plant campaigns. The effects of different types of structured packing, packing height, column internals, and intercooling configuration were systematically studied. Experimental data collected from these pilot plant experiments were reconciled and used for model validations. Earlier campaigns were run with synthetic flue gas containing 12 mol% of CO_2 using 40 wt% PZ (8 *m*). The CO_2 concentrations in

the flue gas were extended to 4-20% to represent various sources including coal-fired (12%), gas-fired (4%), and cement plant (20%). With more understanding of absorber and overall system performance, 30 wt% (5 m PZ) was found more favorable over 40% wt because of the low viscosity.

The Texas Carbon Engineers have developed a systematic methodology for pilot plant data reconciliation and model validation. Solvent CO_2 concentration and packing wetted area were adjusted collectively in the model to match the experimental results. The rigorous absorber modeling and validation help understand the fundamentals of absorber performance and provide guidance for absorber design and optimization.

1.2 RESEARCH OBJECTIVES

Four major research objectives in this work include rigorous model validation with pilot plant experiments, countercurrent absorber design and optimization for different flue gas conditions and removal, and the development of innovative absorber configurations. The overall goals of the work are:

- Validate the rigorous model with pilot plant experiments and improve the accuracy of model predictions for 5 m PZ to facilitate process design and scale-up.
- Demonstrate the effect of process fundamentals on the absorber performance and generalize the correlation between performance and important design variables.
- Develop an optimal countercurrent absorber for various design requirements, including flue gas conditions, removal requirements, and cooling capabilities.

- Develop innovative absorber design to debottleneck the limiting factor, improve performance, and reduce the capital and operating cost.

1.2.1 Model Validation

The absorber model was developed based on bench-scale experimental data, and it may not predict the absorber performance accurately for three reasons:

1. The bench-scale data are collected for the purpose of solvent screening and development could be inaccurate in the operating condition.
2. The rate-based model was development for 8 m PZ then extrapolated to 5 m PZ. The change of amine concentration may introduce model error or uncertainty.
3. The large-scale absorber can perform differently and less ideal than the model, which is built upon bench-scale and small-scale pilot plant experiments.

Therefore, the large-scale pilot plant experiments provide opportunities to validate the model with real absorber performance and adjust the model to correct the intrinsic model error or the non-ideality of large column.

There are three major activities for the model validation:

1. Develop test plan for pilot plant test. The parametric test is designed to provide a wide range of operating conditions and long-term test is to study the system stability and the variation caused by ambient conditions and solvent degradation.
2. Collect experimental data, quantify the uncertainties of the measurements, reconcile results by different analytical methods and redundant measurements.
3. Minimize the error between model prediction and experimental results. Adjustment of both mass transfer and solvent equilibrium parameters can be used to match the absorber performance over a wide range of conditions.

1.2.2 Absorber Design and Optimization

The absorber design involves the most important tradeoff between capital cost and operating cost for amine scrubbing system. The absorber optimization requires evaluation of both process performance and project economics; therefore, it varies with flue gas sources and plant locations. The major activities of absorber design and optimization are:

1. Determine process design basis, including flue gas conditions, CO_2 removal target process cooling availabilities, ambient temperature, relative capital and energy cost, etc.
2. Perform absorber modeling and sensitivity analysis to evaluate the effect of important design variables including packing height, loading, intercooling conditions, and temperatures, etc.
3. Perform preliminary economic analysis to determine the optimal absorber design. Absorber performance for off-design conditions such as high/low ambient temperature, low flue gas rate will also be simulated.

1.2.3 Innovative Absorber Design

The innovative absorber design will study NGCC applications and focus on improving the gas liquid contacting and intercooling configurations. Based on the understanding of the countercurrent absorber and the limiting mechanism, the absorber innovation aims to enhance mass transfer performance, mitigate the temperature effect, and reduce absorber size. The major activities are:

1. Develop absorber configurations that could potentially debottleneck the countercurrent absorber and enhance performance.
2. Simulate/Approximate the performance of the innovative design using current modeling framework and rate-based methodology.

3. Optimize the innovative designs and compare them to traditional absorber. Explain the benefits and the disadvantages with performance results. Provide recommendations and potential applicable scenarios of the innovative design.

1.2.4 High Removal with Amine Scrubbing

With the urgent request to reduce CO_2 emission and the development of amine scrubbing technology, achieving greater than 90% removal for power plant becomes increasingly interesting. In this work, PZ and MEA solvent have been used to study the absorber and economic performance for high removal. The major objectives include:

1. Study the technical feasibility by developing absorber design to achieve high removal for coal and NGCC flue gas. Optimize the absorber design for high removal with advanced intercooling configuration.
2. Perform economic analysis and evaluate the cost for high CO_2 removal, develop recommendation on the removal target for capture plant.
3. Develop cost estimation on zero and negative emission of power plant, evaluate the possibility of deep decarbonization using amine scrubbing, and compare to other capture technologies.

Chapter 2: Pilot Plant Data Reconciliation and Absorber Model Validation[1]

2.1 INTRODUCTION

Model validation is an important stage of the process model development. The PZ Independence model was built from the bench-scale data to represent solvent physical properties, thermodynamics, and kinetics. However, accurate modeling of fundamentals does not guarantee good predictions of absorber performance in large scale for several reasons.

1. The bench-scale data were collected for the purpose of solvent screening and development. Proper regressions lead to least error over a wide range of conditions. However, the model may not be accurate or have high uncertainty in the absorber conditions, i.e., in the low lean loading region, the equilibrium vapor pressure may have relatively large experimental uncertainty because of the low pressure reading.
2. The rate-based model was developed for 8 m PZ then extrapolated to 5 m PZ. The change of amine concentration may introduce model error or uncertainty. The lean loading of interest for previous pilot plant campaigns was around 0.24 then reduced 0.2 to enhance the performance. The effect of these extrapolations has not been evaluated.
3. The large-scale absorber may perform less ideal than the bench-scale experiments. For example, non-ideal flow in the packing including rivulets and

[1] Part of this chapter has been published in Gao, T., Rochelle, G.T., 2019. "CO_2 Absorption from Gas Turbine Flue Gas by Aqueous Piperazine with Intercooling", Industrial & Engineering Chemistry Research and Gao, T., Selinger, J.L., Rochelle, G.T., 2019. "Demonstration of 99% CO_2 removal from coal flue gas by amine scrubbing", Int. J. Greenh. Gas Con. 83, 236-244. I am the primary contributor under the supervise of Dr. Rochelle.

droplets creates additional mass transfer, and the wall effect is less significant compared to pilot plant, etc.

The pilot plant experiments therefore provide opportunities to validate and adjust the process model using the "top-down" method. Solvent equilibrium, reaction kinetics, and packing performance model can be tuned to match the experimental data. The validation is crucial to improve the model accuracy and understand the process scale-up.

Prior Texas Carbon Engineers have developed a methodology to reconcile the pilot plant data and validate process model using Aspen Plus®. Attempts at correcting the model to match the results from the Separations Research Program (UT-SRP) pilot plant have been made using two global corrections, including the interfacial area factor and CO_2 concentration in the solvent. Table 2.1 summarizes the interfacial area and CO_2 correction factors for campaigns at UT-SRP. The model corrections made by different investigators show a poor consistency for the 7 pilot plant campaigns over the years. The discontinuity may be caused by the variation in absorber packing type and height, intercooling configurations, CO_2 inlet concentration, analytical methods, data quality, and the specific choice of correction factors by the researcher. For example, for the first four campaigns from 2008 to 2011 studied by Plaza (ref), both interfacial factor and CO_2 factor were used to tune the model. However, Sachde and Zhang decided to use only 1 correction (interfacial factor or CO_2 factor) for later campaigns to avoid model over-fitting (Zhang et al., 2017) .

The development of model adjustment is also limited or affected by the data quality and the analytical methods. For earlier campaigns, the decision of using both two adjustments was driven by the fact that the CO_2 correction was required to close the material balance and the interfacial area adjustment was used to match the experimental removal (Plaza, 2011). For later campaigns, with multiple analytical methods measuring both gas and liquid compositions, a more rigorous data reconciliation was performed, and

the model adjustment was not constrained by the mass balance. Thus, the interfacial area or the CO_2 can be used interchangeably to match the removal data (Sachde, 2016).

Because of the height limitation of the pilot plant absorber, the absorber performance was controlled by both solvent equilibrium and mass transfer. The discrepancies between model prediction and experiment are the collective results of solvent model and packing model. The contribution of the individual component was not examined.

Table 2.1: Model corrections for piperazine pilot plant campaigns at UT-SRP

Pilot Plant Campaign	Nov. 2008	Sept. 2010	Dec. 2010	Oct. 2011	Nov. 2013	Mar. 2015	Apr. 2017
Packing	Structured 205X	Hybrid 250	Hybrid 250	Structured 350Z	Hybrid 250	Hybrid 250	Hybrid 250
CO_2 Inlet (mol%)	12	12	12	12	12	6-12	4-20
Interfacial Area Factor	1.17	1.02	0.72	0.74	(0.61)	(0.61)	1
CO_2 Factor	1.05	1.05	1.06	1.08	(1.07)	(1.07)	1.05
Reference	(Plaza, 2011)	(Plaza, 2011)	(Plaza, 2011)	(Sachde et al., 2013)	(Sachde, 2016)	(Zhang et al., 2017)	(Zhang , 2018)

Chinen and Morgan, et al. also proposed a method to estimate multiple parameters simultaneously for monoethanolamine (MEA) (Morgan et al., 2017; Morgan et al., 2018). The main difference between this model and the Independence model is that the MEA model includes parametric uncertainty for solvent physical property models, the thermodynamic framework, and mass transfer models of the packing. Using the tools developed by CCSI^2, the parameter distribution can be studied to minimize the model uncertainty. The Independence model on the contrast, is a deterministic model and was validated with the averaged performance data. Based on the test MEA campaign at NCCC, four parameters on packing performance, including interfacial area, liquid mass transfer,

and two liquid holdup factors were regressed through a statistical method and applied to the model at the same time. Their validation process heavily relies on the numerical method, which includes the experimental design to evenly cover the full input space and the optimization of parameters to minimize the overall uncertainty. While for the PZ process, data reconciliation and model adjustment are mostly made to meet practical constraints, such as the closure of material balance or the difference between analytical methods.

2.2 PILOT PLANT OVERVIEW

The Piperazine Advanced Stripper^{TM} (PZAS) process has been tested in the pilot solvent test unit (PSTU) at the National Carbon Capture Center (NCCC) in 2018 and 2019 and at UT-SRP pilot plant in 2018. This chapter focuses on the data analysis, reconciliation, and model validation of these three campaigns. The NCCC 2018 campaign tested system performance for coal flue gas with 12% CO_2 and 2019 campaign tested simulated NGCC flue gas with 4% CO_2. The UT-SRP pilot plant uses synthetic flue gas and 2018 campaign tested absorber performance for 4%, 12%, and 20% CO_2.

2.2.1 PSTU, NCCC

The PSTU is located in Birmingham, Alabama. The test facilities allow development of post-combustion CO_2 capture technology using coal-fired flue gas in an industrial setting. The flue gas is generated from Plant Gaston Unit 5 coal-fired boiler, an 880 MW gross supercritical pulverized coal boiler. The coal burned at this site is medium-sulfur bituminous coal and the flue gas is treated for control of nitrogen oxides (NO_x), SO_3, particulate, and SO_2, using selective catalytic reduction, sodium bicarbonate injection, hot-

side electrostatic precipitation, and wet flue gas desulfurization, respectively. Therefore, the flue gas fully represents the gas conditions of a commercial coal-fired power plant.

Up to 0.5 MW flue gas is split and fed to the amine scrubbing system after the flue gas desulfurization unit. The major units of PSTU are: a SO_2 pre-scrubber, a direct contact cooler (DCC), an absorber, a water wash tower (WW), and the advanced stripper system. A simplified flowsheet of the absorption and stripping process is shown in Figure 2.1. The flue gas was treated with NaOH solution in the pre-scrubber to remove SO_2, then cooled in the direct contact cooler to remove excessive moisture and fed to the bottom of the absorber. The absorber has 3 sections of 6 m Sulzer MellapakPlus® 252Y structured packing but only the bottom 2 sections were used during the campaign. An in-and-out intercooler was used between the bottom 2 sections to mitigate the temperature rise due to the exothermic absorption. The solvent was introduced to the absorber column from the top and counter-currently contacted with flue gas. The CO_2 depleted flue gas was then fed to a water wash column to control the water content and to remove the entrained and volatile amine before being vented to the atmosphere.

The rich solvent exiting the absorber entered the rich storage tank and then was pumped up to stripper pressure and sent to the stripper system for regeneration. Most of the rich solvent was preheated by lean solvent exiting the stripper and further heated by a convective steam heater. The rest was split as cold rich bypass and warm rich bypass before the cold and hot exchangers. The cold rich bypass was heated by hot vapor exiting the stripper and mixed with warm rich bypass, and then entered the stripper at the top. This bypass feed stream was colder than the top feed for a conventional simple stripper, which benefited the energy performance by condensing water vapor and recovering the latent heat. At elevated temperature, the vapor and liquid were separated in the stripper and lean solvent was sent back to the absorber after two cross exchangers and a trim cooler. The

stripper had 2 m RSR® #0.5 and 2 m RSR® #0.7 random packing. Table 2.2 summarizes the configurations of the test facilities.

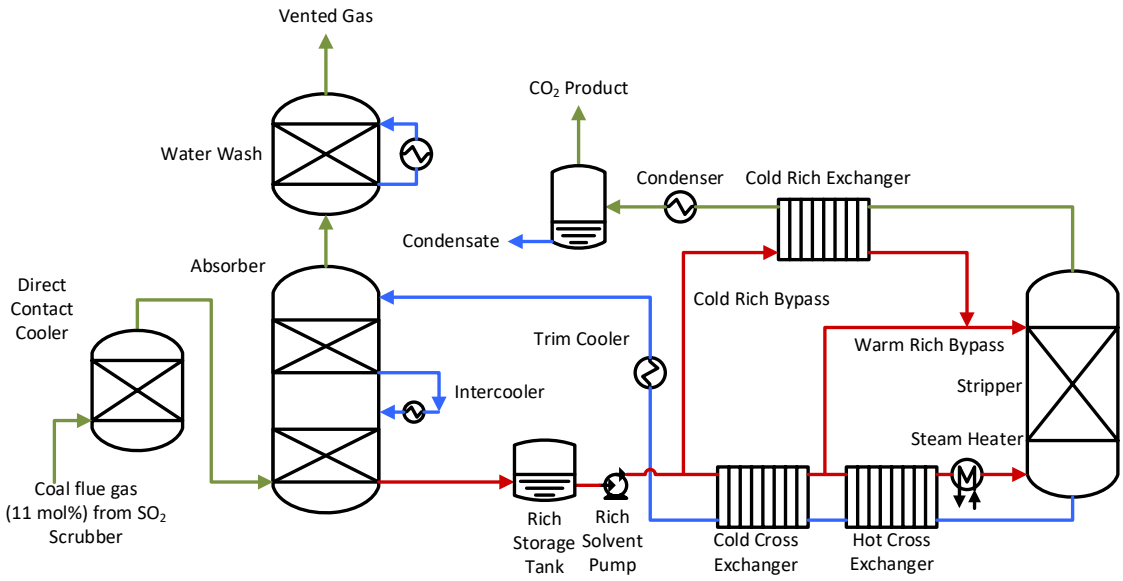

Figure 2.1: Simplified PZAS flowsheet for NCCC 2018 campaign

Table 2.2: Summary of pilot plant equipment specifications of PSTU

Absorber	Column Inner Diameter (m)	0.66
	Packing Height (m)	2 × 6.10
	Packing type	M252Y
	Material	Stainless
Stripper	Packing Height (m)	2 × 2
	Packing Type	RSR #0.5, #0.7
	Cold Cross Exchanger Area (m^2)	31.9
	Hot Cross Exchanger Area (m^2)	114.0
	Cold Rich Exchanger Area (m^2)	8.5

For the 2019 NCCC campaign, the flue gas pretreatment and absorber were modified to test the performance for 4% CO_2 and the stripper section remained the same as the previous test. After the SO_2 scrubber, coal flue gas was diluted with air to reduce the

CO_2 to about 4.3 mol % to simulate NGCC flue gas. The diluted gas could be cooled in the direct contact cooler (DCC) and saturated with water at 40 °C or bypass the DCC and feed to the absorber directly. In the bypass mode, the flue gas was heated to 78 °C by the blower to partially simulate hot NGCC gas conditions. Both simple in-and-out and advanced pump-around intercooling were tested. Figure 2.2 shows the three absorber configurations: (A) absorber with in-and-out intercooling and DCC, (B) with pump-around intercooling and DCC, and (C) with pump-around intercooling but no DCC. When the DCC was online, the mixed gas was cooled and saturated with water at 40 °C and when it was bypassed, the gas was heated to 78 °C and fed directly to the absorber column. NCCC 2019 campaign compared the performance between traditional design (A) and the innovative design (C) and demonstrated the benefits of the design.

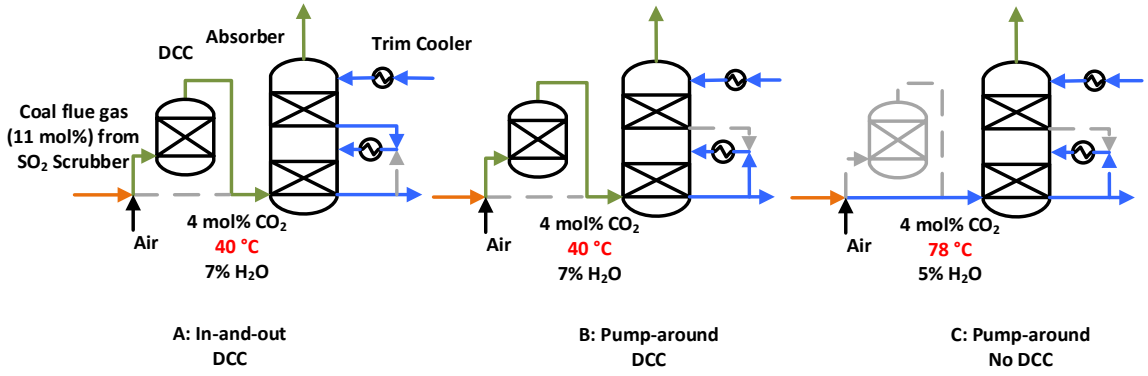

Figure 2.2: Simplified process flow diagram of absorber section for 2019 campaign at NCCC.

2.2.2 UT-SRP

Figure 2.3 shows the simplified PZAS flowsheet tested at UT-SRP in 2018. The pilot plant uses synthetic flue gas and recycles the captured CO_2. The absorber column is packed with 3 sections of RSR 250 structured packing, 3.1 m (10 ft) high for each section. The bottom two sections are used for CO_2 absorption and the top section is the water wash.

The absorber has an inner diameter of 0.43 m and can treat 0.1 MW equivalent coal flue gas. A simple in-and-out intercooling is applied in the middle of the two absorption packings. The CO_2 concentration can be varied easily and the SRP campaign tested the absorber performance for 4%, 12%, and 20% CO_2.

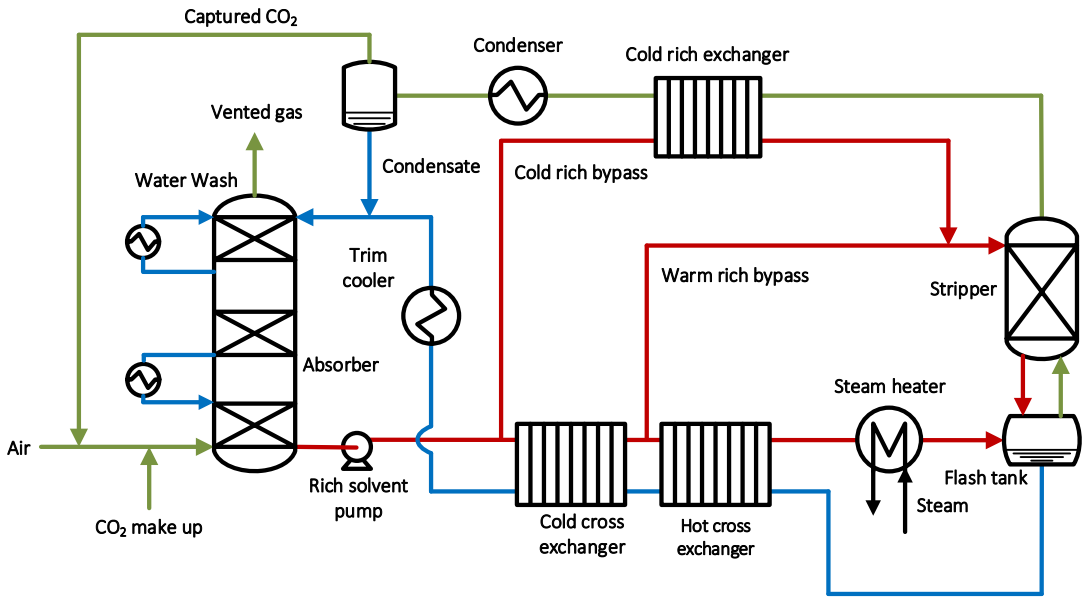

Figure 2.3: Simplified PZAS flowsheet tested at UT-SRP pilot plant.

2.3 Analytical Methods and Pilot Plant Measurements

2.3.1 NCCC pilot plant

To evaluate the absorber performance and study the material balance in the system, both gas and liquid flowrates and compositions were measured. Figure 2.4 shows the relative location for the gas and liquid measurements. The inlet and outlet gas composition of CO_2 was determined by online nondispersive infrared (NDIR) analyzers. For the liquid composition, both online and offline methods were implemented during the campaign. The auto-titrator measured PZ and CO_2 in the lean and rich solvent. The titrator collected samples approximately every 70 minutes. Samples of lean, rich, and midpoint

(intercooling) solvent were collected manually and analyzed by gas chromatography (GC) and total inorganic carbon (TIC) for PZ and CO_2 content on a daily basis. These samples were then shipped to UT-Austin and analyzed by cation chromatography (IC) for PZ in the lab.(Wu and Rochelle, 2021)

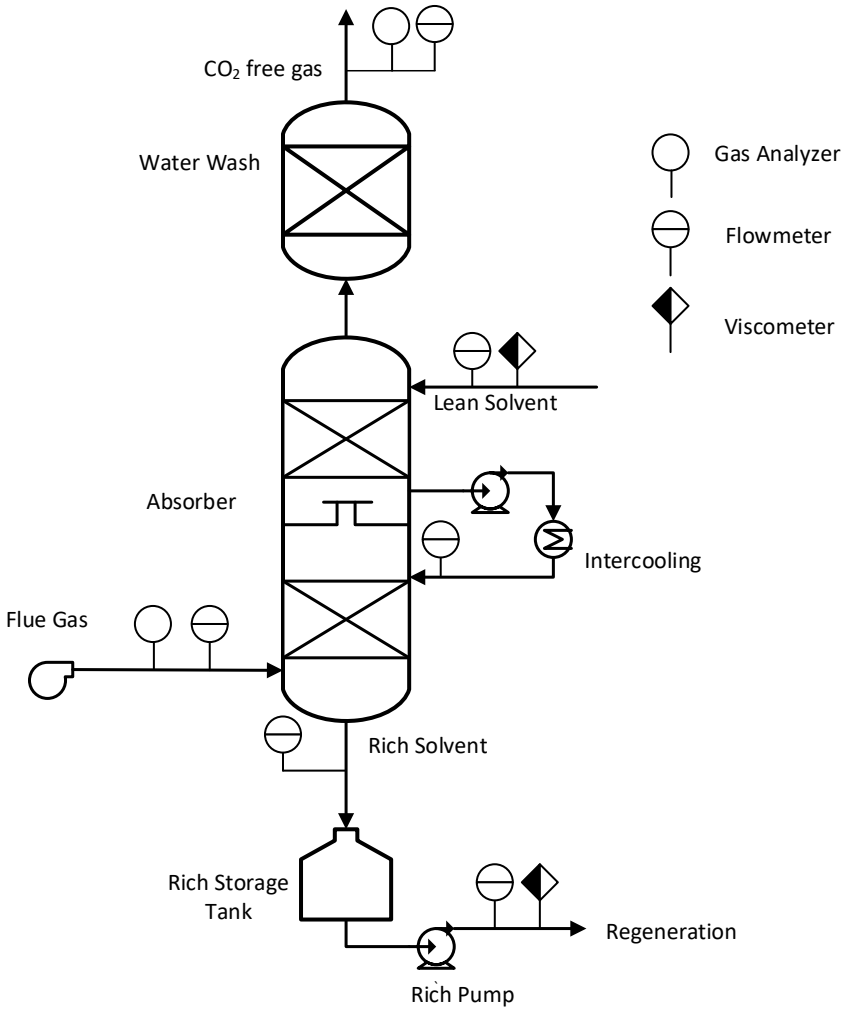

Figure 2.4: Simplified absorber PFD shows the relative locations of gas and flow measurement for NCCC pilot plant.

The solvent density and viscosity were measured continuously by online micromotion flowmeters and viscometers. The density has been shown to be an accurate

and reproduceable measurement during previous PZ campaigns (Lin et al., 2016; Zhang et al., 2017) and is related to PZ and CO_2 concentration by Equation 2.1 (Freeman, 2011). Viscosity is also a function of solvent composition as shown in Equations 2.2 and 2.3. Correlations between solvent viscosity and composition were regressed using experimental data of 2 to 9 m PZ at different loading conditions (Freeman, 2011). The regression results for 5 m PZ are shown in Figure 2.5. The predicted viscosities match experimental viscosities with good accuracy between 40 to 60 °C. The solvent loading measured by different methods was compared and the density and viscosity method was considered accurate throughout the campaign because it was consistent when compared to analytical measurements. Details on the loading reconciliation will be shown in next section.

$$\rho_{PZ} = \rho_w \cdot (0.0407 \cdot C_{CO2} + 0.008 \cdot C_{PZ} + 0.991) \quad (2.1)$$

$$\mu = \mu_w \cdot exp[\,(\frac{26.16}{T} - 0.0265) \cdot (7.69 \cdot C_{PZ} - 7.80 \cdot C_{CO2} + 3.37 \cdot C_{PZ} \cdot C_{CO2})] \quad (2.2)$$

$$\mu_W = 2.41 \times 10^{-5} \times 10^{247.8/(T-140)} \quad (2.3)$$

where:

ρ = liquid density (kg/m^3);

C = PZ/CO_2 concentration in the solution (mol/kg);

μ = liquid viscosity (cP);

T = temperature (K)

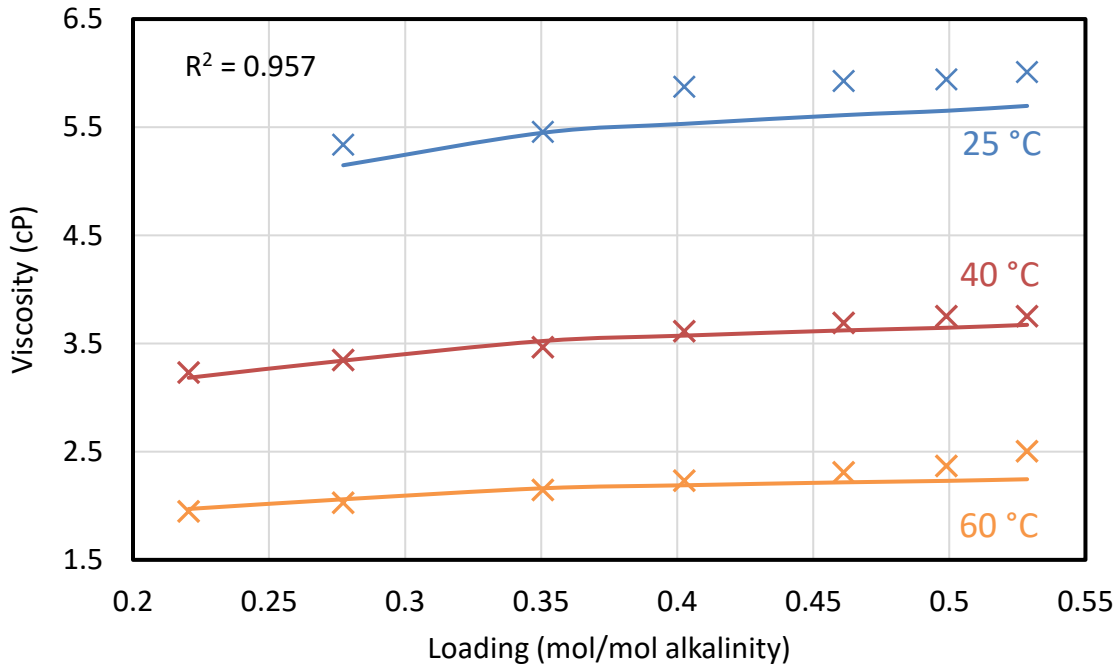

Figure 2.5: Comparison of solvent viscosities measured by experiment (cross points) and predicted by correlations (solid lines) for 5 m PZ at 25, 40 and 60 °C.

2.3.2 UT-SRP Pilot Plant

A similar analytical setup was also used in UT-SRP pilot plant. Figure 2.6 shows the relative locations of the online gas analyzers, flowmeters, and viscometer around the absorber. CO_2 concentration in gas phase is analyzed by NDIR and Fourier-transform infrared spectroscopy (FTIR). Solvent density and viscosity are measured and used for loading calculation using the method showing in equation 2.1-2.3.

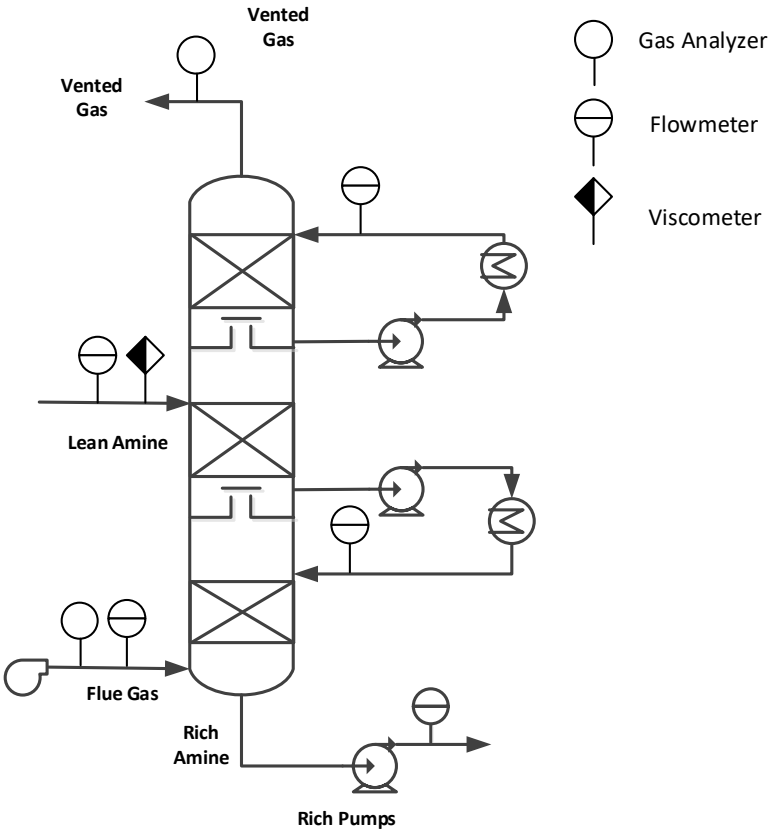

Figure 2.6: Simplified absorber PFD for UT-SRP showing measurement locations.

Column temperature profile is measured by multiple temperature sensors in the absorber column. The locations of the sensors are shown in Figure 2.7.

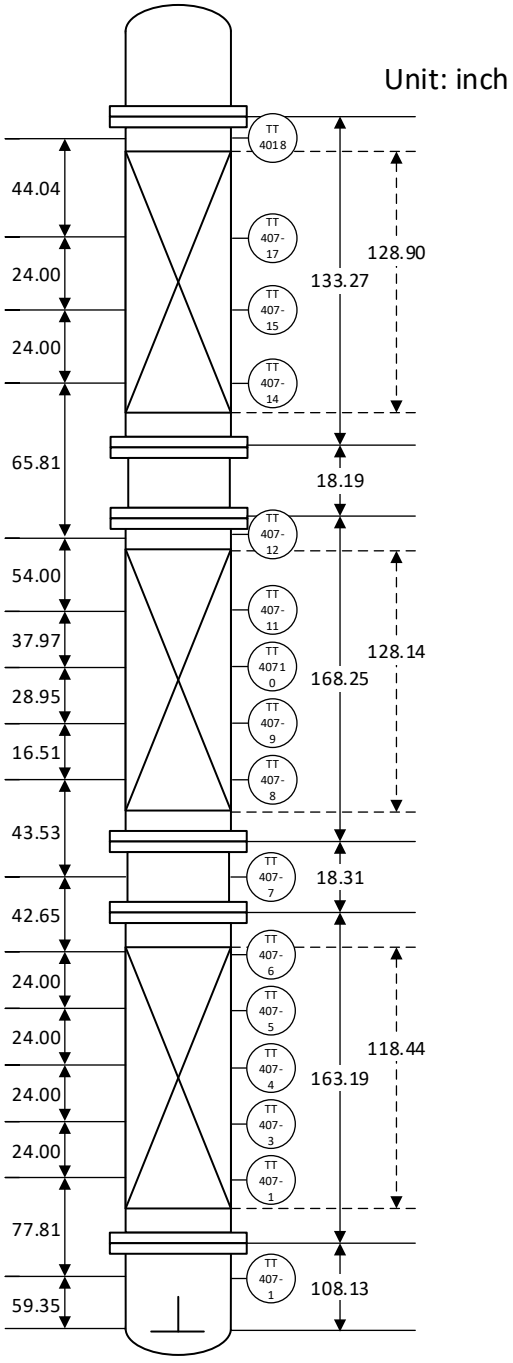

Figure 2.7: Locations of temperature sensor in the absorber column for UT-SRP

2.4 MODELING METHOD

The rigorous rate-based process modeling method was developed in Aspen Plus® RateSep™ and used to evaluate the absorber performance. The model contains solvent and packing models. The PZ model ("Independence" model) (Frailie, 2014) predicts the solvent properties and the packing models describe interfacial area and mass transfer performance.

The "Independence" model consists of thermodynamics, kinetics, and physical properties. The thermodynamics was built within the electrolyte non-random two liquid (e-NRTL) framework. The reaction rate was modeled with the Arrhenius equation using rate data collected from wetted wall column measurements. The remaining physical properties were regressed with solvent compositions and temperature.

The CO_2 absorption into PZ solvent has been modeled as fast reaction in the boundary layer. The method for film discretization was previously developed to model the concentration profile accurately in the boundary layer in Aspen V7 and V8. However, manual control of the film discretization is no longer supported in newer versions (V10 or later) of Aspen Plus®. Comparisons of simulation results between the versions were made and no significant differences were found between different versions of Aspen Plus®.

The packing characterization was built from the data collected from the UT-SRP air water column. This model includes mass transfer coefficients in gas and liquid phase (k_G and k_L) and the wetted area (a_e). The latest model was regressed from measurements of 39 packings, and incorporated the role of liquid viscosity and packing section height (Song, 2017; Song et al., 2014, 2017).

2.5 PILOT PLANT EXPERIMENTAL RESULTS

Table 2.3 Absorber operating conditions for three pilot plant campaigns

Pilot Plant Campaign	NCCC 2018	NCCC 2019	SRP 2018
CO_2 in flue gas (mol % dry)	10.6-12.3	4.0-4.3	11.9-12.0 18.8-19.9 4.4-4.6
Steady-state runs	68	80	47
PZ molality (m)	4.1-5.9	3.5-5.6	4.5-5.5
Flue gas rate (kg/s)	0.46-0.66	0.63-1.01	0.19-0.33
Lean Solvent rate (kg/s)	1.38-2.90	0.61-1.77	0.25-1.36
CO_2 removal	83.1-99.1%	80.0-95.8%	74.5%-98.5%
Lean loading (mol CO_2/mol alkalinity)	0.199-0.268	0.186-0.254	0.165-0.255
Rich loading (mol CO_2/mol alkalinity)	0.378-0.358	0.364-0.410	0.360-0.417
Solvent inlet T (°C)	31.2-49.8	40.3-53.5	36.1-40.1
Gas inlet T (°C)	36.7-62.1	39.7-83.0	38.2-48.8
Intercooling T (°C)	27.2-40.2	34.9-42.6	33.6-46.3

The three pilot plant campaigns tested absorber performance over a wide range of operating conditions in the parametric test, demonstrated the concept of innovative design and optimization, and studied the system stability and variation in the long-term test. The first campaign at NCCC started with fresh PZ solvent and operated for about 2100 hours. This campaign tested the baseline performance for coal flue gas with 12% CO_2. 68 steady state runs with 1 hour interval were defined when the solvent flowrate, loading, removal, and temperature varied less than 5%. The 2019 campaign focused on 4% CO_2 and 80 steady

state runs were defined similarly. The same PZ inventory from previous campaign was used and the tested for another 2000 hours. This campaign studied the absorber performance for NGCC conditions and demonstrated the innovative design using pump-around intercooling. Effects of ambient temperature variation were studied throughout these two tests. The maximum CO_2 removal achieved was 99.1% and 95.8% for coal and NGCC flue gases, respectively.

For the SRP campaign, experiments with 4%, 12%, and 20% CO_2 were run to represent different flue gas sources. There are total 47 parametric steady state runs for this campaign and data for each run was collected over 30 minutes.

2.5.1 Reconciliation of Solvent Composition

For the campaigns at the NCCC pilot plant, multiple methods were used to determine solvent composition, including the calculation based on online density and viscosity, online auto-titration, offline onsite GC and TIC analysis, and offline IC analysis at UT Austin. These methods are commonly used in amine scrubbing plants, but the results may not match because they measure different physical quantities and need to be reconciled. For example, GC and IC measure the PZ concentration but the titration measures solvent alkalinity. Although PZ is the source of alkalinity for fresh solvent, the difference between methods can show up as the solvent degrades. These methods also have different source of error and measurement uncertainty. Compared to the offline analytical methods, the online calculation has better reproducibility and smaller uncertainty because the density and viscosity measurements are precise.

2.5.1.1 NCCC 2018 Campaign

Figure 2.8 compares PZ (alkalinity) by offline IC and online titration to the calculation by online density and viscosity measurements for NCCC 2018 campaign. During this campaign, the lean viscometer was not working properly. To calculate lean composition with density measurements only, the PZ molality was assumed to be the same as the rich solvent. The rich molality and loading were calculated based on measurements by rich flowmeter and viscometer, and both were found consistent throughout the campaign.

The alkalinity measured by titration is about 3% less than the PZ concentration calculated by density and viscosity. The standard error between titration and calculation is 0.039, making the difference between these two methods statistically insignificant. There is no significant difference found between lean and rich solvent, showing the same molality assumption is valid during steady state conditions.

Similarly, the IC and calculation is not significantly different either. The online titration shows a smaller variance than the offline IC, suggesting there might be extra uncertainty introduced by offline sample collection, packing and shipment, and manual sample analysis. The error between cation and calculation shows a time dependent behavior, but the trend is not showing up for the titration, indicating PZ may degrade during the operation but the degradation product does not lose the alkalinity.

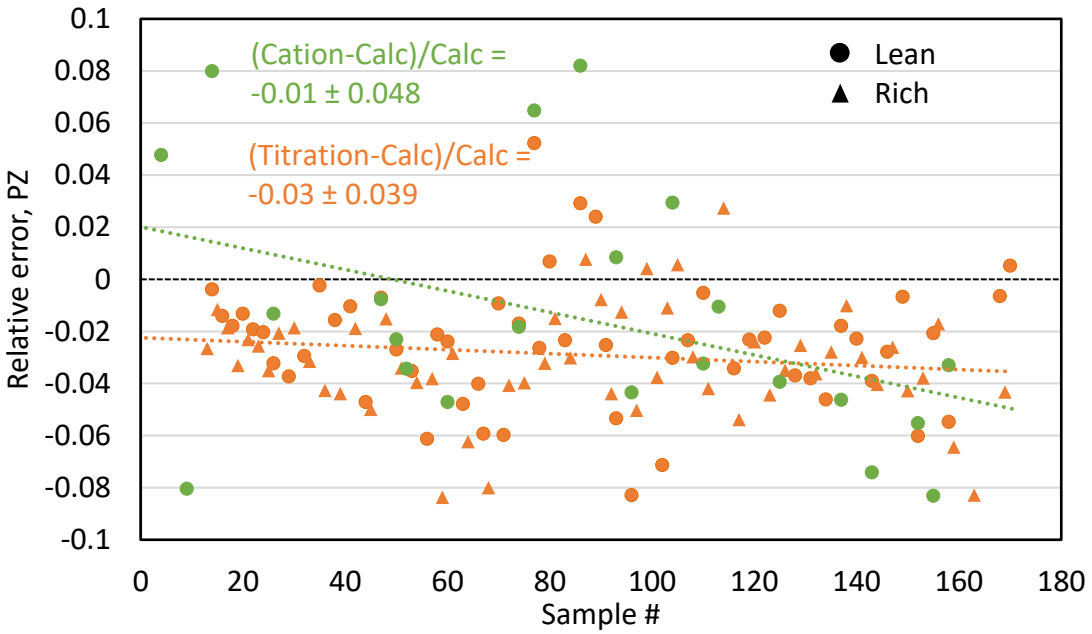

Figure 2.8: Comparison of PZ measured by offline IC (green) and titration (orange) and PZ calculated from online density and viscosity for NCCC 2018 campaign.

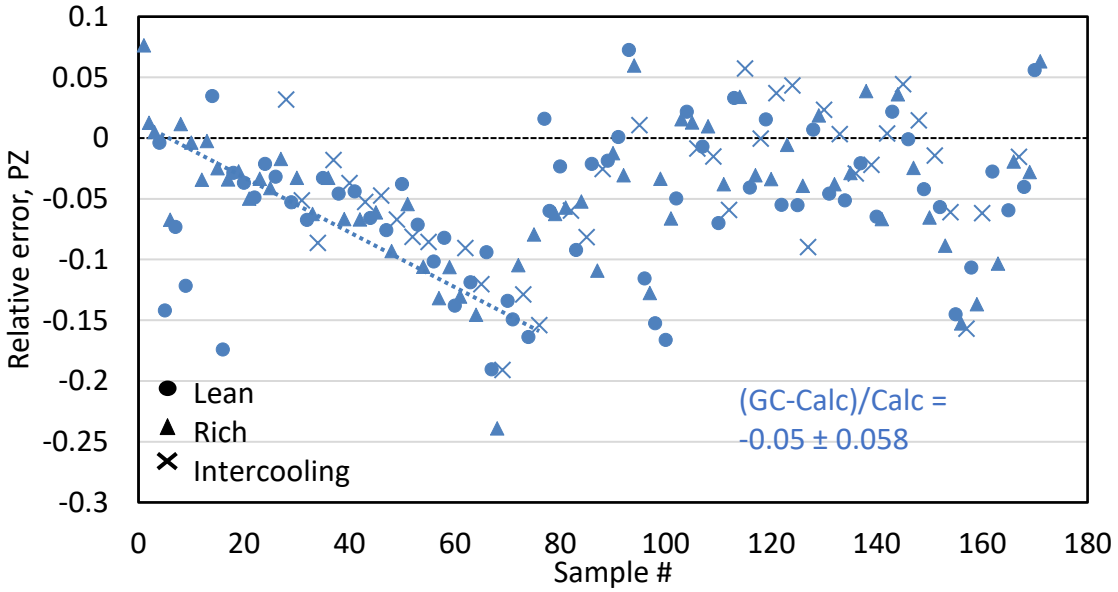

Figure 2.9: Comparison of PZ measured by offline GC and PZ calculated from online density and viscosity for NCCC 2018 campaign.

The comparison between offline GC measurements and online calculation is shown in Figure 2.9. The error for offline GC shows the largest standard error and a time-dependent trend for the first 90 samples. This trend cannot be reproduced later, thus considered as random error associated with offline analytical analysis.

Figure 2.10 compares solvent CO_2 measured by TIC and titration and to online calculation for lean, rich, and intercooling solvent. Offline TIC agrees with calculation but there is a step change around sample number 90. The shift in the TIC at May 29 (sample number 90) is correlated with the shift in PZ by GC, suggesting a sampling or common dilution error in the onsite laboratory.

The titration measurements are consistently lower (17% on average) than the online calculation and the error is not time dependent. A constant offset is adequate to reconcile the measurements by these two methods.

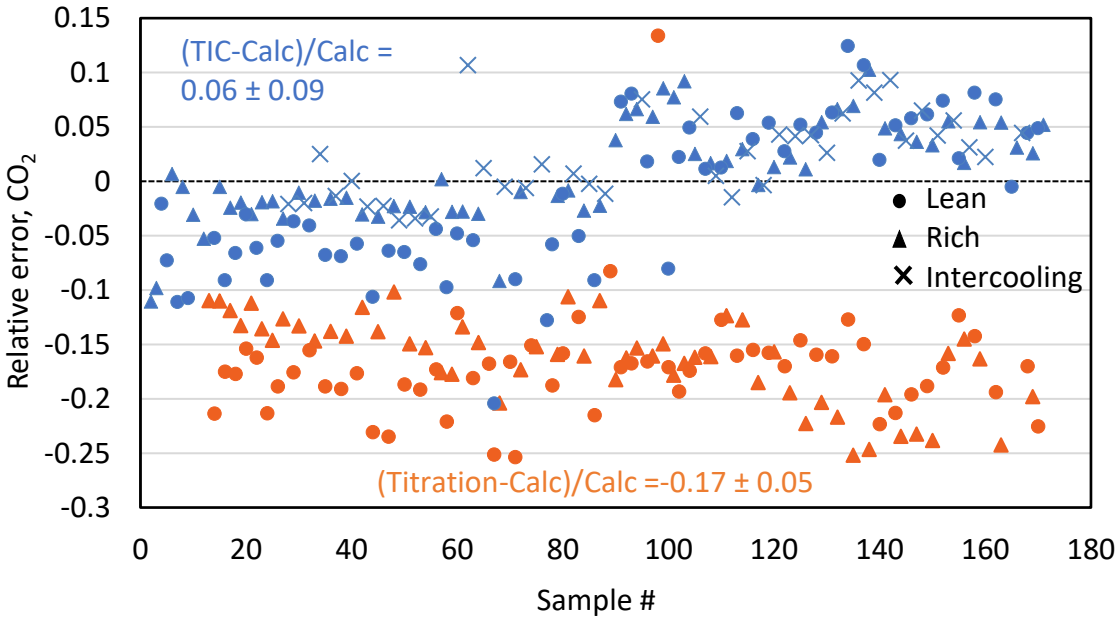

Figure 2.10: Comparison of CO_2 measured by offline TIC and online titration to CO_2 calculated from online density and viscosity for NCCC 2018 campaign.

Solvent loading is the molar ratio of solvent CO_2 to alkalinity. The relative errors of loading between different methods are shown in Figure 2.11. The loadings by titrated PZ and CO_2 are shown in orange. PZ by GC and CO_2 by TIC are blue. PZ by titration and CO_2 by TIC are green. Given the large uncertainty associated with analytical methods, loadings measured by GC & TIC, titration & TIC agrees with calculation based on density and viscosity within 1 standard error. For lean samples, errors for all three analytical methods are corelated with calculated loading: lower loadings tend to have greater errors. This indicates a systematic shift in the density and viscosity correlation. However, this trend is not observed in the intercooling and rich samples.

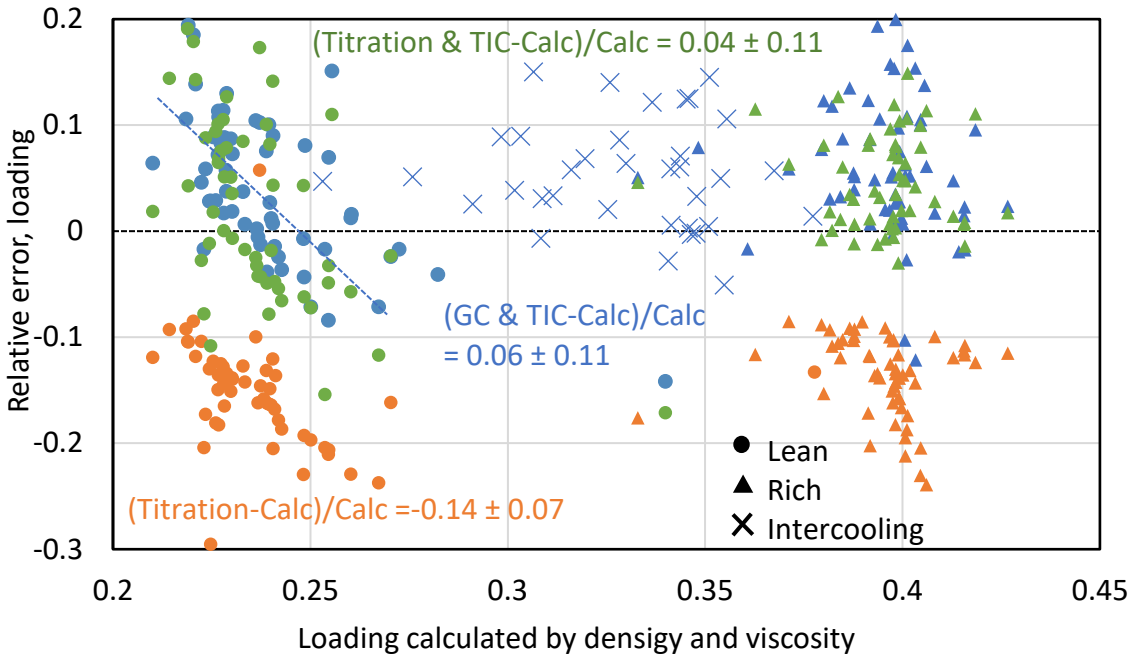

Figure 2.11: Comparison of loading measured by titration (orange), GC & TIC (blue), and titration & TIC (green) to loading calculated from density and viscosity measurements for NCCC 2018 campaign.

For NCCC 2018 campaign, multiple analytical methods were used to analyze PZ and CO_2 concentration. The PZ calculated by density and viscosity shows consistent offset

with analysis by GC, IC, and titration. The CO_2 by calculation agrees with TIC within 1 standard deviation. Compared to calculation, the averaged PZ by titration is 3% smaller and by TIC is 1% smaller. The CO_2 by titration is consistently 17% less than TIC and calculation.

Density and viscosity calculation is used as base method for the reconciliation for two reasons: the good availability and precision. Solvent density and viscosity are measured every minute by online flowmeter and viscosity. This method enables real time monitoring of the solvent composition and greatly improves the data availability compared to other analytical methods. The density and viscosity measurements also have good reproducibility and show low variations in the steady state. The standard deviations are usually less than 2%.

2.5.1.2 NCCC 2019 Campaign

The methods developed for NCCC 2018 campaign continued to be used for the NCCC 2019 campaign. The lean viscometer worked properly for this campaign, so the lean and rich solvent were calculated independently using density and viscosity measurements for each stream. The second viscosity measurement also provides the opportunity to validate the assumption made during the 2018 campaign.

Figure 2.12 compares the measured lean viscosity to calculated viscosity based on the assumption that the lean and rich solvent have the same PZ molality. The two viscosities agree well, suggesting the method using density and viscosity is reproducible and the assumption is valid for steady state testing.

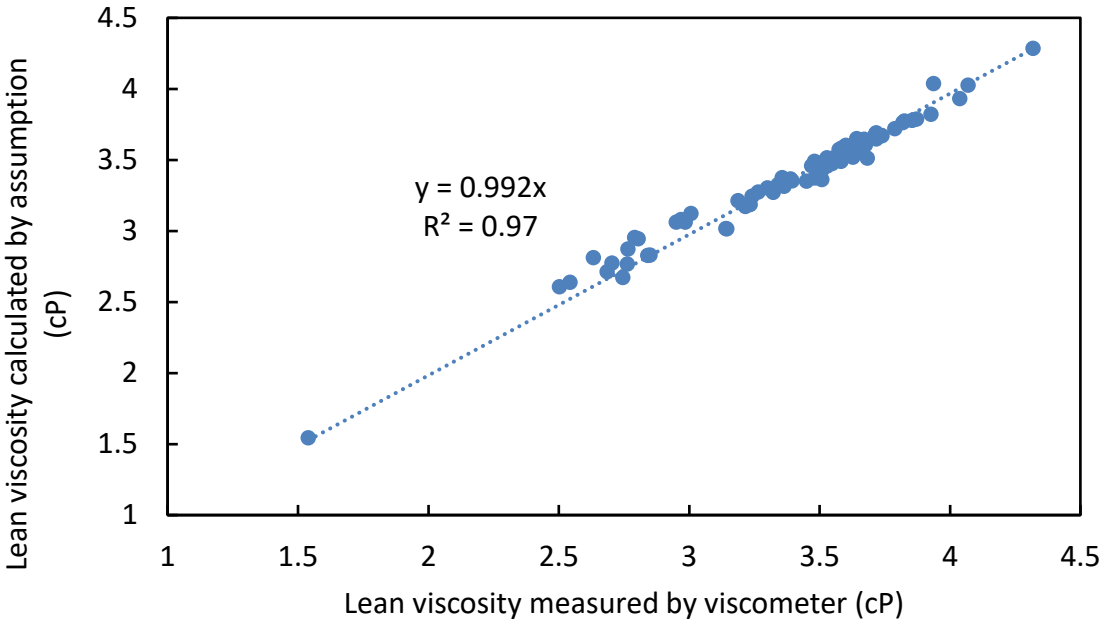

Figure 2.12: Comparison of lean viscosity measured by viscometer and calculated based on "equal molality" assumption.

The variations of solvent viscosity are plotted against calendar time in Figure 2.13 and the uncertainty of the two viscosity measurements is shown. The gaps represent plant shut down. The lean viscometer generally shows a greater reproducibility than the rich viscometer. It is likely that the rich pump downstream of the rich viscometer introduces turbulence in the flow and the rich viscosity therefore has greater uncertainty. Both lean and rich viscometers became more scattered after May 15th, on which day the carbon bed filter was turned on. Another pump in the carbon bed section was put online near the rich viscometer sample point, but it is not clear why the lean measurement was also affected. There are several step changes in solvent viscosities, and they are related to the addition of fresh PZ and the use of carbon bed. When the carbon bed was online, it absorbs water, increases the PZ concentration and solvent viscosities. During the long-term test (latter half

of the campaign), the viscosities decrease over time, suggesting possible PZ loss during the operation.

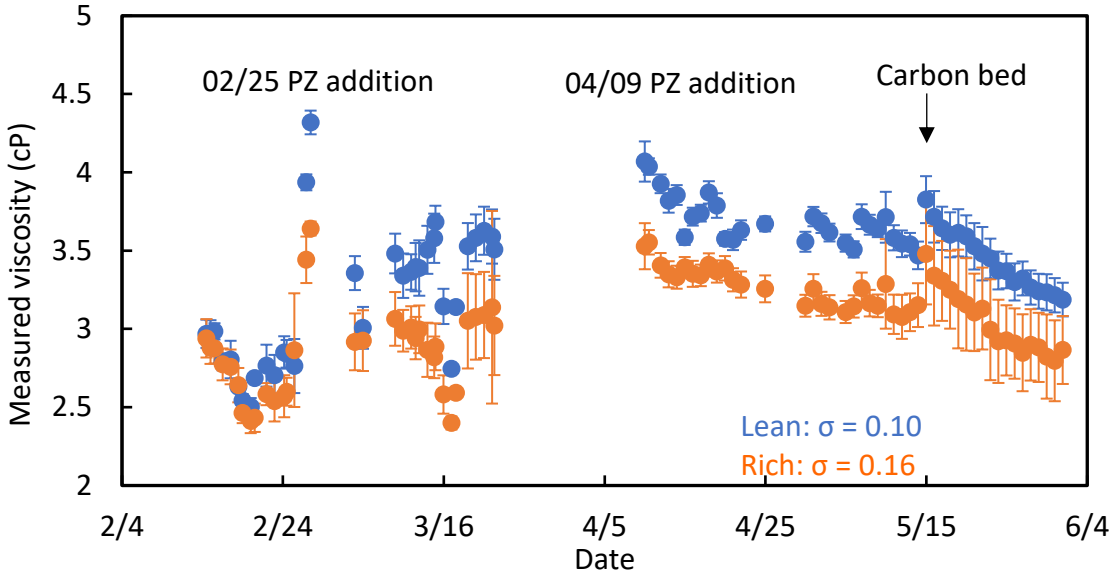

Figure 2.13: Lean (blue) and rich (orange) solvent viscosity measurements for steady state runs, the error bar shows the uncertainty of the measurements.

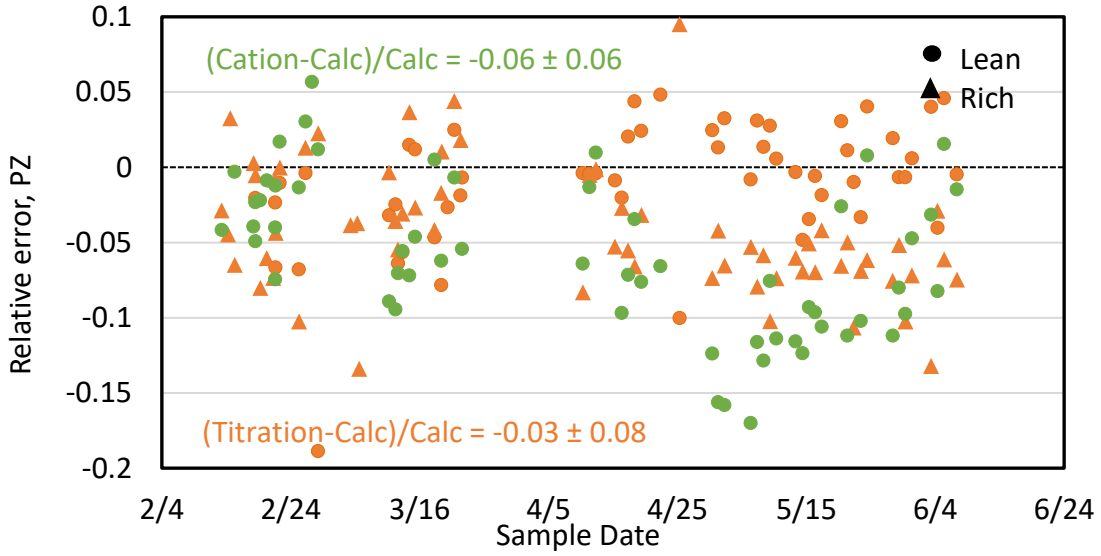

Figure 2.14: Comparison of PZ measured by offline IC (green) and titration (orange) to PZ calculated from online density and viscosity for NCCC 2019 campaign.

Figures 2.14 and 2.15 compare the PZ analyzed by titration, IC, and GC to the calculated by online density and viscosity. The averaged PZ concentrations by titration and GC are 3% lower than the calculation, and IC measurements are 6% lower. The standard errors of analytical methods are 6-8%, making the different between the average value statistically insignificant. There are some variations associated with operating time, but it is not a strong time dependence. The lean and rich PZ concentrations by titration diverge after April 10th: the errors for lean solvent are consistently higher than (about 6%) the rich. A similar trend is also observed in GC measurements, indicating the plant shutdown before April 10th may cause systematic error on the flowmeter or viscometer. The calculation based on density and viscosity tends to overpredict the PZ concentration in the rich solvent by 6%.

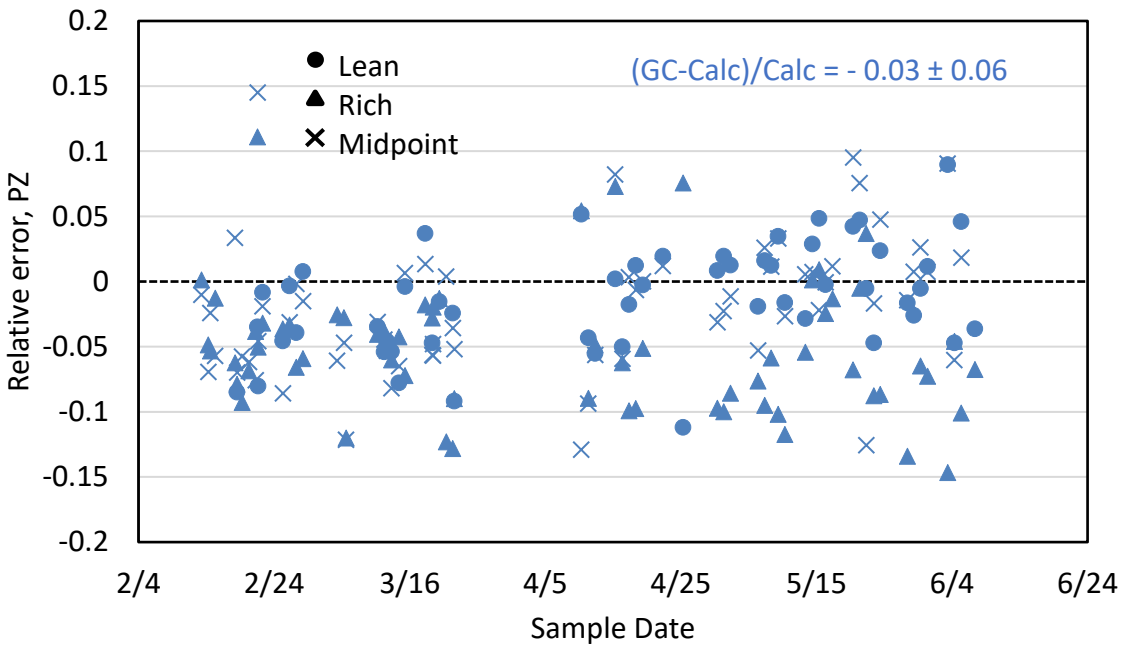

Figure 2.15: Comparison of PZ measured by GC to PZ calculated from online density and viscosity for NCCC 2019 campaign.

CO_2 concentrations by titration and TIC are compared in Figure 2.16. Both titration and TIC measurements show good reproducibilities. The averaged CO_2 by TIC is 3% greater than the calculation and the averaged titration is 18% less. Based on the two campaigns at NCCC, the online auto-titration consistently undermeasures CO_2 compared to other methods, indicating a systematic offset associated with the experimental setup or instrument calibration.

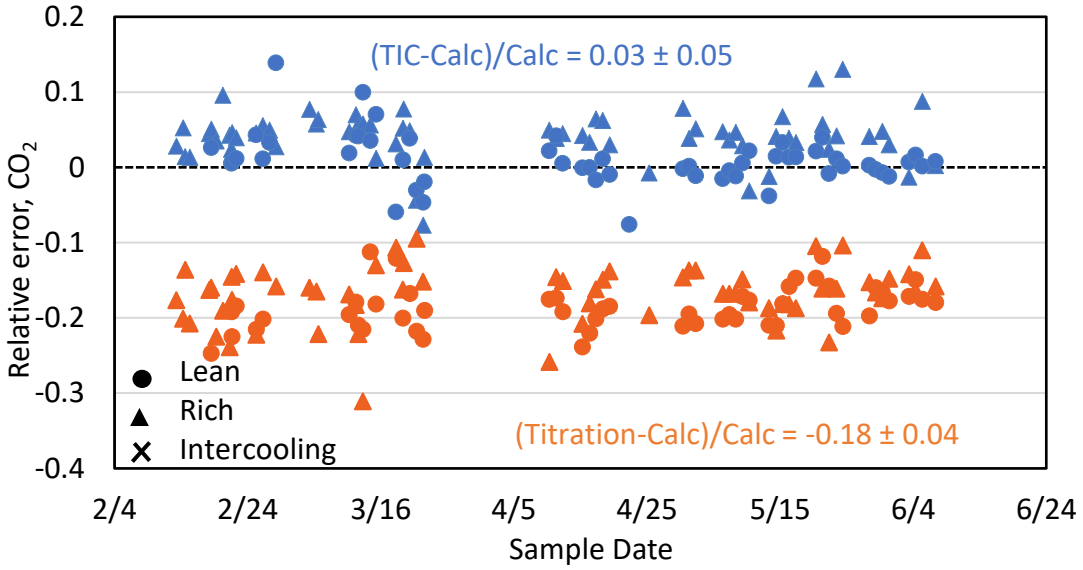

Figure 2.16: Comparison of CO_2 measured by TIC (blue) and titration (orange) to CO_2 calculated from online density and viscosity for NCCC 2019 campaign.

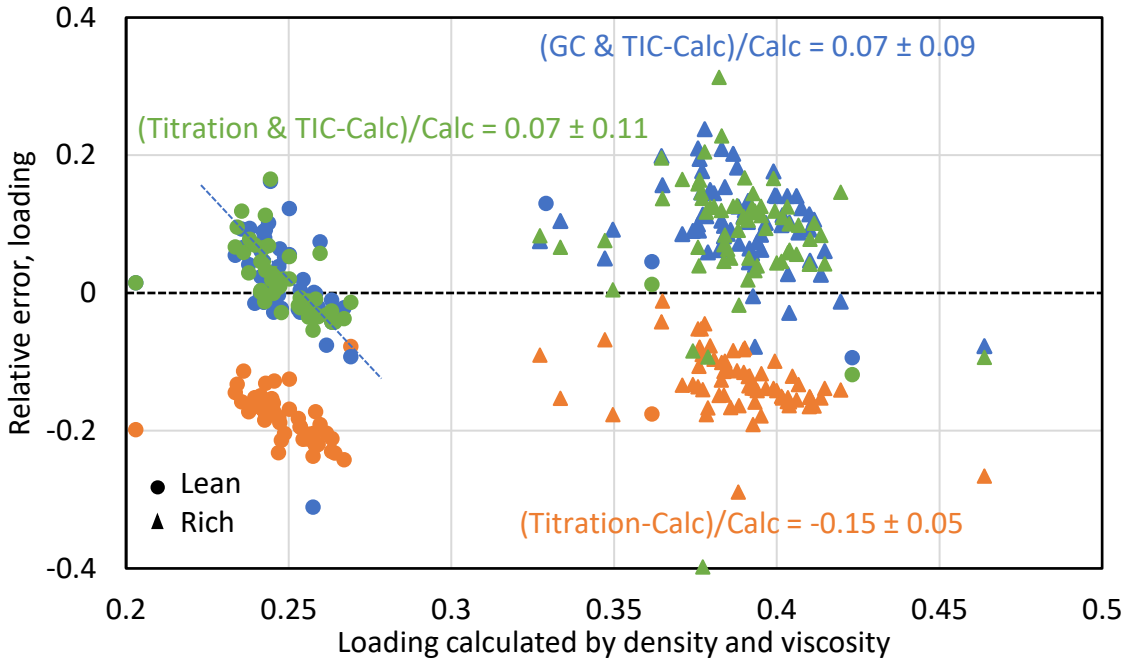

Figure 2.17: Comparison of loading measured by titration (orange), GC & TIC (blue), and titration & TIC (green) and loading calculated from density and viscosity for NCCC 2019 campaign.

PZ and CO_2 measured by different methods are converted to loading and compared to density and viscosity calculation in Figure 2.17. The PZ by titration matches TIC, therefore the loadings using PZ from GC and titration and CO_2 from TIC are very close, and they are 7% lower than the loading calculated by density and viscosity. The loading calculated using titrated CO_2 is 15% less than the calculation, mainly caused by the offset in the CO_2 content. The loading reconciliation for NCCC 2019 campaigns leads to similar conclusions as the 2018 campaign.

2.5.1.3 SRP 2018 Campaign

For the SRP 2018 campaign, lean and rich samples were collected during the campaign and manually titrated for PZ and CO_2 concentration. Online measurements of density for lean and rich solvent were available. One viscometer was measuring lean

solvent and the viscosity along with density can be used to determine solvent compositions at SRP for the first time. However, the viscometer readings were found consistently higher than the expected viscosity of 5 m PZ based on prior pilot plant and bench-scale measurements. Figure 2.18 compares the measured viscosity to that calculated using Equations 2.2 and 2.3 based on solvent compositions from titration. The points are coded to represent the different inlet CO_2 concentrations, and the error bar shows the standard deviations over the 30-minute steady state. Despite some large variations in the measurements, the measured viscosities are well-correlated with the calculated viscosities with R^2 close to 1. The viscometer reading needs to be divided by a factor of 1.51 to reconcile with prior data collected from pilot plants and laboratories. This correction is applied for all the following analyses.

A possible cause for the large variation of the viscometer is the flowrate. The designed flowrate of viscometer is around 10 gpm, and it is close to the actual solvent flowrate for 12% CO_2. Therefore, the variations of the orange points (12% CO_2) are smaller than the green (4% CO_2, low flowrate) and blue (20% CO_2, high flowrate). There are three outliers showing in the red circle where the viscometer readings are high, they are the runs at very high liquid flow (around 20 gpm).

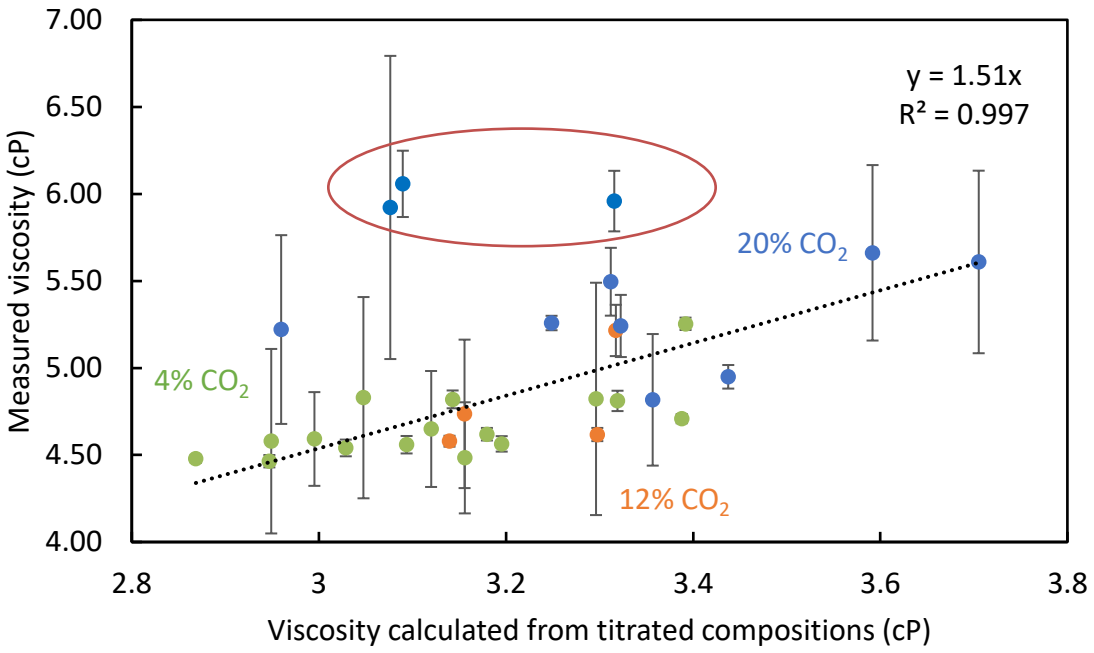

Figure 2.18: Comparison of lean viscosity measured by viscometer and calculated based on compositions from titration. Points are color coded to represent the inlet CO_2 concentration.

Figure 2.19 shows the relative error between solvent loading analyzed by titration and calculated based on online density and corrected viscosity. On average, the titrated loading is about 7% lower than the density and viscosity calculation. Since the viscosity was first calibrated using the titration results, and the correction accounts for most of the variation in the viscosity data (R^2> 0.99), density measurements become the main source of the error.

There are two possible causes of the error: the measurement or the correlation. Based on prior experience from pilot plant data reconciliation, density measurements are reliable and have good reproducibility (standard deviation around 0.01). It is likely that Equation 2.1 does not corelate solvent density and composition with good accuracy. This hypothesis is also confirmed by the tendency of loading error showing in both NCCC and

SRP campaigns. For both lean and rich solvent, instead of randomly distributed at different loading, the relative error is linearly related to loading as showing by the dashed in in Figures 2.11, 2.17 and 2.19. Furthermore, the 7% offset on loading has been observed in multiple prior pilot plant campaigns at SRP (Sachde, 2016; Sachde et al., 2013), indicating a systematic error in the density correlation because these campaigns using density only. Therefore, more bench-scale measurements of solvent density in a narrower loading range may help improve the accuracy.

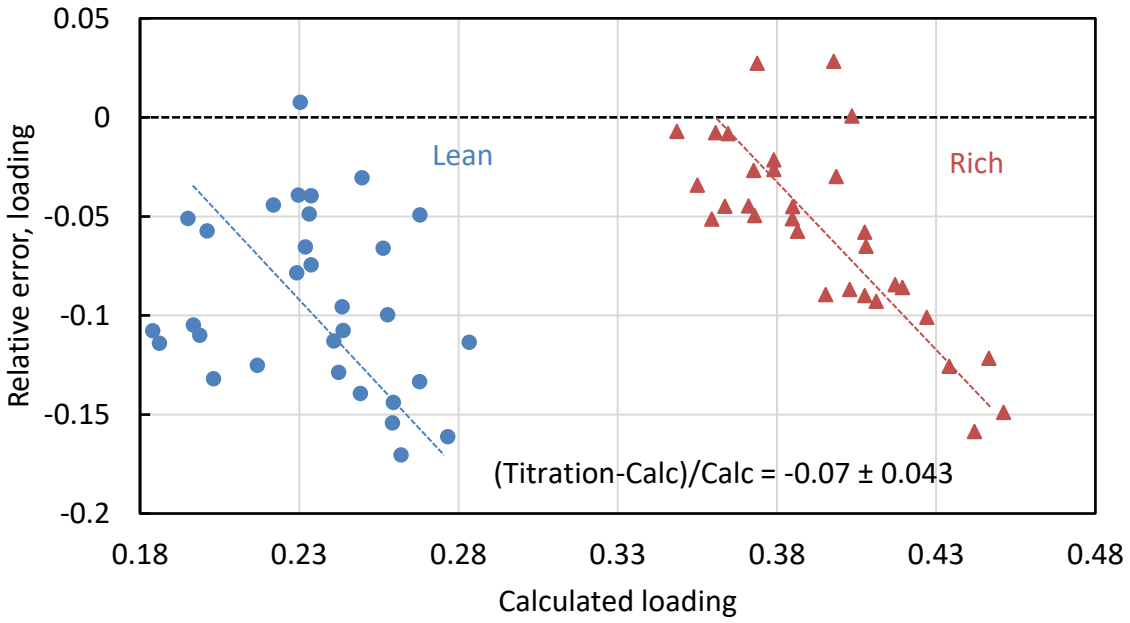

Figure 2.19: Comparison of loading measured by titration and loading calculated from density and viscosity for SRP 2018 campaign.

2.5.2 Material Balance

Studying the CO_2 material balance provides opportunities to evaluate the consistency of flow measurements and concentration measurements in both gas and liquid phase. Three CO_2 rates around the system are commonly used to exam the material closure: the CO_2 removed rate from the gas phase, the capture rate into the solvent, and the

production rate in the stripper overhead stream. The liquid phase CO_2 rate is calculated from solvent flow measurements and compositions from online density and viscosity using equation 2.4.

$$R_{CO2,Liq} = \frac{\dot{m}_{LiqOUT}(x_{CO2,LiqOUT}) - \dot{m}_{LiqIN}(x_{CO2,LiqIN})}{M_{CO2}} \quad (2.4)$$

where:

$R_{CO2,Liq}$ = CO_2 absorption rate in liquid (kmol CO_2/hr)

$\dot{m}_{LiqOUT}$ = mass flow of outlet liquid (lb/hr)

$\dot{m}_{LiqIN}$ = mass flow of inlet liquid (lb/hr)

$x_{CO2,LiqOUT}$ = mass fraction of CO_2 in absorber rich solvent calculated from density and viscosity

$x_{CO2,LiqIN}$ = mass fraction of CO_2 in absorber lean solvent calculated from density and viscosity

M_{CO2} = CO_2 mole mass (lb/kmol)

The gas phase CO_2 removed rate is calculated using inlet and outlet flowrates and CO_2 concentrations measured by NDIR through equation 2.5. The stripper overhead product rate is measured as the flowrate and is assumed to be pure CO_2.

$$R_{CO2,Gas} = \frac{\dot{m}_{GasIn}(y_{CO2,GasIN})}{M_{GasIn}} - \frac{\dot{m}_{GasOUT}(y_{CO2,GasOUT})}{M_{GasOUT}} \quad (2.5)$$

where:

$R_{CO2,Gas}$ = CO_2 removed rate in flue gas (kmol CO_2/hr)

$\dot{m}_{GasIn}$ = mass flow of inlet flue gas (lb/hr)

$\dot{m}_{GasOUT}$ = mass flow of outlet flue gas (lb/hr)

$y_{CO2,GasIN}$ = mole fraction of CO_2 in inlet flue gas measured by online NDIR

$y_{CO2,GasOUT}$ = mole fraction of CO_2 in outlet flue gas measured by online NDIR

M_{GasIN} = mole mass of inlet flue gas (lb/kmol)

M_{GasOUT} = mole mass of outlet flue gas (lb/kmol)

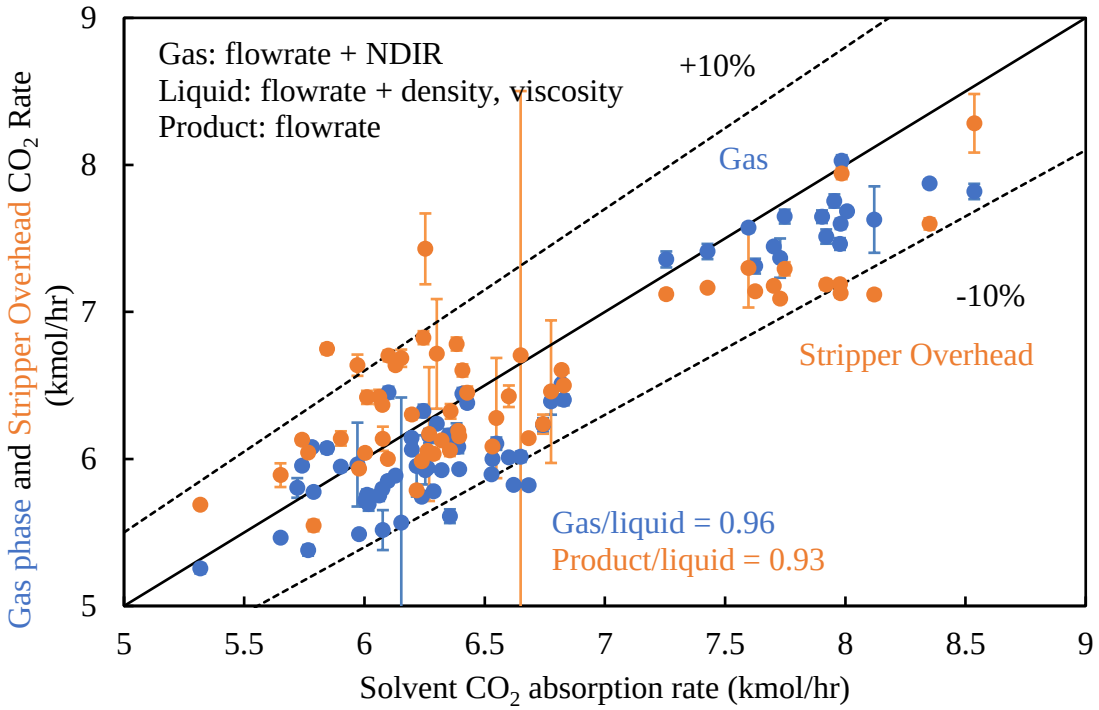

Figure 2.20: CO_2 rates in the gas and liquid phases and the stripper overhead product for NCCC 2018 campaign.

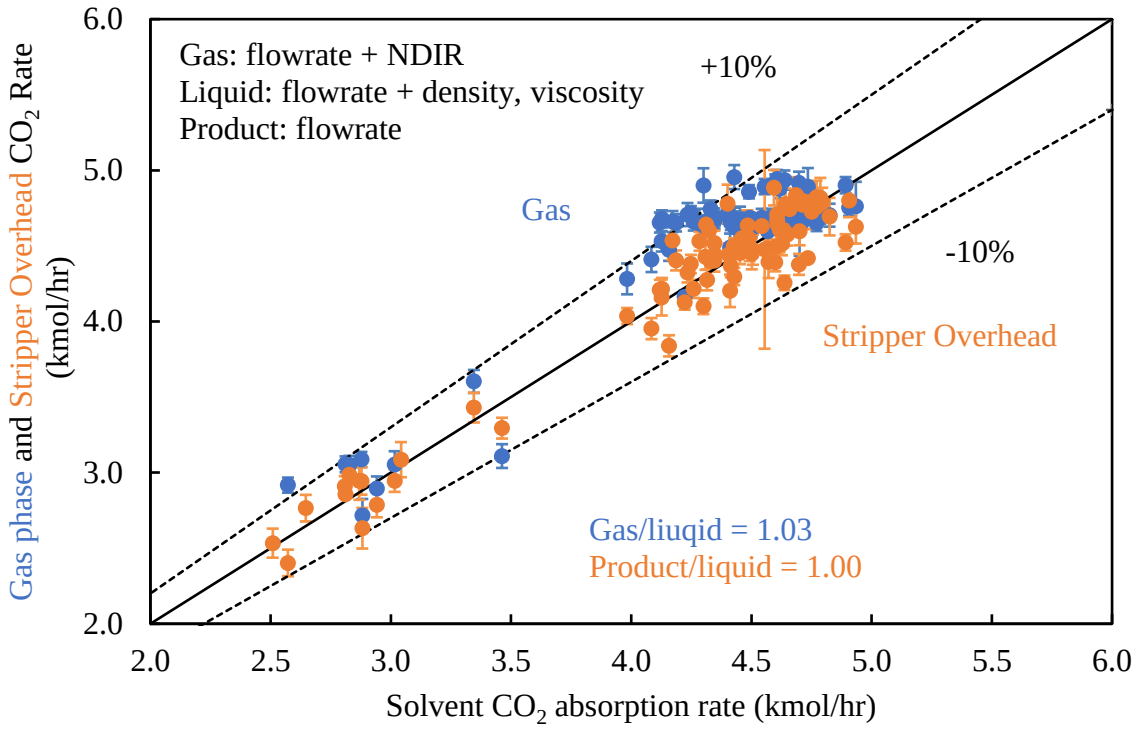

Figure 2.21: CO_2 rates in the gas and liquid phases and the stripper overhead product for NCCC 2019 campaign.

Figures 2.20 and 2.21 compare the three CO_2 rates and the uncertainties measured in NCCC pilot plant for 2018 and 2019 campaigns. The CO_2 material balance closes within 10% for most of the steady state runs during these two campaigns. For the 2018 test, the averaged CO_2 rate in the gas phase and product are 4% and 6% smaller than the absorption rate in the solvent. For the 2019 campaign, the CO_2 production rate matches the absorption rate in the solvent phase, and they are 3% smaller than the gas phase. The production rate shows large variations for some runs because the stripper overhead is at high pressure and can be affected by the stripper operation. Stripper flooding occurred for some runs and caused the large fluctuation in the flowrate.

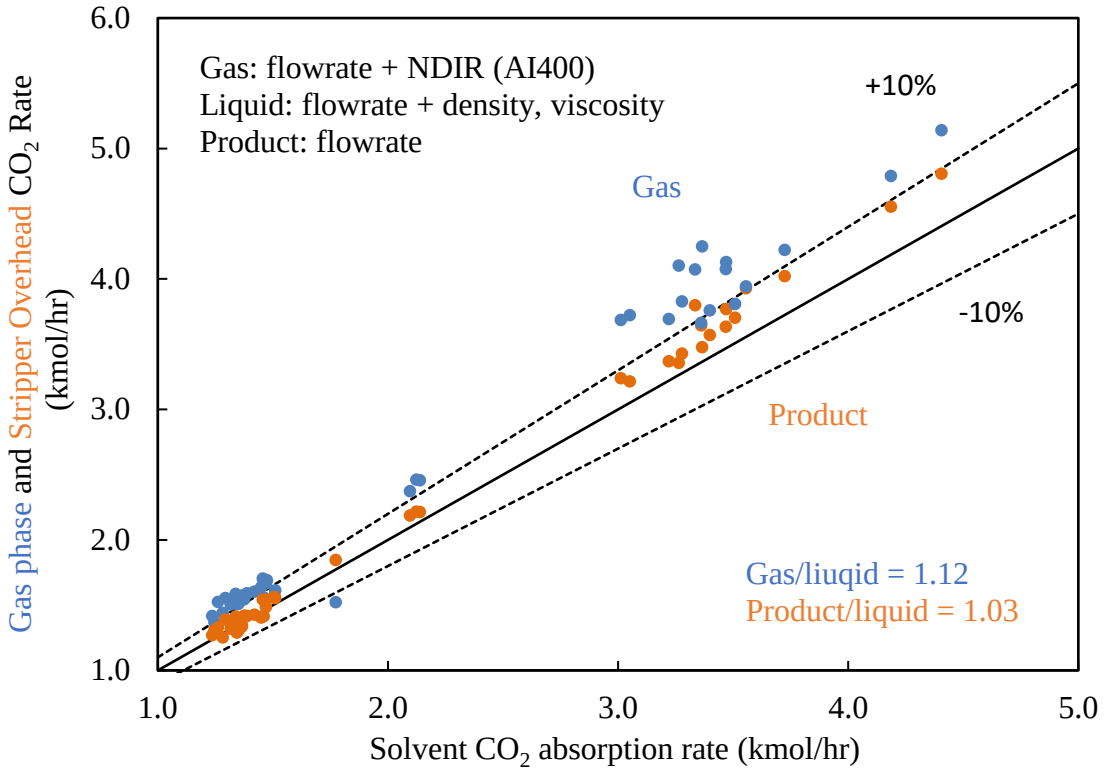

Figure 2.22: CO_2 rates in the gas and liquid phases and the stripper overhead product for SRP 2018 campaign.

Figure 2.22 compares the three CO_2 rates measured at SRP pilot plant for 2018 campaign. The CO_2 captured in the solvent side is calculated based on density and corrected viscosity and it matches the stripper overhead CO_2 flowrate. The gas side CO_2 removed rate is 12% higher than liquid side CO_2 absorption rate and 9% higher than the stripper overhead flowrate, which is in accordance with the overprediction of inlet CO_2 concentration by NDIR. The material balance indicates that the CO_2 rate in the gas phase is consistently high and needs correction.

During the campaign, online FTIR measurements were available during some of steady state runs. FTIR measurements and CO_2 material balance were used to adjust the NDIR measurements as shown in Figure 2.23. After NDIR measurements of inlet CO_2

were reduced by 11%, the corrected CO_2 concentrations can match the FTIR measurement, and closed the CO_2 balance within 1% difference.

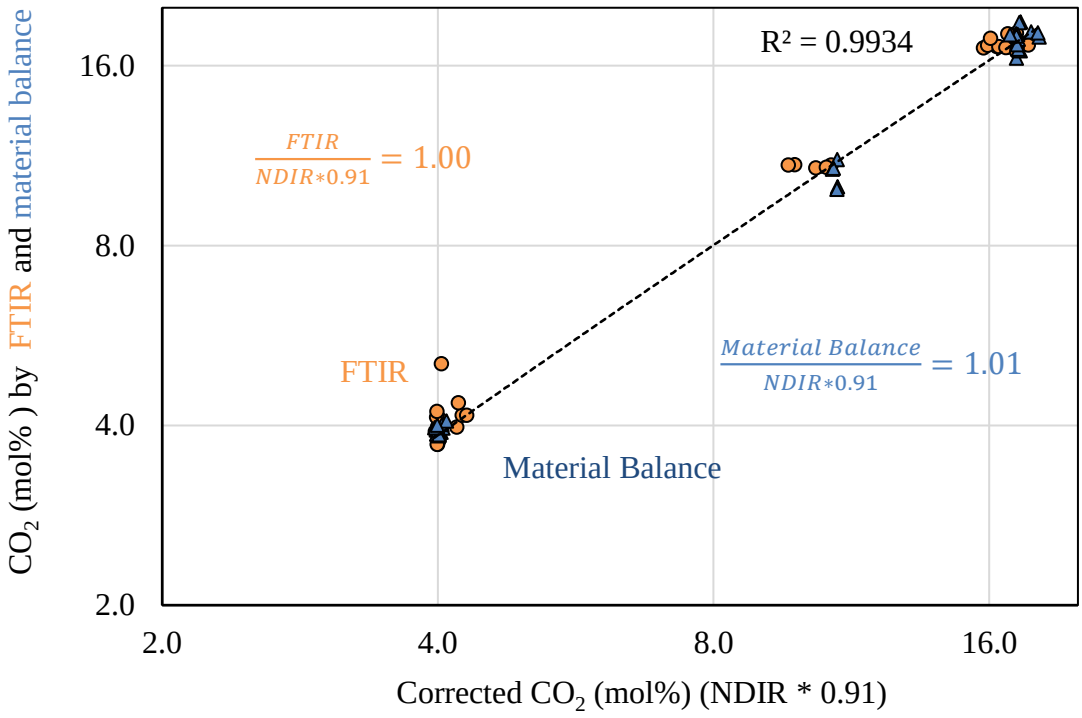

Figure 2.23: Correction of inlet NDIR measurement based on FITR (orange) and material balance (blue).

2.5.3 Absorber Performance

CO_2 penetration and absorber number of transfer unit (NTU) are defined to help study the absorber performance. The CO_2 removal and penetration in mole basis are defined in Equation 2.6. The NTU is commonly used in mass transfer studies and is simplified as in Equation 2.7. NTU can capture the nonlinear increase of the amount of transfer area required to achieve a high CO_2 removal. For gas film controlled mass transfer with no equilibrium limit (Equation 2.8), the total packing height required is the product

of the height of transfer unit (HTU) and the number of transfer unit (NTU). For example, it takes twice as much packing area to achieve 99% removal (NTU = 4.6) as 90% (NTU = 2.3) if it is gas film controlled and there is no equilibrium limit. The CO_2 absorption into amine solvent is more complicated than the ideal model but the use of NTU can help understand the absorber performance, especially for the higher removal condition.

$$removal = 1 - \frac{N_{CO_2,out}}{N_{CO_2,in}} = 1 - Penetration \tag{2.6}$$

$$NTU = -\ln(Penetration) \tag{2.7}$$

$$H = \left(\frac{G}{K_G A}\right)\int_{y_{in}}^{y_{out}} \frac{-dy}{y - y^*} = -\underset{(HTU)}{\frac{G}{K_G A}} \underset{(NTU)}{\ln\left(\frac{y_{out}}{y_{in}}\right)} \tag{2.8}$$

2.5.3.1 NCCC 2018, coal conditions

Among 68 absorber steady state runs for NCCC 2018 campaign, 36 parametric tests were performed to test the system over a wide range of conditions. The base CO_2 removal target was 90% but high removal cases were achieved for both low and high gas rates. Figure 2.24 shows the measured CO_2 penetration (color-coded dots) at different loading and temperature as well as the Aspen Plus® modeled predictions (blue triangles) at corresponding conditions.

The operating temperature of the absorber varied during the campaign as indicated by the color of points. The colors are the rich solvent temperature exiting absorber sump and represent average temperatures along the column. At constant CO_2 penetration around 90%-93%, lower temperature (darker) leads to greater rich loadings, indicating better absorber performance. The solvent and gas inlet temperature were controlled to be 40 °C at the beginning of the campaign in the winter and then increased to about 46 and 49 °C

due to elevated ambient temperature in the summer. At normal temperature, 90% removal can be achieved with a rich loading around 0.4. The rich loading increases to 0.41 at lower temperature and decreases to 0.38 at higher temperature. This seasonal variation affects the system cooling performance and causes about 12% change in the solvent flow to achieve the same CO_2 removal level.

By increasing the solvent rate, a higher removal rate was achieved at reduced rich loading. There were 4 cases at 99% removal and the corresponding rich solvent decreased to 0.38. This is an 8% decrease in delta loading compared to 90% cases, and it is also associated with the energy penalty to raise CO_2 removal by 10%.

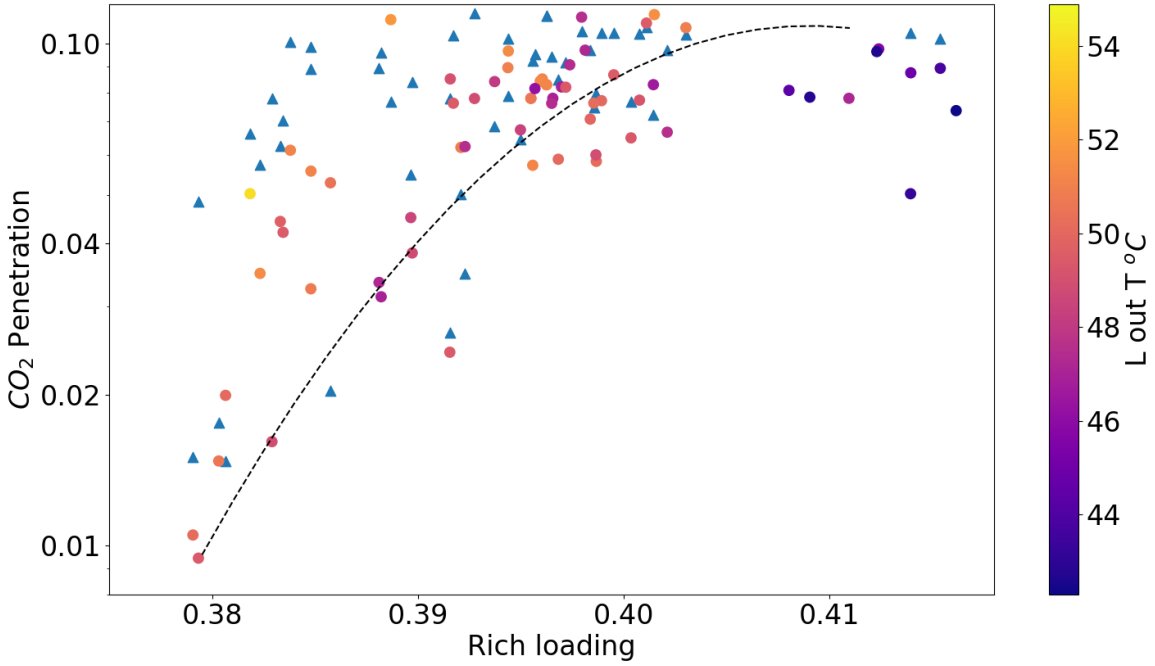

Figure 2.24: Experimental absorber performance (round dots) at different loading and temperature and the modeled results at corresponding conditions (Blue triangles). The color of experimental points shows the rich solvent temperature exiting the absorber. The dashed line is the empirical correlation at 0.24 lean loading and 49 °C. (Equation 2.9)

$$NTU = -1701.7 + 57.22 * lldg + 2164.5 * rldg - 0.07 * Tout - 15.2 * ln(lldg) - 885.4 * ln(rldg) \quad (2.7)$$

With the experimental absorber performance for 36 parametric runs, an empirical correlation for NTU as shown in Equation 2.7, was regressed as a function of lean loading (lldg), rich loading (rldg) and solvent outlet temperature (Tout). Variables and the form of the function were chosen empirically so the expression has reasonable physical meaning and captures experimental results. Among the four temperatures around the absorber (gas, liquid inlet and outlet), the liquid outlet temperature had the most significant influence on absorber performance. This suggests the absorber is likely to pinch at the bottom and the rich solvent temperature becomes important because it defines the equilibrium near the bottom, and the mass transfer driving force is enhanced at lower temperature.

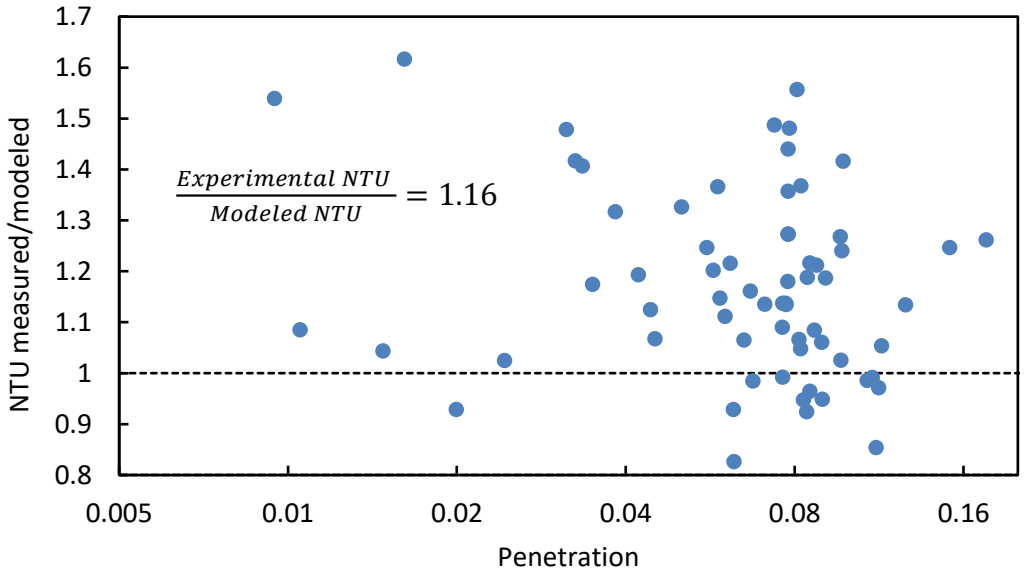

Figure 2.25: The ratio of experimental and model predicted NTU at variable CO_2 penetration for NCCC 2018 campaign.

The modeling results for each steady state run are simulated using the rigorous rate-based method in Aspen Plus® without adjustment. The lean solvent composition for model input were calculated from density and viscosity. Figure 2.25 shows the ratio of measured number of transfer units to modeled results. The model under-predicted the absorber performance for most of the cases, and on average, the experimental transfer unit is 16% greater than modeled value. This may result from the disagreement of loading measured by different methods: the CO_2 (wt %) by titration was consistently lower than the density and viscosity prediction by 14% in this campaign. Therefore, the model was simulated at higher lean loading conditions thus the performance was worse than the experiments. Detailed model adjustment will be discussed in next section.

2.5.3.2 NCCC 2019, NGCC conditions

Data from 80 absorber steady-state runs were obtained over 2100 operating hours in 2019. The first 22 runs were parametric tests, which examined the absorber performance over a wide range of conditions, and the rest was long-term testing designed to study the system stability, solvent oxidation, and other operational problems including maintaining system water balance. There were four major absorber operating conditions tested during the campaign: in-and-out (40 °C) with 40 °C gas inlet temperature, pump-around (40 °C) with 40 °C gas, pump-around (40 °C) with 78 °C gas, and pump-around (35 °C) with 78 °C gas. The CO_2 removal varied between 85% and 96% with lean loading from 0.19 to 0.25 mol CO_2/mol alkalinity.

Figure 2.26 shows the experimental absorber performance grouped with four operating conditions. The rich loading varied between 0.36 and 0.41, and it shows correlation with CO_2 penetration: the rich loading decreases from 0.4 to 0.38 as the removal increases from 90% to 95%. The delta loading reflects the energy penalty for high CO_2

removal at the NGCC condition. The long-term runs achieved rich loading exceeding 0.4, which is greater than the rich loading from the 2018 campaign at coal conditions. This means that low CO_2 in the NGCC flue gas does not necessarily lead to a lower rich loading, nor to worse energy performance. This is because the column temperature is well-managed with pump-around intercooling, which increases the rich loading even at the low CO_2 partial pressure.

This campaign demonstrated the effect of pump-around intercooling and the innovative design eliminating the DCC for NGCC flue gas. The blue and orange points are the comparison between in-and out and pump-around intercooling. At roughly the same rich loading, the pump-around absorber can achieve higher removal. The effect of gas inlet temperature is shown in the different between orange and grey points. When the hot flue gas was fed into absorber directly, the rich loading only reduced slightly. This is because with the pump-around intercooling, the hot gas can be quenched and cooled quickly in the absorber bottom. Therefore, the DCC column can be eliminated in the NGCC application. Similar to the temperature effect found in the 2018 campaign, lowering pump-around temperature is an effective strategy to improve the absorber performance. By lowering the pump-around intercooling from 40 °C to 35 °C, the rich loading increases from around 0.38 to 0.4, that is about 15% reduction in the solvent circulation rate.

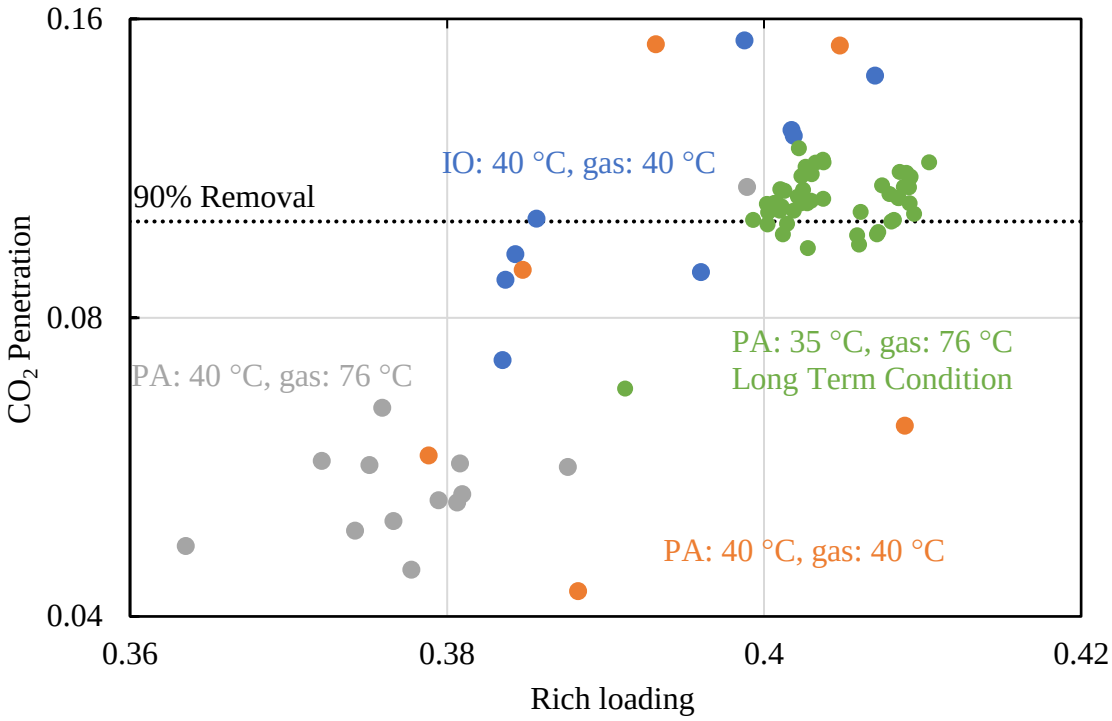

Figure 2.26: Experimental absorber performance for NCCC 2019 campaign. Points are color coded to represent the conditions (IO: in-and-out intercooling, PA: pump-around intercooling).

The raw model predictions are compared to the experimental results in Figure 2.27. The model underpredicts the NTU by 52% on average but the error is different for the two intercooling configurations. For in-and-out configuration, the model underpredicts NTU by 39% and for pump-around absorber it underpredicts by 54%. This difference suggests the absorber performance is controlled by different mechanisms for the two intercooling configurations.

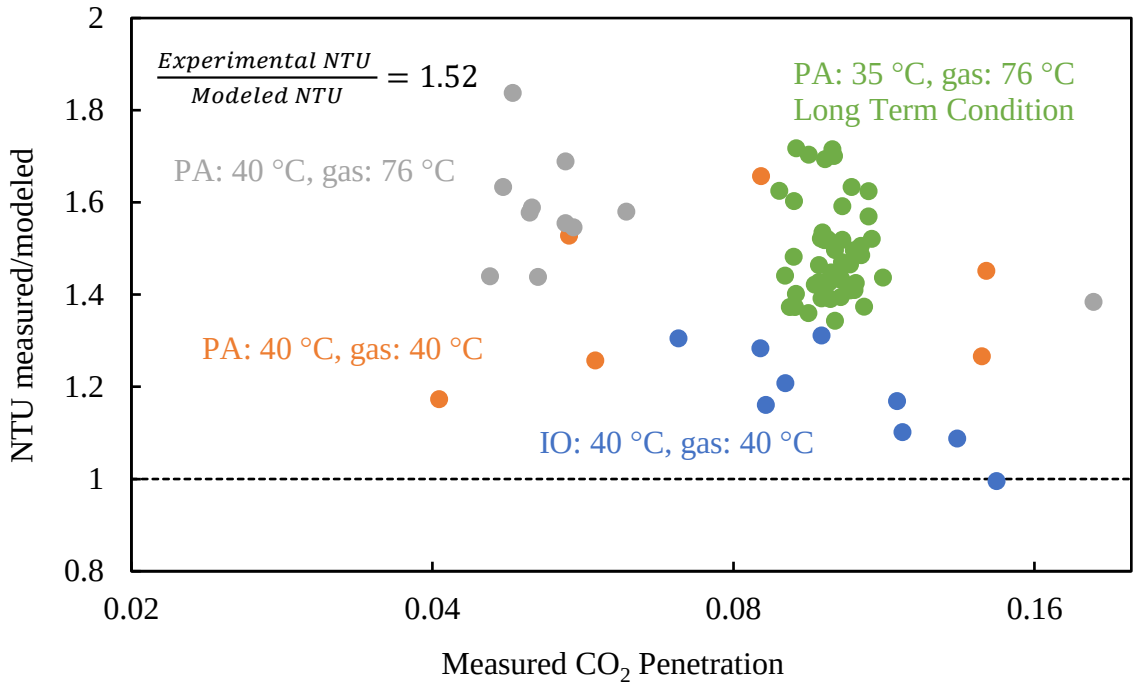

Figure 2.27: The ratio of experimental and model predicted NTU at different CO_2 penetration for NCCC 2019 campaign. Points are color coded to represent the conditions.

2.5.3.3 SRP 2018

During the SRP 2018 campaign, 47 steady-state tests were completed with three CO_2 concentrations. Most of the runs aimed at 90% removal and the highest removal achieved for 20% and 4% CO_2 was 98.5% and 96.7% respectively. Figure 2.28 shows the experimental performance for the three different CO_2 concentrations. The rich loading for the 12% and 20% CO_2 are close for 90% removal, suggesting there could be mass transfer pinch in the absorber. At 4% CO_2, greater mass transfer driving force is required to achieve 90% removal, giving a lower rich loading compared to the other cases. The unadjusted model predictions are shown in Figure 2.29. On average, the measured NTU is about 39% greater than the simulation, and the error at variable CO_2 concentration is roughly the same.

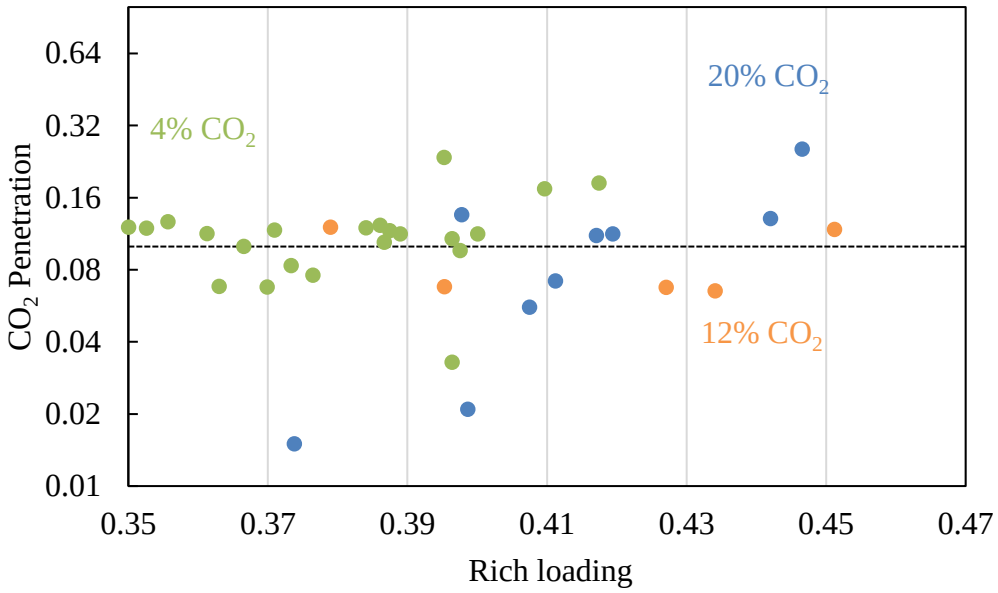

Figure 2.28: Experimental absorber performance for SRP 2018 campaign. Points are color coded to represent the inlet CO_2 concentration.

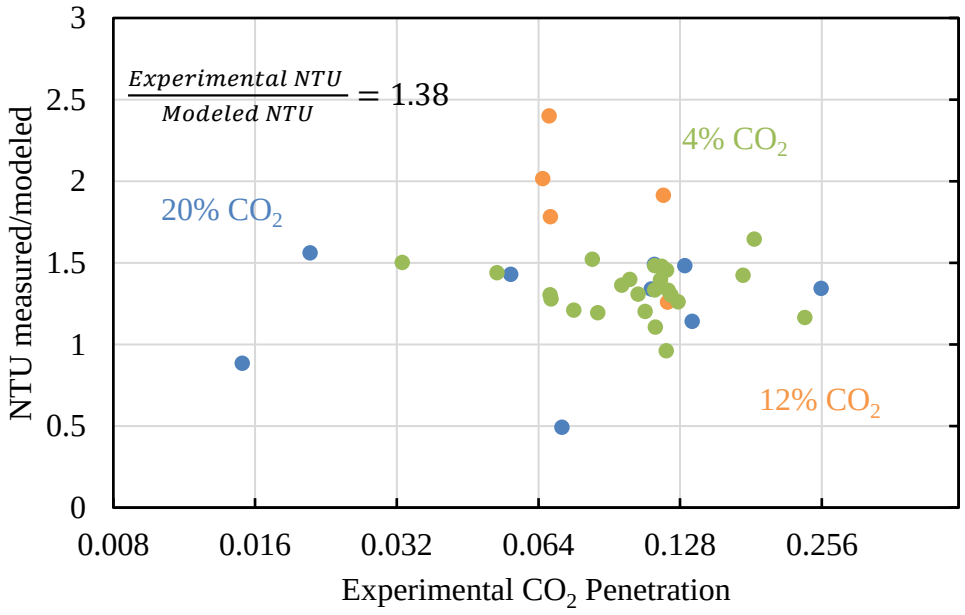

Figure 2.29: The ratio of experimental and model predicted NTU at different CO_2 penetration for SRP 2018 campaign. Points are color coded to represent the inlet CO_2 concentration.

2.6 MODEL VALIDATION AND ADJUSTMENT

Experimental data from the three pilot plant campaigns are used to validate the rigorous absorber model and improve its accuracy. The pilot plant measurements are first reconciled or adjusted to make sure the consistency as described in previous section. The model input of solvent composition is calculated using density and viscosity for the three campaigns for the consistency. The raw model consistently underpredicts the CO_2 removal and absorber NTU, but the error is correlated with CO_2 concentration and the intercooling configuration. For the NCCC absorber with in-and-out intercooling, the model underpredicts NTU by 16% and 41% for coal and NGCC flue gas, and NGCC with pump-around intercooler, the model underpredicts by about 51%. For the SRP campaign with in-and-out intercooling, the model underpredicts about 40% for all the three CO_2 concentrations. This means that the CO_2 concentration, intercooling, and absorber packing height collectively determine the controlling mechanism of the performance.

To understand the effect of intercooling and the controlling factor of absorber, also to provide insight for model adjustment, sensitivity on mass transfer performance and solvent equilibrium was studied first. The 2019 pilot plant campaign at NCCC is used as an example for the sensitivity analysis because the two types of intercooling configuration can be directly compared. Figure 2.30 shows the sensitivity to interfacial area (a) and liquid and gas mass transfer coefficients (k_L and k_G) for pump-around and in-and-out intercooling. The NTU shows a relatively greater dependence on wetted area (a) than k_L and k_G, but overall, the dependence on the mass transfer model is significantly lower than the dependence on the equilibrium model, suggesting that the equilibrium is the major controlling factor for the absorber performance.

The sensitivity to “equilibrium” parameters is shown in Figure 2.31. The NTU ratio shows a greater dependence on both the CO_2 and PZ. Compared to in-and-out intercooling,

the pump-around absorber is more sensitive to the equilibrium adjustment. The recycle flow in the pump-around section increases the solvent loading and makes the overall performance more pinched.

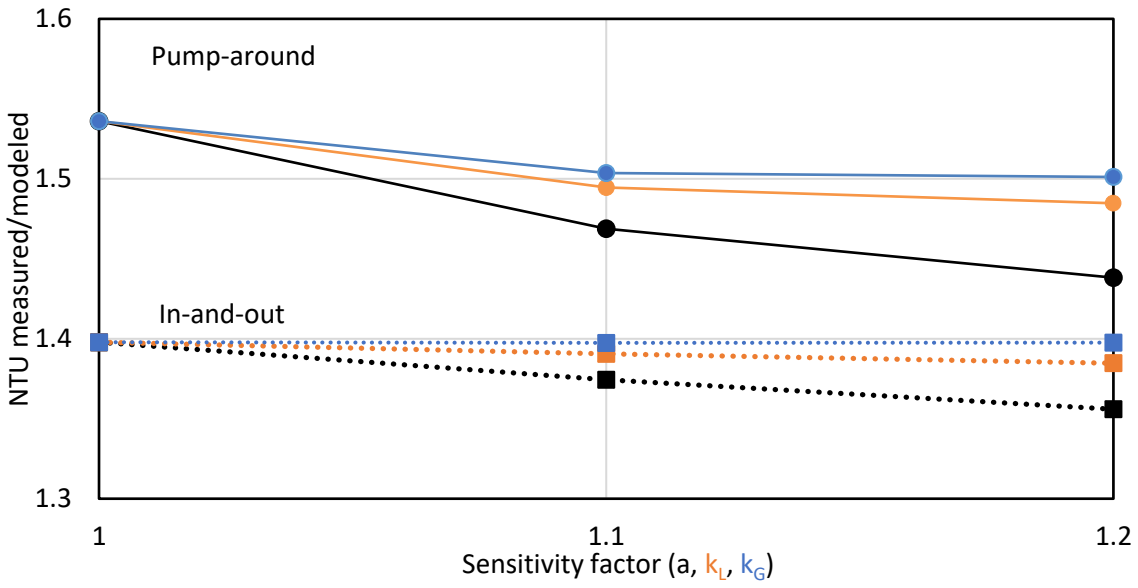

Figure 2.30: Sensitivity of absorber performance to mass transfer model (a, k_L, and k_G) for pump-around (solid line) and in-and-out (dashed line) intercooling.

The sensitivity analyses indicate the absorber performance is equilibrium controlled. Because of the fast absorption rate of PZ, 40 ft of packing is excessive even for the 4% CO_2 and the model correction using this set of experiments should focus on the equilibrium correction. In this campaign, a different set of experiments were run with only 1 section of packing (20 ft), these data can be used to validate the mass transfer model after the equilibrium correction.

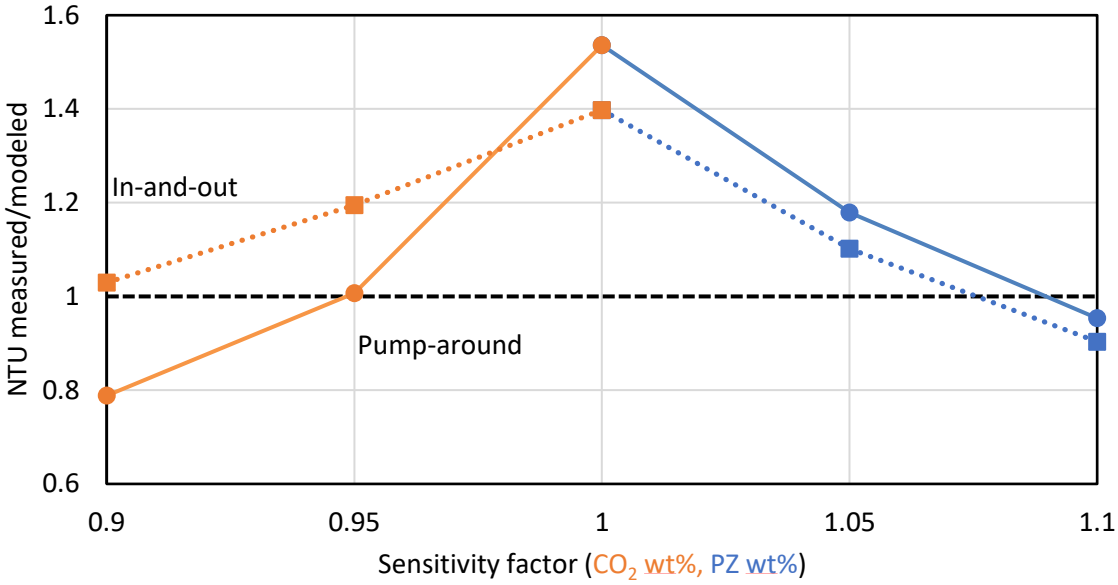

Figure 2.31: Sensitivity of absorber performance to solvent equilibrium model (PZ and CO_2 weight fraction) for pump-around (solid line) and in-and-out (dashed line).

To adjust the equilibrium and match the pilot plant experiments, a factor on the calculated PZ was applied for the model input. This adjustment could be consistent with systematic analytical error or with systematic degradation of the solvent. Figure 2.32 compares the measured and modeled absorber NTU in chronological order with color coding for the five major absorber conditions for NCCC 2019 campaign as illustrated in Figure 2.2. The hollow represents the raw model predictions, and the solids points are with the correction factor of 1.08 on PZ weight fraction. The model is able to predict CO_2 removal accurately for all of the configurations over the wide range of operation. The pump-around data are more scattered because the viscosity measurements showed a greater variation at these conditions. The relative difference in NTU between the model and the experiments shows a decreasing trend during the long-term testing, and it reflects the extent of solvent degradation.

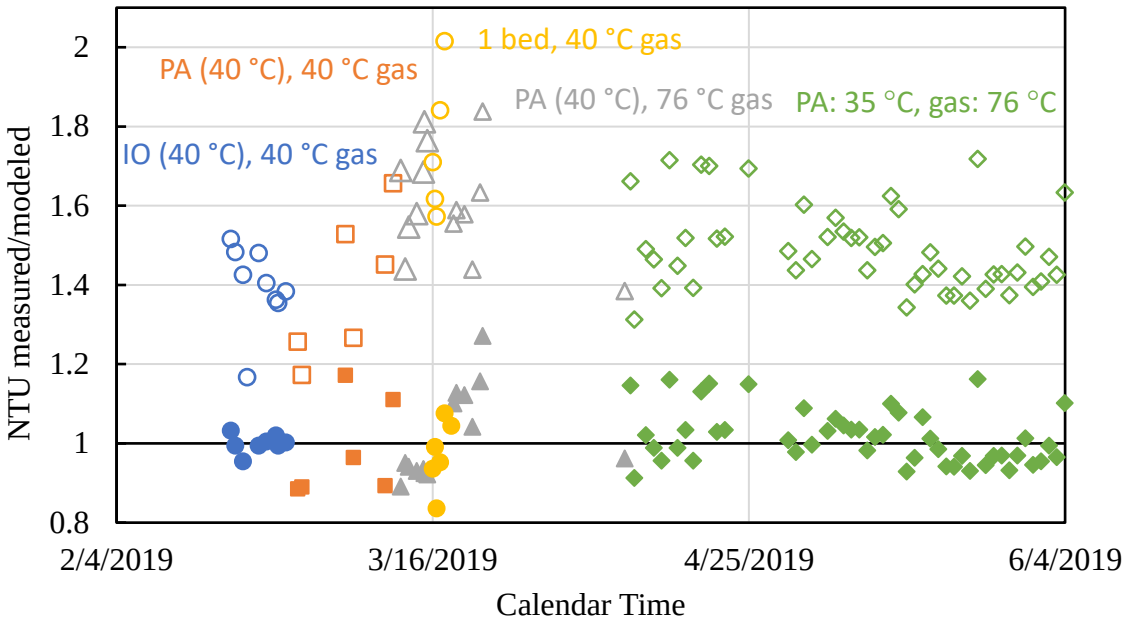

Figure 2.32: Absorber model validation for 2019 campaign at NCCC. Points are color-coded to represent 4 major operating conditions. The hollow points are the raw model predictions, and the solids are after the correction on PZ weight fraction.

The measured temperature profile was also compared to the model predictions. Figures 2.33, and 2.34 show results for 2 representative cases of in-and-out and pump-around intercooling configurations. In both figures, the temperature on the primary axis is plotted against the relative position, with 0 and 1 representing the top and bottom of the absorption column. The calculated CO_2 flux is shown on the secondary axis.

As shown in the two figures, the shape of the temperature profile varies with the conditions of L/G, and intercooling. Figure 2.33 shows the conventional absorber design with in-and-out intercooling. In the absorber column, the gas carries the heat of absorption, pushes the temperature bulge to the top of the column, and leads to a cold bottom. 90% removal is achievable because the over-stripped solvent provides adequate CO_2 driving force even at elevated temperature, and the rich loading is high because the rich solvent is relatively cold.

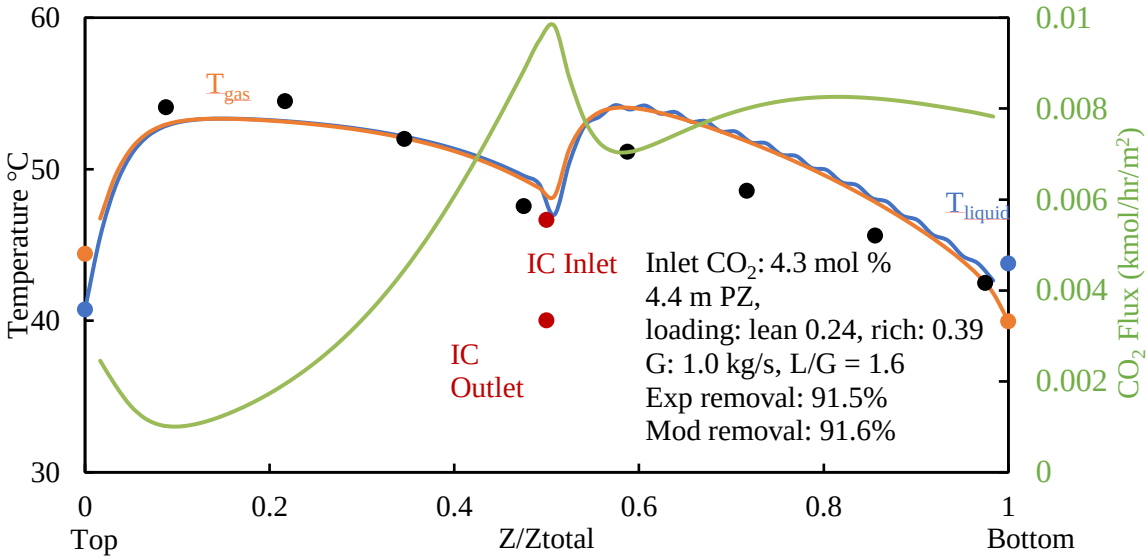

Figure 2.33: Absorber profile for in-and-out intercooling and 0.24 lean loading. Temperature measurements (points) and model predictions (curve) are shown on the primary axis; CO_2 transfer flux is shown on the secondary axis.

With pump-around intercooling as showing in Figure 2.34, the solvent rate in the bottom section can be enhanced to provide effective cooling. The liquid flow in the pump-around is three times as many as the top. At this solvent rate, the intercooling is sufficient, and the temperature is low even with a hot flue gas inlet. As a result, the pump-around intercooling increases the rich loading and reduces the solvent requirement by 30% compared to in-and-out.

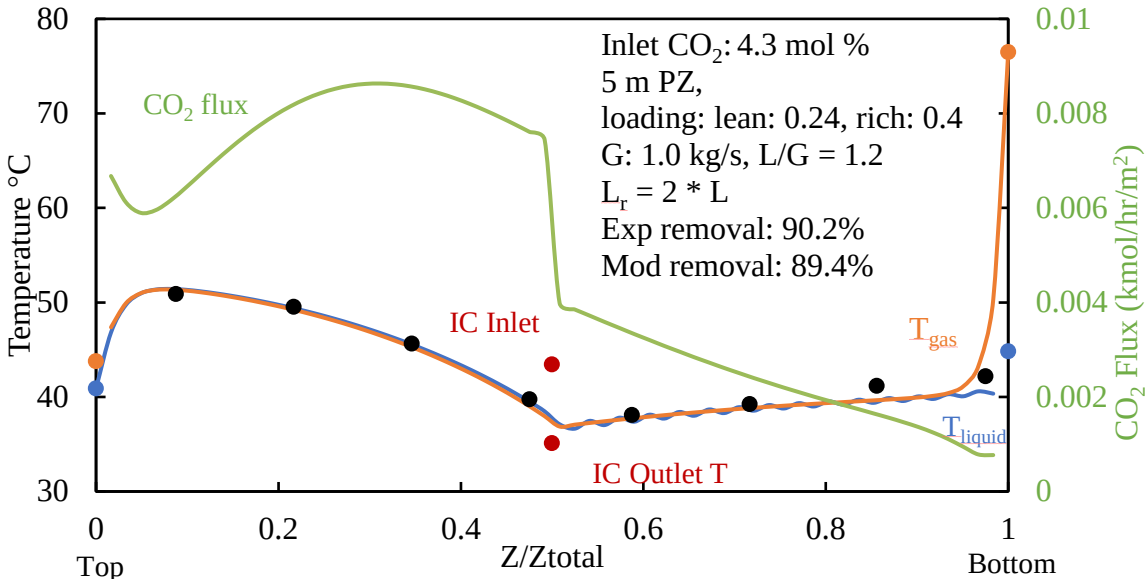

Figure 2.34: Absorber profile for pump-around intercooling and 0.24 lean loading. Temperature measurements (points) and model predictions (curve) are shown on the primary axis; CO_2 transfer flux is shown on the secondary axis.

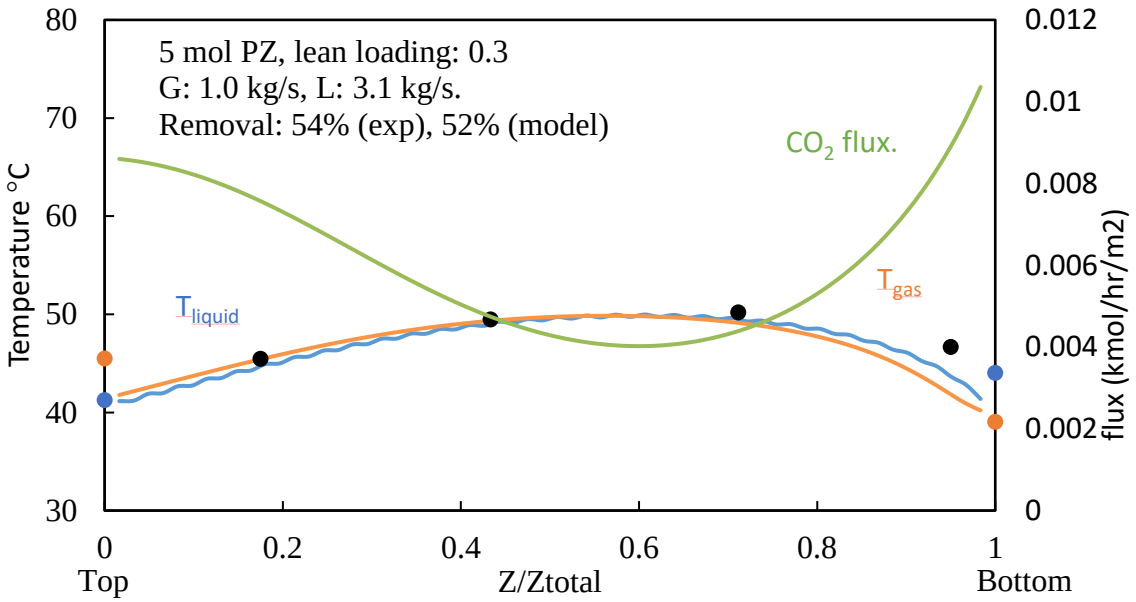

Figure 2.35: Absorber profile for experiments with only 1 section of packing (20 ft). Temperature measurements (points) and model predictions (curve) are shown on the primary axis; CO_2 transfer flux is shown on the secondary axis.

After the equilibrium adjustment, the packing characterization model is validated using experiments with only 1 section of bed. Figure 2.35 shows the temperature and mass transfer profile for Case 32. This experiment is designed to validate mass transfer performance with less mass transfer area and greater solvent flowrate, making it far from equilibrium pinch and mass transfer controlled. The model predicts the NTU and temperature profile accurately, suggesting good accuracy of the packing performance model.

Similar model adjustment was also done for SRP campaign as shown in Figure 2.36. With the 8% adjustment of PZ weight fraction, the model can predict absorber NTU for all three CO2 concentrations with 3% error. This 8% adjustment reduces the loading by 8%, which also matches the loading measured by titration. For the NCCC 2018 campaign, the factor of 1.08 on PZ overcorrects the NTU and the model with 3% adjustment makes the error between experiments and model to be 0. The validation of two campaigns at NCCC leads to different factor and it could be related to solvent degradation. More analytical analysis could be done to study the effect of solvent degradation on the density and viscosity correlation and the absorber performance.

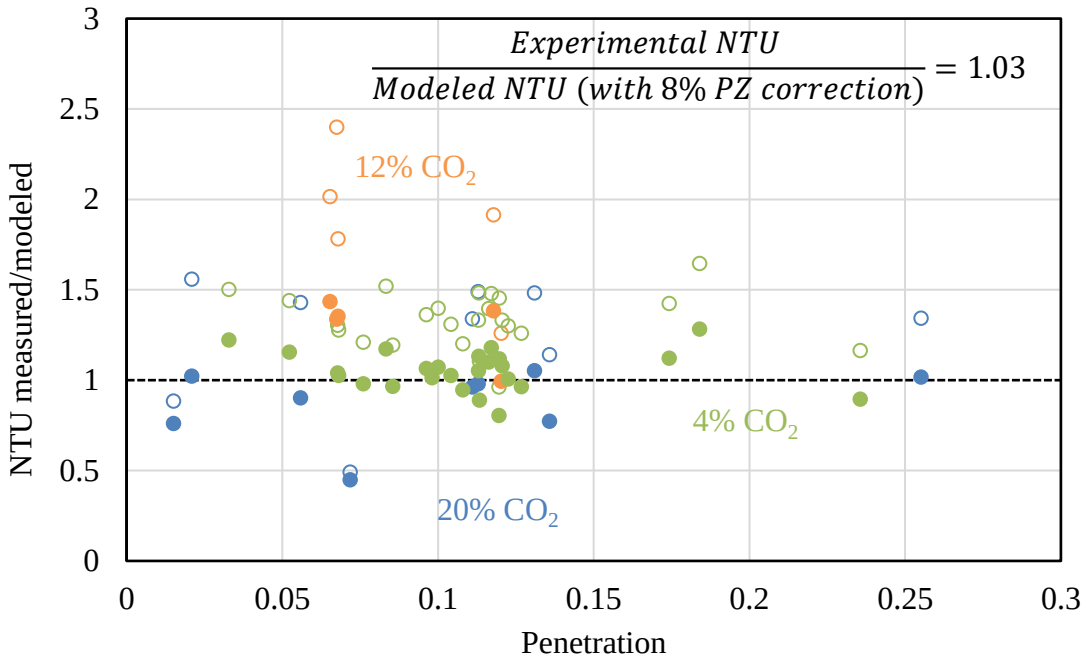

Figure 2.36: Absorber model validation for 2018 SRP campaign. Points are color-coded for 3 CO_2 concentrations. The hollow points are the raw model predictions, and the solids are after the 8% correction on PZ weight fraction.

The model adjustment clearly shows the discrepancies between loading measurements and the model inputs. The adjustment on PZ concentration works to predict absorber performance and NTU, but it makes the model inappropriate for other modeling activities including estimate of physical property and volatile amine emission because the PZ concentration is varied. To solve this problem, the solvent equilibrium in the absorber can be adjusted by varying the reaction rate.

In the rate-based absorber modeling, the solvent equilibrium is defined by the ratio of forward and reverse rate of the CO_2 absorption reactions as shown in Equation 2.8-2.10.

$$PZCOO^- + H_2O + CO_2 \leftrightarrow H^+PZCOO^- + HCO_3^- \quad (2.8)$$

$$2PZ + CO_2 \leftrightarrow PZCOO^- + PZH^+ \quad (2.9)$$

$$2\,PZCOO^- + CO_2 \leftrightarrow PZ(COO)_2^- + H^+PZCOO^- \quad (2.10)$$

By varying the forward and reverse rate of these three reactions, the equilibrium constant can be varied to match the pilot plant results. Figure 2.38 compares the model correction using 8% adjustment on PZ (solid points) and 60% adjustment on the reverse rate (hollow points). Both models match the pilot plant results with an averaged NTU ratio of 1 but the model using PZ adjustment is less scattered. This means adjusting solvent loading is not exactly the same as adjusting the equilibrium partial pressure. The equilibrium near lean and rich end needs to be corrected differently to match the shift in the PZ concentration.

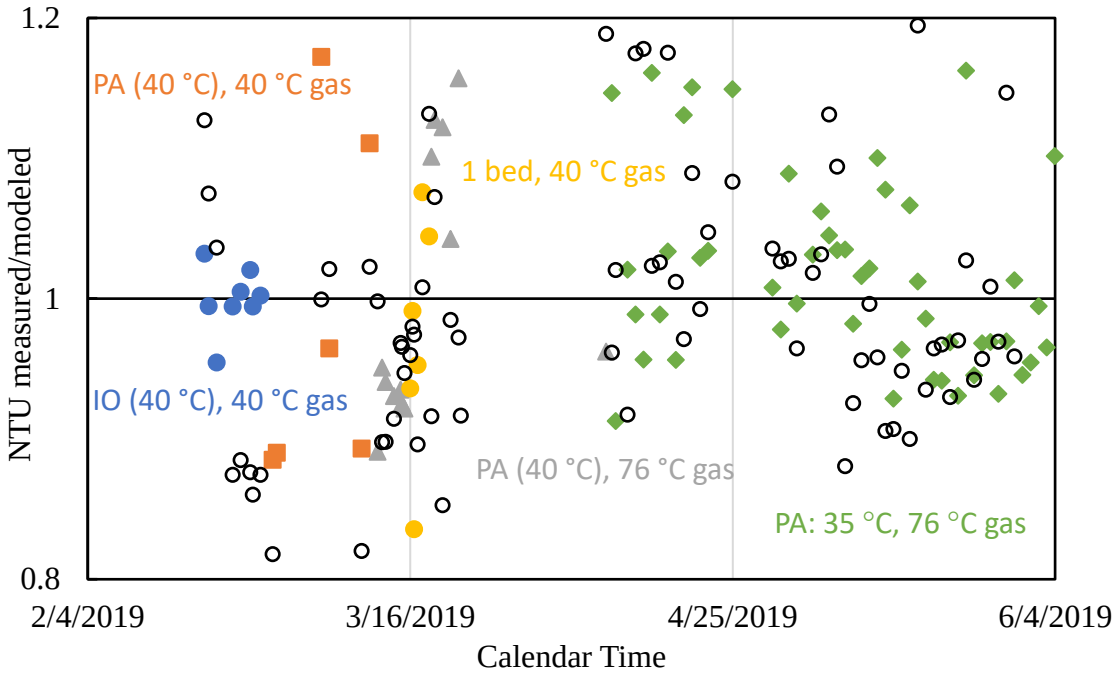

Figure 2.37: Comparison of model adjustment with +8% PZ (solid points) and -60% reverse reaction rate (hollow points). The solid points are color-coded to represent the operating conditions.

To help understand the adjustment made for the absorber validation and its implication, Figure 2.38 summaries the procedures for the pilot plant operation and

absorber modeling and the connections between them. For the pilot plant operation, 5 m PZ is loaded based on analytical methods and the lean loading is determined by controlling striper temperature and pressure. This operation sets the equilibrium pressure of lean solvent at the stripper condition (high temperature and pressure) and the loading agrees well with the model. Solvent rate is then reported at different removal and process conditions.

To model the absorber, the solvent composition needs to be determined as the model inputs and there are uncertainties with the method. The density and viscosity are used because of the good reproducibility and accessibility, but it may not represent the true compositions of the solvent. With the adjustment of 8% on PZ or 60% on the reverse rate, the model agrees with the experiments, and it predicts the same solvent flowrate and column temperatures as the pilot plant experiments.

The solvent equilibrium is well-controlled at stripper conditions but needs to be adjusted at absorber conditions, suggesting the temperature dependence of the equilibrium could be a source of this adjustment.

When use the model for process design, this adjustment should not be misinterpreted or used for other modeling activities such as estimating physical properties. The equipment should be designed at model predicted solvent flowrate to achieve the removal targe but with 5 m PZ (without 8% adjustment), because this presents the practical operating of the plant.

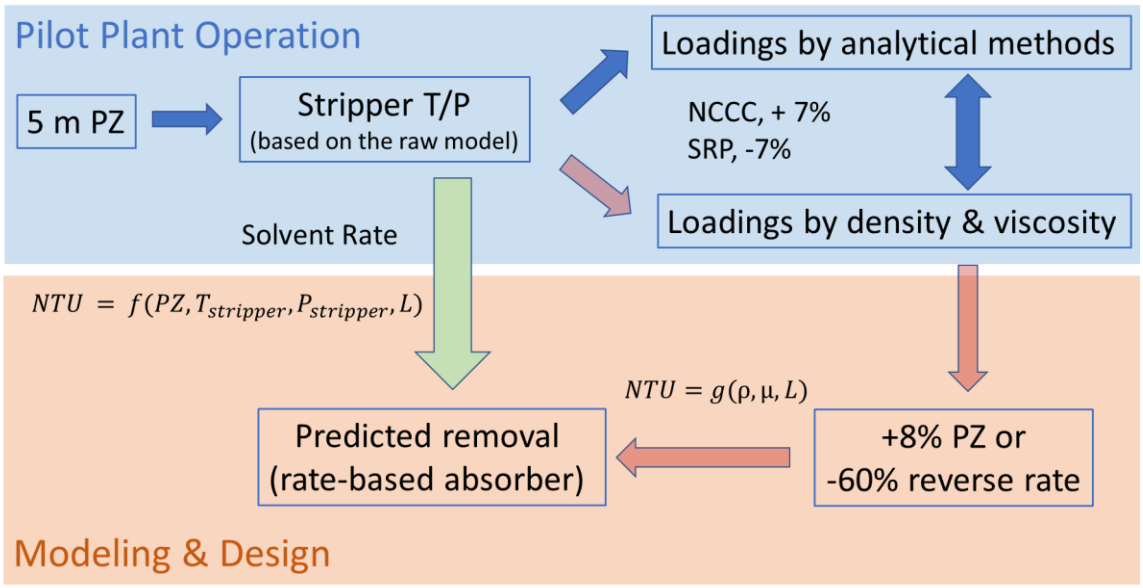

Figure 2.38: Scheme shows the procedures and connections of pilot plant operation and model simulation.

2.7 CONCLUSIONS

A rigorous PZ absorber model has been validated using the steady-state experiments from the NCCC 2018, 2019, and SRP 2018 campaigns. The tests cover wide range of operating conditions included CO_2 concentrations (4%, 12%, and 20%), lean loadings (0.18–0.25 m CO_2/mol alkalinity), gas inlet temperatures (40, 78 °C), and intercooling configurations (in-and-out and pump-around). With 12 m of packing and intercooling, the maximum CO_2 removal of 99.6% and 96% was achieved using 5 m PZ for coal and NGCC flue gas.

Pilot plant experiments and absorber modeling demonstrated benefits of innovative absorber design using pump-around intercooling without DCC for NGCC condition. Pump-around intercooling is always better than in-and-out at NGCC conditions because it cools the gas effectively with an enhanced solvent flow. The absorber bottom temperature

is dominated by the intercooling temperature and lowering that temperature can improve the performance dramatically.

Data reconciliation was implemented to study the uncertainty of the pilot plant measurements and analytical methods. The CO_2 material balances were examined for the three campaigns. The raw absorber model underpredicts absorber NTU by 16%, 52%, and 38% for the NCCC 2018, NCCC 2019, and SRP 2018 campaign. Adjustment on solvent equilibrium was needed to match the pilot plant results. For NCCC 2019 and SRP 2018, the absorber model can be corrected by increasing the PZ calculated from density and viscosity by 8% or reducing the CO_2 desorption rate by 60%. The pack characterization model was also validated using less pinched experiments with only one section of packing.

The absorber modeling relies heavily on the accurate input of solvent composition. For the SRP campaign, loading calculated from density and viscosity measurement on average is 7% greater than the titration, which could explain the 8% adjustment for the model validation. For the NCCC campaign, the analytical loading is 7% greater than the density and viscosity and is not consistent with the model adjustment.

The validated model provided a good basis for process design to determine CO_2 removal and solvent circulation rate. But the adjustment should not be over-interpreted and used to model other properties.

2.8 RECOMMENDATIONS

The method of calculating solvent composition based on density and viscosity greatly improves the data availability and reproducibility compared to analytical methods. However, it also introduces uncertainty associated with the experimental data previously collected and model regression. The reconciliation of loading for the three campaigns as well as previous work clearly shows the error associate with the density and viscosity

correlation. Also, the solvent degradation will affect solvent density and viscosity, but it is missing in the current model It will be helpful to validate the correlation with more measurements and incorporate the role of solvent degradation.

Greater than 90% removal cases should be validated using pilot plant results. When the removal is high, the absorber is close to a lean-end pinch and these cases can be used to validate solvent equilibrium at lean conditions. The uncertainty of equilibrium adjustment and the temperature dependence of the solvent equilibrium model can be studied.

Chapter 3: Absorber Design and Optimization for CO_2 Capture with Aqueous Piperazine[2]

3.1 INTRODUCTION

Amine scrubbing for CO2 capture from power plants using the natural gas combined cycle (NGCC) is now being considered for commercial application with a number of Front End Engineering Designs (FEED) completed (Awtry et al., 2021; Bhown et al., 2021; OBrien et al., 2021; Oddvar Lie et al., 2021) or in process. Practically all of these FEED's evaluate proprietary systems so there have been and will probably not be any significant public reports on the detailed process evaluations required to set the design conditions of the absorber. This chapter presents the detailed evaluation of the absorber design for a FEED using the piperazine Advanced Stripper (PZAS)TM process.

The PZAS^{TM} process has been demonstrated and published as a benchmark for second-generation amine scrubbing with many pilot-plant experiments and modeling results (Chen et al., 2014; Gao and Rochelle, 2019; Gao et al., 2019; Sachde et al., 2013; Zhang et al., 2017). 5 m PZ (30 wt %) is known for its fast kinetics, good energy performance, resistance to thermal and oxidative degradation, and low corrosivity. PZAS was operated with simulated Natural Gas Combined Cycle (NGCC) flue gas (4.3 mol % CO2) at the National Carbon Capture Center (NCCC) in Wilsonville, Alabama in 2019 (Rochelle et al., 2021). During about 2000 hrs of operating, the system performance was tested at various operating conditions including gas temperature, absorber intercooling temperature, solvent flowrate, and lean loading.

A rigorous, rate-based absorber model for PZAS was validated with pilot plant results as described in Chapter 2 and can accurately predict the CO2 removal and temperature profile over a wide range of conditions. With the validated model, the effects

[2] Part of this chapter has been submitted to International Journal of Greenhouse Gas Control.

of key process variables including flue gas temperature, liquid flowrate, intercooling temperature, and pump-around flowrate were accurately predicted (Gao and Rochelle, 2019)

A FEED is being developed using the PZAS process to capture CO2 from a 460 MW NGCC in west Texas (Clossman et al., 2021). The site is characterized by low fuel cost. Duct burners are installed and use supplementary firing to increase electricity output. The site has a semi-arid climate with limited annual precipitation., so air cooling will be used for the capture plant to reduce freshwater usage. The ambient temperature varies dramatically annually, with a highest daily averaged temperature of 34 °C during hot summers and a lowest daily averaged temperature of -2 °C in cold winters.

The primary objective for the FEED is to develop a detailed and comprehensive cost estimate of the PZAS^{TM} system on a commercial scale (Clossman et al., 2021). For NGCC flue gas, the absorber will be the largest cost center (around 30–40% of the equipment cost) for the capture plant, and the optimization of the absorber will be important to reduce overall capital cost and operating cost.

In this work, the rigorous absorber model is used to design and explore the operating conditions of the absorber. Previous simulation of the absorber shows the importance of intercooling for NGCC flue gas and the benefits of the pump-around configuration. The enhanced solvent flow in the bottom section cools the gas effectively and eliminates the direct contact cooler (Sachde and Rochelle, 2014; Zhang, 2018; Zhang et al., 2016). This pump-around intercooling reduces absorber packing and improves the performance and is adopted for this FEED.

The conventional absorber section design consists of a direct contact cooler (DCC), an absorber, and a water wash (Faramarzi et al., 2017; Gjernes et al., 2017; Morgan et al., 2018). Simple in-and-out intercooling is usually applied to mitigate temperature bulge and

improve the performance. For the conventional design, water balance is maintained by setting the temperature of DCC, trim cooler, and water wash to around 40 °C to control the water content in the gas streams. Based on previous pilot plant results and process modeling, the FEED proposed the first of its kind absorber design using pump-around intercooler without DCC or trim cooler in commercial scale. The column temperature and system water balance are managed by pump-around intercooling and water wash. This design reduces the absorber packing requirement, capital cost, and improves the performance. Real flue gas conditions at different ambient temperatures are used in the design to demonstrate the flexible operating strategy in response to the seasonal and diurnal ambient temperature swing. In this paper, important variables affecting absorber performance will be studied to select conditions expected to produce lower cost. Risk of the proposed design is evaluated based on model predictions and pilot plant results.

3.2 METHODS

3.2.1 Simulation Method

Aspen Plus® was used for the absorber and water wash modeling. A rigorous, rate-based absorber model was developed and reconciled with previous campaign data from the National Carbon Capture Center (NCCC). The model consists of the solvent model "Independence" (Frailie, 2014) and packing characterization models. The reaction kinetics were regressed from wetted wall column measurements and modeled as fast reaction in the boundary layer. The packing performance model developed by Song was regressed from pilot plant results (Song, 2017; Song et al., 2014). An adjustment of 1.08 on PZ weight fraction was made to match the 2019 pilot plant results at 4% CO2 in the flue gas (Gao and Rochelle, 2019).

3.2.2 Design Basis

A simplified process diagram of the absorber and water wash is shown in Figure 3.1. The flue gas from the NGCC unit is mixed with the flue gas from the gas boilers, which were added to the scope of the FEED (Clossman et al., 2021) to provide steam for the solvent regeneration. Two absorber trains will be designed for the FEED to reduce the size and the cost of each absorber column.

The flue gas specifications are provided by the host site and listed in Table 3.1. The case E-007 represents the median year-round temperature and is taken as the base case. Cases E-004 and E-001 are two lower temperature cases and cases E-010 and E-013 are two higher temperature cases.

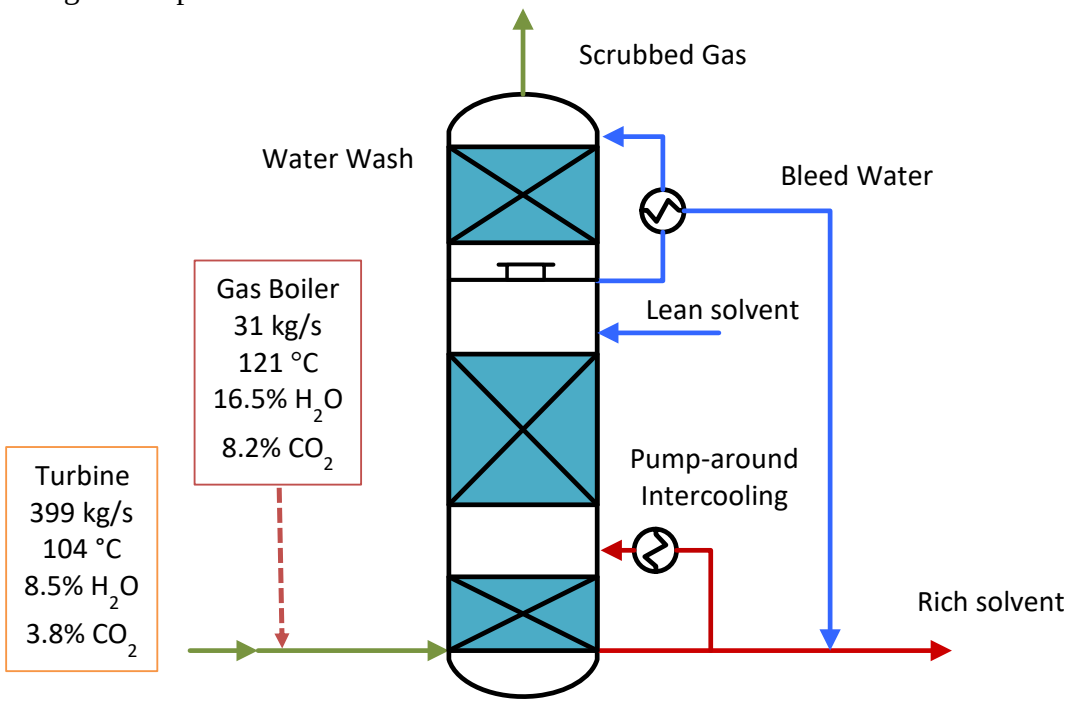

Figure 3.1: The absorber configuration for the FEED

Table 3.1: Flue gas specifications for 1 NGCC unit (1 absorber train)

Case	E-007 (Base)	E-004	E-001	E-010	E-013
Ambient Temperature (°C)	18.3	13.8	-13.3	35.0	40.6
Flue Gas Temperature (°C)	104.4	105.0	107.2	103.3	102.8
Flue Gas Rate (kg/s)	399.3	403.8	429.0	382.4	376.9
CO_2 (vol %)	3.81	3.81	3.78	3.79	3.78
H_2O (vol %)	8.45	8.26	7.45	9.49	9.99
O_2 (vol %)	13.35	13.39	13.62	13.16	13.06

Table 3.2: Flue gas specifications for 1 gas-fired package boiler (1 absorber train)

Flue Gas Temperature (°C)	121.1
Flue Gas Rate (kg/s)	31.2
Vol % CO_2	8.28
Vol % H_2O	16.46
Vol % N_2	72.35
Vol % O_2	2.41

Table 3.3: Gas production or consumption rate in 1 duct burner

Production/consumption	kg/s
H_2O	1.9
CO_2	2.4
N_2	0.08
O_2	3.9

3.3 BASE CASE DESIGN

3.3.1 Process description

The hot flue gas from turbines (104 °C) and boilers (121 °C) is mixed and fed to the absorber bottom directly. Flue gas flows upward through two sections of packing and counter-currently contacts with the solvent. The bottom pump-around intercooling enhances the solvent rate and provides adequate cooling to cool the hot flue gas and to remove the heat generated during the absorption. The gas then flows through another section of packing to remove PZ and excess water. The lean solvent leaving the cold cross exchanger feeds into the absorber at about 52 °C. All the cooling in the absorber section including pump-around and water wash uses air-cooling. The air cooler is designed to cool the liquid with a temperature approach of 11 °C to ambient.

3.3.2 Absorber Design

The absorber design includes the column configuration (column diameter, packing height, packing type, packing area, and intercooling location) and the operating conditions (lean loading, lean solvent flowrate, pump-around rate, and cooling temperature).

3.3.2.1 Column Internal and diameter

The absorber diameter is primarily determined by the gas rate, and it affects the capital cost of the packing and the column flooding. The cost associated with flooding is reflected in the gas pressure drop. The liquid rate also affects the gas velocity and the flooding. With the pump-around in the absorber bottom, the liquid rate is increased, and the flooding will be greater than in the top section. One objective for the absorber design is to balance the flooding in both sections and to minimize the pressure drop in the column.

Electricity-driven blowers are used to provide header pressure for the flue gas, and they require a large power input. The power inputs for blowers with 70% isentropic efficiency at different pressure heads are shown in Figure 3.2. The electricity consumption for blowers is about 5–7 MW for reasonable pressure drops and is on the same order as the power for CO_2 compression (around 10 MW). The capital cost for blowers is also significant. According to the techno-economic analysis (TEA) done with PZAS at 12% CO_2 conditions (Farmer et al., 2019), the blower Purchase Equipment Cost (PEC) takes up 3.4% of the PEC for the CO2 capture plant. At the same basis of CO_2 production rate, an NGCC capture unit treats about 3 times more flue gas than a coal plant. The blower PEC is projected to be around 9–10% of the total PEC for the capture unit.

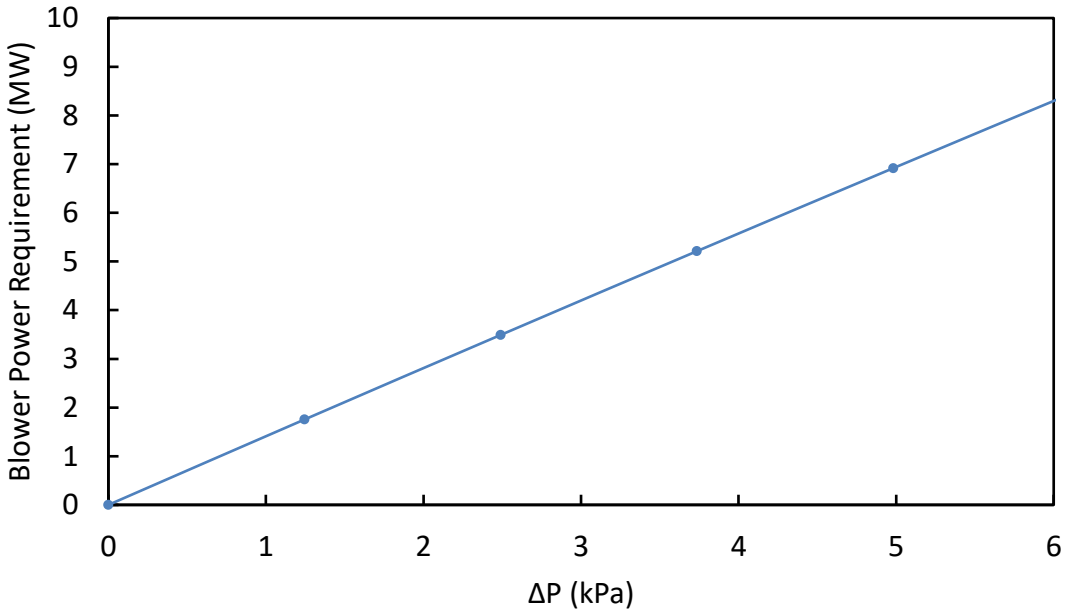

Figure 3.2: Power requirements for flue gas blowers with 70% isentropic efficiency at different pressure head (2 absorber trains).

3.3.2.2 Height of Packing

The absorber packing height is the most important specifications for column design. Figure 3.3 shows the sensitivity analysis of packing height to define the tradeoff between capital cost and energy cost. At constant CO_2 removal, the solvent flowrate decreases with more packing area, and it approaches a minimum flowrate L_{min} when the packing is excessive, representing the equilibrium limits of the solvent. Points to the left use less packing and require more energy for regeneration. Previous optimization shows the optimal absorber packing height generally leads to a flowrate equals to 1.1-1.2 L_{min} (Sachde, 2016). Optimal L/L_{min} represents the balance between capital cost and energy cost therefore varies for different plant site. The west Texas capture plant is featured as low energy cost therefore the optimization favors relatively less absorber packing and greater energy consumption. At 7.6 m packing as the design point, the L/L_{min} equals 1.16, indicating a reasonable tradeoff between the capital cost and the energy cost.

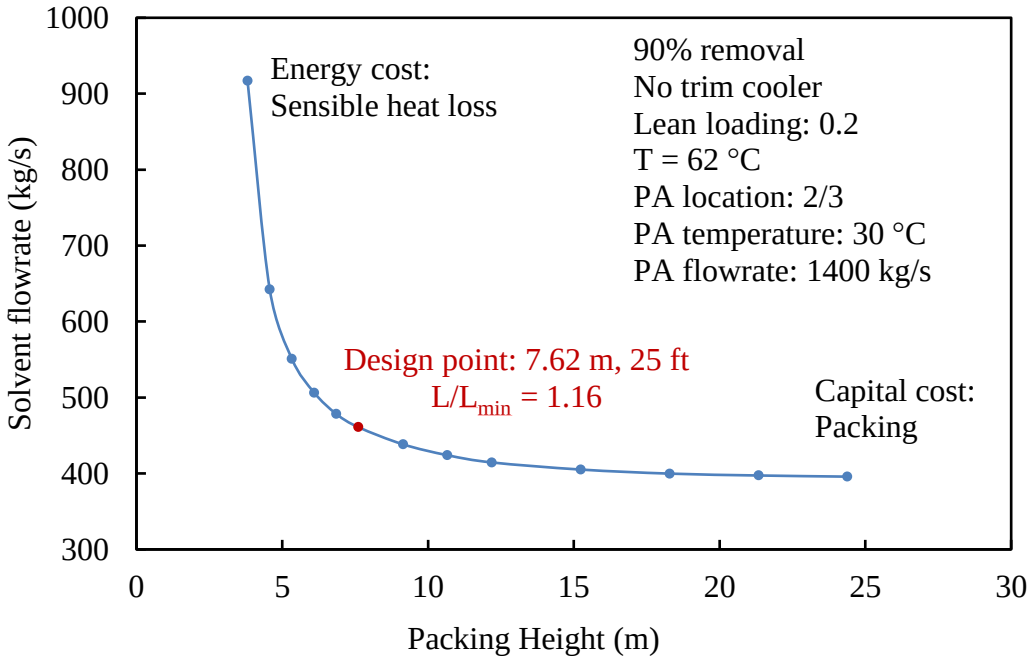

Figure 3.3: Sensitivity analysis of absorber packing height for 90% CO_2 removal.

3.3.2.3 Trim Cooler Temperature

The effect of lean solvent temperature is studied to explore opportunities to simplify the air-cooling loop and to predict the system performance at high ambient temperature. Figure 3.4 shows the effect of trim cooler temperature on solvent flowrate and water content of the gas leaving the absorber. For the absorber with 25 ft packing, the flowrate increases by less than 1% when the temperature increases from 40 to 62 °C, and the water concentration increases from 10% to 14%. It is important to monitor the water flow to make sure there is more water leaving than coming into the absorber, so there is enough water to run the water wash. When the flue gas contains more water during summer because of the high ambient temperature, the water wash needs to be run at a higher temperature to maintain the water balance.

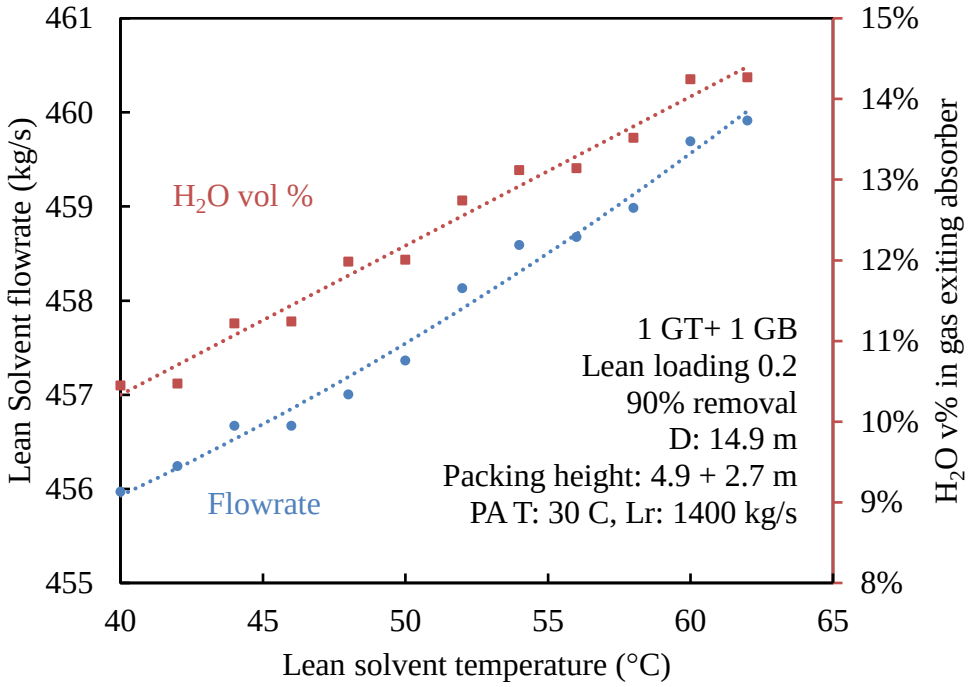

Figure 3.4: Effects of trim cooler temperature on solvent flowrate (blue dots, primary y axis), and water content (red squares, secondary axis) of the gas leaving absorber.

For the FEED design, lean temperature appears to be less important than pilot plant experiments and conventional design for two reasons: the lower lean loading and smaller packing height. Both factors make the top of absorber column away from equilibrium pinch and more mass transfer controlled. Therefore, the limitation of higher temperature and less absorption driving force is less significant for the design condition.

The lean temperature has little effect on CO_2 removal, but it affects how the heat is removed from the system. Figure 3.5 shows the heat duties of the three cooling inputs in the absorber section at variable trim cooler temperature. In the design without a trim cooler, the heat is transferred to and removed from the water wash while the total duty remains constant. Therefore, eliminating the trim cooler does not reduce the cost of the heat exchangers. However, this design is adopted over the traditional design for three reasons.

1. Eliminating the trim cooler simplifies the cooling loop in the system and the process control.

2. The design simplifies the solvent loop and reduces the solvent holdup in the trim cooler. Avoiding the circulation of solvent to air coolers, which are located away from the capture plant, reduces the environmental risks associated with solvent leaking.

3. Cooling water wash is more effective. The liquid is dilute PZ in water wash and is less viscous, so the heat transfer performance is better. The water wash runs at higher temperature and provides a larger temperature approach.

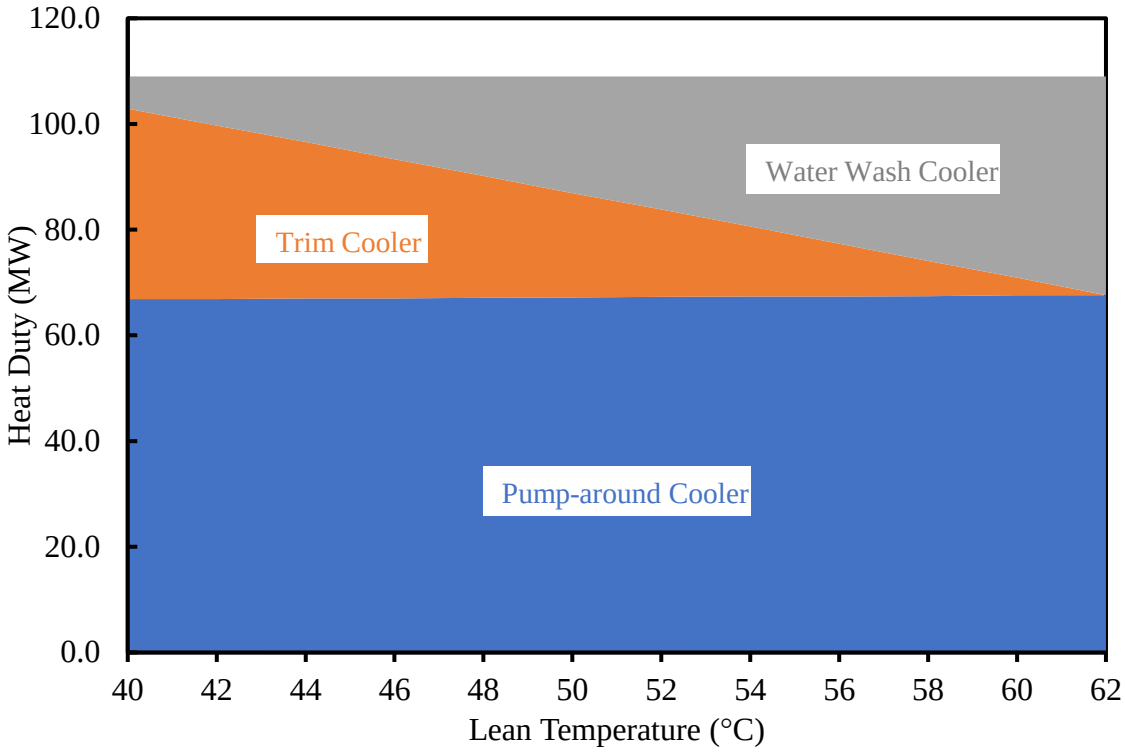

Figure 3.5: Heat duties of three cooling inputs in the absorber section at variable trim cooler temperature

The temperature and mass transfer rate profiles in the absorber shown in Figure 3.6 explain the effect of the trim cooler. The solid lines are the profiles for the absorber with the trim cooler and the dashed are without. The temperature profile and mass transfer rate for the two cases are similar except in the top sections, which explains the minor effect of trim temperature. At the low liquid rate for NGCC flue gas, column temperature is primarily determined by the gas enthalpy. The cooling provided by lean solvent cannot propagate to the column because of the low L/G. For the temperature profile, difference between absorber with or without trim cooler only appears near the top 0.5 m of packing. This also justifies the choice of pump-around intercooling because a greater solvent rate is required to provide effective cooling. At the bottom section, where the solvent flowrate is greater, the liquid temperature is flat, and the gas is cooled quickly in the bottom.

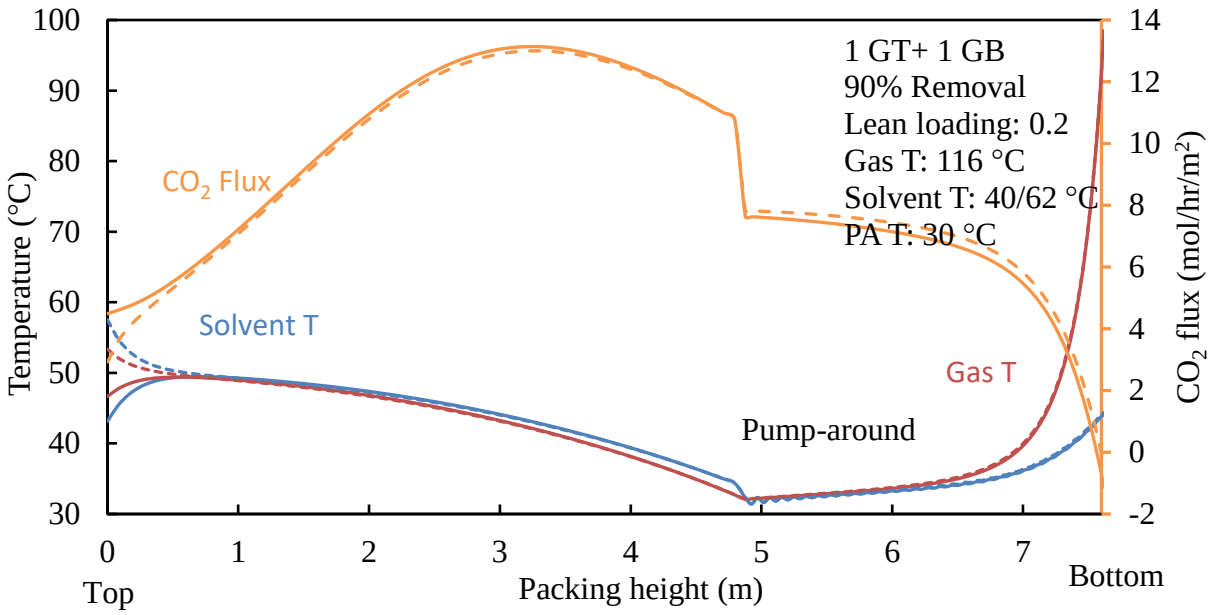

Figure 3.6: Vapor temperature (red), liquid temperature (blue), and mass transfer rate (orange) profile in the absorber with trim cooler at 40 °C (solid) and without trim cooler (dashed).

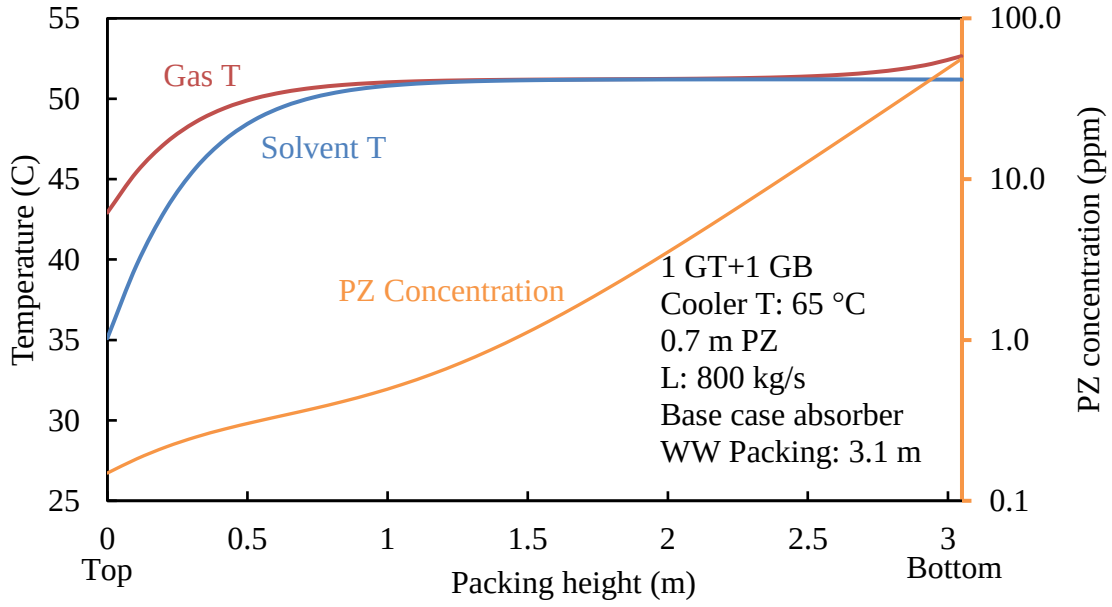

Figure 3.7: Vapor temperature (red), liquid temperature (blue), and PZ concentration in the vapor (orange) in the water wash section.

The main disadvantage of eliminating the trim cooler is more PZ in the flue gas leaving the absorber. The water wash needs to be designed to remove more volatile PZ. Gaseous PZ and the temperature profile in the water wash section are shown in Figure 3.7. The PZ decreases to 1 ppm using about 5 ft (1.5 m) packing, and the gas and liquid temperature are pinched in the middle of the column. The profiles indicate 10 ft (3.0 m) packing is excessive for gaseous PZ removal and for heat transfer. The water wash is overdesigned and is able to remove volatile PZ even without the trim cooler. The excessive packing benefits the aerosol removal and reduces the temperature approach on the top, which helps maintain the water balance during high ambient temperature conditions.

3.3.2.4 Pump-around Location

The pump-around (PA) intercooling breaks the packing and introduces the pump-around location as another variable for the column design. Figure 3.8 shows the optimization of the pump-around location for three values of total packing height. At constant lean solvent flow, the absorber shows a maximum CO_2 removal when the pump-around location varies, as indicated by the ratio of the height above the pump-around to the total height. For three different total packing heights (6.1 m, 7.6 m, and 9.1 m), the optimal pump-around location is at the bottom one third of the column. The optimum configuration for 6.1 m of total packing is 4.9 m above the pump-around and 2.7 m below.

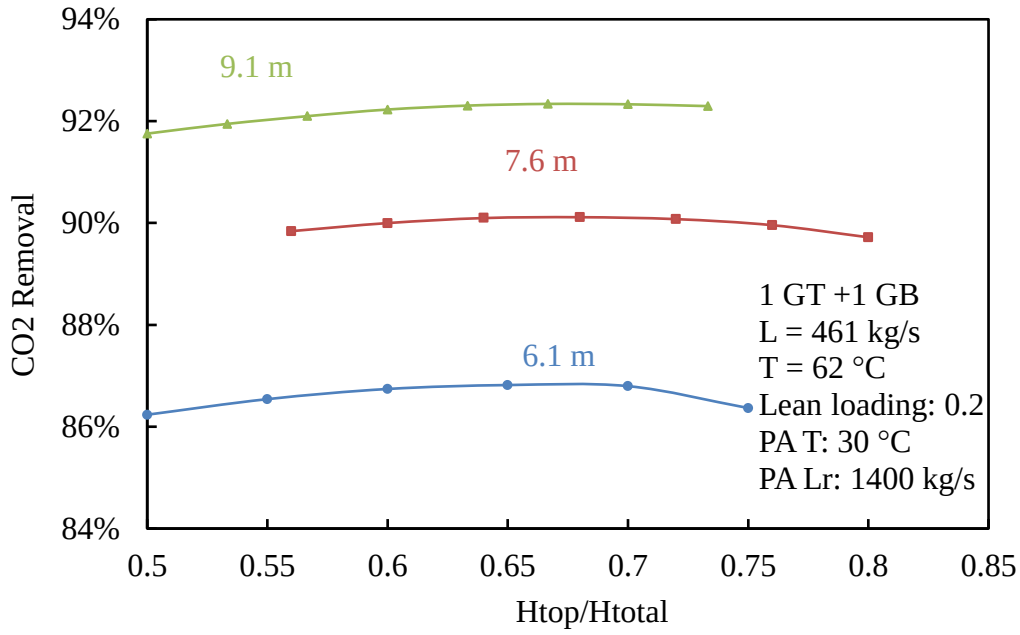

Figure 3.8: Optimization of the pump-around location for 3 total packing heights (6.1 m: blue, 7.6 m: red, 9.1 m: green).

3.3.2.5 Pump-around Temperature and Flowrate

Pump-around intercooling is designed to improve the absorber performance. The effects of cooling temperature and pump-around circulation rate are studied through sensitivity analysis. As shown in Figure 3.9, lowering the pump-around temperature improves the absorber performance significantly. By reducing the temperature from 40 to 30 °C, the solvent flowrate decreases by about 13%. Lower column temperature always improves the absorber performance, but there might be practical issue with operating PZ solvent at low temperature. The transition temperature of solid precipitation for 5 m PZ is 24 °C for 0.2 loading and it decreases at higher loading. Since the solvent at the intercooling heat exchanger is rich therefore the risk of precipitation is minimized with the pump-around intercooling. The absorber is designed at low temperature (30 °C) to improve the performance.

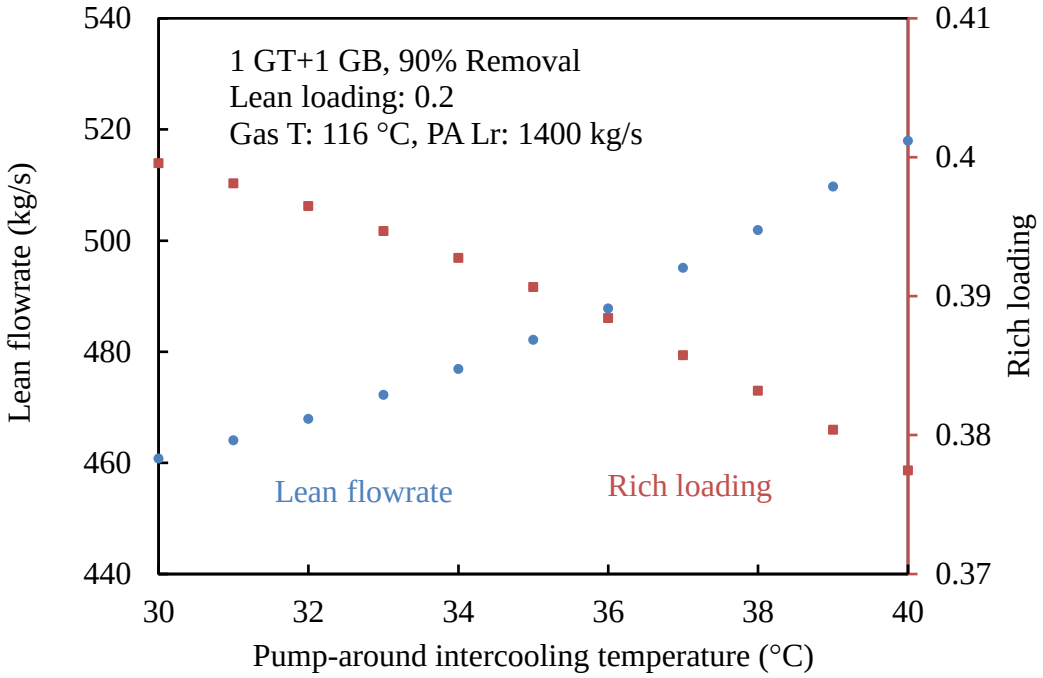

Figure 3. 9: Effects of pump-around temperature on solvent flowrate (blue triangles, primary y axis) and rich loading (red dots, secondary y axis) for fixed column configuration and 90% removal.

The sensitivity analysis of pump-around flowrate for fixed absorber column configuration and CO_2 removal is shown in Figure 3.10. As the pump-around rate increases, the lean solvent flowrate decreases and approaches a minimum value. At high pump-around rate, the local cooling cost of the absorber, including the cost of the intercooling pump distributors, chimney trays, and air cooler increases while the global cost of the system associated with less solvent circulation, including the capital cost of heat exchangers, sensible heat loss, and steam consumption is minimized. Without rigorous cost optimization, it is reasonable to save the global cost by using a high circulation rate. In the base case design, the pump-around rate is 140 kg/s and leads to a L/L_{min} = 1.03 based on the pump-around rate.

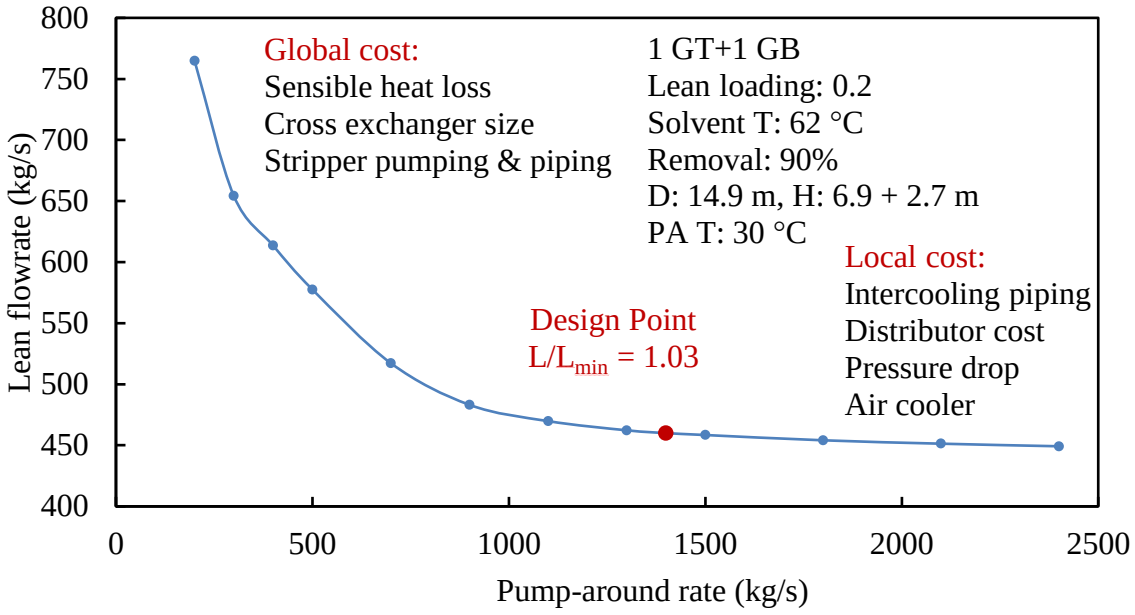

Figure 3.10: Sensitivity analysis of pump-around flowrate on lean solvent flowrate for fixed column configuration and 90% removal

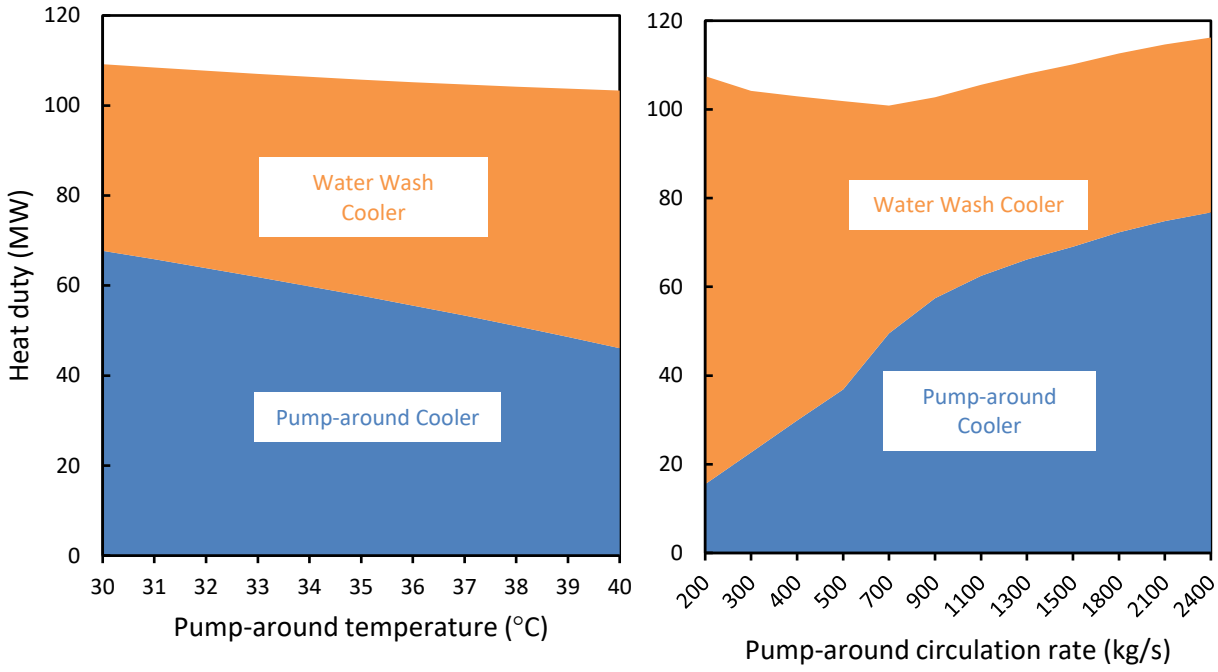

Figure 3.11: Heat duties in the absorber section during the sensitivity analysis of pump-around intercooling temperature and flowrate

The effects of pump-around conditions on heat duty in the absorber section are shown in Figure 3.11. When pump-around intercooling is at a lower temperature and a higher flowrate, more heat is removed from the intercooler, but the total heat duty in the system remains the same. The increase in cost when the intercooling is designed at maximum duty is caused by a lower temperature approach and worse heat transfer performance because of viscosity, instead of a greater total duty.

3.3.3 Comparison with Conventional Design

The conventional absorber design uses a DCC to chill the flue gas before it enters the absorber. A simple in-and-out intercooler is used in the absorber to remove the heat and improve the performance. However, at the low L/G ratio for NGCC, the cooling effect of simple the in-and-out intercooler and DCC is not as effectives as the pump-around intercooler. Figure 3.12 shows the temperature profiles and CO_2 transfer flux in the conventional absorber design with DCC and in-and-out intercooler. The conventional design uses the same amount of packing as the pump-around for CO_2 absorption with an additional DCC column to precool the flue gas to 40 °C. The location of in-and-out intercooler is optimized to maximize the removal and the temperature is the same as the pump-around intercooler. At the same lean solvent flowrate as the pump-around design, the conventional design achieves 86% CO_2 removal. With the same lean solvent and intercooling temperatures, the average liquid temperature in the column for the in-and-out design is 45.5 °C and is 4.3 °C higher than the pump-around. The pump-around is a better intercooling configuration for NGCC because it enhances the liquid flow, provides more cooling, and improves the absorption driving force. The FEED design combines gas cooling and intercooling into one section using the pump-around and eliminates the DCC column. Although the pump-around requires a greater circulation rate, the total cost is

offset by the significant reduction in the capital of the column. This paper mainly focuses on the process design and absorber performance and more economic analysis on the benefits of the pump-around absorber will be discussed in detail after the FEED is completed.

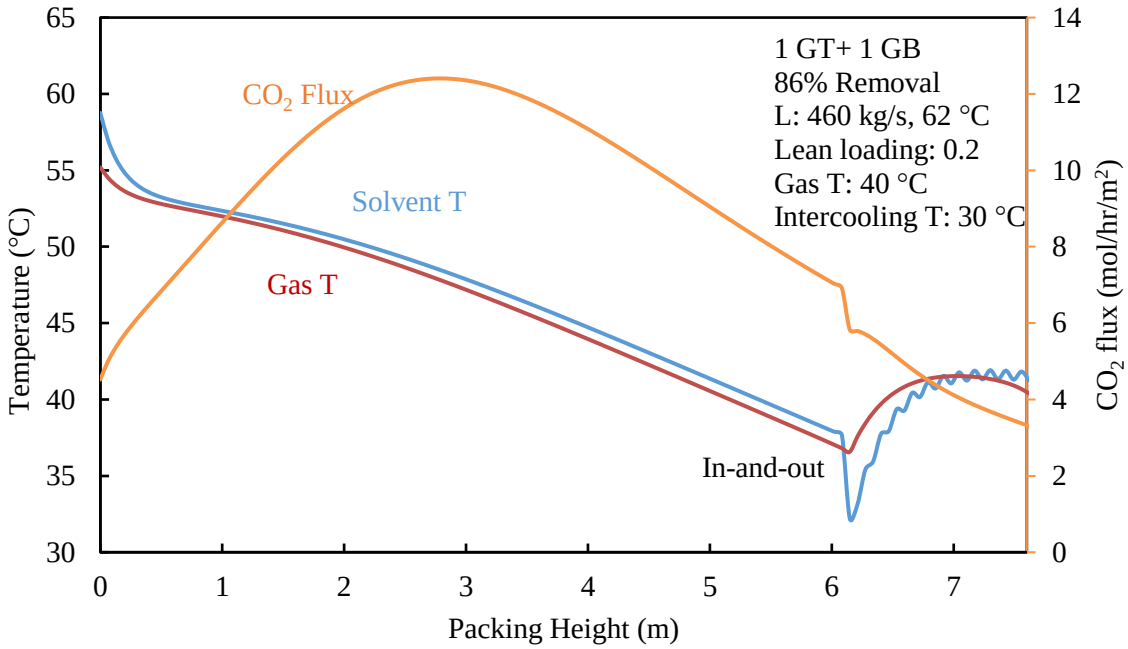

Figure 3.12: Vapor temperature (red), liquid temperature (blue), and mass transfer rate (orange) profile in the conventional absorber design with DCC and in-and-out intercooler

3.3.4 CO_2 Removal

Figure 3.13 shows the CO_2 removal at different solvent flow rates for the base case column design. High temperature of the lean solvent affects the CO_2 absorption at top stages and makes high CO_2 removal (>95%) difficult. As the solvent rate increases, CO_2 removal increases to a maximum and then drops. At high flowrate, the hot lean solvent brings more heat into the system and reduces the CO_2 absorption driving force.

The absorber will be designed for 90% removal, and it is possible to increase the CO_2 capture rate by increasing the solvent flowrate, e.g., 95% capture rate can be achieved by increasing the flow by 18%. Operating at greater than 90% removal will take advantage of the fact that equipment will be overdesigned for the FEED and increase the cash flow and profitability of the project.

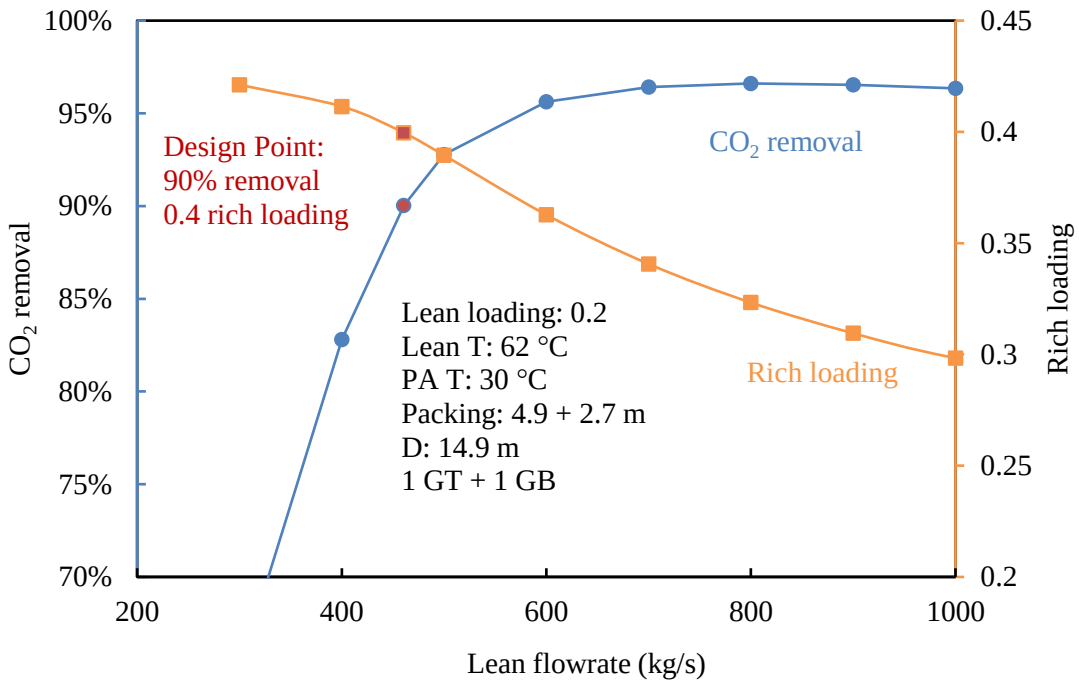

Figure 3.13: CO_2 removal (blue) and rich loading (orange) lean solvent flowrates for fixed column configuration.

Removing more than 95% CO_2 is difficult in the base design for two reasons: the low CO_2 driving force and the high temperature at the top of absorber. Figure 3.14 shows the temperature and CO_2 transfer flux at 95.6% removal. The high temperature reduces the absorption driving force, and even strips CO_2 out (negative flux). To achieve a higher removal, the top section needs to be cooled to retain the driving force.

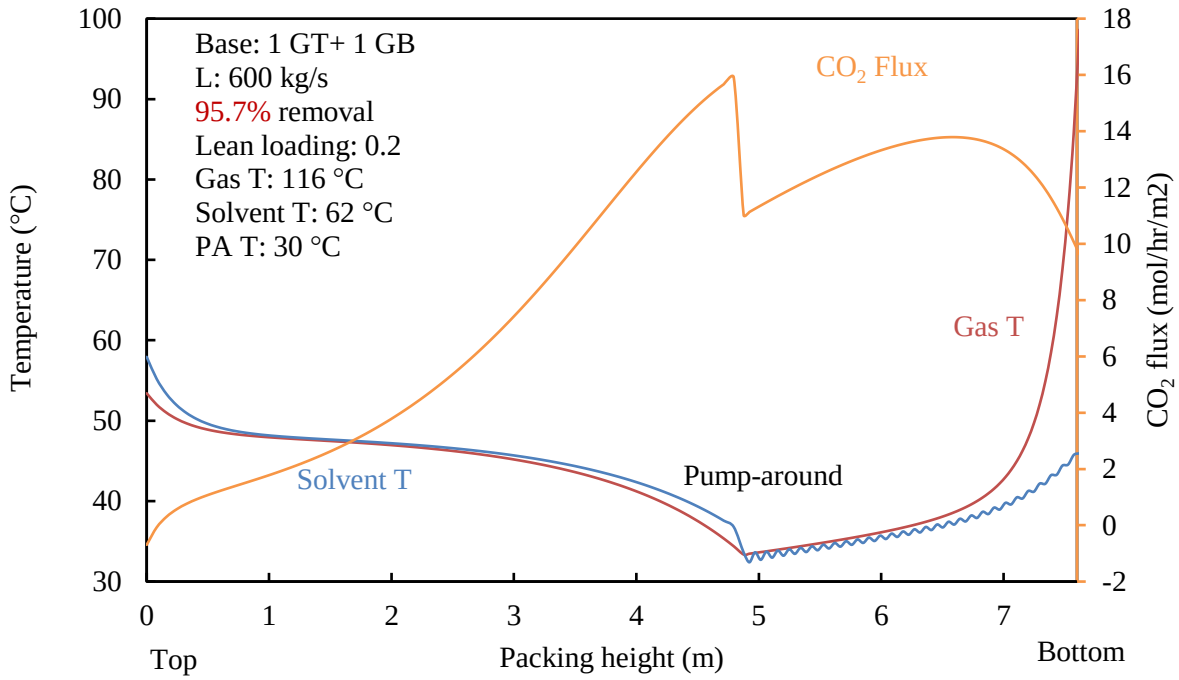

Figure 3.14: Vapor temperature (red), liquid temperature (blue), and mass transfer rate (orange) profile in the absorber at 95.7% removal.

Figure 3.15 compares the absorber performance at high CO_2 removal conditions for the base case design and with additional trim cooler at 40 °C. At a removal between 90% and 95%, adding the trim cooler for the lean solvent only makes minor improvement because of the low L/G ratio. As the solvent flowrate increases to achieve greater than 95% removal, the trim cooling becomes more effective, and the temperature bulge moves downwards. The difficulty of high CO_2 capture at NGCC conditions lies in cooling the top section of the absorber, and trim cooling has greater benefits when the target is greater than 95% capture.

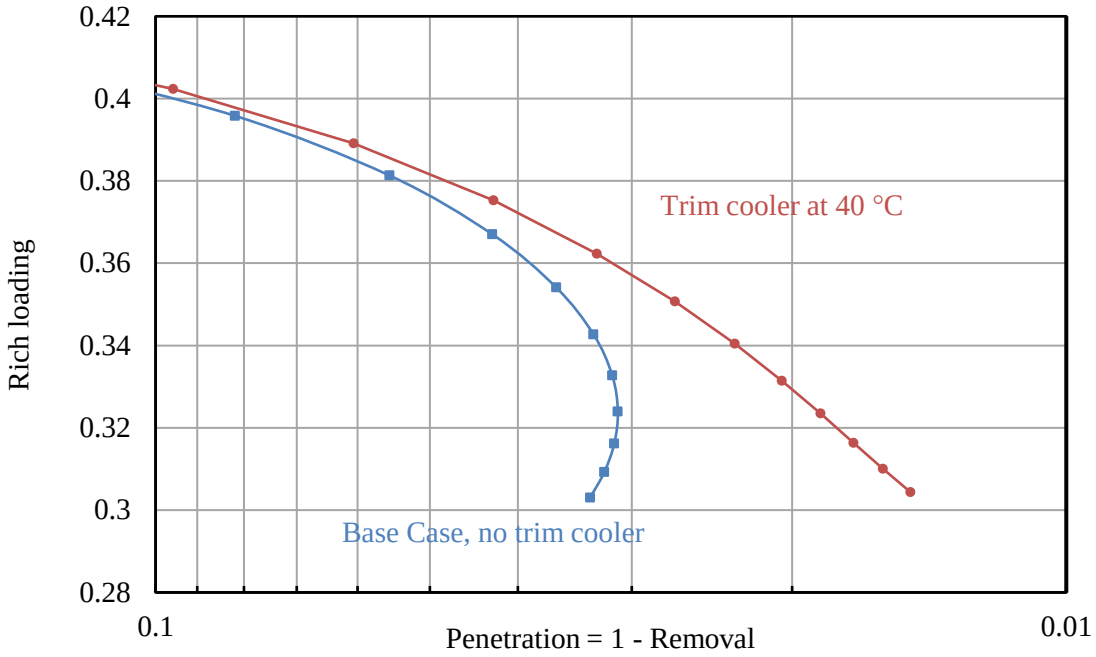

Figure 3.15: Absorber performance at high CO_2 removal for base case design (blue curve) and base case with additional trim cooler at 40 °C (red curve).

3.3.5 Lean Loading

The overall lean loading optimization requires the economic analysis of both absorption and stripping sections. For the absorber, a lower lean loading is always beneficial because it provides greater driving force. The solvent circulation rate decreases at lower lean loading, which reduces the pumping and piping cost and the heat exchanger area. The effects of lean loading on absorber packing height and solvent flowrate are shown in Figure 3.16. The flowrate and packing height are optimized based on $1.16*L_{min}$. When the lean loading decreases from 0.24 to 0.2, absorber packing height decreases by 10 ft and the solvent rate decreases by 18%. Steam consumption in the stripper area goes up slightly to get lower lean loading because of the over-stripping, but the cost for cross-exchangers goes down and sensible heat loss is minimized. The cost for CO_2 compression increases

because the stripper operating pressure will be lower. A lower lean loading improves the absorber performance, but the risk of low lean loading includes PZ precipitation and volatile PZ leaving the absorber. During the 2019 NCCC campaign, the system was operated at 0.2 lean loading without precipitation issues, therefore a lean loading of 0.2 is recommended for the FEED.

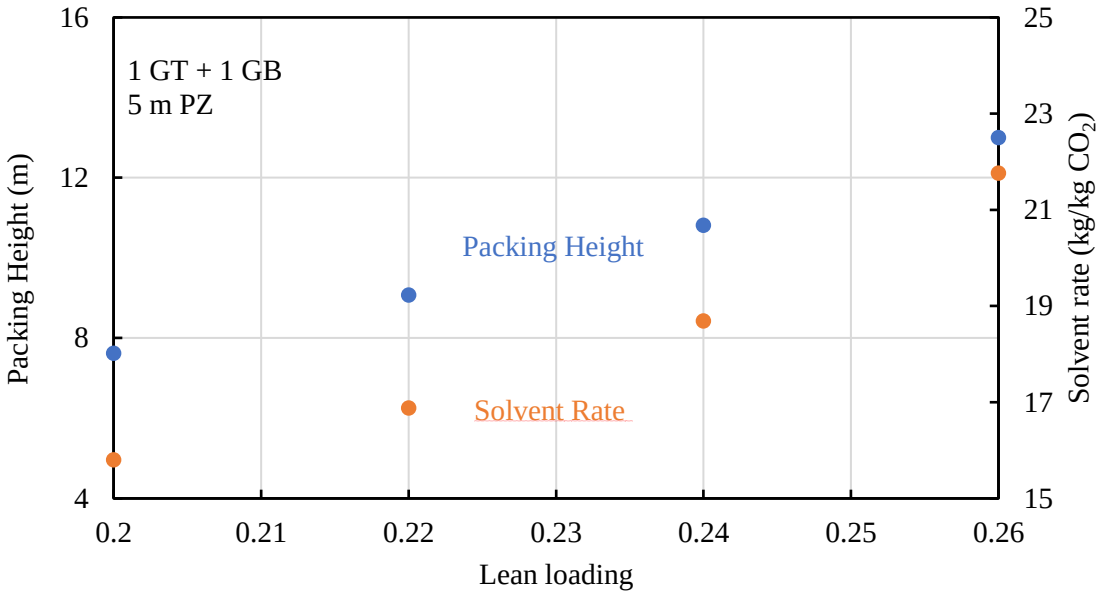

Figure 3.16: Optimized absorber packing height and solvent flowrate based on 1.16*L_{min} at varying lean loading for 90% CO_2 removal.

3.3.6 Risks of the Design

The absorber performance for the FEED study is simulated using the Independence model. Although the model has been validated with pilot plant results, some key process variables are extrapolated and the impact or the risk of the extrapolation need to be evaluated. Figure 3.17 summarizes the effect of the key process variables and compares them to the pilot plant results from NCCC. The delta loading from the long-term test at NCCC is about 14% less than the design, and the difference can be explained by different

lean loading, pressure, packing height, pump-around temperature, flowrate, and trim cooler. The low lean loading, low pump-around temperature, and high flowrate improves the absorber performance, while the lower ambient pressure (12.95 psia) and shorter packing reduce the performance.

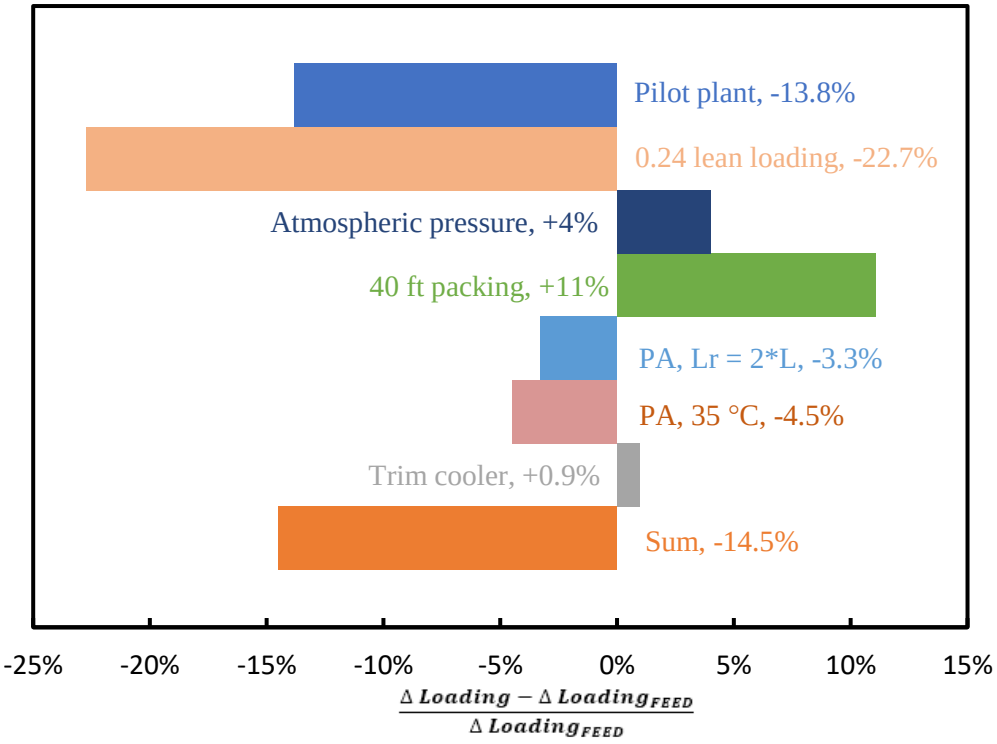

Figure 3.17: Effects of key process variables on absorber performance

Lean loading and the absorber height are the two major differences between the FEED design and the pilot plant long-term test. During parametric testing, a wide range of lean loading (0.19–0.25) was tested and used for model validation. The design point of 0.2 lean loading is therefore not considered as an extrapolation and poses a limited risk. The pilot-plant experiments were conducted with 12 m (40 ft) M252Y packing that was not varied, and the 7.6 m (25 ft) packing has not been tested before. However, the packing performance has been validated through the parametric testing. The FEED design uses

shorter packing sections (4.9 m and 2.7 m) and will be more efficient because of the better liquid distribution.

3.4 ABSORBER FOR OFF-DESIGN CONDITIONS

Previous section developed the base case absorber design for the FEED. This section will discuss the absorber operating for off-design conditions including the seasonal variation caused by different ambient temperature and greater than 90% removal.

3.4.1 Ambient Temperature

The flue gas rate and composition vary at different ambient conditions and operation modes of the power plant The performance of air cooler also changes at different ambient temperature, and this work assumes constant temperature approach between air cooler outlet and ambient. At low ambient temperature, turbines can handle more mass flowrate of the gas because of the high density, and therefore produce more electricity and more flue gas. At low ambient temperature (-13.3 °C), the flue gas mass flow increases by about 8%. Using the same solvent flow as in the base case, the CO_2 removal will be 87% and the CO_2 production rate will be 4% greater. The air cooler can intercool the solvent below the design temperature (30 °C) during the winter, but the pump-around temperature is still set as 30 °C to prevent solid precipitation.

At high ambient temperature, the flue gas rate decreases, and the absorber column operates at higher temperature because the air cooling has a temperature approach of 11.1 °C to the ambient. At 40.5 °C ambient temperature, the pump-around can only cool the liquid to about 52 °C, and removal drops to 77% because of the lower CO_2 transfer driving force at higher temperature.

Aside from lower CO_2 removal, the high ambient temperature creates water balance issues in the absorber section. At high temperature, gas leaving the system contains a greater amount of water and creates net water loss in the system. Given the large temperature swing in Denver City, the strategy to maintain the water in the summer is condensing water during the night when the ambient temperature is low and making up water for day-time loss. Figure 3.18 shows the water production or loss rate as a function of ambient temperature at two water wash circulation rates. A greater rate provides more cooling to the gas and retains more water in the system. At a circulation rate of 800 kg/s, the system starts to lose water around 26.6 °C ambient temperature. By increasing the flowrate to 1800 kg/s, the system can maintain the water balance below 33.3 °C. A detailed analysis examined the temperature profile of Denver City and concluded an intermediate circulation of 1300 kg/s would maintain the water balance most of the time.

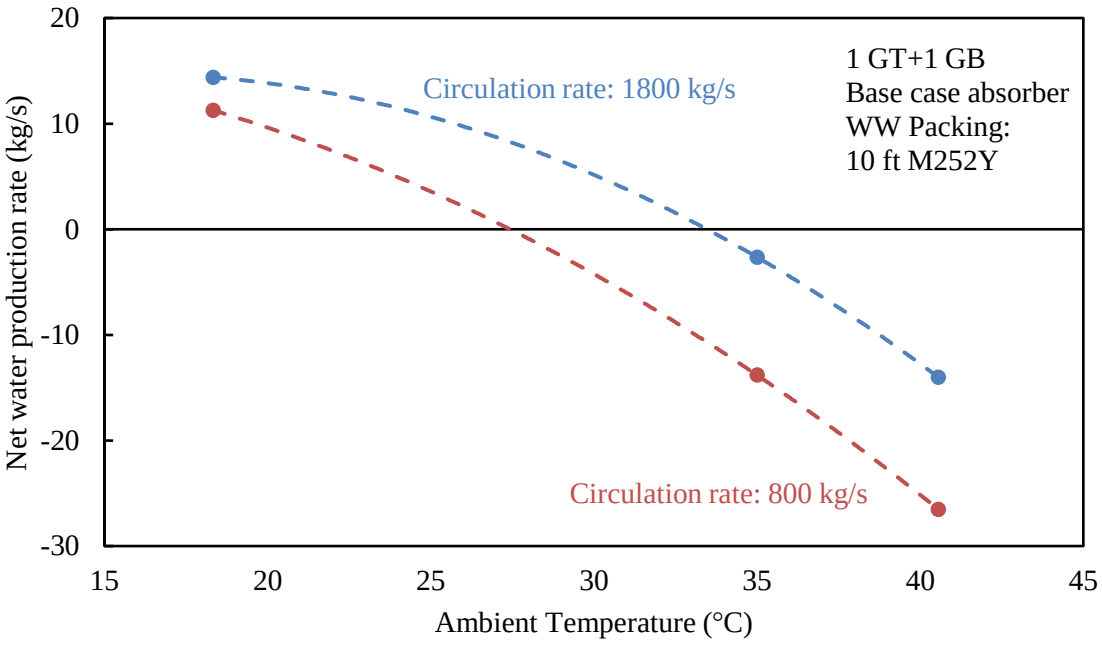

Figure 3.18: Net water rate in the absorber section at varying ambient temperature

3.4.2 Higher CO_2 removal

The FEED absorber is design at 90% CO_2 removal, but higher removal is achievable when the power plant is operating at partial load. Figure 3.19 shows the CO_2 removal and the temperature of gas leaving absorber at different gas flowrate. The base case is designed at 90% removal with duct burner. At constant solvent flowrate, the removal reaches 92% when the duct burner is off. As the flue gas rate reduces, the CO_2 removal shows a maximum around 97.7% when the flowrate is about 60% of the design. This is because as the flue gas rate reduces, the L/G increase in the absorber and the hot inlet solvent starts to raise the column temperature near the top and reduces the driving force. The maximum removal is achieved where the gas temperature is lowest.

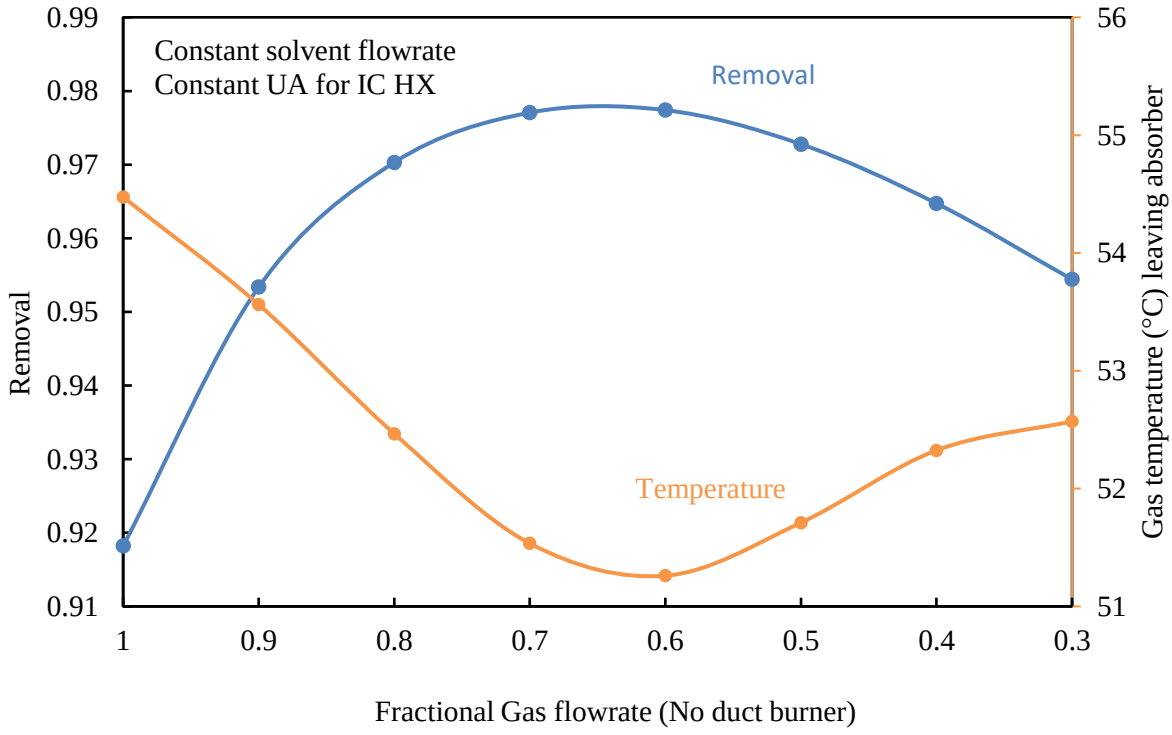

Figure 3.19: CO_2 removal and temperature of gas leaving absorber at various gas flowrate.

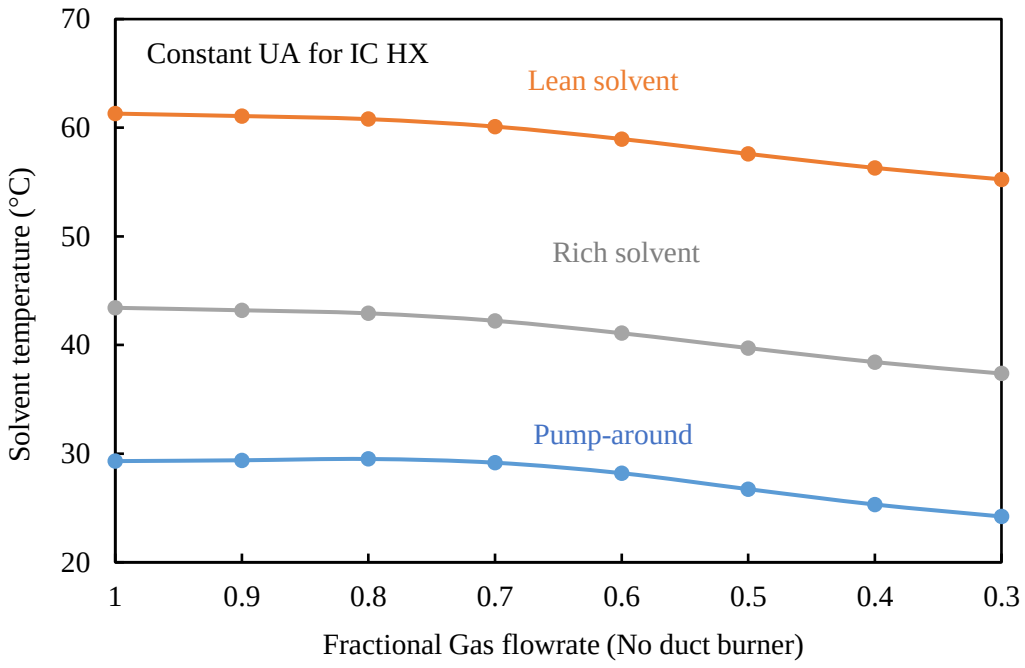

Figure 3.20: Temperatures of lean solvent (orange), rich solvent (grey), and intercooled solvent (blue) at varying gas flowrate under the assumption of constant UA.

Figure 3.20 shows the temperatures of lean, rich, and intercooled solvent at various gas flowrate. The intercooler heat exchanger is assumed to have constant UA and performs better with less cooling load at low gas flowrate.

With less CO_2 product in the stripper column, the lean loading can be further reduced to increase removal by lowering stripper pressure. Figure 3. 21 shows the CO_2 removal at various gas flowrate with three different lean loading. By reducing the stripper pressure by 6%, the lean loading decreases to 0.18 and the maximum CO_2 removal increases to 98.4% when the gas rate is 70%. Compressor should be able to handle the low stripper pressure because the mole flow of CO_2 is reduced more than the stripper pressure, therefore the overall volumetric of the CO_2 product is less than the design condition.

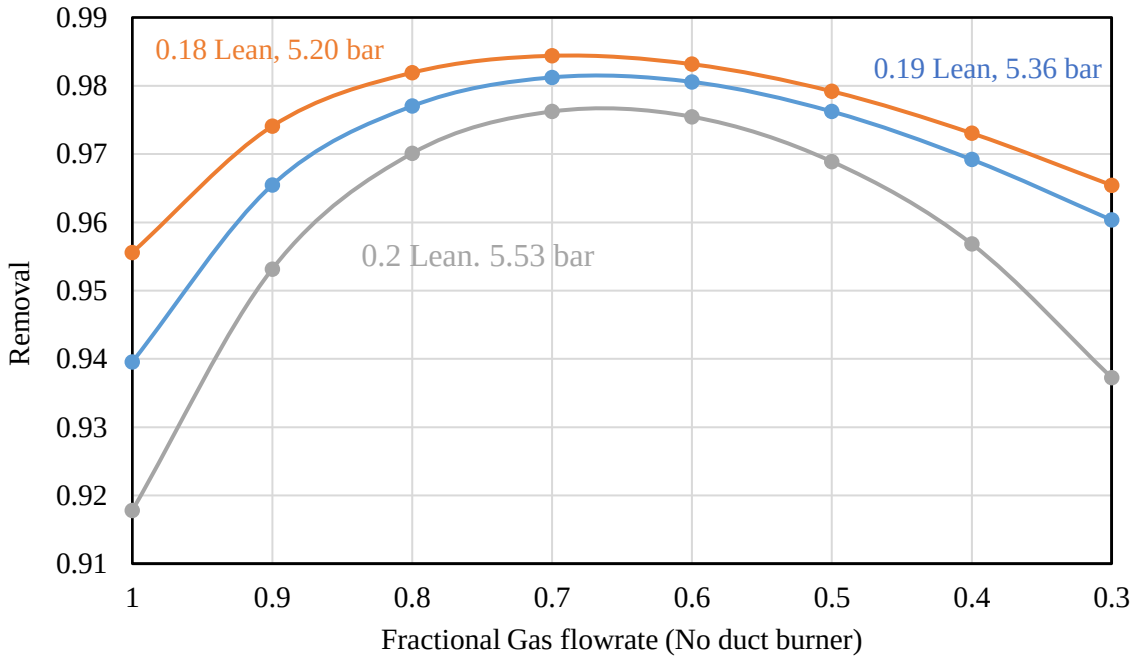

Figure 3.21: CO_2 removal at various gas flowrate using three lean loading.

For the summer cases, the maximum CO_2 removal 95.7% can be achieved with 60% of the designed gas flow. With less intercooling duty and the assumption of constant UA, air cooler will perform better than the design conditions and lead to a temperature approach about 10 °F.

The operating strategies discussed above for the partial plant load uses constant solvent flowrate as the base case to maximum the CO_2 removal and to reduce carbon emission. The rich loading is significantly lower than the base case for the low gas rate conditions and the energy performance will be worse. To maximum the profit, solvent flowrate should be reduced to increase the rich loading.

3.5 CONCLUSIONS

Based on the validated model for PZ at NGCC conditions, the following integrated absorber and water wash design was proposed for the NGCC power plant (1 out of 2 absorber trains):

Packing: M252Y, 3.0 m, 4.9 m, and 2.7 m from top to bottom

Column cross-section area: 174 m2

No direct contact cooler, no trim cooler

Lean solvent: 0.2 lean loading, 472 kg/s

Pump-around intercooling: return temperature: 30 °C, flowrate: 1400 kg/s

Maximum column flooding: 83%

Overall pressure drop of the flue gas through the absorber column: 2 kPa

Water wash circulation rate: 1300 kg/s

Given the fast reaction rate of PZ, reducing the packing height saves the capital cost of the absorber column. The design proposes a first -of -its -kind commercial scale absorber design using pump-around intercooling to improve absorber performance and eliminating DCC and trim cooler to reduce capital cost. The lean loading, low pump-around temperature, and high circulation rate is designed to improve the absorber performance and to reduce the operating cost. Compared to conventional absorber design with DCC and in-and-out intercooling, at similar operating conditions, the pump-around absorber design removes 4% more CO_2 and eliminates the DCC column.

The absorber can operate with the varied gas flowrate caused by ambient temperature. The base CO_2 removal is 90% and varies from 78% to 90% depending on ambient temperature. During the summer, water balance can be maintained by condensing water during the night to make up for the water lost during the day. A circulation rate of 1300 kg/s in the water wash enables operation for most of the time.

Greater than 90% removal can be achieved for operating with partial plant load. The maximum CO_2 removal for the base case and summer case is about 98.4% and 95.7% at 70% and 60% flue gas rate as the base case.

Chapter 4: Innovative Absorber Design using Aqueous Piperazine for Gas Turbines

4.1 INTRODUCTION

The PZAS^{TM} process has been demonstrated as a promising second-generation amine scrubbing technology for CO_2 capture by extensive pilot plant experiments and modeling results (Gao and Rochelle, 2019; Gao et al., 2019; Rochelle et al., 2021; Rochelle et al., 2019). A rigorous, rate-based absorber model was validated with the pilot plant experiments and can accurately predict the CO_2 removal and temperature profile over a wide range of conditions. With the validated model, the effects of key process variables including flue gas temperature, liquid flowrate, intercooling temperature, and pump-around flowrate were accurately predicted. In chapter 3, this model was used to design the absorber for the FEED and to predict its performance.

This chapter proposes two innovative absorber designs for NGCC applications: the hybrid absorber and crossflow absorber. Figure 4.1 shows the pump-around absorber design for the FEED (left), the hybrid absorber (middle), and the crossflow absorber (right). For the FEED absorber, the CO_2 absorption section consists of 2 beds of MellapakPlus® 252Y structured packing: the top section is 16 ft, and the bottom section is 9 ft. The absorber uses a pump-around intercooler to circulate solvent around the bottom section. The high pump-around flowrate and low temperature (30 °C) are chosen to improve the absorber performance. The hot flue gas (111 °C) and lean solvent (62 °C) are fed into the absorber directly without precooling. The absorber is designed at 0.2 lean loading and can remove 90% of the CO_2 with a rich loading of 0.4.

Two disadvantages of the pump-around design are the back mixing of the solvent in the pump-around section and the low utilization efficiency of the column space. The high liquid flux in the bottom section helps manage the column temperature and cools the

hot flue gas at the cost of reduced CO_2 absorption rate because of the back mixing of the rich solvent. The detailed column design reveals the second disadvantage of the pump-around design, which is a common one for the countercurrent absorber in amine scrubbing. A large portion of the "open volume" in the column is associated with gas turning direction, gas distributions, packing break, and mechanical supports. For example, the height below the bottom packing section is around 30 ft, and the space between the packing sections is another 30 ft. Each packing break creates about 10-15 ft of open space above and below it. The open space increases the height of the column and takes up a significant portion of the shell cost. For the FEED column, with additional 10 ft water wash on top, the total packing height is 35 ft, and the column height is 117 ft.

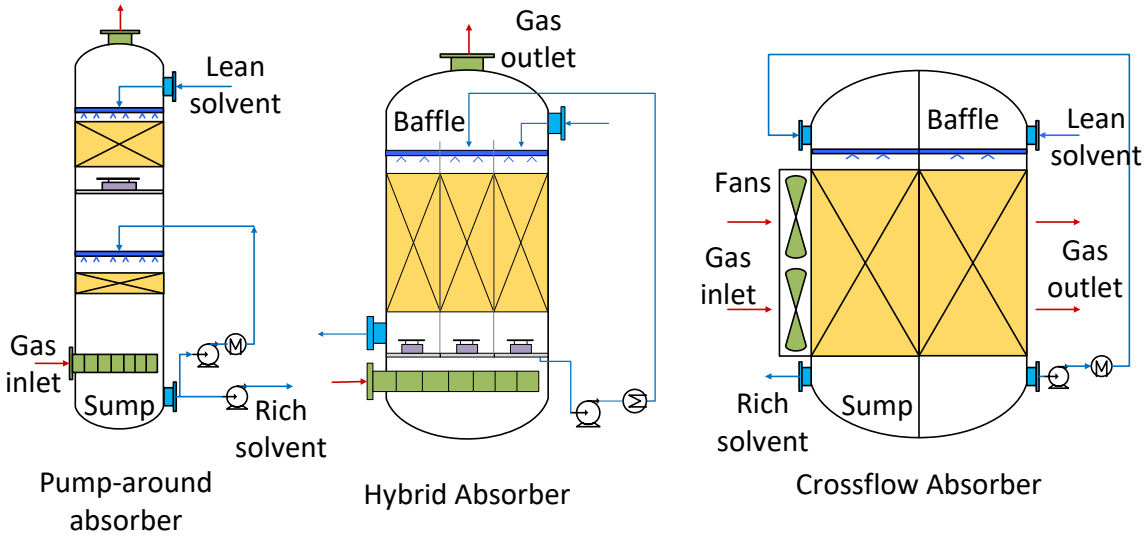

Figure 4.1: Three absorber configurations (without water wash section): pump-around absorber (left), hybrid absorber (middle), and crossflow absorber (right).

The hybrid configuration and crossflow absorber are proposed as process intensifications of the pump-around absorber to improve CO_2 absorption efficiency and reduce the open volume in the absorber. Figure 4.2 shows the simplified flowsheet diagram for the hybrid configuration: the flue gas is split into three portions, and the solvent

countercurrently contacts with each split in one section of packing and is intercooled between the sections. In each section, the liquid to gas ratio (L/G) can be increased by 3 times compared to the countercurrent absorber because the gas rate is only one third of the total gas rate. At this high L/G ratio, the solvent will carry most of the heat of absorption and can be cooled effective by the intercooler. The high liquid flux will also increase the liquid film mass transfer coefficient (k_L), the interfacial area (a), and improve the gas-liquid distribution. The water wash section is above the CO_2 absorption section and manages the water balance. In this configuration, solvent flows in sequence without back mixing and maintains a high L/G similar to the pump-around configuration. In large commercial-scale absorber column, these sections can be integrated into one column as shown in Figure 4.1.

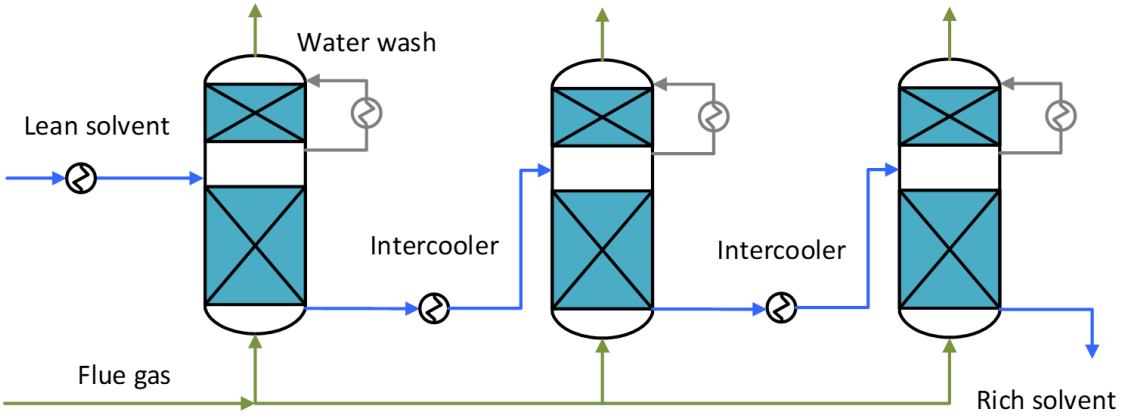

Figure 4.2: Simplified flowsheet diagram for the hybrid absorber configuration

The crossflow absorber shown in Figure 4.1 represents another option for intensification. Flue gas flows horizontally into the packing bed and the solvent flows vertically in each packing bed. Intercooling is applied in the right bottom. While the countercurrently packed columns are more common, the crossflow absorber may present some favorable characteristics: (1) The column is more compact and has less visual impact. The column could be directly integrated in the flue gas pathway with rectangular ductwork.

The space required to turn the gas flow direction from horizontal to vertical is eliminated. (2) The gas and liquid velocities can be optimized separately because the flow area can be varied independently. The crossflow absorber can be operated at a greater gas velocity because the flooding limitation is significantly delayed compared to countercurrent flow. The pressure drop can also be optimized by varying the angle between the directions of gas flow and packing channels.

The crossflow gas liquid contactor has been commonly used for cooling towers and recently gained attention for direct air capture (DAC) applications. Figure 4.3 shows a crossflow cooling tower design (left) and a cell of a crossflow cooling tower (right) from SPX Cooling Technologies.

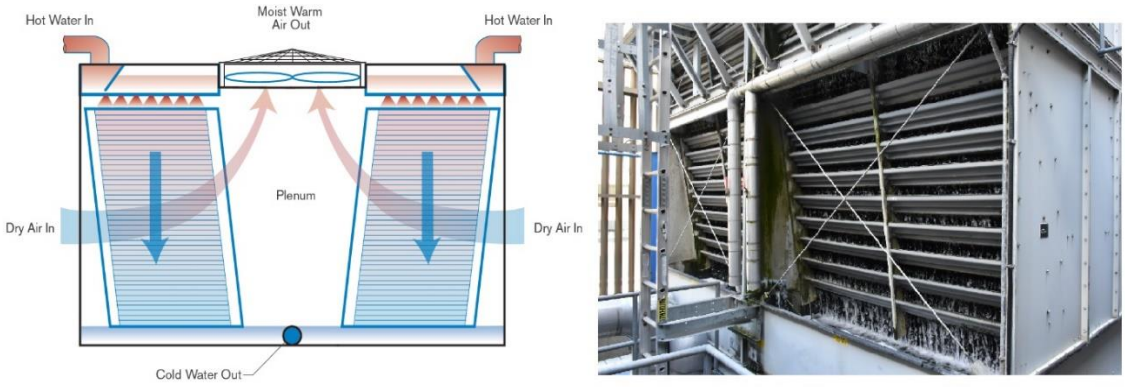

Figure 4.3: Crossflow cooling tower (SPX Cooling Technologies)

In a crossflow tower, the process water is pumped to the top of the tower and discharges into a water basin with nozzles. The crossflow tower also has the advantage of maintaining an even liquid and gas distribution at low flow conditions. With the use of nozzle cups, a crossflow tower can utilize as little as 30% of the design flow and keep good water distribution across the packing, whereas for countercurrent flow, the water needs to be distributed across the entire cross section of the structure, which limits the low flow

capability to about 70% of design flow. At flows under 70% of the design rate, channeling begins to develop as shown in Figure 4.4.

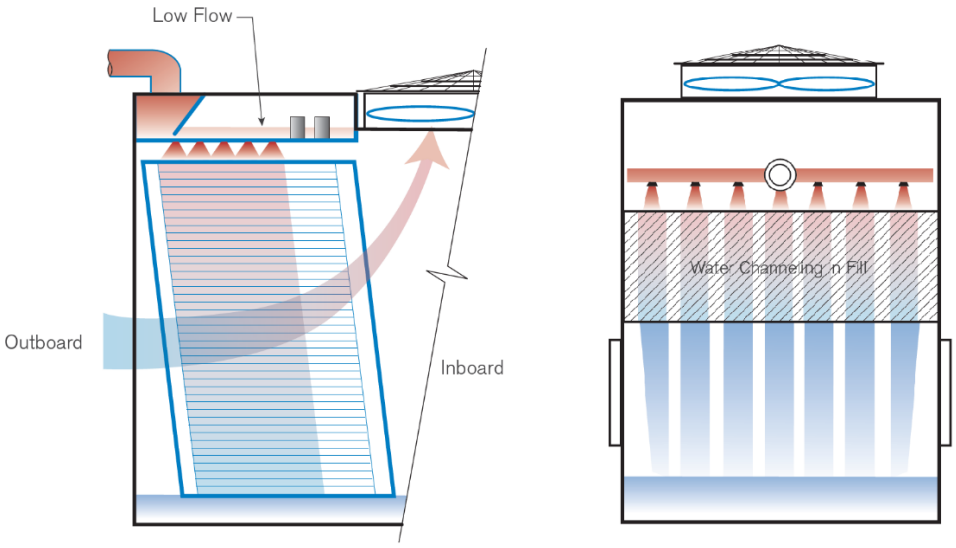

Figure 4.4: Water distribution for crossflow (left) and countercurrent flow (right) tower at low flow conditions.

Figure 4.5 shows a crossflow tower fill (structured packing) and an example of crossflow tower internals from SPX Cooling Technologies. The tower is usually designed at an angle to accommodate the liquid flow drifting in the air flow direction. Generally, crossflow towers have inlet louvers. The purpose of louvers is to equalize air flow into the fill and retain the water within the tower. A drift eliminator is installed at the air outlet to remove entrained liquid in the gas stream.

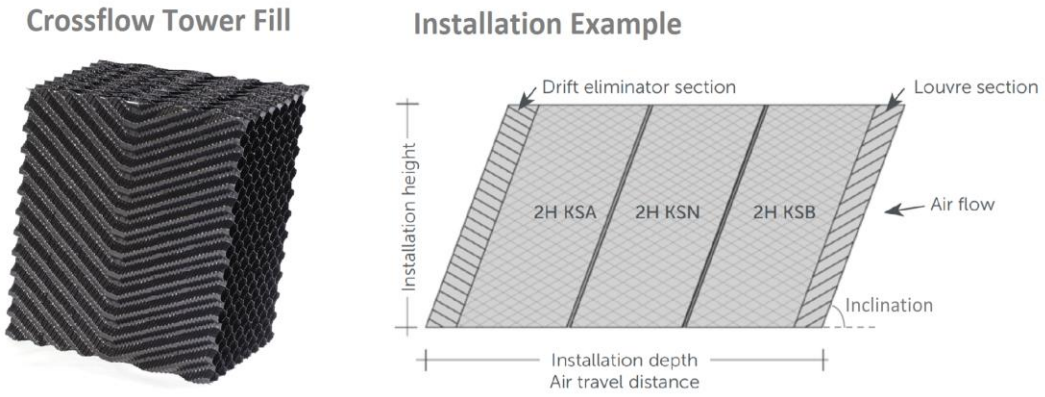

Figure 4.5: Crossflow tower fill (left) and installation example (right) (SPX Cooling Technologies).

Lavalle et al. studied the hydraulic performance of crossflow contacting by computational fluid dynamics (Lavalle et al., 2018). They simulated the conventional structured packing cell (shown in Figure 4.6) to investigate the potential application for CO_2 capture. The liquid flows from top to bottom and the gas flows from left to right. The gas and liquid crossflow form a countercurrent and a co-current channel in half of the element. The co-current channel can delay column flooding and reduce the gas phase pressure drop.

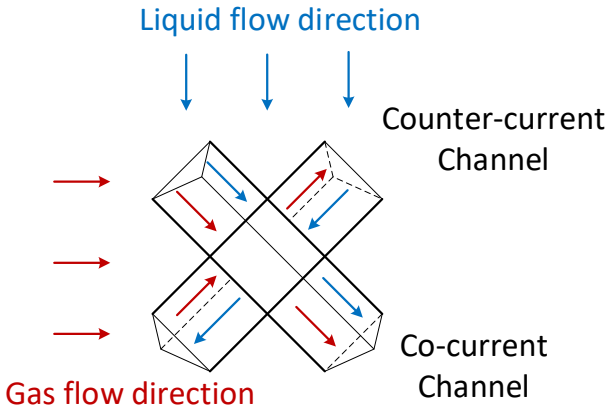

Figure 4.6: Schematic of the crossflow elementary cell

Figure 4.7 shows the simulated wet pressure drop of crossflow and countercurrent flow for various structured packing. The packing used for crossflow (green points) pressure drop calculation has a geometry similar to Mellapak® 500Y. Results from Lavalle showed that for structured packing with similar density, crossflow can reduce the pressure drop and the column can be operated at a higher gas velocity. However, when compared to the MellapakCC™, which is optimized to minimize the pressure drop for carbon capture application, the pressure drop for crossflow is still significantly greater. The optimization of packing geometry to reduce pressure drop for crossflow may not be as effective as for countercurrent flow because there is not large volume of liquid holdup in the packing joint for crossflow. Therefore, the advantages of the crossflow absorber are high gas velocity and smaller column size to reduce the capital cost.

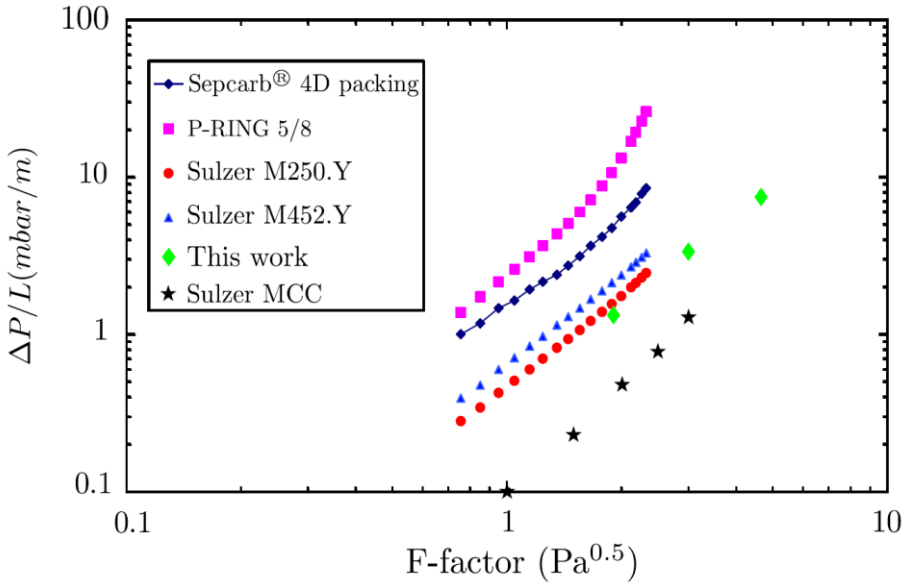

Figure 4.7: Comparison of wet pressure drop of crossflow (green) and countercurrent flow for various structured packing (Lavalle et al., 2018).

Because of the advantages of low pressure drop and compact size, crossflow contacting is favored to when large volume of gas needs to be treated. Carbon Engineering

has proposed a crossflow absorber configuration for DAC and performed bench and pilot scale experiments using NaOH solutions (Heidel et al., 2011; Holmes and Keith, 2012; Holmes et al., 2013; Keith et al., 2018). Compared to amine scrubbing, the NaOH process is less complicated because the mass transfer is wetted area controlled only with no equilibrium limitation, and the column temperature is more uniform because of the low CO_2 concentration. This chapter explores the possibility of using crossflow contactor for CO_2 capture on NGCC condition and optimizes the configuration by rate-based modeling.

4.2 SIMULATION METHOD

Aspen Plus® is used for the absorber and water wash modeling. The rigorous, rate-based absorber model was developed and reconciled with previous campaign data from the National Carbon Capture Center (NCCC). An adjustment of 1.08 on PZ weight fraction was made to match the 2019 pilot plant results at 4% CO_2 in the flue gas.

Multiple Radfrac columns are used to simulate the different absorber configurations and to mimic the gas and liquid flow patterns. Within each Radfrac block, the liquid and gas flow countercurrently as limited by the software: the gas is fed to the bottom and the liquid is fed to the top. For computational stages, the choice of mixing rule for pump-around and hybrid absorber is countercurrent, and for crossflow it is well-mixed. Figure 4.8 shows a hybrid configuration with 3 absorber and 3 water wash in series as simulated in Aspen Plus®.

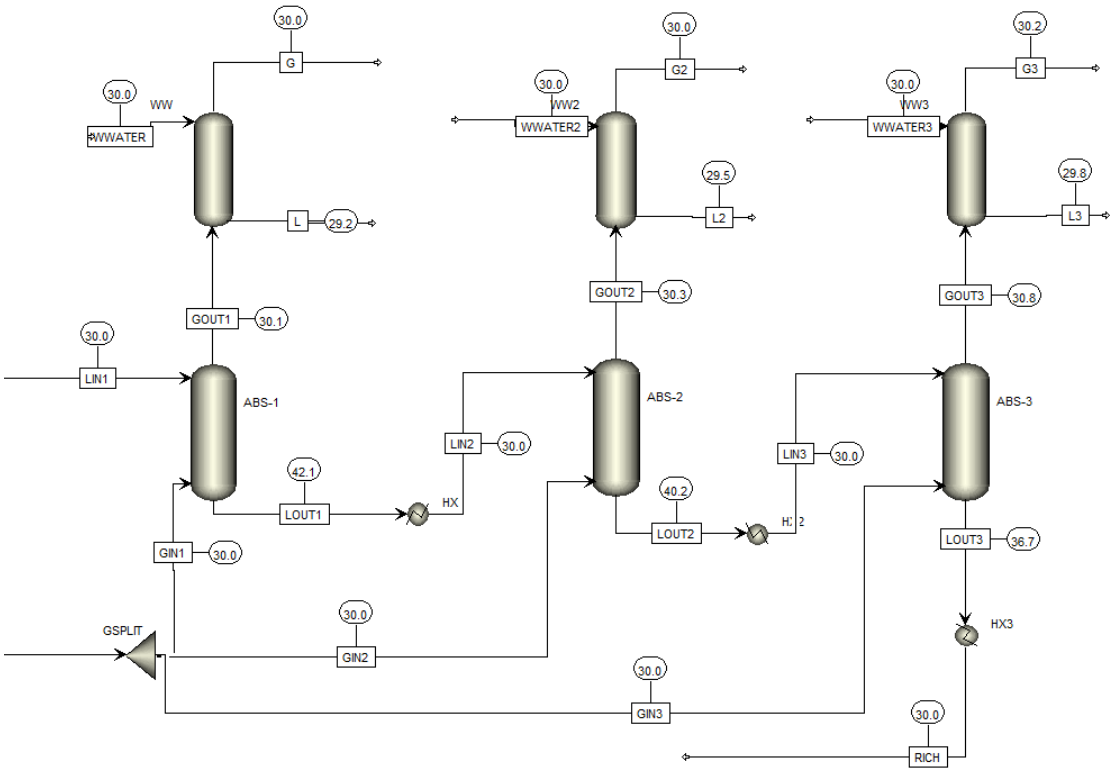

Figure 4.8: The hybrid absorber configuration as simulated in Aspen Plus®

The crossflow absorber is mimicked using small countercurrent elements with connecting streams flowing in the crossflow directions. Figure 4.9 shows the simplified flowsheet as simulated in Aspen Plus® and the geometries of the element, the slice, and the column. The 2D matrix represents a slice of the crossflow absorber as the green slab in Figure 4.9. The liquid leaving the top element feeds into the next element below and the gas leaving the left element feeds into the next one on the right. The element has a cross-section area of 25 ft^2 and a packing height of 5 ft to represent a 5×5×5 cubic element. The 2D matrix simulates the performance of a slab with dimensions of H×L×5 ft^3. In each element, the gas and liquid flow have the same pathlength, so the gas phase pressure drop is additive in horizontal direction. In each element, the hydraulics and driving force are

calculated as countercurrent flow, therefore this method only provides an approximate estimate of the performance considering the crossflow driving force and it will converge to a real crossflow column when the element is sufficiently small.

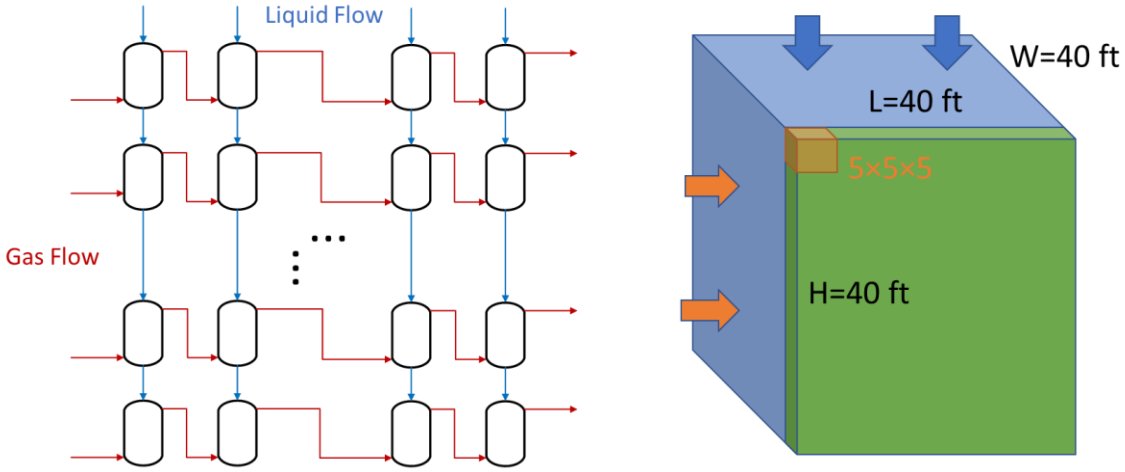

Figure 4.9: Simplified flowsheet as simulated in Aspen Plus® (left) and geometries (right) of the crossflow absorber (blue cube), simulated slice (green slab) and the countercurrent element (orange cube).

4.3 Results and Discussions

4.3.1 Hybrid Absorber

The most important design variable introduced by the hybrid absorber configuration is the number of small sections in series (the number of solvent paths), and it represents the major tradeoff between capital and energy cost. Figure 4.10 shows the designs for hybrid absorber with 3 sections (left) and 2 sections (right). At constant total packing volume, more small sections in series increase the L/G in each section because the gas is evenly split to each section and contacts with all the solvent. Solvent intercooling is more effective at higher L/G because more liquid can capture a greater portion of the heat of absorption. Figure 4.11 shows the temperature profiles in the first absorber for the hybrid configurations with 2 and 3 sections in series. Both configurations have same amount of

packing and the same cooling temperatures. The L/G with 3 sections is about 50% greater than the 2 sections. As a result, the temperature bulge moves to the bottom and the overall column temperature is significantly lower. There are more locations for intercooling to manage the temperature, and the column is closer to isothermal with a greater number of sections. Therefore, more sections improve the absorber performance.

However, more sections lead to a greater system complexity, even though the system can be integrated in large one column. The proposed design uses non-load bearing curtains between the packing sections and these curtains prevent mixing of the solvent. Solvent will be distributed to each section, collected by chimney trays, intercooled, and redistributed to next section. The column design does not differ significantly from a regular absorber vessel. Adding extra solvent paths also increases the capital cost of pumps, pipes, and exchangers. The operating and the dynamic behavior of the absorber may be more complicated, requiring sophisticated design and control for solvent delivery.

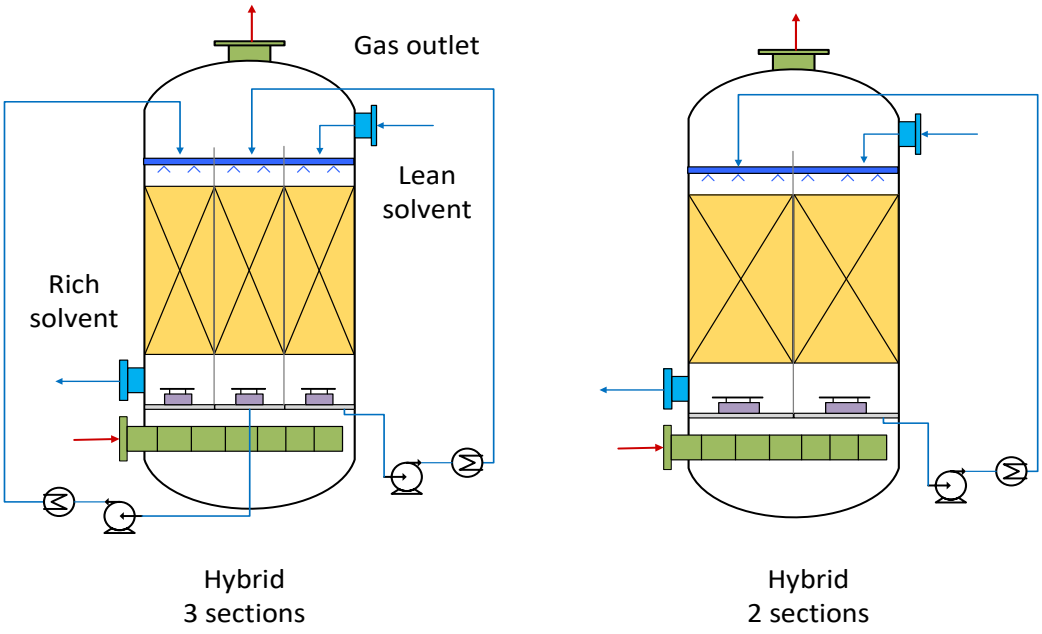

Figure 4.10: Hybrid absorber configuration with 3 sections (left) and 2 sections (right).

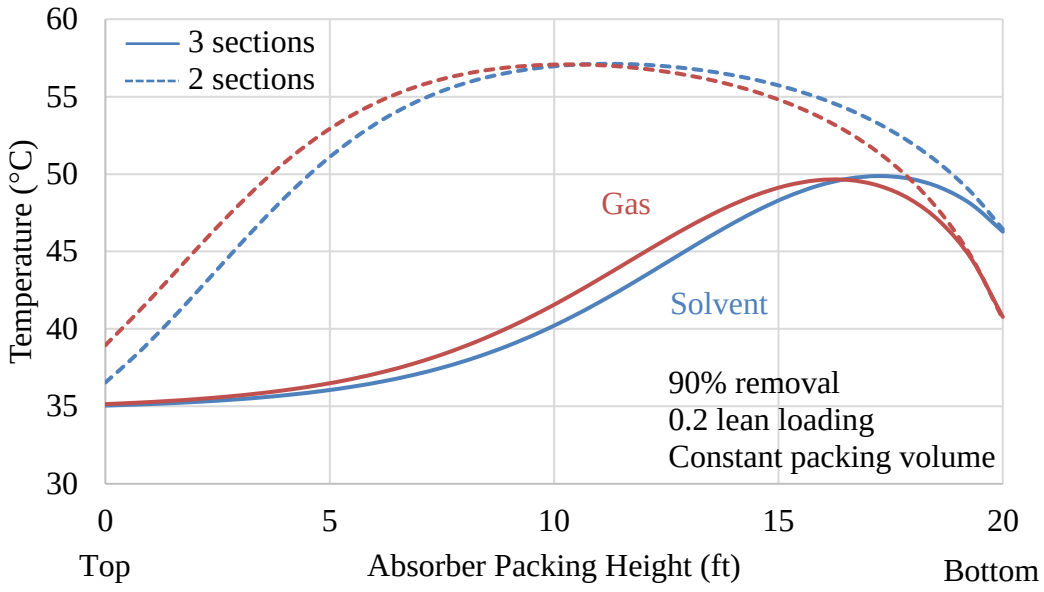

Figure 4.11: Solvent (blue) and gas (red) temperature profiles in the first absorber column for hybrid configurations with 2 (dashed) and 3 (solid) absorbers sections.

Figure 4.12 proposes a base case hybrid configuration with 3 sections. Each section has a 20 ft high absorption bed and a 10 ft high water wash section. The total packing volume is the same as the pump-around absorber in the FEED, but the solvent rate is about 30% greater than the FEED. The main reason for the worse performance is that the cooling temperature is constrained by the water balance and cannot be lower than 43 °C. For the pump-around absorber, the gas leaving the absorber is at high temperature, having been heated by the hot lean solvent. Water vapor in the gas leaving the absorber enters the water wash section, is condensed, and recycled back to the solvent to maintain the water balance in the system. It is important to ensure the gas leaving the absorber has greater than 8% water vapor, so the solvent temperature for the hybrid configuration has to be greater than 43 °C. For the pump-around absorber, the intercooling can be as low as 30 °C, and this low cooling temperature greatly improves the absorber performance.

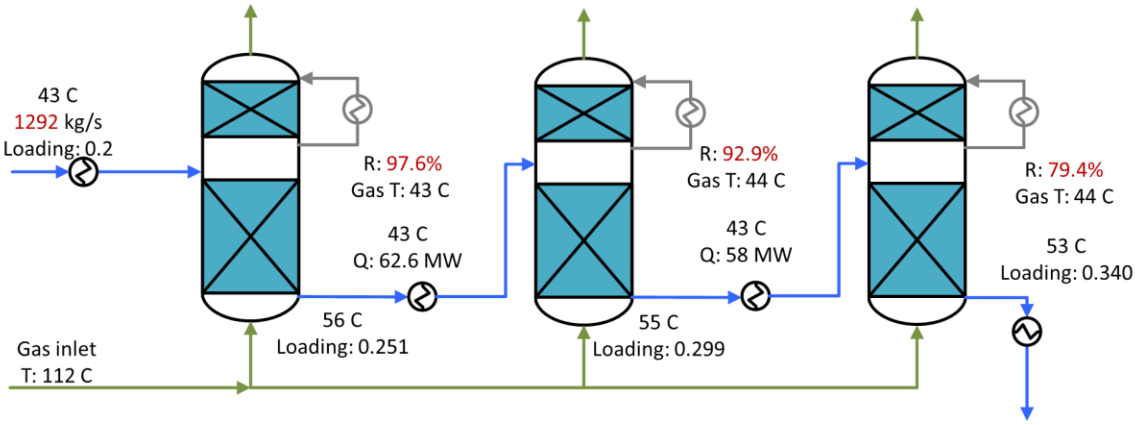

Figure 4.12: Absorber performance of a base case hybrid configuration with 3 sections

To demonstrate the effect of the cooling temperature, the flue gas is first cooled to 28 °C before entering the absorber. Practically, this is done by using a direct contact cooler (DCC). Excess water is removed before entering the absorber, and the solvent can be cooled to 30 °C. As shown in Figure 4.13, at 90% removal, the solvent flowrate can be reduced by 26% at this temperature. The implementation of this design involves a greater capital investment because a DCC is required to cool the flue gas. The solvent flow for 90% CO_2 removal is about 5% greater compared to the pump-around absorber. The performance is slightly worse than the pump-around because the first column achieves about 99.3% removal and approaches lean-end pinch. Sensitivity analysis shows that the performance of the third column is also limited by the mass transfer area but increasing the packing area for only this column may cause difficulty for the integrated column design.

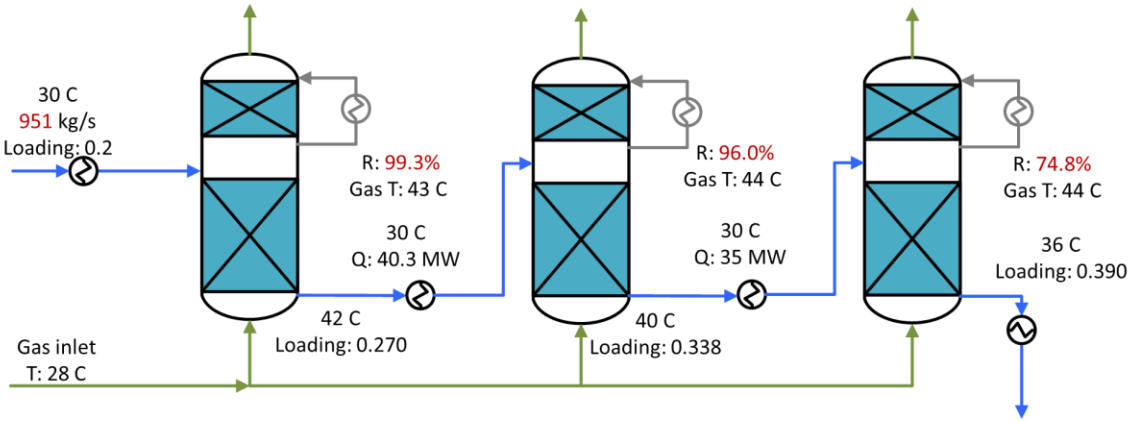

Figure 4.13: Absorber performance of hybrid configuration with 3 columns and DCC

Another variation of the hybrid absorber design is shown in Figure 4.14. The top three sections treat the flue gas from NGCC turbines, and the bottom section treats the gas from the gas boiler and is relatively small. The hot lean solvent is fed into the first absorber and is then intercooled to 30 °C. The lean solvent absorbs CO_2 from the turbine exhaust which contains about 4% CO_2. After removing the CO_2 in the 3 sections, the solvent then further enriches by contacting with the boiler exhaust containing 9% CO_2. This configuration takes advantage of the high CO_2 concentration and results in a rich loading of 0.398. The boiler exhaust needs to be cooled to remove the excessive water before entering the small absorber. The overall water balance can be managed by controlling the temperature of DCC and the circulation rate of the first high temperature water wash section. This design can outperform the pump-around absorber but increase the capital cost significant because of the additional small absorber.

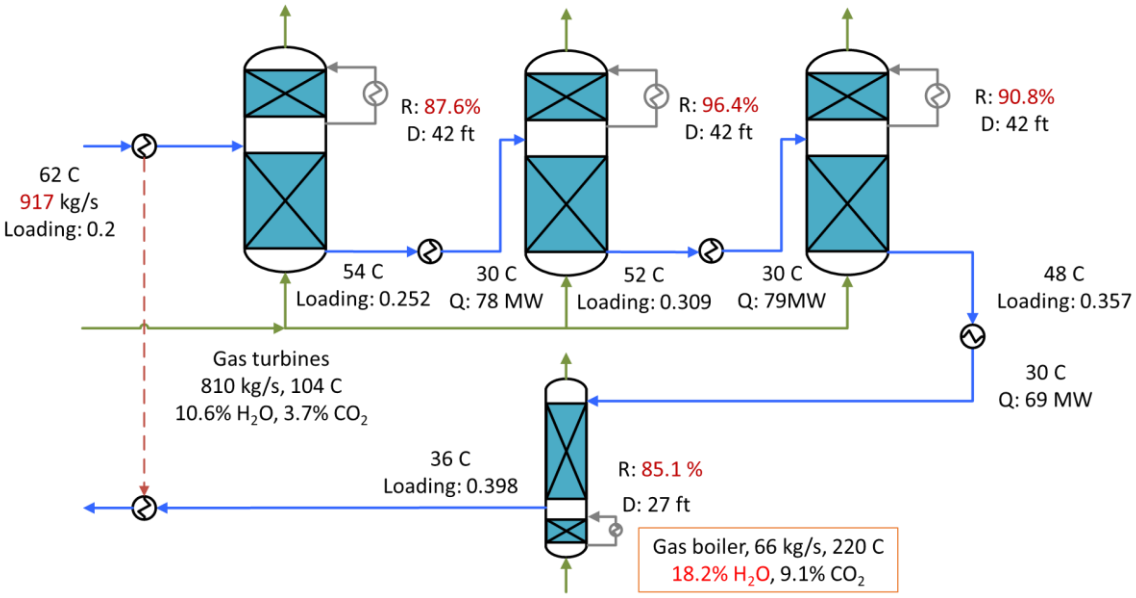

Figure 4.14: Absorber performance of hybrid configuration with 4 sections.

Compared to the pump-around absorber, the hybrid configuration could potentially reduce energy cost for two major reasons:

1. High L/G in each section of the absorber. The solvent flowrate per packing area is three times greater than the countercurrent absorber. The high liquid rate enhances the liquid mass transfer coefficient (k_L) in the packing and is less likely to be maldistributed. The high L/G also provides better intercooling. The liquid carries more enthalpy in the column and cooling the liquid will reduce column temperature effectively.

2. Better CO_2 transfer driving force. The hybrid design preserves the CO_2 driving force by avoiding back mixing the solvent and diluting the concentrated CO_2 from the boiler. One disadvantage of the pump-around design is the back mixing of the solvent. The hybrid avoids mixing the rich solvent with lean solvent and retains the high L/G as in the pump-around section. Instead of mixing with the flue gas from the turbines, concentrated CO_2 from the boiler is maintained in this design. The last column is small, but it enriches the rich solvent because of the high CO_2 concentration.

However, the base case hybrid absorber design with only 1 vertical packing section is worse than the pump-around design because of the temperature limitation. To maintain the water balance without DCC, the solvent temperature cannot be below 43 °C or water will accumulate in the absorber and dilute the solvent.

A big drawback of the hybrid configuration is its complexity. Although the integrated equipment design could be simpler than the flowsheet suggests, the system requires more sophisticated flow control. The overall water balance is harder to control because the water wash sections operate at different conditions.

Another disadvantage of the design is the difficulty of pilot plant testing. There are no pilot plant results available, and it is hard to test the system at pilot plant scale. The proposed design uses multiple absorber sections can only be integrated into one column at large scale, where the packings are installed in small sections naturally. It will be cost ineffective to test this configuration at small pilot scale.

4.3.2 Crossflow Absorber

The performance of the crossflow absorber is estimated using a 2D matrix consisting of small absorbers. The base case of the crossflow absorber with 40×40×5 ft^3 (L×H×W) packing is simplified and simulated using an 8×8×1 matrix with countercurrent elements. The total length in W direction can be divided into multiple slabs and each of them has the same profile, the 3D column therefore can be represented by the 2D matrix.

Figure 4.15 shows the CO_2 removal and the temperature profiles for the base case at 90% removal. Hot flue gas (104 °C) and hot lean solvent (62 °C) enter the absorber directly without cooling. Gas flows horizontally from left to right and liquid flows vertically from top to bottom through the intersections. The CO_2 removal and temperature show a diagonal distributed behavior as the collective results of the liquid and gas flow.

The flue gas near the top contacts with fresh solvent and the CO_2 is absorbed as it flows. The top left therefore has the highest CO_2 removal. As the solvent flows downwards, it absorbers CO_2 and provides less driving force for CO_2 removal. The equal removal contour diagonally crosses the column indicating low removal on the bottom left and high removal at top right as expected.

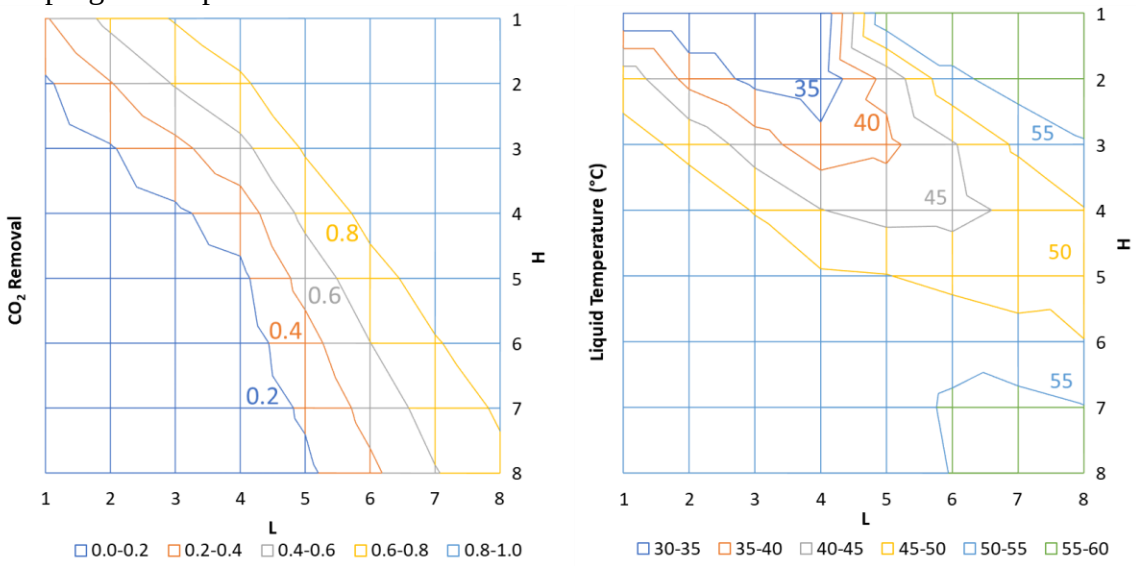

Figure 4.15: CO_2 removal and liquid temperature profiles for the crossflow absorber at 90% removal. The 8×8 matrix represents the slab of 40×40×5 ft^3 (L×H×W).

The temperature profile shows similar diagonal distribution. Solvent and gas carry the heat in their flow directions and lead to a high temperature region near the bottom right. Unlike countercurrent flow, the heat will not be trapped in the middle of the column and can be removed effectively by an intercooler cooling the solvent from the bottom right. The intercooled solvent feeds to the top left of the column and contacts directly with the hot flue gas and gets hotter as it flows.

Based on the profiles, the bottom left region is mostly pinched because of the high temperature. At 90% removal, the crossflow absorber achieves a rich loading of 0.384 using about 34% more packing than the pump-around absorber. The overall performance

of the crossflow design is worse than the pump-around because the solvent temperature near the bottom left is high. The rich solvent leaves the crossflow absorber at 51 °C and is 7 °C hotter than the pump-around, which leads to the high temperature mass transfer pinch. Additional cooling of the rich solvent is needed to improve the performance.

The optimal absorber packing height can be studied using the minimum solvent rate (L_{min}) analysis. Figure 4.16 compares L_{min} of the pump-around absorber and crossflow absorber. Both configurations achieve 90% CO_2 removal using solvent with 0.2 lean loading. The lean solvent is fed at 62 °C and the intercooler is set to 29.5 °C. The curve for the pump-around absorber is acquired by varying column height and keeping the pump-around in fixed position relative to the total height. The column flooding remains roughly constant because the gas velocity is constant when the height varies. The analysis of the crossflow absorber is done using factors (*a, b, c*) on wetted area (a_e), liquid, and gas phase mass transfer coefficients (k_L and k_G) respectively instead of varying the packing volume directly because of the flooding limitation. The crossflow packing remains cubic shape and each dimension is changed to the same extent using the factor a to exclude the effect of geometry. In this design, the cross-section area for gas and liquid flow changes proportionally as the packing volume changes, so the "column flooding" is also changed. One advantage of the crossflow contacting is that there is no flooding limitation as with countercurrent contacting, so the column can be smaller and can be operated at a greater velocity. The effect of high velocity is represented by the factors (*a, b, c*), which are calculated based on the gas and liquid velocity dependence of a_e, k_L, and k_G as shown in Equation 4.1 and compared to the base case velocity. Factors (*a, b, c*) are greater than 1 and capture the enhancement of mass transfer performance as benefits of high gas and liquid velocities. The small absorber is simulated using factors instead of simulated directly as it is in Aspen Plus® to avoid flooding errors.

$$a_e \propto u_L^{0.138}, k_L \propto u_L^{0.165}, k_G \propto u_G^{0.5} \quad (4.1)$$

The crossflow has a greater L_{min} than the pump-around because the rich solvent is heated by the hot flue gas and pinches at lower rich loading. At a flowrate corresponding to 1.2*L_{min}, the optimal packing volume for the crossflow absorber is about 15% less than for the pump-around. The energy performance is worse, but crossflow can reduce the absorber capital cost and may be favored when the energy cost is low.

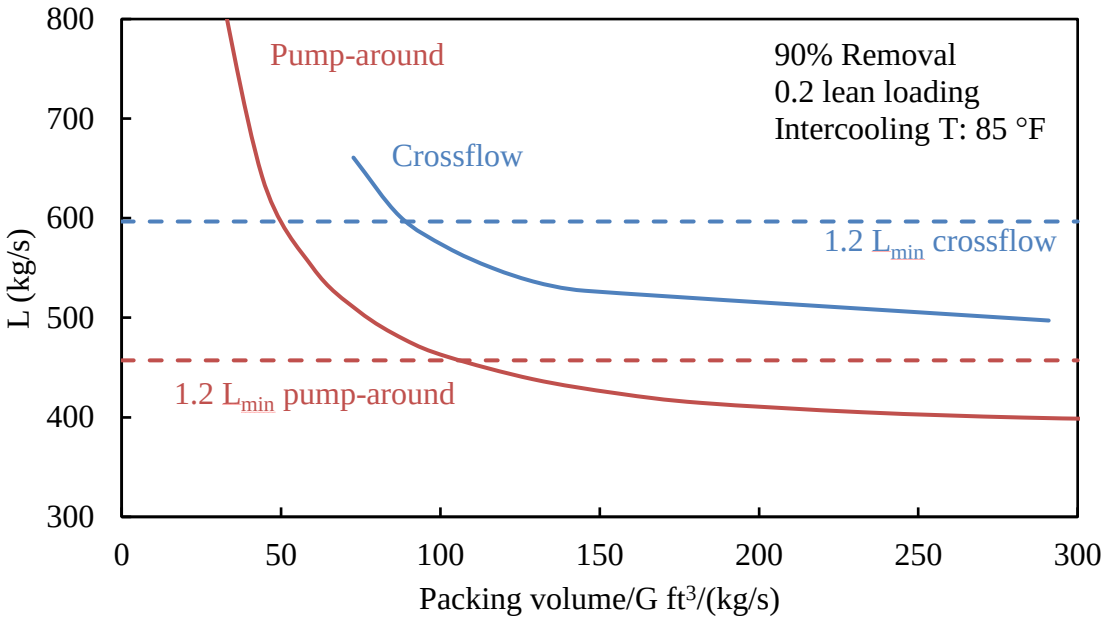

Figure 4.16: Minimum solvent flowrate (L_{min}) analysis for pump-around (red) and crossflow (blue) absorber. Dashed lines are 1.2*L_{min} for both absorber configurations.

The effect of packing geometry on absorber performance is shown in Table 4.1. Packing geometry is varied at constant packing volume. The crossflow contactor introduces an extra degree of freedom to control the gas and liquid velocity independently. The cross-section areas for gas and liquid flow are H×W and L×W, respectively. A large H and small L lead to a greater liquid velocity and smaller gas velocity and vice versa. The dimensions can be optimized for the velocities and mass transfer performance. However,

for the base case design, the geometry only has a minor effect on performance because the high temperature pinch limits the overall performance and overshadows the mass transfer performance.

Table 4.1: The effect of packing geometry on crossflow absorber at 90% removal

H (ft)	60	45	45
L (ft)	30	40	30
W (ft)	30	30	40
Volume (ft^3)	54000	54000	54000
G (kg/s)	300	300	300
Removal	0.90	0.90	0.90
Rich loading	0.3839	0.3843	0.3840

To mitigate the high temperature-induced mass transfer pinch and improve the absorber performance, configurations with extra intercooling as shown in Figure 4.17 are proposed and simulated. For the 3-path column shown on the left, the solvent is fed to one third of the top area, collected at the bottom, intercooled, and sent to the next section on the top left. The liquid velocity is 50% greater than the 2-path configuration because each cross-section area is smaller. For the configuration on the right, a second intercooler is added to the middle of the left section to address the high temperature near the rich end directly. With the same packing volume, the 3 paths and 2 paths absorber achieve 90% CO_2 removal at rich loadings of 0.384 and 0.396, respectively. For the 3 paths column, the rich solvent is still heated by the high temperature flue gas, which leads to the pinch and is similar to the column with one intercooler. Figure 4.18 shows the CO_2 removal and liquid temperature profiles for the 2 paths column. The second cooler in the middle creates a local low temperature region, cools the rich solvent to about 47 °C, and improves the absorber

performance. With the second intercooler, the crossflow can achieve same rich loading as the pump-around absorber.

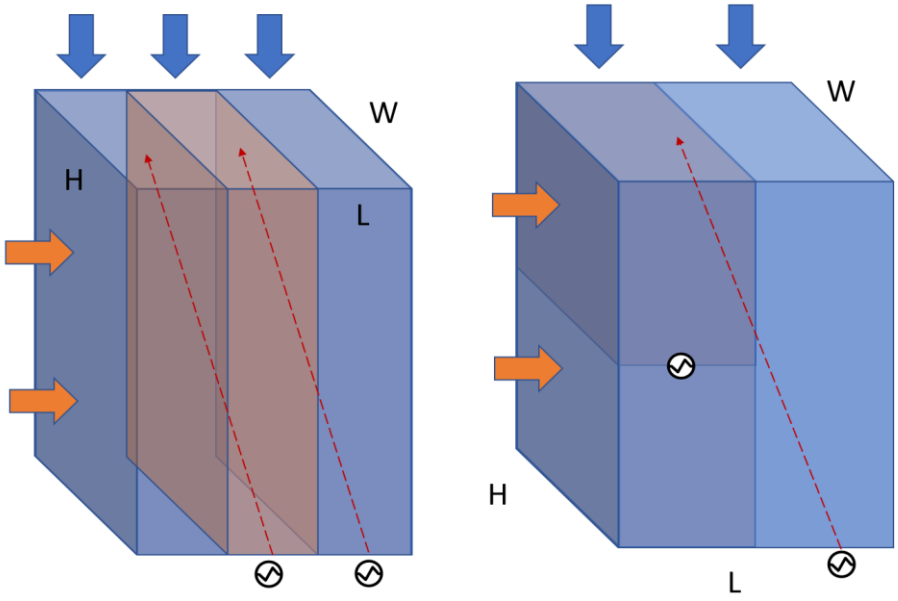

Figure 4.17: Crossflow absorber with 2 intercoolers: 3 paths (left) and 2 paths (right). The blue and orange arrows are liquid and gas flow directions.

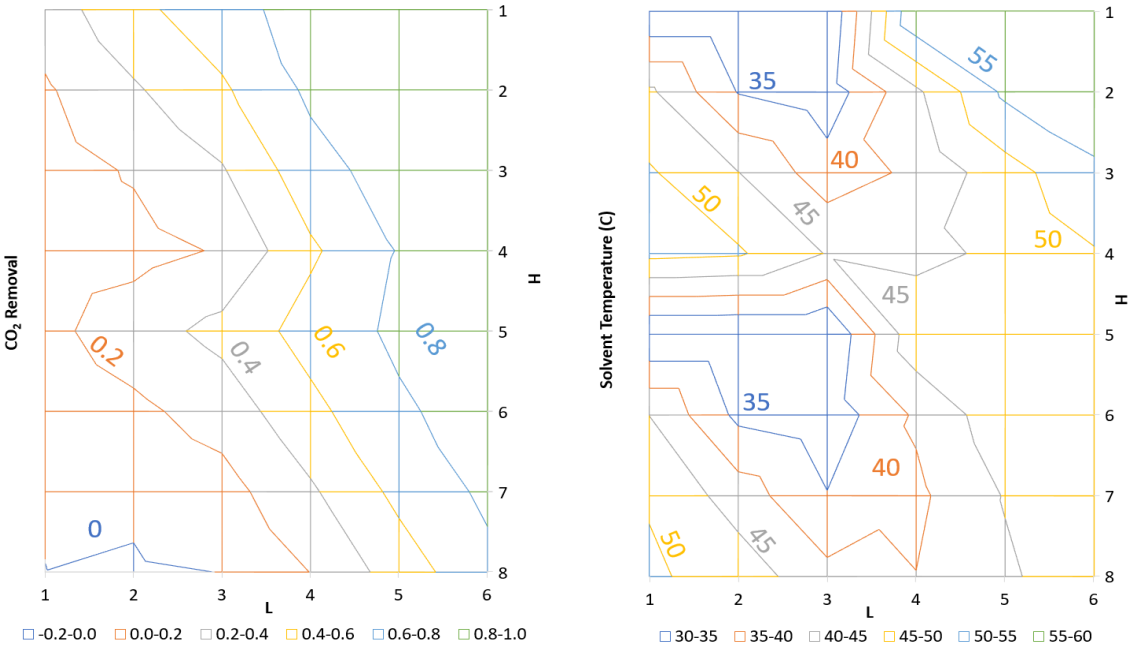

Figure 4.18: CO_2 removal and liquid temperature profiles for the 2 paths crossflow absorber with 2 intercoolers at 90% removal. The 6×9 matrix represents the slab of 30×40×5 ft^3 (L×H×W).

The 2-intercooler configuration shown on the right side of Figure 4.17 draws solvent from the middle of the packing section and redistributes it, which requires a packing break and liquid redistribution. Figure 4.19 proposes a modified configuration that is easier to implement: 1 vertical packing is broken into 2 sections and placed parallel to each other. Solvent flows through packing section 1-4 in sequence and 2 intercoolers are set between sections 2 and 3, 3 and 4. Compared to the pump-around absorber, multiple pumps are required to provide liquid head for each section, but the flowrate for these pumps is the same as the lean solvent, which is about one third of the pump-around flowrate.

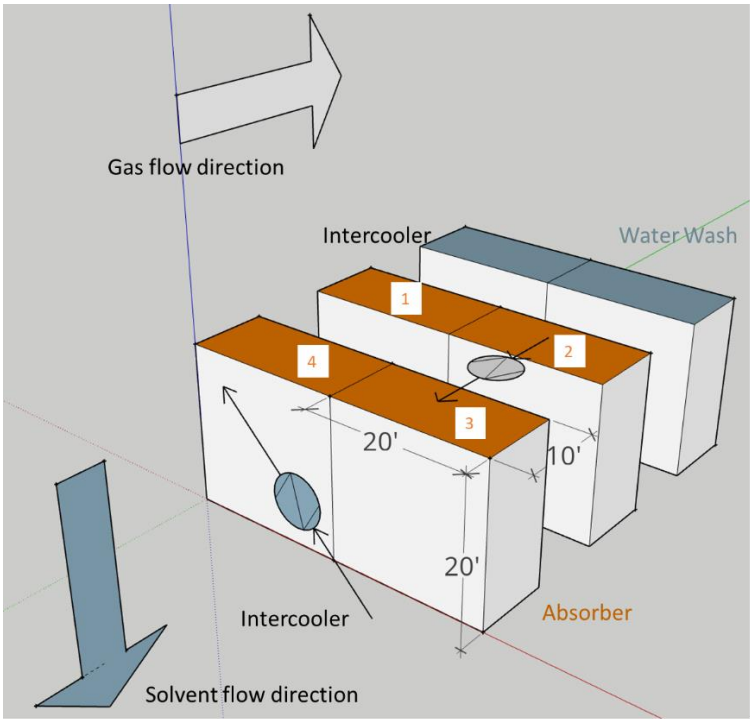

Figure 4.19: Arrangement of crossflow absorber with 2 intercoolers. The numbers shown on the absorber indicate the sequence of solvent flow.

Figure 4.20 shows two possible liquid flow patterns for the crossflow absorber with 2 intercoolers. The driving force for CO_2 absorption is slightly different for each section. The flue gas entering section 1 in flow pattern A has a lower CO_2 concentration than pattern B. Simulations show that the overall performance for pattern A is slightly better than B and the following analyses all show the results for pattern A.

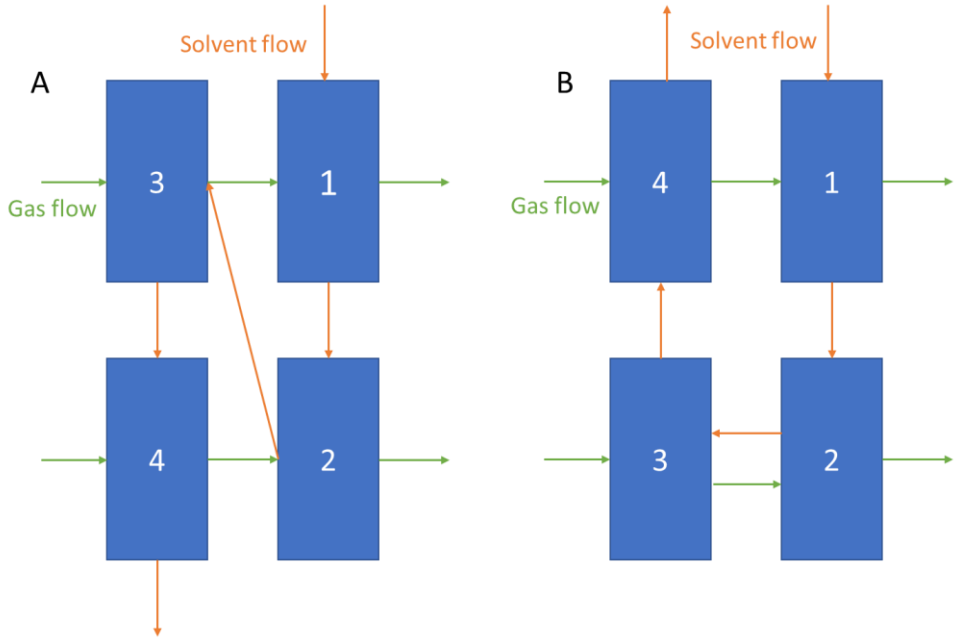

Figure 4.20: Top view of two liquid flow patterns for the crossflow absorber arrangement with 2 intercoolers. The numbers shown on the absorber indicate the sequence of solvent flow.

Figure 4.21 compares the performance of the pump-around absorber and crossflow absorber with 2 intercoolers at 90% removal when the packing volume is varied at the same gas condition. Similar to the L_{min} analysis shown in the previous section, the crossflow with 2 intercoolers should be considered for small column designs. When the packing volume is reduced, the absorber is less equilibrium-controlled and could be better than the pump-around because of the better mass transfer performance caused by high liquid velocity.

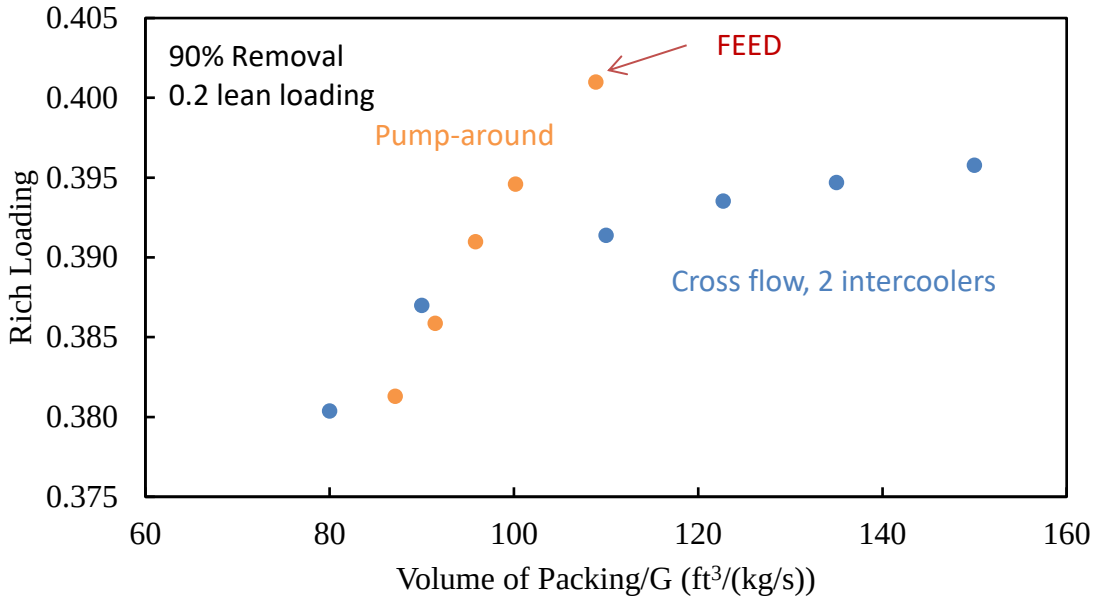

Figure 4.21: Comparison of pump-around and crossflow absorber for 90% CO2 removal at various packing volume

4.4 CONCLUSIONS

Two types of innovative absorber designs—hybrid and crossflow absorbers, are proposed and simulated using Aspen Plus® as the intensification of pump-around absorber.

The hybrid and crossflow absorbers are more compact than the pump-around. The open volume between packing sections and the volume for turning gas are eliminated by using one section only and by avoiding changing gas flow direction.

For the hybrid configuration, at least 3 sections in series are required so the L/G is large enough to manage the column temperature. More columns lead to greater L/G, more cooling abilities, and better energy performance, but also increase the capital cost. The base case design is worse than the pump-around because the cooling temperature is constrained to maintain the water balance and cannot be lower than 43 °C The optimized configuration

take advantage of the high CO_2 concentration from the boiler and achieve the same performance as the pump-around absorber.

The crossflow absorber is simulated using matrix arrangement of countercurrent absorber elements. The base case design indicates a worse performance than the pump-around absorber because of the high temperature-induced mass transfer pinch. Adding a second intercooler near the rich end reduces the solvent temperature significantly and improves the absorber performance. The crossflow absorber design features small size and high velocity, it is favored when the relative capital cost is high and energy cost is low.

4.5 RECOMMENDATIONS

The crossflow absorber is simulated using in the countercurrent modeling framework in Aspen Plus®. This method requires minimum effort on model development and represents the initial estimation of crossflow absorber. Further studies on crossflow contacting, mass transfer performance, and economics are required for a comprehensive evaluation of the innovative design.

Chapter 5: Absorber Design for High CO_2 removal using Aqueous Piperazine for Gas Turbines

5.1 INTRODUCTION

Climate change is one of the biggest challenges facing the world in the 21st century. According to the latest Intergovernmental Panel on Climate Change (IPCC) report, to limit global warming to 1.5 °C, the world needs to reduce carbon emissions by more than 49% of the 2017 level by 2030 and achieve carbon neutrality by 2050 (Masson-Delmotte et al., 2018). To achieve this aggressive goal, implementing carbon capture and utilization (CCS) will be a critical pathway.

Historically, amine scrubbing has focused on removing 90% of the CO_2 from flue gas during the technology development. During the early stage of research, the 90% removal target was inherited from previous experience with flue gas desulfurization (FGD) and was found a reasonable target to balance technical feasibility and economic performance. Rao and Rubin studied the effect of CO_2 capture rate and estimated the optimum for a coal power plant is around 81%-87% using 30 wt% monoethanolamine (MEA) (Rao and Rubin, 2006). Similar estimation by Abu-Zahra et al showed the cost per tonne CO_2 avoided was flat between 80% and 95% removal (Abu-Zahra et al., 2007). These studies used first generation solvent and process such as MEA without absorber intercooling and could be improved by recent progress on process simulation and optimization.

The development of second generation of amine solvent and process shows that capturing greater than 90% CO_2 is feasible. Pilot plant demonstrations at the National Carbon Capture Center (NCCC) achieved 99.91% capture rate from pulverized coal-fired (PC) plant using MEA (Morgan et al., 2018). The PZAS process, a benchmark of a second-generation amine solvent, was also capable of capturing 99.1% CO_2 from coal flue gas and

95.8% from NGCC flue gas based on the pilot plant tests at NCCC (Gao and Rochelle, 2019; Gao et al., 2019). Petra Nova recently reported a 92.4% capture rate through their 3-year demonstration period (Kennedy, 2020). It is well-established that amine scrubbing can do better than 90% capture rate.

Previous studies on high CO_2 capture rate only focused on coal-fired flue gas, and the process was not fully optimized for higher CO_2 capture. Natural gas is cleaner and produces less CO_2 per unit power generated compared to coal. In places where gas is readily available, gas will dominate the electricity production in the future. Therefore, capture on NGCC flue gas is equally important. Higher capture rate on NGCC flue gas is more difficult because of the low CO_2 concentration and the temperature bulge near the absorber top (Gao and Rochelle, 2019). Absorber design for higher capture rate is more important and needs to be optimized. 99% removal on NGCC is an interesting case to study because the exhaust after capture contains about 400 ppm of CO_2, meaning net zero emission of the power plant. Being able to achieve carbon neutrality for power plant using amine scrubbing alone will greatly improve the competitiveness of the technology.

This chapter focuses on the absorber design for greater than 90% removal of NGCC flue gas using 5 *m* PZ, demonstrates the technical feasibility to achieve 95% to 99% removal, and compares the performance of conventional absorber with the two innovative designs introduced in Chapter 4.

5.2 METHOD

The Independence model with 8% PZ adjustment is used to simulate the absorber performance at high CO_2 removal. The model is validated with pilot plant experiments with 4% CO_2 at NCCC, and most of the tests achieved about 90% removal. The pilot plant absorber has 40 ft packing and making the performance mainly controlled by rich-end

equilibrium. The highest CO_2 removal achieved during the pilot plant test was 95.8%. Simulating higher removal represents an extrapolation of the model and could introduce uncertainties because the equilibrium at the lean-end becomes more important at higher removal.

All the cases are designed at the base case E-007 for the FEED are shown in Table 3.1.

5.3 RESULTS AND DISCUSSION

5.3.1 Pump-around absorber

The FEED absorber design eliminates the DCC and trim cooler to reduce the capital cost and uses low intercooling temperature (29.5 °C) to improve the performance. The trim cooler was found unimportant for 90% removal for two reasons. The 0.2 lean loading is low enough to provide the mass transfer driving force for 90% removal and the high temperature region caused by hot solvent feed is only limited in a small portion of the column because of the low L/G. The heat carried by the solvent is small compared to the enthalpy of the gas. However, the lean temperature becomes more important at higher removal. CO_2 absorption pinches near the lean end for high removal and lowering temperature improves the driving force significantly.

A lower column temperature always improves absorber performance, but the temperature is constrained by the water balance. Figure 5.1 demonstrates the strategy to maintain water balance in a conventional absorber design with DCC and without DCC as in the FEED design. For the conventional design with DCC, the flue gas is first cooled to around 40 °C, saturated at this temperature, and contains about 7% water. Excess moisture is removed before entering the absorber. When the gas leaves the system, the water content is controlled by the water wash so that the amount of water leaving the system is the same

as the amount entering. This set the water wash temperature about 2 °C higher than the DCC because the total gas flowrate leaving the system is smaller than the feed as CO_2 being absorbed. The water balance also constrains the trim cooler because water needs to be condensed in the water wash, meaning the temperature of gas leaving absorber needs to be higher than the gas leaving water wash. For example, in the conventional design, the gas leaves absorber at 45 °C and then cooled to 42 °C before leaving the system. For the conventional design, the column temperature is set by DCC and can be lower when the cooling is available and to enhance the absorber performance.

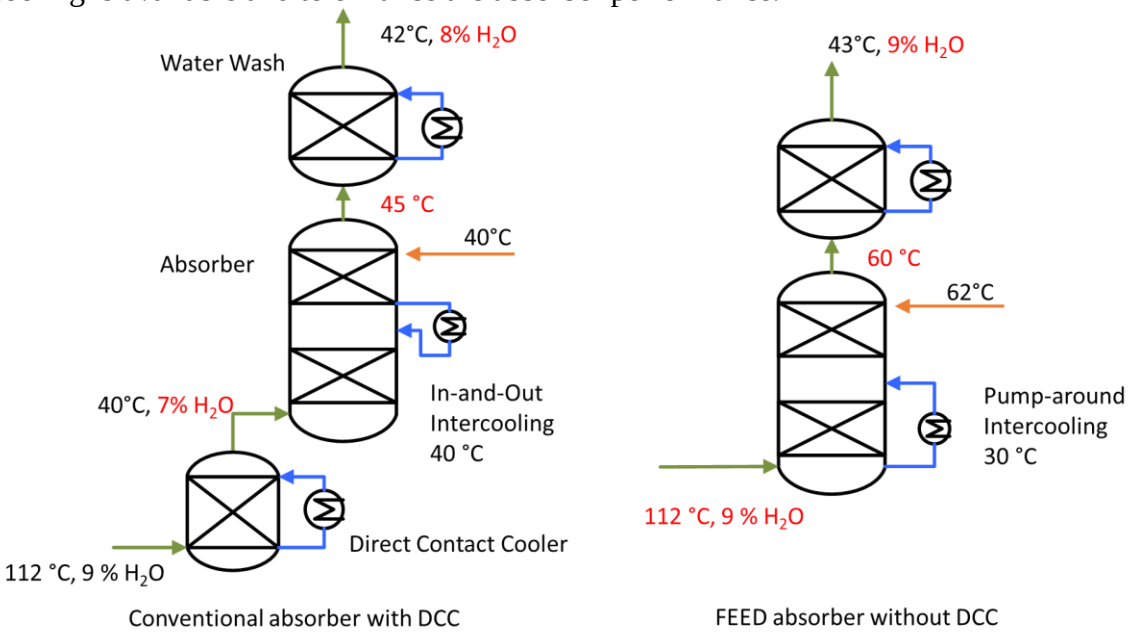

Figure 5.1: Demonstration of strategies to maintain water balance for conventional absorber design with DCC (left) and FEED absorber without DCC (right).

However, for the FEED absorber design without DCC, the hot flue gas containing 9% water enters absorber directly. This water concentration set the temperature of gas leaving the system at 43 °C. Temperatures of water wash and absorber top are slightly higher than the conventional design and cannot be lower even if extra cooling is available.

The FEED design reduces the cost of DCC but is less flexible to vary column temperature while keeping the water balance. The temperature of trim cooler also needs to be high enough so that the gas leaving the absorber is above 43 °C.

Figure 5.2 compares the absorber performance for the FEED absorber without and with trim cooler. Rich loading is used to indicate the operating cost and energy performance. Greater rich loading means smaller solvent circulation rate and lower heat duty. The trim cooler temperature is varied so the gas leaving the absorber is 43 °C. When the solvent rate increases to achieve higher removal, the trim temperature also increases to avoid excessive cooling of the gas and to keep the water balance. The higher temperature further deteriorates the removal performance and defines the maximum CO_2 removal.

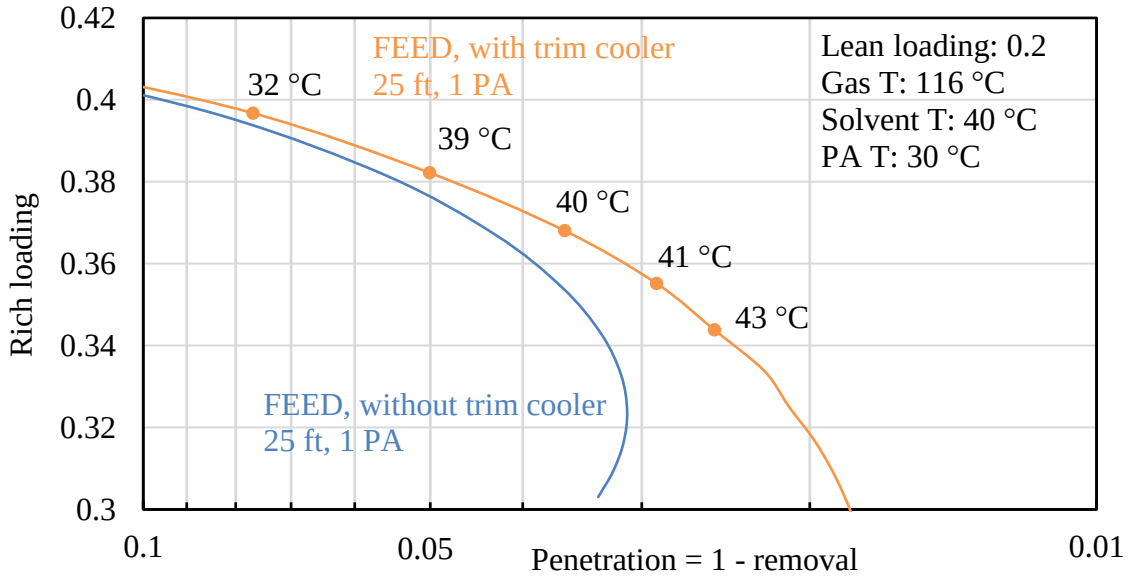

Figure 5.2: Absorber performance at high CO_2 removal for pump-around without trim cooler (blue curve) and with trim cooler (orange curve) (No DCC). The solvent rate is varied to achieve the desired removal. The minimum trim cooler temperature that maintains the water balance is labeled.

Adding packing or intercoolers in the absorber can improve the performance and achieve higher removal. Figure 5.3 compares the performance of the absorber using 1

intercooler with various packing heights and double pump-around intercooling. Compared to the 25 ft design, 15 ft of additional packing increases the rich loading from 0.32 to 0.39 at 98% removal, which is a 58% reduction in the solvent circulation rate. With 40 ft packing, the L/L_{min} equals to 1.15 and the rich loading for 98% removal decreases by 8% compared to 90%. This 8% represents the penalty for providing additional driving force to achieve higher removal.

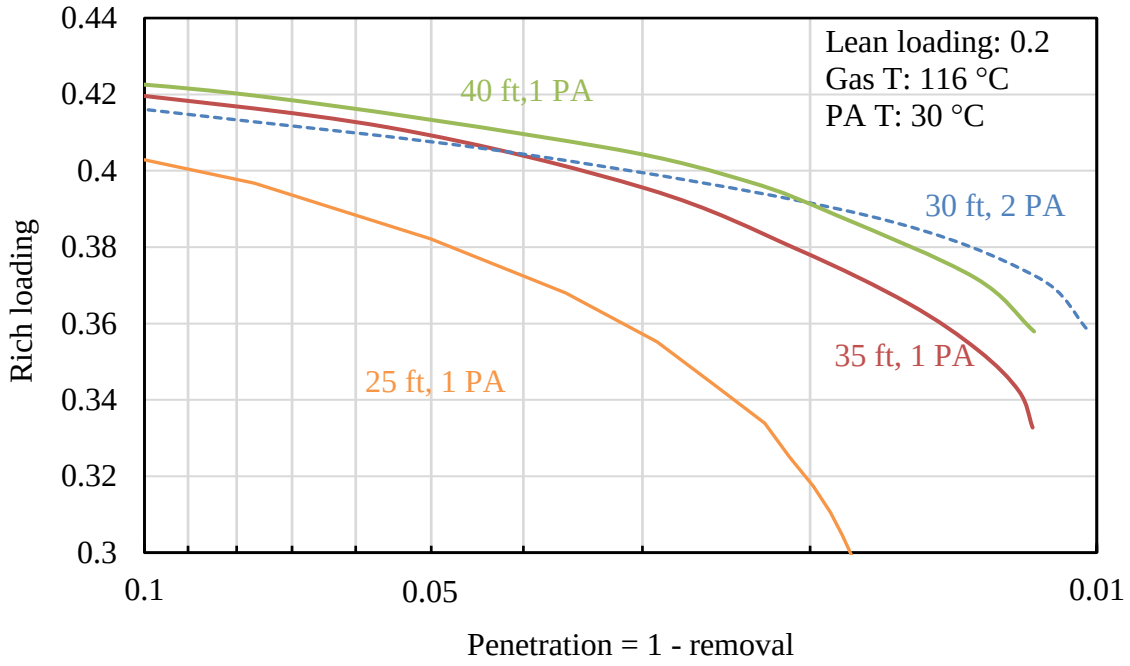

Figure 5.3: Absorber performance at high CO_2 removal for pump-around with 25 ft (orange), 35 ft (red), and 40 ft (green) packing and double pump-around configurations.

Another option to improve absorber performance for higher removal is to use one additional pump-around loop to manage the column temperature. The blue curve in Figure 5.3 shows the performance using intercoolers and 30 ft packing. There are 3 sections of packing and pump-around intercoolers are applied to the bottom two sections. The double pump-around only shows a higher rich loading for removal greater than 98% where the equilibrium matters the most.

None of the absorber configurations shown in Figure 5.3 can achieve 99% removal with good energy performance. The performance deteriorates steeply above 98% because of the equilibrium limits. Lowering the column temperature near the top section or lowering the lean loading can improve the absorption driving force, but they introduce additional cost or problems. The column temperature is set by the water balance for currently design, a DCC column is required to control the water entering the system so the column can be running at a lower temperature. For lean loading, solid precipitation is a practical issue for 5 *m* PZ. The transition temperature for 0.2 loading is 22 °C and it increases at lower lean loading. Lowering temperature and loading will increase the risk of PZ precipitating out on the trim cooler.

5.3.2 Hybrid Absorber

At 90% removal, the hybrid absorber is worse than the pump-around design because the intercooler temperature is constrained by the water balance and cannot be as low as the pump-around. To improve the design for higher CO_2 removal, additional packing is added as shown in Figure 5.4. This two-section column design is similar to the pump-around absorber and improves the flexibility of intercooling temperature. For the top section, the lean solvent is distributed to the packings then collected by the chimney tray. All the liquid from the top is sent to only one third of the section on the bottom and contacts with one third of the gas, which increases the L/G ratio by 3. There are two intercoolers between the three bottom sections. This configuration keeps the large L/G and intercooling capability in the pump-around absorber and avoids solvent back-mixing. The exchangers are about the same size because of the similar heat duty. There are more pumps used in this configuration, and each one needs a spare. However, these pumps are smaller than the

pump-around design because they only deliver the lean flow whereas the pump-around circulates 3 times more solvent.

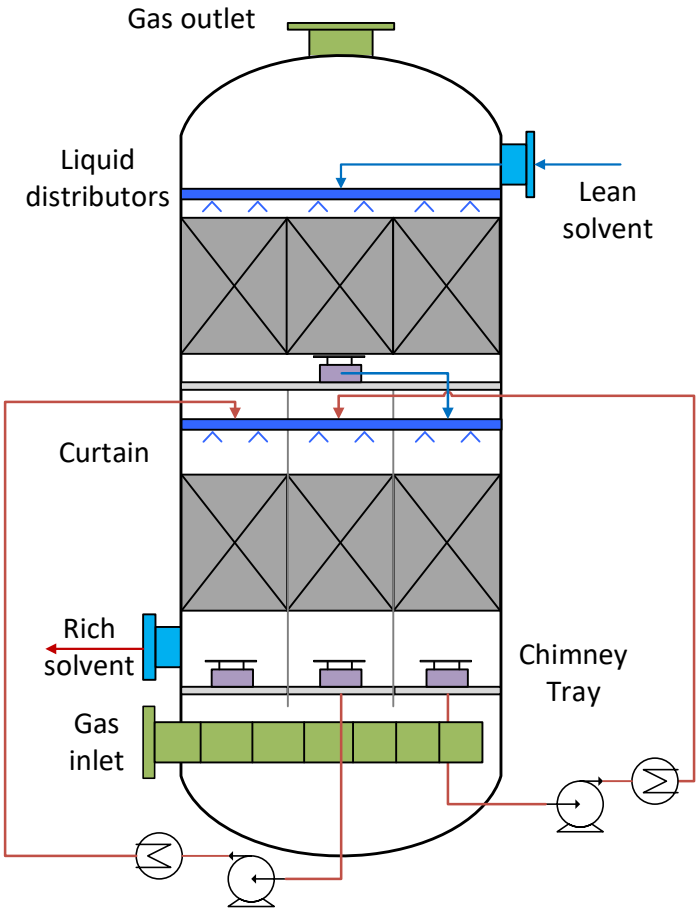

Figure 5.4: Hybrid absorber design for high CO_2 removal.

Figure 5.5 compares the performance of pump-around and hybrid absorber. Two absorbers are designed with same amount of packing volume and same cooling temperatures. The pump-around absorber outperforms the hybrid below 95% removal because the pump-around enhances the bottom L/G to a large ratio by circulating more solvent while the hybrid can only increase it by three times. As the removal increases, the lean flowrate increases, and the hybrid absorber starts to perform better with better cooling.

The hybrid also avoids back mixing and preserves the driving force better. However, 99% removal is not achieved because of the temperature and equilibrium limits.

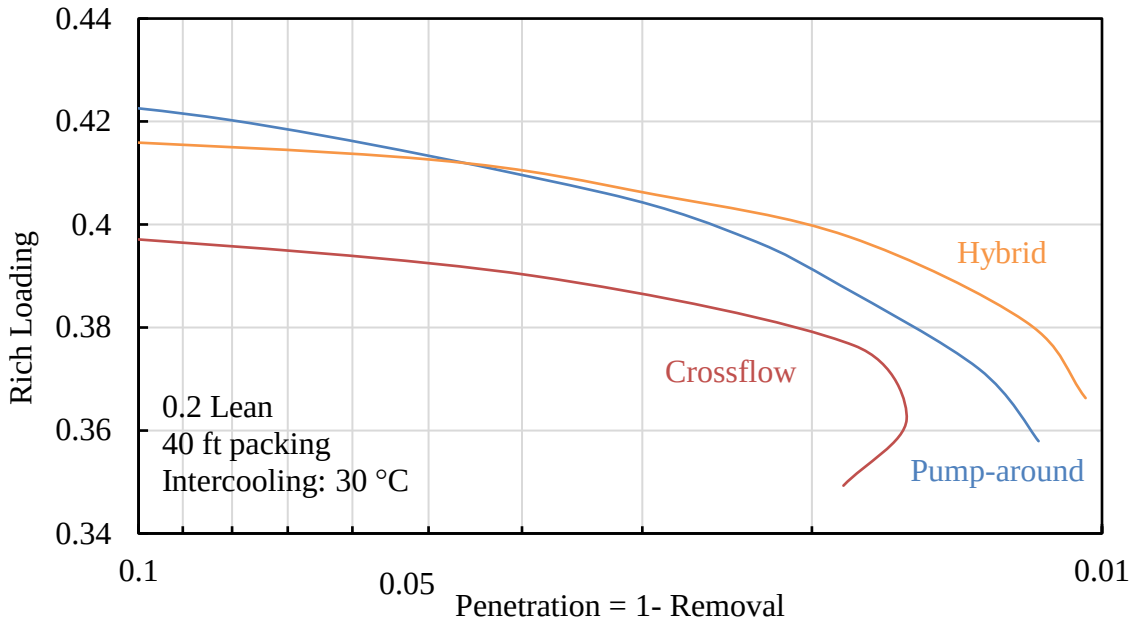

Figure 5.5: Absorber performance at high CO_2 removal for pump-around (blue), hybrid (orange), and crossflow absorber (red).

5.3.3 Crossflow absorber

The performance of a crossflow absorber is also shown in Figure 5.5. The rich loading with crossflow is consistently lower than the pump-around and hybrid absorber because the rich solvent is heated by the hot flue gas. The comparisons are made for configuration using same amount of packing, and the crossflow absorber will perform better for smaller sized column.

Because of the temperature and equilibrium limitation, neither absorber design achieves 99% removal with reasonable rich loading. An additional DCC column is required to manage the water balance and to reduce the column temperature. Figure 5.6 demonstrates the effect of lowering temperature by using a DCC. The DCC is running at

30 °C and the trim cooler is running at 35 °C. All three designs can achieve 99% removal with rich loading around 0.36 to 0.39. Compared to the FEED absorber designed for 90%, the rich loading decreases by less than less than 10%. The major cost increase is reflected in the absorber capital cost, including the DCC, trim cooler, and 15 ft extra packing.

The hybrid absorber shows the best performance for high removal because it takes advantage of the high L/G and avoids the solvent back-mixing. The crossflow absorber gains the most benefit from the addition of the DCC because the flue gas entering absorber now is cold and can cool the rich solvent and increase the rich loading.

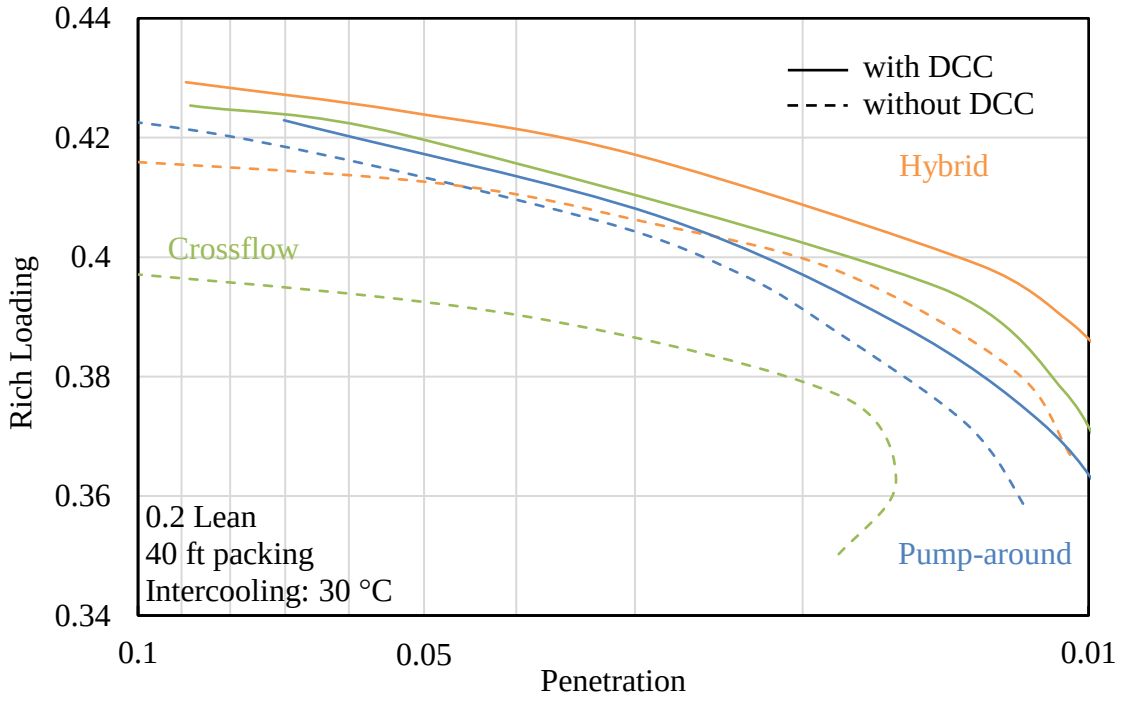

Figure 5.6: Compare absorber configurations with (solid lines) or without (dash lines) at high CO_2 removal for pump-around (blue), hybrid (orange), and crossflow absorber (red).

5.4 Conclusions

With the development of amine scrubbing technology, greater than 90% removal becomes more important. This chapter compares performance of pump-around, hybrid, and

crossflow absorbers for high CO_2 removal and proposes modifications to the base case design.

With 40 ft packing (L/L_{min} = 1.15), the pump-around absorber can achieve 98% removal with a rich loading of 0.39. Compared to the 90% base case, the major cost increase is in the absorber section, including a trim cooler and 15 ft extra packing. The hybrid absorber performs better than the pump-around when removal is greater than 95%. However, because of the temperature limitation to maintain the water balance, absorbers without a DCC cannot achieve 99% with reasonable energy performance at 0.2 lean loading.

A DCC is required to achieve 99% removal and it will increase the cost for capture. All the configurations can achieve 99% removal and the rich loading decreases by less than less than 10% compared to 90% removal. The hybrid absorber has the best performance and crossflow absorber benefits the most from the DCC.

5.5 RECOMMENDATIONS

The process model was validated with pilot plant experiments at NCCC for 90% removal, and those cases are mainly equilibrium controlled at rich end. When extrapolating the model to 99% removal, the equilibrium in the lean end is more important. More pilot plant experiments at higher CO_2 removal should be run and used to validate the equilibrium model at the lean conditions.

This chapter focuses on the analysis of absorber performance and the process fundamentals. Economics analysis should be done using the detailed cost estimate from the FEED to provide quantified conclusions on the cost of higher removal and the benefits of innovative absorber design.

Chapter 6: Evaluation of High Removal for CO_2 Capture using Aqueous MEA

6.1 INTRODUCTION

Amine scrubbing is the most mature technology for post-combustion carbon capture. Most pilot-scale demonstrations and process optimizations for amine scrubbing have been focused on CO_2 capture at 90% removal. Recent progress on process development shows that capturing greater than 90% CO_2 from power plants is feasible. A pilot plant demonstration at National Carbon Capture Center (NCCC) achieved 99.91% capture from a pulverized coal (PC) plant using monoethanolamine (MEA) (Morgan et al., 2018). Piperazine (PZ), a benchmark of second-generation amine solvents, was also capable of capturing 99.1% CO_2 from coal flue gas and 95.8% from Natural Gas Combine Cycle (NGCC) flue gas based on the pilot plant test at NCCC (Gao and Rochelle, 2019; Gao et al., 2019). Petra Nova, the world's largest capture facility, recently reported a 92.4% capture rate through their 3-year demonstration period (LLC, 2020). It is well established that amine scrubbing can exceed a 90% capture rate.

Rigorous economic analysis using validated process models for higher CO_2 removal has not been performed. Rao and Rubin studied the CO_2 capture rate and estimated the optimum for a coal power plant is around 81–87% using 30 wt % MEA (Rao and Rubin, 2006). Similar estimation by Abu-Zahra et al. showed the cost per tonne CO_2 avoided was flat in the range between 80% and 95% removal (Abu-Zahra et al., 2007). These studies were performed during the early stage of process development and could be improved by recent progress on process simulation and optimization. A similar study was done by private technology providers. Mitsubishi Heavy Industries (MHI) modeled the advanced KM CDR process and demonstrated that zero-emission can be achieved at 6% incremental cost compared to 90% capture (Hirata et al., 2020). SaskPower reported that the new carbon

capture project at Shand Power Station would be designed at 95% removal instead of 90% based on the sensitivity analysis, but the detailed economic analysis was not revealed (Bruce et al., 2018).

This work aims to evaluate the economics of deep decarbonization (>90% CO_2 capture) of flue gas from both coal-fired and NGCC power plants, using the conventional 30 wt % MEA. MEA the benchmark first-generation solvent for amine scrubbing and is used in this study to represent the general performance of amine scrubbing technology. The main objective is to evaluate the incremental cost for different CO_2 removal rates and determine the optimal removal for amine scrubbing. The process optimization and equipment design for higher CO_2 removal are also studied using a rate-based MEA model.

6.2 METHODS

6.2.1 Simulation Methods

The rigorous rate-based MEA model developed in Aspen Plus by Carbon Capture Simulation for Industry Impact ($CCSI^2$) was used in this study (Morgan et al., 2017; Morgan et al., 2018). This model consists of solvent physical properties, reaction kinetics, and packing characterization sub-models, and is validated with pilot plant experiments at NCCC over a wide range of operating conditions (Morgan et al., 2018; Soares Chinen et al., 2018).

6.2.2 Costing Methods

The detailed equipment designs were developed based on heat and material balance from the simulation. Purchase Equipment Costs (PEC) was estimated by using a combination of quote from Aspen In-Plant Cost Estimator and from Engineering Procurement and Construction (EPC) firms. The associated cost for installation, support,

and labor is scaled based on the equipment size. The choice of scaling factor for size follows the methodologies recommended by NETL (Turner et al., 2019). Total Plant Cost (TPC) for CO_2 capture and compression system is estimated using a Lang factor on the PEC. (Peters et al., 1968). A value of the Lang factor (5.1) was estimated by EPC firm and used for this work, and it is close to the factor for fluid-processing plants (4.83) suggested in the literature.

The annualized capital cost is calculated using Capital Charge Factor (CCF) as shown in Equation 6.1. Based on the recommendation by NETL, PC and NGCC cases with CO_2 capture are classified as high-risk project. With an operational period of 30 years, CCFs of 0.124 and 0.111 are used for natural gas plants and coal plants because of the difference in the capital expenditure period (3 years for NGCC and 5 years for PC) (NETL, 2012).

$$CAPEX = \frac{TPC \times CCF}{CO_2 \ captured \ per \ year} \tag{6.1}$$

where:

CAPEX: annualized capital cost, $\left(\frac{\$}{tonne\ CO_2}\right)$;

TPC: total plant cost, estimated by Lang factor × PEC;

CCF: capital charge factor, converting the total cost to annual basis

The operating expenditure (OPEX) includes the utilities cost of steam, electricity, and cooling water. These utilities are extracted from the power plant at a fixed cost.

The economic model generally follows the methodology for CO_2 capture recommended of NETL with some simplifications. The fixed CAPEX and OPEX is neglected because they are independent of CO_2 removal and will not affect the incremental

cost. The important conclusions from this work are the difference between costs at variable CO_2 removal rather than the absolute values because this work does not aim to provide an accurate and comprehensive cost estimate.

6.3 RESULTS AND DISCUSSION

6.3.1 Process Description and design basis

The general absorption-stripper process using 7 *m* MEA is shown in Figure 6.1. Flue gas from coal-fired power plant must be pretreated to reduce the SO_2 content before entering the capture process. The pretreated coal flue gas or NGCC flue gas is cooled using a direct contact cooler (DCC) that fed to the absorber. Flue gas flows up and countercurrently contacts the solvent in the absorber. Intercooling is applied in the middle of the column to remove the heat generated during absorption. The conventional in-and-out intercooling collects the solvent from the top section, cools it, and sends it to the next section. The gas leaving the absorber flows through a water wash section to control the amine emission and maintain the water balance in the system. The rich solvent leaving the absorber is pumped to stripper pressure and sent to regeneration. The cross exchanger preheats the rich solvent and recovers the sensible heat from the lean solvent. A reboiler in the stripper provides the heat for regeneration. The CO_2 and water vapor from the top of the stripper are cooled and separated and the CO_2 product is then purified and compressed to the pipeline pressure.

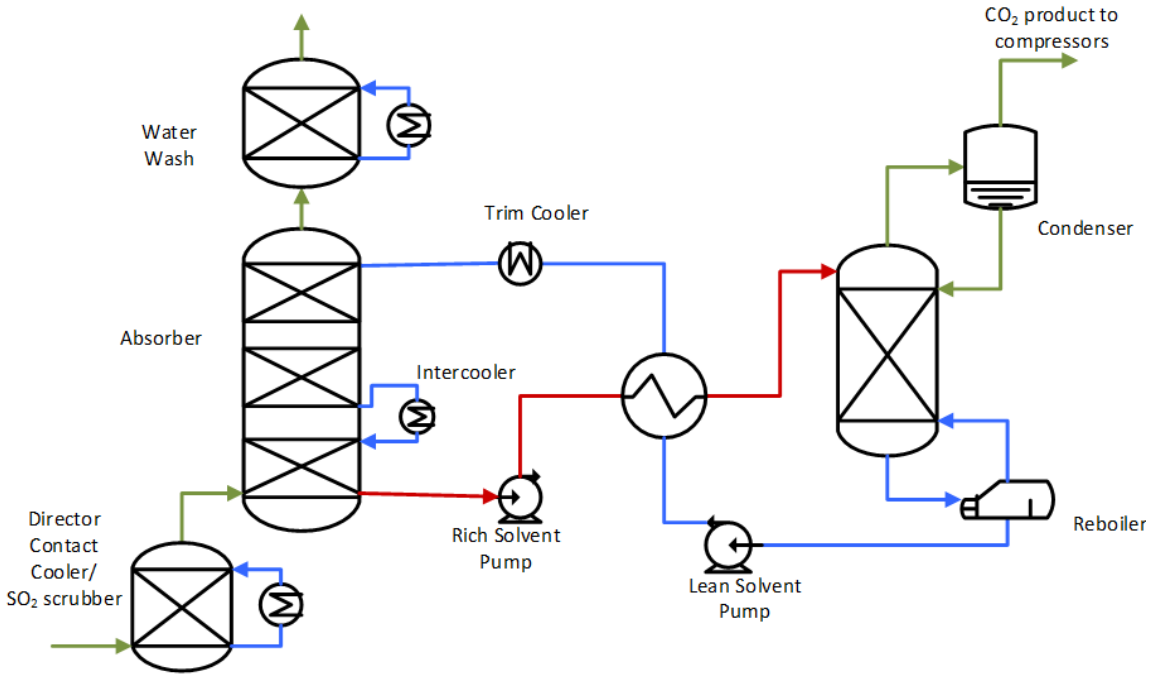

Figure 6.1: Simplified process flow diagram of MEA simple stripper process.

The flue gas specifications and design basis are from the 2019 DOE baseline for PC and NGCC power plants with CO_2 capture units (Case B12B and Case B31B), and the details are summarized in Table 6.1. Two absorber trains are used to treat the large volume of gas flow, and the solvent from two absorbers is combined and sent to one stripper column for regeneration. The absorber using in-and-out intercooling and the strippesr are designed at 70% flooding. For the pump-around absorber, the column is sized for 80% flooding for the pump-around section with a greater solvent flowrate, and the top section is at about 50-60% flooding. For PC flue gas, the integrated SO_2 scrubber and DCC are used as in the NETL baseline report. For the NGCC, the DCC section is integrated with the absorber column. Sulzer MellapakPlus^{TM} 252Y structured packing is used for both absorbers and strippers. The cross exchanger is designed at 10 °C logarithmic mean

temperature difference (LMTD). Two eight-stage compressors are used to compress the CO_2 product to 2200 psig for CO_2 transportation and storage.

Table 6.1: Flue gas specification for PC and NGCC power plant based on NETL baseline.

	PC (Case B12B)	NGCC (Case B31B)
Temperature (°C)	57	111
Flowrate (kg/hr)	3386000	3927000
Mole fraction, CO_2	0.125	0.040
Mole, fraction, H_2O	0.150	0.088
Mole fraction, N_2	0.689	0.752
Mole fraction, O_2	0.036	0.120

To study the incremental cost of high CO_2 capture, evaluate the system performance, and provide guidance for selecting a removal target, three scenarios are proposed. Case 1 is a base case design of a capture unit aimed at 90% removal. Case 2 examines the system performance and capture cost using the equipment specifications from Case 1 to represent the ramping-up of existing capture plant. Case 2 is a suboptimal design for higher capture and is likely to be limited by the capacity of the process equipment, but it takes advantage of the overdesigned features of the existing plant and increases the CO_2 production. Case 2 also reveals strategies on flexible operation and the cost for extra CO_2 capture after the capture plant is built. For Case 3, the capture unit will be designed and optimized for a higher removal. The cost to achieve high removal is minimized by process optimization, which is important for industry and policymaker to evaluate technology and its potential to achieve zero CO_2 emission, or even negative emission.

6.3.2 Absorber performance

The absorber is the most important piece of equipment in comparing variable CO_2 removal, and the optimization of the absorber plays an essential role in reducing the cost at high removal. This chapter mainly focuses on optimizing the absorber. The key process variables to be optimized include packing height, solvent flowrate, column temperatures, and intercooling configurations.

6.3.2.1 Absorber packing height

The absorber packing height represents the tradeoff between capital cost and energy cost. Increasing absorber packing height provides more mass transfer area for CO_2 absorption, reduces the solvent circulation rate, and improves the energy performance. The optimization of absorber packing height follows the rule of thumb using the concept of minimum flowrate (L_{min}) as demonstrated in Figures 6.2 and 6.3.

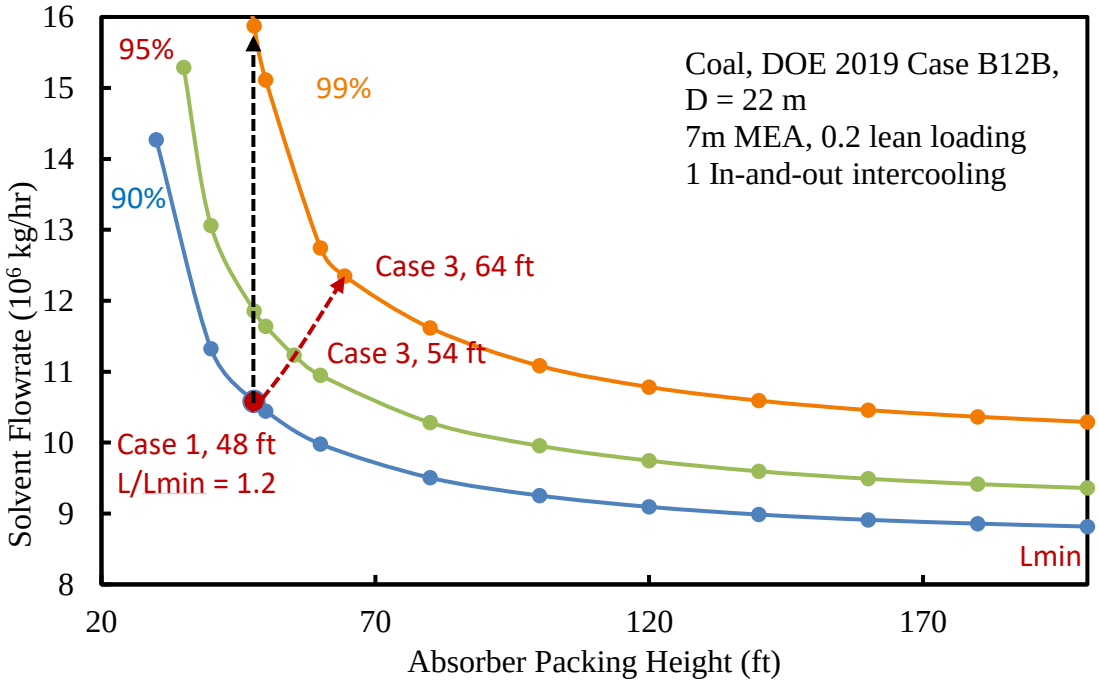

Figure 6.2: Absorber packing height and the optimization using L_{min} for PC flue gas.

As the packing height in the absorber increases towards "infinity" and the mass transfer area does not limit the performance, the solvent circulation rate approaches a minimum, and it represents the minimum absorption driving force required for given CO_2 removal. Based on previous literature, the optimal absorber packing height usually gives a solvent rate in the range of 1.1-1.3 L_{min}. In this work, $L/L_{min} = 1.2$ is used for the packing height optimization (Sachde, 2016). Figures 6.2 and 6.3 show the trade-off for absorber packing height for PC and NGCC flue gas at different removal conditions. The red point at 90% removal defines Case 1: optimized absorber packing height for 90% removal. The black dashed line represents the Case 2, where the equipment is designed for 90% removal but operated to capture more CO_2. The red dashed line is the absorber height optimization for higher CO_2 removal and corresponds to Case 3.

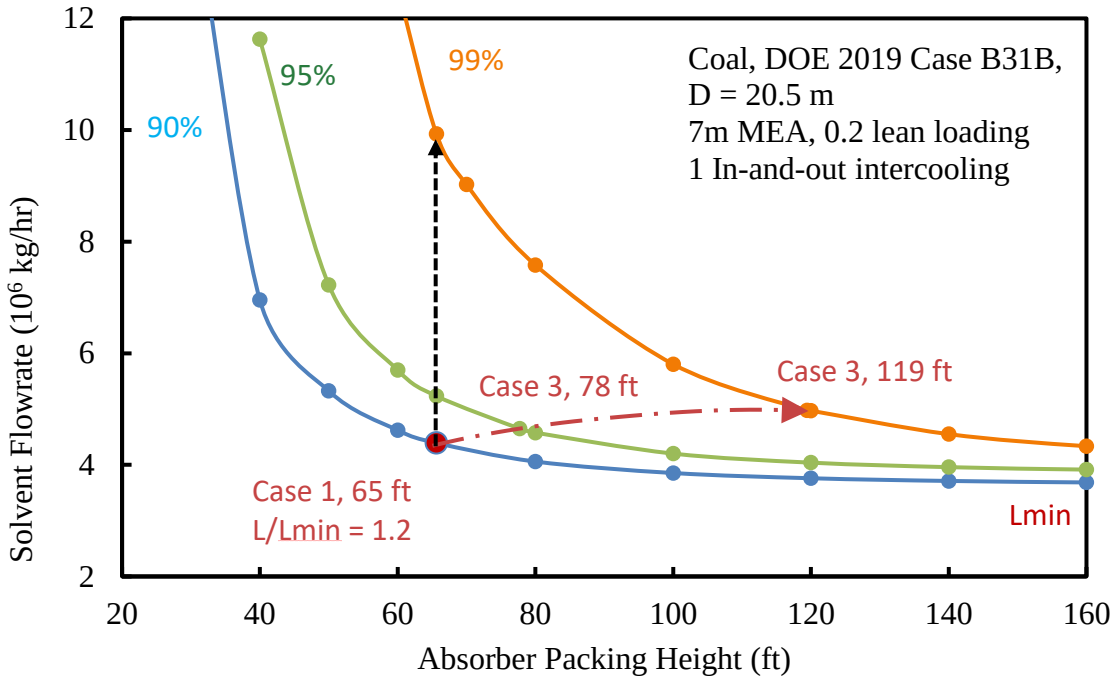

Figure 6.3: Absorber packing height and the optimization using L_{min} for NGCC flue gas.

Table 6.2 summarizes absorber height and stripper energy consumption for PC and NGCC flue gas at different CO_2 removal conditions. For Case 1, absorbers for PC and NGCC flue gas require 48 ft and 66 ft height of packing, respectively. With the same packing height as case 1, the Case 2 requires more solvent circulation and greater heat duties. The Case 2 is a suboptimal design for high removal and the steam consumption increases dramatically for 99% conditions. The energy cost is reduced in Case 3 by increasing the absorber packing as the results of optimization for higher capture rate. The optimized design for 95% removal requires less than 20% increase in the absorber packing height and the energy requirement remains the same. 99% removal is more difficult and the absorber packing height requirement increases by 33% and 80% for PC and NGCC flue gas. Capturing 99% of the CO_2 from NGCC flue gas by the simple absorber is considerably more expensive than the base case as reflected in the packing height.

Table 6.2: Summary for absorber packing and heat duty for solvent regeneration.

		PC				NGCC			
	Removal	Absorber Packing		Reboiler Heat Duty		Absorber Packing		Reboiler Heat Duty	
	%	ft	% to Case 1	GJ/t CO_2	% to Case 1	ft	% to Case 1	GJ/t CO_2	% to Case 1
Case 1	90	48	-	3.81	-	66	-	4.02	-
Case 2	95	48	-	4.00	105	66	-	4.40	109
Case 2	99	48	-	4.81	126	66	-	7.03	175
Case 3	95	55	115	3.84	101	78	118	4.03	100
Case 3	99	64	133	4.00	105	119	180	4.12	102

As shown in Table 6.2, 99% removal is significantly more difficult than 95% removal. This is because of the transfer increases quickly when CO_2 removal is greater

than 95%. To demonstrate the effect of CO_2 removal, Figure 6.4 shows the optimal absorber packing height at variable CO_2 penetration, and the height shows a good correlation to the logarithm of penetration, which is connected to the concept of the number of transfer units (NTU).

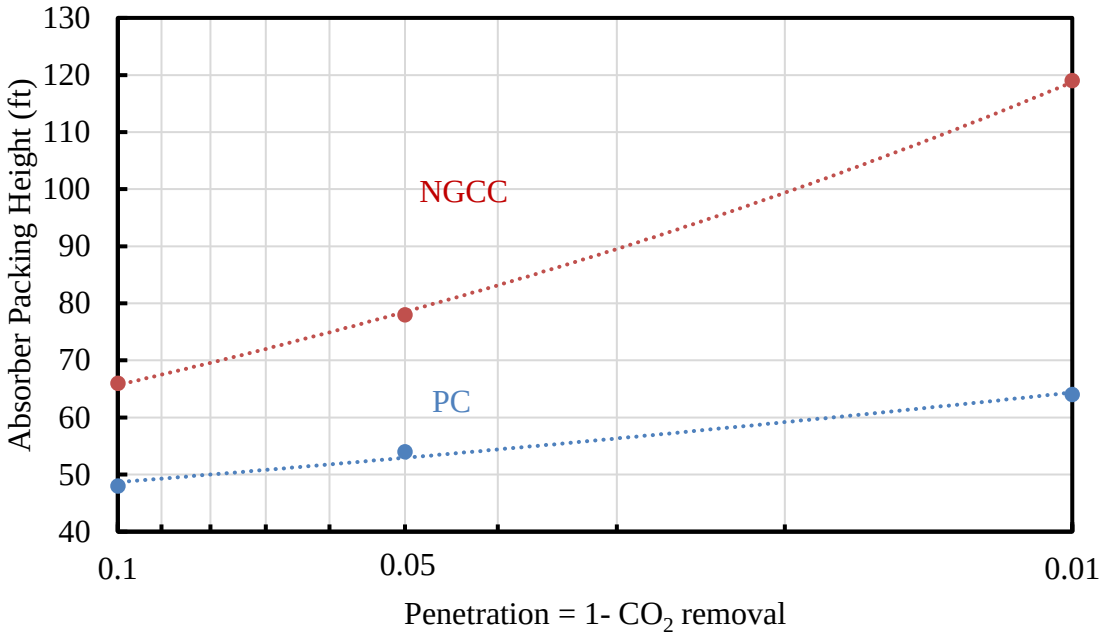

Figure 6.4: Optimal absorber packing height at variable CO_2 penetration.

Compared to PC, CO_2 capture from NGCC requires greater packing area and steam duty. There is a greater penalty for higher CO_2 removal too, which can be seen from the increase of absorber packing height or reboiler heat duty. This is caused by the low CO_2 concentration and the top temperature bulge in the absorber column. Because of the lower CO_2, the liquid-to-gas ratio (L/G) is about 3 times smaller than that of coal flue gas. The temperature bulge moves to the top of the absorber because of the low L/G, raises the column temperature, and reduces the driving force. The high removal cases are closer to a lean-end mass transfer pinch because of the high temperature and low CO_2 partial pressure.

Mitigating the temperature bulge at NGCC conditions can improve the absorber performance significantly.

6.3.2.2 Intercooling configurations

As described previous chapters, absorber with pump-around intercooling is proposed for NGCC flue gas because it can provide greater cooling with enhanced L/G. For CO_2 removal greater than 99%, a double pump-around configuration is proposed to further cool the column by adding a second intercooling loop to the second top section. Figure 5 shows the integrated absorber, DCC, and WW column design with in-and-out intercooling and double pump-around intercooling. The cooling capacity is limited by the liquid flowrate for in-and-out intercooling, and it can be improved by the pump-around configuration: the liquid flowrate in the section can be enhanced locally. The trade-offs for the pump-around section are the back-mixing of the solvent, greater column flooding in the section, and greater cost for pumping, intercooling, and liquid distribution. Pump-around intercooling can be effective, nonetheless, in managing absorber temperature because of the low L/G at NGCC conditions.

With the cooling provided by the pump-around in the bottom section, the DCC section can be eliminated. The NGCC flue gas enters the absorber at 111 °C with a H_2O concentration of 9%. The superheated gas picks up water and can be cooled quickly in the absorber bottom. The solvent temperature remains low (below 50 °C) because of the high flowrate. The water balance in the system is maintained by controlling the WW temperature at around 42 °C, so that the gas leaving the system contains the same amount of water as the flue gas entering the absorber.

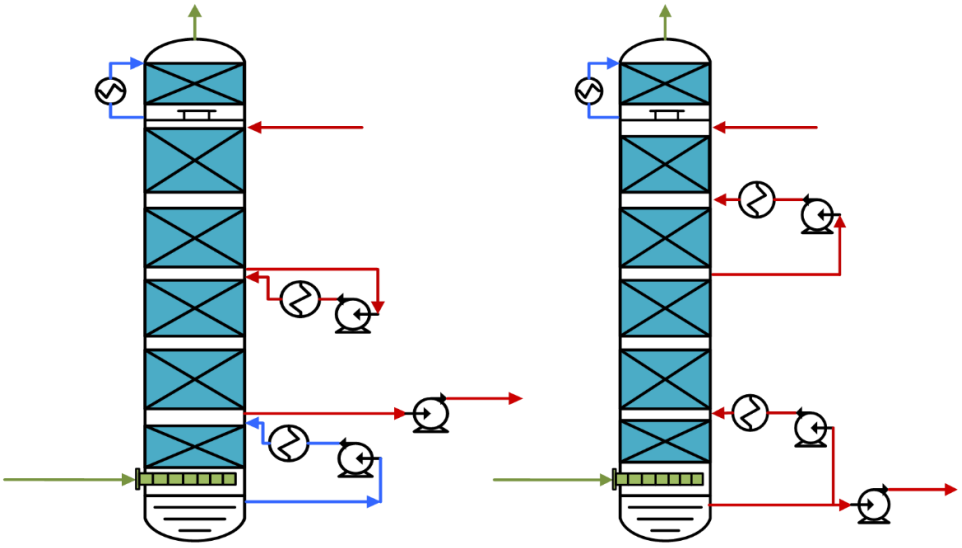

Figure 6.5: Integrated absorber, DCC, and WW design with in-and-out intercooling (left) and with pump-around intercooling (right).

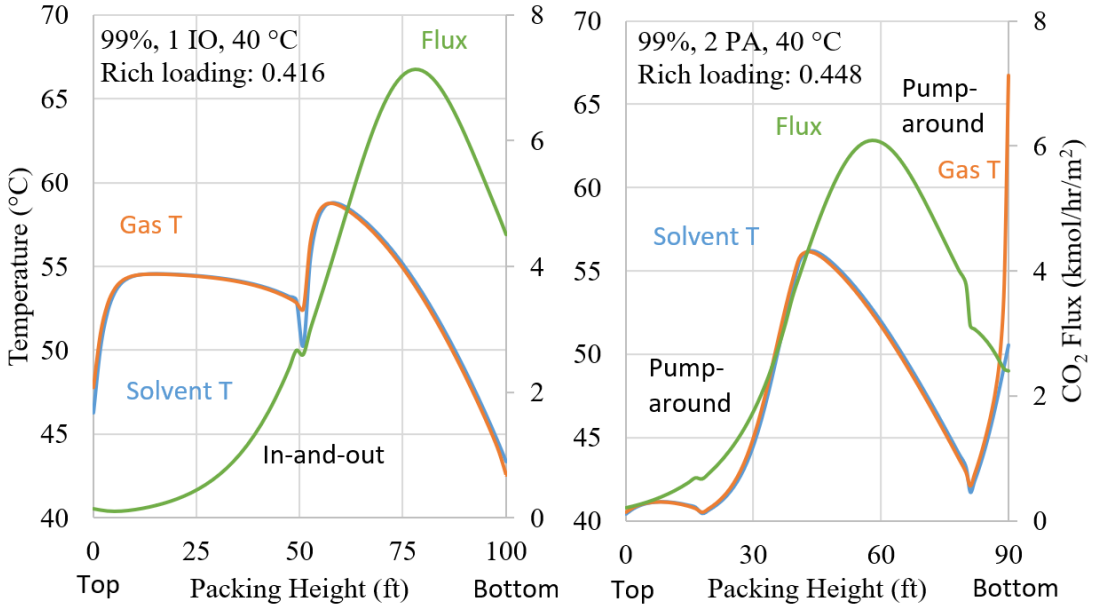

Figure 6.6: Temperature profiles (gas: orange, liquid: blue) and CO_2 transfer flux (green) in the absorber with in-and-out intercooling and DCC (left), and pump-around intercooling without DCC (right) for 99% removal of NGCC flue gas.

The optimal location of the top intercooling loop is found to be around the second packing section. It cools the absorber top effectively without reducing the absorption driving force because of the solvent back mixing.

Figure 6.6 shows the temperature profiles and CO_2 transfer flux in the absorber column at 99% removal for NGCC flue gas using the two absorber configurations shown in Figure 6.5. Because of the low L/G ratio for the NGCC flue gas, the gas carries the enthalpy and pushes the temperature bulge to the top. The simple in-and-out intercooling is not efficient, and most of the top section is at elevated temperature. The CO_2 flux approaches zero at the temperature bulge in the top section, indicating the temperature bulge near absorber top is the limiting mechanism at near-zero emission. The pump-around intercooling, on the contrary, can cool the column effectively with enhanced flow rate. With the pump-around intercooling around the second top section, the temperature is managed around 42 °C, and the mass transfer driving force is preserved. The bottom pump-around section cools the hot flue gas and keeps the solvent temperature low. With shorter packing height and lower temperature, the pump-around configuration outperformances the in-and-out intercooling. The improvement is more evident for higher capture rate because the CO_2 transfer driving force is more important as the CO_2 concentration decreases.

6.3.3 Economic analysis

Table 6.3 shows the PEC of major equipment in the capture unit for Cases 1 and 3. The total PEC for the 90% removal base case for PC and NGCC plants are 131 and 75 $MM, respectively. The absorber column and the compressor are the two largest cost centers. The absorber cost increases quickly at higher CO_2 removal because the packing height scales linearly to the logarithm of penetration as shown in Figure 6.4. The absorber

PEC increases by 26% and 59% for PC and NGCC conditions, respectively, as the capture ratio increases from 90% to 99%. The downstream equipment after the absorber is roughly linearly scaled to the CO_2 rate because the constant cyclic capacity is achieved by the optimized absorber design. The cost of the compressor is independent of removal within the range of 10% additional CO_2. Given the large share of the compressor cost in the overall plant PEC, a higher capture rate could result in a lower annualized capital cost with greater CO_2 removal.

At 90% removal, the pump-around configuration can reduce the absorber cost by 14% by eliminating the bottom DCC section.

Table 6.3: PEC of major equipment for Case 1 and Case 3

Equipment		90%, PC, IO	95%, PC, IO	99%, PC, IO	90%, NGCC, PA	90%, NGCC, IO	95%, NGCC, PA	99%, NGCC, PA
Absorber	PEC, $MM	28.3	32.5	35.7	29.1	33.2	33.5	46.2
	ratio to Case 1	-	1.15	1.26	-	1.14	1.15	1.59
Striper	PEC, $MM	18.4	19.3	22.6	8.2	7.8	8.7	8.7
	ratio to Case 1	-	1.05	1.23	-	0.95	1.06	1.06
HX	PEC, $MM	17.6	18.4	21.1	9.4	8.8	9.8	10.8
	ratio to Case 1	-	1.05	1.2	-	0.94	1.04	1.15
Pumps	PEC, $MM	5.1	5.4	5.9	3	3.2	3.1	4.1
	ratio to Case 1	-	1.06	1.16	-	1.07	1.03	1.37
Compressor	PEC, $MM	55.4	55.5	56.1	22.7	22.7	22.9	23
	ratio to Case 1	-	1	1.01	-	1	1.01	1.01
Total	PEC, $MM	130.8	137.1	147.5	74.8	79.2	80.3	96.1
	ratio to Case 1	-	1.05	1.13	-	1.06	1.07	1.28

The CAPEX is estimated using PEC and OPEX only, and includes the cost for steam in the stripper, electricity, and cooling water. It varies according to removal rates.

Figures 6.7 and 6.8 show the CAPEX, OPEX, and total cost for different CO_2 removal rates, configurations, and flue gas conditions.

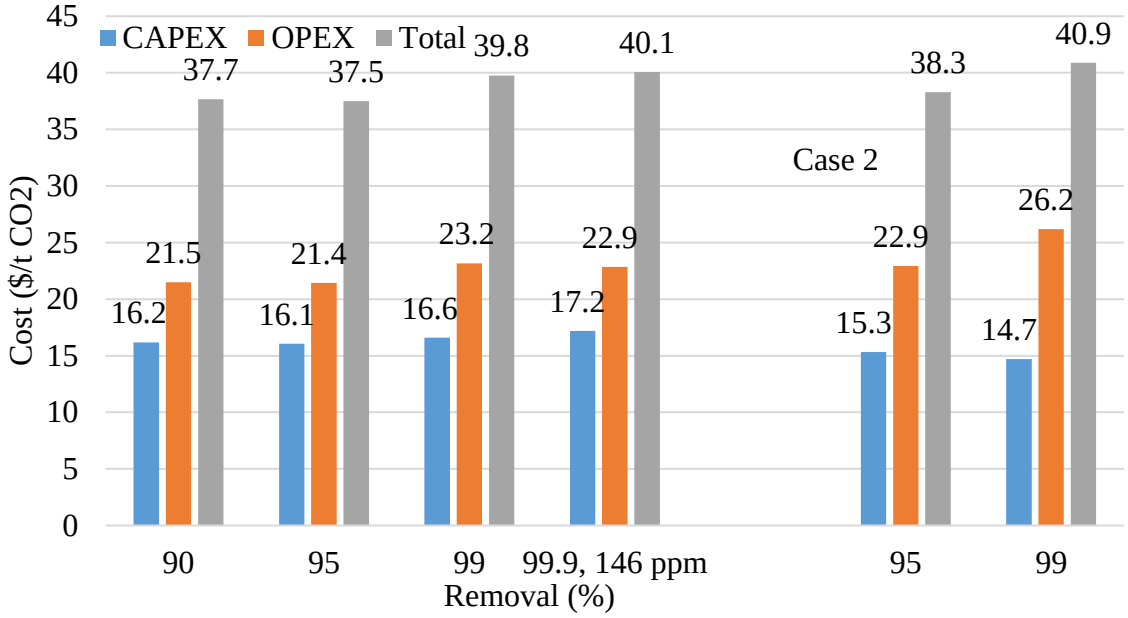

Figure 6.7: CAPEX, OPEX, and total capture cost for PC flue gas. The group on the left is the optimized design (Cases 1 and 3), and the group on the right is the non-optimized design (Case 2).

For coal-fired power plants with the optimized process design, the total cost of CO_2 capture is minimized at a removal rate around 95%. Compared to the 90% case, the increase in absorber capital cost is offset by the reduction in compressor cost. The rich loading for 95% removal is the same as for 90%, resulting in the same heat duty for the stripper. The OPEX decreases slightly because a greater CO_2 production rate reduces the cost of flue gas handling and delivery per unit CO_2. For 99% capture, OPEX increases by about 8% compared to the 90% case and drives a 6% increase in the total cost. With in-and-out intercooling, MEA solvent can achieve 99.9% removal for coal flue gas, where the CO_2 in the exhaust gas is about 146 ppm. With optimized absorber packing height, the total cost reaches 40.1 $/tonne of CO_2.

Case 2 demonstrates the cost of achieving a higher capture rate with the equipment designed for 90% capture. This mode of operation takes advantage of the over-designed equipment and maximizes the capacity. The PEC in Case 2 is the same as Case 1, but the CAPEX is reduced because of the extra CO_2 production. Limitations of system capacity will be discussed later. The total annualized cost for this ramp-up operation increases by 2% and 8% for 95% and 99% capture rate, respectively.

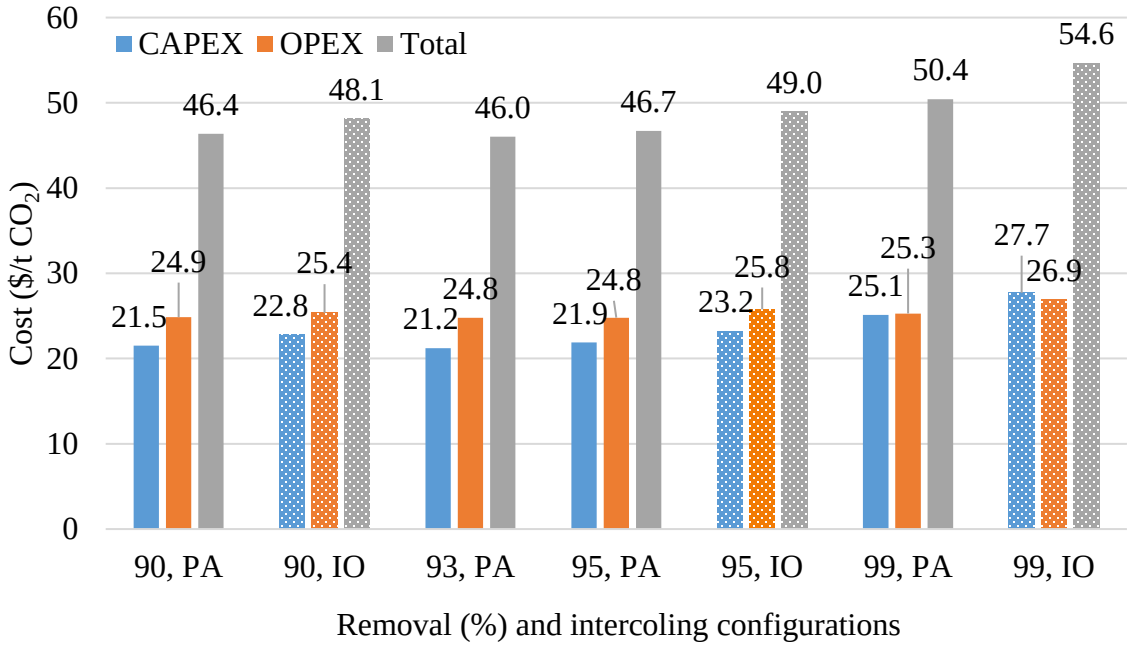

Figure 6.8: CAPEX, OPEX, and total capture cost for absorber with in-and-out and pump-around intercooling for NGCC flue gas.

A similar economic analysis for NGCC flue gas is shown in Figure 9. The optimized capture cost at 90% removal is about 46.4 $/tonne and is 23% greater than the coal flue gas, as the result of low CO2 concentration. Compared to the conventional absorber using in-and-out intercooling and DCC, the absorber with pump-around intercooler reduces the cost by 1.7, 2.3, 4.2 $/tonne for 90%, 95%, and 99% removal, respectively. The difference increases at greater CO2 removal, indicating that effective

cooling is more important for high removal and the absorber performance is more likely to be limited by the mass transfer pinch at the high removal conditions.

The optimal removal is 93% for NGCC. It is lower than the PC flue gas because the absorber takes up a larger portion of the total cost for the NGCC, so the penalty for higher removal is greater.

The economic analysis shows that the capture cost remains roughly constant for 90–95% removal but it increases rapidly after 95%. An incremental cost of CO2 capture is defined in Equation 6.2 to quantify the marginal cost of capturing between two removal or two CO2 concentrations.

$$Incremental\ Cost_{r_1,r_2} = \frac{Cost_{r_2} * r_2 - Cost_{r_1} * r_1}{r_2 - r_1} = Incremental\ Cost_{y_2,y_1} \qquad (6.2)$$

where:

r: CO_2 removal, $r_2 > r_1$, and

y: CO_2 concentration in the vented gas corresponding to the removal, $y_2 < y_1$.

The marginal cost from 90% to 95% removal is 33.9 and 52.1 $/tonne of CO_2 for coal and NGCC flue gas, which is close to the cost at 90% removal, which means low additional cost is required to achieve 95% removal. However, the marginal cost for 95% to 99% is significantly higer, reaching 94.4 and 138.3 $/tonne for coal and NGCC.

6.3.4 Zero and Negative Emission of Power Plant

Achieving zero or even negative emission of power plant with the MEA is technically feasible, and the economic analysis is shown in Figure 6.8. At 99% removal for NGCC, the CO_2 from the exhaust is around 400 ppm with an overall cost of 50.6 $/tonne. This means zero-emission for power plants. The removal can be pushed further to 99.7%,

leaving only 135 ppm of CO_2 in the scrubbed gas at an overall cost around 54.5 $/tonne. The cost for even higher removal becomes prohibitive using MEA because it reaches the equilibrium limits of the solvent.

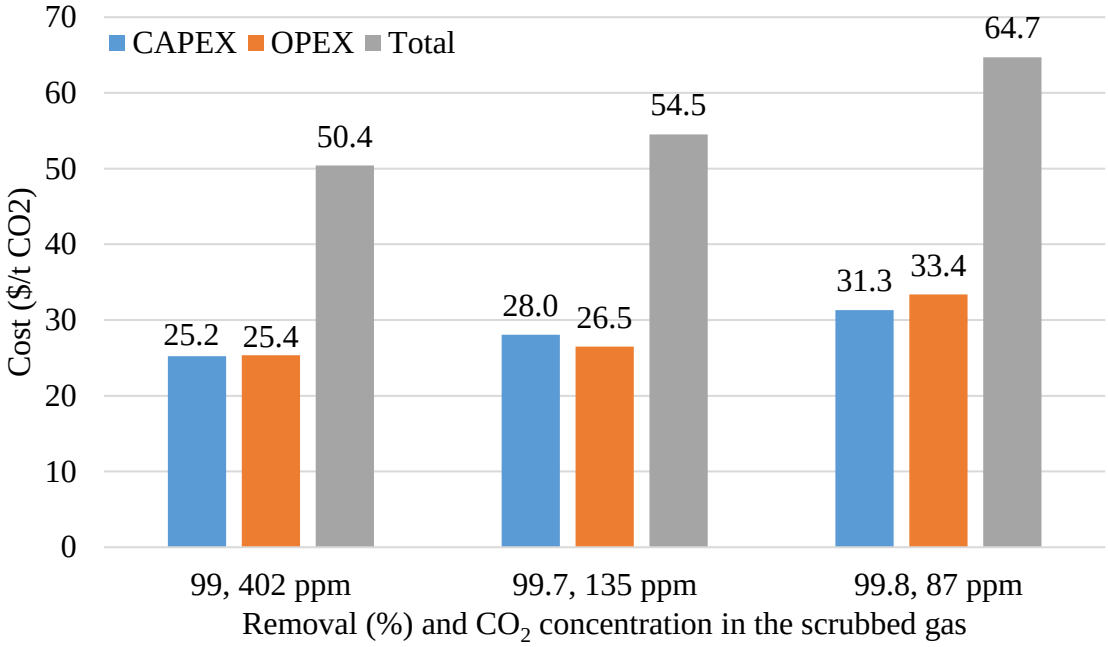

Figure 6.9: Cost analysis for zero and negative emission for an NGCC power plants.

Figure 6.10 summarizes the marginal capture cost for NGCC power plants using MEA. At the optimal CO_2 removal of 93%, the incremental cost is about 36 $/tonne. The incremental cost then increases rapidly to 139 $/tonne at the zero emission case. Capturing below 100 ppm using MEA costs over 10000 $/tonne because it approaches the equilibrium partial pressure of 82 ppm of the solvent.

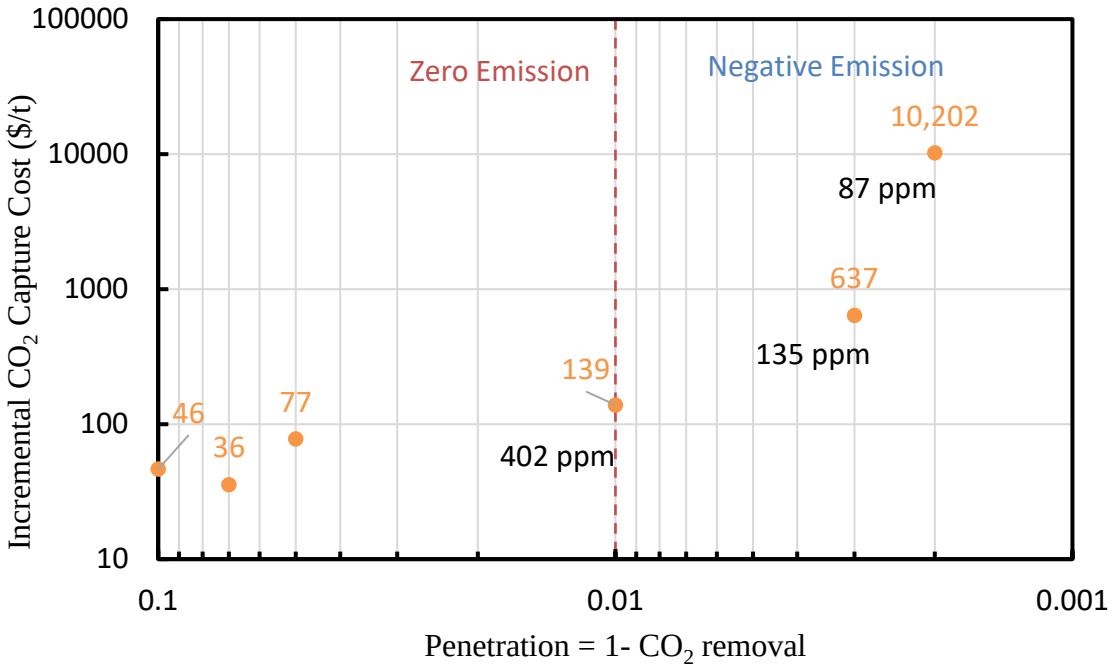

Figure 6.10: Incremental capture cost for NGCC power plant using MEA. The CO_2 concentrations are labeled for zero and negative emission cases.

The concept of direct air capture (DAC) has been increasingly popular as researchers start to explore pathways to achieve negative emissions. Being a novel technology without any large-scale demonstration, the estimated costs for DAC vary from \$100 to \$1000/tonne CO_2 captured (Keith et al., 2018; Minx et al., 2018; Socolow et al., 2011; Zeman, 2014). The cost estimated by the American Physical Society is often considered as the benchmark for DAC, which is \$550/tonne CO_2 captured for a "realistic" case, and \$430/tonne CO_2 captured for an "optimistic" case (Socolow et al., 2011). Carbon Engineering (CE), which is planning to build the largest DAC plant in the world, identified many cost reduction opportunities from the APS study and claimed a cost range of \$168 – \$232/tonne CO_2 captured in the base case scenario (Keith et al., 2018). As a comparison, the MEA-based amine scrubbing technology can achieve zero emission for power plant at

the marginal cost of 139 $/tonne CO_2. This suggests the amine scrubbing technology alone is favored to achieve zero emission from the power plant, as opposed to only capturing 90% of the CO_2 from the power plant and then achieving zero emission by capturing the vented CO_2 from atmosphere using the DAC.

For the development of emission control technologies, DAC should be considered as a complementary technology to amine scrubbing to achieve the ultimate goal of negative emission and reducing CO_2 concentration in the atmosphere. But the economic analysis clearly shows that DAC is not practical and deployed at large scale until amine scrubbing is fully implemented for power plants.

6.3.5 Lean Loading Optimization

Lean loading is an important variable in the process optimization, especially for higher CO_2 removal. Table 6.4 summarizes the effect of lean loading and the optimum for variable removal from NGCC flue gas. The optimized lean loading decreases from 0.18 to 0.16 as the CO_2 removal increases because a lower lean loading provides greater absorption driving force. But the cost curve is flat for lean loadings between 0.16 and 0.2, and the cost reduction is less than 0.5 $/tonne.

Table 6.4: Optimization of lean loading for NGCC conditions.

Removal, %	90	90	90	99	99	99	99.7	99.7	99.7
Lean Loading	0.2	0.18	0.17	0.18	0.17	0.16	0.18	0.16	0.15
CAPEX	21.5	21.3	21.3	25.0	24.8	24.8	27.7	27.5	27.4
OPEX	24.9	24.7	25.2	25.0	25.0	25.3	25.6	25.7	26.2
Total	46.4	46.0	46.5	50.0	49.8	50.1	53.3	53.2	53.7

6.3.6 System Capacity

As discussed in previous section, Case 2 simulates ramping-up system capacity to capture more CO_2. This operating model will increase the cash flow or profitability of the capture plant with a marginal increase of the capture cost. The maximum capture capacity is, however, limited by the equipment capacity and steam availability. The effect of CO_2 removal on major equipment will be discussed, including columns, compressor, heat exchangers, and pumps. Two possible operational strategies are studied for higher capture rate: increasing the circulation rate at fixed lean loading; or lowering the lean loading by reducing the stripping pressure and increasing the flowrate. Figure 6.11 shows the relative increase of the solvent circulation rate and column flooding as the result of ramping-up for the two strategies.

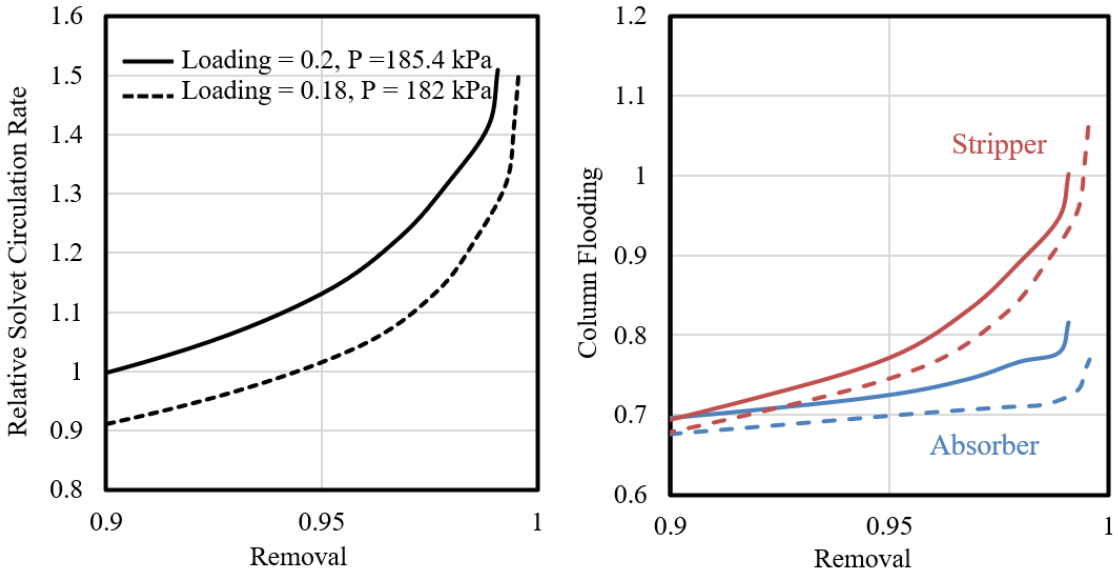

Figure 6.11: Relative solvent circulation rate and column flooding during system ramping-up.

At fixed lean loading, the solvent flowrate must increase by 12% to reach 95% capture. The pumps will need to deliver 25% more pressure head for exchangers because

of the greater flow. A greater circulation rate and CO_2 rate increase the column flooding, too. The absorber flooding is less sensitive to the capture rate because the flooding is primarily determined by the flue gas velocity, but the stripper flooding is determined by the CO_2 and water vapor rate and is more sensitive to the removal. The CO_2 rate scales linearly to the removal and the water vapor increases at the lower rich loading for higher removal. As a result, the capacity of the stripper is likely to limit the maximum CO_2 rate. The compressor will also have a greater inlet flowrate at higher removal and deviate from the optimal operating conditions. More steam is required for a higher CO_2 capture rate. With the existing reboiler, it will require a greater steam flow and higher-pressure steam for regeneration.

Another operating strategy is to lower the stripper pressure and reduce the lean loading. With a greater absorption driving force at lower loading, the solvent flowrate is smaller, and the column flooding is less limiting compared to fixed lean loading. However, the compressor will have a smaller inlet pressure and will constrain the CO_2 rate. By assuming no additional capital cost is required for ramping up to 95% removal, the total cost is 48.2 and 47.4 $/tonne for the two cases of fixed and reduced lean loading. The increase is less than 2 $/tonne compared to 90% base case operation. With the value of the CO_2 product, it is economically desirable to maximize the capture rate under the capacity of existing equipment and utility supply.

6.3.7 Discussion of the methodology

The TPC for the capture system is estimated using a Lang factor to the PEC. The PEC for higher capture rates is scaled from the 90% case based on characterized variables, such as flowrate, heat duty, etc. However, this methodology is likely to overestimate the incremental cost for higher removal for two reasons:

1: It is likely that PEC for equipment does not scale continuously to the size or the characterized variable in the range of interest, i.e., it could roughly remain constant. For example, the solvent circulation rate will increase by 5% to capture more CO_2, but the cost of the solvent delivery system such as pumps or liquid distributors may not increase within the range. Therefore, the increase of PEC is overestimated by this method.

2: The TPC includes Bare Erected Cost (BEC), engineering services, and contingencies (process and project), among which many would remain roughly constant and are independent of the size of the equipment. For example, the labor cost for installing a pump that delivers a 5% greater flowrate should be the same as a smaller pump, and the same will apply to services and contingencies. The increase of TPC is also overestimated by this Lang factor method.

Therefore, the incremental cost for higher removal is likely to be overestimated by the scaling method. Our estimation of cost at higher removal is conservative. It makes environmental and even economic sense to raise the target for CO_2 capture rate beyond 90%.

6.4 CONCLUSIONS

The MEA simple stripper process is used as a baseline to study the feasibility and economics of greater than 90% CO_2 removal, zero emission, and negative emission for power plants. The total capture cost for PC and NGCC power plants at 90% removal are 37.7 and 46.4 $/tonne CO_2, respectively,

Great than 90% removal for PC and NGCC is demonstrably feasible using the validated MEA model. The economics for higher capture is evaluated with optimized process design. The optimal removal for PC and NGCC power plant is 95% and 93%, respectively. Compared to 90% removal, the incremental cost for increased absorber

packing height is offset by a lower compression cost per tonne of CO_2 because the compressor cost remains constant. The cost at 99% removal is 6% and 9% higher compared to 90% capture for PC and NGCC power plants.

Capturing from NGCC power plants is more expensive than from PC plants, and the penalty for higher removal is also greater. This is because of the lower CO_2 concentration and the temperature bulge near the top of the absorber. The pump-around configuration can mitigate the temperature bulge and reduce the packing requirement; therefore, it outperforms the in-and-out configurations for NGCC flue gas.

Zero emission and negative emission for power plants are possible using the MEA scrubbing process. The overall cost of zero emission for the NGCC power plant is about 50.4 $/tonne with an incremental cost of 139 $/tonne near 400 ppm. The cost of reducing CO_2 concentration to around 100 ppm is prohibitive because it approaches the equilibrium limits of the solvent.

For an existing capture plant designed for 90% removal, it is possible to increase the capture rate at a marginal penalty: the cost increases by less than 2% to ramp up to 95% removal. It will increase the cash flow or revenue for the capture plant, but the maximum capture rate is limited by the equipment capacity and utility availability.

In sum, CO_2 removal by amine scrubbing should not be limited at 90%. It is economically optimal to capture around 93–95%. Zero emission for power plants is achievable with moderate incremental cost, which provides a viable solution to further reduce the CO_2 concentration in the atmosphere. Amine scrubbing should be implemented to achieve the goal of zero emission before the deployment of DAC technologies.

Chapter 7: Conclusions and Recommendations

7.1 Summary of Work Completed

The ultimate goal of this work is to develop recommendations for the absorber design in the amine scrubbing process. PZAS process was selected as a case study for the research of absorber design and optimization as it has been demonstrated as the benchmark of second-generation process. The rigorous rate-based model previously built from bench-scale experiments was validated using pilot plant experiments and then used for absorber design and optimization.

Three campaigns at the NCCC and UT-SRP pilot plants were done with 5 *m* PZ to evaluate absorber performance, demonstrate the concept of innovative design, and provide experimental data for model validation. To study the effect of key process variables, the parametric test was designed and performed over a wide range of operating conditions, including inlet CO_2 concentration, gas rate, liquid rate, lean loading, intercooling configuration, and column temperature. The long-term test further studied the variation of system performance over long time of operation with solvent degradation and changes in the ambient temperature.

The pilot plant measurements were first reconciled, and their uncertainties were quantified before being used for model validation. With an adjustable parameter on the solvent equilibrium model, the model can predict the CO_2 removal and temperature profile over the wide operating conditions for both NCCC and UT-SRP pilot plant.

The validated absorber model was then used to develop a detailed absorber design for a commercial scale CO_2 capture plant in west Texas. The design proposes a first-of-its-kind commercial scale absorber using pump-around intercooling to improve absorber

performance and eliminating DCC and trim cooler to reduce capital cost. The variation of performance, operating strategies were also studied for different ambient temperature.

Two innovative absorber designs: the hybrid and crossflow absorber were proposed to reduce the capital cost of the absorber, and their performance were simulated using Aspen Plus® under countercurrent modeling framework.

Achieving greater than 90% removal using amine scrubbing was studied with MEA and PZ solvent. MEA was chosen as the baseline first generation solvent to evaluate the technical feasibility and economic performance for the high removal. For PZ, high removal using countercurrent, hybrid, and crossflow absorbers was studied and compared to the 90% base case design. Absorber designs were optimized for high removal and configurations with DCC were proposed to achieve zero emission for the power plant.

7.2 Conclusions and Recommendations by Research Objective

7.2.1 Pilot Plant Test and Model Validation

The absorber performance with 5 *m* PZ was tested with three pilot plant campaigns: NCCC 2018, NCCC 2019, and SRP 2018. The key conclusions for the experiments are:

- 5 *m* PZ achieved 90% removal with 12 m packing for flue gas with 4% and 12% CO_2 at NCCC and with 9.1 m packing for 4%, 12%, and 20% CO_2 at SRP.
- With 12 m of packing and intercooling, the maximum CO_2 removal of 99.6% and 96% can be achieved by 5 *m* PZ for flue gas with 12% and 4% CO_2.
- The method of calculating solvent composition based on density and viscosity was used during the campaigns. Online density and viscosity measurements had good reproducibilities and availabilities. However, the

calculated solvent loading consistently deviated from the analytical methods, indicating the density and viscosity correlation may be intrinsically biased.

- The CO_2 material balance for three campaigns closed within the variation of measurements using the liquid composition calculated from solvent density and viscosity.

The steady state runs from the three campaigns were used for model validation and adjustment. The raw model underpredicts absorber NTU by 16%, 52%, and 38% for the NCCC 2018, 2019, and SRP 2018 campaigns, respectively. Adjustment of the solvent equilibrium model was required to match the experimental results. For NCCC 2019 and SRP 2018, the absorber model was corrected by increasing the PZ calculated from density and viscosity by 8% or reducing the CO_2 desorption rate by 60%. For NCCC 2018 , the PZ adjustment was 3%. The process model also predicted the absorber temperature profile accurately with both in-and-out and pump-around intercooler.

The packing characterization model was validated using experiments with only one section of packing from NCCC 2019 campaign.

Based on the pilot plant experiments and process modeling, the absorber performance with in-and-out and pump-around intercooling for NGCC flue gas was compared. The pump-around absorber performed better than in-and-out because it increases the liquid flux and L/G in the bottom section and provides more effective cooling at the low CO_2 concentration.

Recommendations

- The reconciliation of loadings for the three campaigns and previous pilot plant work at SRP indicates the possible systematic error associated with the density correlation. Solvent degradation will also affect the solvent

density and viscosity and should be included in the correlation. It will be helpful to validate the correlation with more experimental measurements and incorporate the role of solvent degradation.

- Cases with greater than 90% removal cases should be validated using pilot plant results. When the removal is high, the absorber is close to a lean-end pinch and these cases can be used to validate solvent equilibrium at lean conditions. The uncertainty of equilibrium adjustment and the temperature dependence of the solvent equilibrium model should be studied.

7.2.2 Absorber Design for Capture Plant in West Texas

Based on absorber model validated with pilot plant experiments at NCCC, a first-of-its-kind commercial scale integrated absorber and water wash design was proposed for a NGCC capture system in west Texas.

The design uses three sections of M252Y packing with height of 3.0 m, 4.9 m, and 2.7 m from top to bottom. The top section is a water wash, and the bottom section is the pump-around section. All the cooling will be done using air cooler. The design eliminates DCC and trim cooler to reduce capital cost, and uses 0.2 lean loading, low pump-around temperature (30 °C), and high pump-around rate to improve the performance and to reduce the operating cost.

Compared to conventional absorber design with DCC and in-and-out intercooling, the proposed design removes 4% more CO_2 at similar operating conditions and reduces capital cost by removing the DCC column.

Variation in ambient temperature affects the performance of the air cooler and absorber. The base case removal is 90% and decreases to 78% during hot summer days. In the summer, water balance will be maintained by condensing more water during the night

when the ambient temperature is low to make up for the water loss during the daytime when the temperature is high.

Greater than 90% removal can be achieved when the power plant is operated in partial load. The maximum CO_2 removal for the base and summer case is about 98.4% and 95.7% at 70% and 60% flue gas rate.

The FEED project will provide detailed cost estimation on equipment and project. The economics of the project and the optimal operating conditions should be further studied.

7.2.3 Innovative Absorber Design

The hybrid and crossflow absorber are proposed and simulated for process intensification from the pump-around absorber at NGCC conditions. These two configurations are more compact and reduce the open volume between packing sections in the absorber column.

For the hybrid absorber, three sections in series are required to provide large L/G and effective intercooling. The base case design is constrained by water balance and performs worse than the pump-around design because of the high intercooling temperature. The optimized configuration takes advantage of the high CO_2 concentration from the gas boiler and achieves the same performance as the pump-around absorber.

The base case crossflow absorber design performs worse than pump-around absorber because of the high temperature mass transfer pinch in the rich end. Adding a second intercooler reduces temperature significantly and improves the performance.

The crossflow absorber features small size and high velocity, it is favored when the relative capital cost is high and energy cost is low.

The performance of the crossflow absorber was simulated using countercurrent contacting and modeling framework in Aspen Plus®. Further model development to study the crossflow contacting and mass transfer performance can increase the accuracy of the process model. The equipment cost of innovative absorber should also be studied to evaluate the design comprehensively.

7.2.4 High Removal with Amine Scrubbing

The absorber performance for high removal with 5 *m* PZ was studied and compared to 90% base case. With 40 ft packing (L/L_{min} = 1.15), the pump-around absorber can achieve 98% removal with a rich loading of 0.39. Compared to the 90% base case, the major cost increase is in the absorber section, including a trim cooler and 15 ft of extra packing. 99% removal is difficult because it approaches a lean end pinch at the top temperature bulge. With an additional DCC to maintain the water balance, the absorber column temperature can be further reduced to achieve 99% removal.

The economic performance of achieving greater than 90% removal using amine scrubbing was studied using MEA solvent. The optimal removal for coal and NGCC power is 95% and 93%. Compared to 90% removal, the increase cost for absorber packing is offset by a lower compression cost per CO_2 because the compressor cost remains constant. The cost at 99% removal is 6% and 9% higher compared to 90% capture for coal and NGCC.

Zero emission and negative emission for power plant are possible using MEA scrubbing process. The overall cost of zero emission of NGCC power plant is about 50.4 $/tonne with an incremental cost of 139 $/tonne near 400 ppm of CO_2. The cost of reducing CO_2 to below 100 ppm is prohibitive because it approaches the equilibrium limit of the solvent.

For an existing capture plant designed for 90% removal, it is possible to increase the capture rate at a marginal cost penalty: the cost increases by less than 2% to ramp up to 95% removal.

The CO_2 removal for amine scrubbing process should not be limited at 90%. It is economically favorable to capture around 93-95%. Zero emission for power plant is achievable with moderate incremental cost, which provides a viable solution to further reduce the CO_2 emission to the atmosphere. Amine scrubbing should be implemented to achieve the goal of zero emission before the deployment of DAC technologies.

Appendices

APPENDIX A: ASPEN SUBROUTINES, PACKING CHARACTERIZATION MODEL

The packing characterization subroutines include the mass transfer coefficients model (MCWH) and the wetted area model (AREA).

A.1 Mass transfer coefficients

```
      SUBROUTINE mcwh(KSTG,     NCOMPS, IDX,       NBOPST, KPDIAG,
     1                XCOMPB, FRATEL, YCOMPB, FRATEV, PRESS,
     2                TLIQ,     TVAP,     AVMWLI, AVMWVA, VISCML,
     3                DENMXL, SIGMAL, VISCMV, DENMXV, AREAIF,
     4                PREK,     EXPKD,    COLTYP, USRCOR, TWRARA,
     5                COLDIA, HTPACK, PACSIZ, SPAREA, CSIGMA,
     6                PFACT,    PKPRMS, VOIDFR, IPAKAR, IPTYPE,
     7                IVENDR, IPMAT,    IPSIZE, WEIRHT, DCAREA,
     8                ARAACT, FLOPTH, NPASS,    WEIRL,    IFMETH,
     9                SYSFAC, HOLEAR, ITTYPE, TRASPC, PITCH,
     A                IPHASE, NINT,     INT,       NREAL,    REAL)
      IMPLICIT NONE
c #include "dms_global.cmn"
c #include "dms_maxwrt.cmn"

      INTEGER KSTG, NCOMPS, IDX(NCOMPS), NBOPST(6), KPDIAG,
     +          COLTYP, USRCOR, IPAKAR, IPTYPE, IVENDR, IPMAT,    IPSIZE,
     +          NPASS, IFMETH, ITTYPE, NINT, INT(NINT), IPHASE, NREAL
      REAL*8   XCOMPB(NCOMPS), FRATEL, YCOMPB(NCOMPS), FRATEV,
     +          PRESS, TLIQ, TVAP, AVMWLI, AVMWVA, VISCML, DENMXL,
     +          SIGMAL, VISCMV, DENMXV, AREAIF, PREK, EXPKD,
     +          TWRARA, COLDIA, HTPACK, PACSIZ, SPAREA, CSIGMA,
     +          PFACT,    PKPRMS(20), VOIDFR, WEIRHT, DCAREA, ARAACT,
     +          FLOPTH, WEIRL, SYSFAC, HOLEAR, TRASPC, PITCH,
     +          REAL(NREAL)
C***********************************************************************
*
C    LICENSED MATERIAL.    PROPERTY OF ASPEN TECHNOLOGY, INC.    TO
BE           *
C    TREATED AS ASPEN TECH PROPRIETARY INFORMATION UNDER THE
TERMS          *
C    OF THE ASPEN PLUS SUBSCRIPTION AGREEMENT.
*
```

```
C***********************************************************************
*
C-----------------------------------------------------------------------
C               COPYRIGHT (C) 2004
C                 ASPEN TECHNOLOGY, INC.
C                 CAMBRIDGE, MA
C-----------------------------------------------------------------------
C
C       DESCRIPTION: User provided RateSep routine to calculate the
C                           liquid (IPHASE=0) and vapor (IPHASE=1) binary mass
C                           transfer coefficient parameters (PREK, EXPKD).
C
C       VARIABLES IN ARGUMENT LIST
C
C       VARIABLE I/O    TYPE     DIMENSION     DESCRIPTION AND RANGE
C       -------- ---    ----     ---------     ---------------------------------
C       KSTG          I      I             -           SEGMENT NUMBER
C       NCOMPS        I      I             -           NUMBER OF COMPONENTS
C       IDX           I      I          NCOMPS         COMPONENT INDEX VECTOR
C       NBOPST        I      I             6           PHYSICAL PROPERTY OPTION
C                                                      SET BEAD POINTER
C       KPDIAG        I      I             -           PHYSICAL PROPERTY
C                                                      DIAGOSTIC CODE
C       XCOMPB        I      R          NCOMPS         BULK LIQUID MOLE
FRACTION
C       FRATEL        I      R             -           FLOW OF LIQUID (KMOL/SEC)
C       YCOMPB        I      R          NCOMPS         BULK VAPOR MOLE
FRACTION
C       FRATEV        I      R             -           FLOW OF VAPOR (KMOL/SEC)
C       PRESS         I      R             -           PRESSURE (N/SQ.M)
C       TLIQ          I      R             -           LIQUID TEMPERATURE (K)
C       TVAP          I      R             -           VAPOR TEMPERATURE (K)
C       AVMWLI        I      R             -           AVERAGE MOLECULAR
WEIGHT
C                                                      OF LIQUID MIXTURE
C                                                      (KG/KMOL)
C       AVMWVA        I      R             -           AVERAGE MOLECULAR
WEIGHT
C                                                      OF VAPOR MIXTURE (KG/KMOL)
C       VISCML        I      R             -           VISCOSITY OF LIQUID
C                                                      (N-SEC/SQ.M)
C       DENMXL        I      R             -           DENSITY OF LIQUID MIXTURE
C                                                      (KMOL/CU.M)
```

```
C       SIGMAL      I      R            -        SURFACE TENSION OF LIQUID
C                                                (N/M)
C       VISCMV      I      R            -        VISCOSITY OF VAPOR MIXTURE
C                                                (N-SEC/SQ.M)
C       DENMXV      I      R            -        DENSITY OF VAPOR MIXTURE
C                                                (KMOL/CU.M)
C       AREAIF      I      R            -        INTERFACIAL AREA
C                                                (SEE NOTE-1 BELOW)
C       PREK        O      R            -        BINARY MASS TRANSFER =
C       EXPRKD      O      R            -              PREK*DIFFUSIVITY**EXPKD
C                                                (SEE NOTE-2 BELOW)
C       COLTYP      I      I            -        TYPE OF COLUMN
C                                                1 = PACKED
C                                                2 = TRAY
C       USRCOR      I      I            -        CALCULATION METHOD (I.E.
C                                                CHOICE OF USER CORRELATION)
C                                                  1   = USER1
C                                                  2   = USER2
C                                                  3   = USER3
C                                                  4   = USER4
C       TWRARA      I      R            -        CROSS-SECTIONAL AREA OF
C                                                TOWER (SQ.M)
C       COLDIA      I      R            -        COLUMN DIAMETER (M)
C       HTPACK      I      R            -        HEIGHT OF PACKING IN THE
C                                                SEGMENT (M)
C       PACSIZ      I      R            -        SIZE OF PACKING (M)
C       SPAREA      I      R            -        SPECIFIC SURFACE AREA OF
C                                                PACKING (SQ.M/CU.M)
C       CSIGMA      I      R            -        CRITICAL SURFACE TENSION
C                                                OF PACKING MATERIAL (N/M)
C       PFACT       I      R            -        PACKING FACTOR (1/M)
C       PKPRMS      I      R           20        PACKING PARAMETERS
C                                                PKPRMS(1) = STICHLMAIR
CONSTANT C1
C                                                PKPRMS(2) = STICHLMAIR
CONSTANT C2
C                                                PKPRMS(3) = STICHLMAIR
CONSTANT C3
C                                                PKPRMS(4) = CL IN BILLET 93
C                                                PKPRMS(5) = CV IN BILLET 93
C                                                PKPRMS(6) = B IN BRF 85
C                                                PKPRMS(7) = S IN BRF 85
C                                                PKPRMS(8) = H IN BRF 85
```

```
C                                          PKPRMS(9) = Fse IN BRF 92
C                                          PKPRMS(10) = CE IN BRF 92
C                                          PKPRMS(11) = THETA IN BRF 92
C       VOIDFR    I     R          -       VOID FRACTION OF PACKING
C       IPAKAR    I     I          -       PACKING ARRANGEMENT
C                                            1 = RANDOM
C                                            2 = STRUCTURED
C       IPTYPE    I     I          -       PACKING TYPE
C                                          See IPTYPE in packsr.f
C       IVENDR    I     I          -       PACKING VENDOR CODE
C       IPMAT     I     I          -       PACKING MATERIAL CODE
C       IPSIZE    I     I          -       PACKING SIZE CODE
C       WEIRHT    I     R          -       AVERAGE WEIR HEIGHT (M)
C       DCAREA    I     R          -       TOTAL AREA OF DOWNCOMER
C                                          ON TRAY (SQ.M)
C       ARAACT    I     R          -       TOTAL ACTIVE AREA
AVAILABLE
C                                          ON TRAY (SQ.M)
C       FLOPTH    I     R          -       AVERAGE FLOWPATH LENGTH
(M)
C       NPASS     I     I          -       NUMBER OF TRAY PASSES
C       WEIRL     I     R          -       AVERAGE WEIRH LENGTH (M)
C       IFMETH    I     I          -       FLOODING CALCULATION
C                                          METHOD; REQUIRED FOR SIEVE
C                                          TRAY
C       SYSFAC    I     R          -       SYSTEM FACTOR; REQUIRED
FOR
C                                          SIEVE TRAY
C       HOLEAR    I     R          -       HOLE AREA/ACTIVE AREA;
REQUIRED
C                                          FOR SIEVE TRAY
C       ITTYPE    I     I          -       TRAY TYPE
C                                            1 - BUBBLE CAPS
C                                            2 - SIEVE
C                                            3 - GLITSCH BALLAST
C                                            4 - KOCH FLEXITRAY
C                                            5 - NUTTER FLOAT VALVE
C       TRASPC    I     R          -       TRAY SPACING (M)
C       PITCH     I     R          -       SIEVE TRAY HOLE PITCH (M)
C       IPHASE    I     I          -       PHASE QUALIFIER
C                                            0 = LIQUID
C                                            1 = VAPOR
C       NINT      I     I          -       Size of INT
```

```
C        INT          I/O     I          NINT          User correlation INT array
C        NREAL         I      I           -            Size of REAL
C        REAL         I/O     I          NREAL         User correlation REAL array
C
C       NOTE-1:
C               SPECIFIC INTERFACIAL AREA "AREAIF" HAS THE FOLLOWING
UNITS.
C                 FOR PACKED COLUMNS, THE UNITS IS "SQ.M/CU.M OF
PACKING"
C                 FOR TRAY COLUMNS, THE UNITS IS "SQ.M/SQ.M ACTIVE TRAY
AREA"
C
C       NOTE-2:
C               BINMTP = PREK * DIFFUSIVITY**EXPKD
C               BINARY MASS TRANSFER COEFFCIENTS "BINMTP" HAVE UNITS
(KMOL/SEC)
C               DIFFUSIVITY HAVE UNITS (SQ.M/SEC)
C               BINMTP HAS MOLAR DENSITY AND INTERFACIAL AREA
INCLUDED
C
C**********************************************************************
*
C        Declare local variables used in the user correlations
C
         REAL*8 RS_BennettHL
         REAL*8 RS_BennettA
         REAL*8 RS_BennettC
         REAL*8 ScLB,     ScVB,     rhoLms,       rhoVms,
        +           uL,         uV,         Fs,       QL,    tL,    dEQ,    C,
        +           uSV,        alphae, hL,       ShLB,    ReV,
        +           dTemp,    theta,    PACKHT


         PACKHT = REAL(1)
C
C        Instead of computing BINMTP from diffusivity as in RATEFRAC
C        compute PREK and EXPKD for RateSep
C
         IF (COLTYP .EQ. 1) THEN
C
C**** PACKED COLUMN
C
              IF (USRCOR .EQ. 1) THEN
```

```
C       1ST PACKING TYPE
C       User subroutine for pack column using Di's Correlation in his Dissertation

              IF (IPHASE.EQ.0) THEN
C
C              Liquid phase

C       kL = 0.12 * uL**0.565 * (miuL/rhoL)** -0.4 * g**(1/6) * ap**(-0.065) *
(z/1.8)**(-0.54) * Diffusivity**0.5

C       Liquid phase density
                  rhoLms = DENMXL * AVMWLI
C       Superfical velocity
                  uL = FRATEL / TWRARA / DENMXL

                  dTemp = 0.12D0 * uL**0.565D0 * (VISCML/rhoLms)**(-0.4D0)
     +                    * 9.81D0**(0.16666667D0) * SPAREA**(-0.065D0)

                  dTemp = dTemp * (PACKHT/1.8D0)**(-0.54D0)

C       Conversion of kL from m/s to kmol/s
                  PREK = dTemp * DENMXL * AREAIF * HTPACK * TWRARA
                  EXPKD = 0.5D0
              ELSE

C              Vapor phase
C
C       kG = 0.28 * uV**0.62 * (miuV/rhoV)** -0.12 * ap**0.38 * sin(2*alpha)**0.65 *
Diffusivity**0.5
                  rhoVms = DENMXV * AVMWVA
                  uV = FRATEV / TWRARA / DENMXV

                  IF (IPAKAR .EQ. 1) THEN
                     theta = 45
                  ELSE
                     theta = PKPRMS(11)
                  END IF
C                  END OF IF (IPAKAR)

                  dTemp = 0.28D0 * uV**0.62D0 * (VISCMV/rhoVms)**(-0.12D0)
     +                    * SPAREA**(0.38D0) * (sin(2.0D0*theta))**0.65D0
C              Conversion of K from m/s to kmol/s
                  PREK =    dTemp * DENMXV * AREAIF * HTPACK * TWRARA
```

```
                  EXPKD = 0.5D0
               END IF
C              END OF IF (PHASE)
C
            END IF
C           END OF IF (USRCOR)
C
         ELSE IF (COLTYP .EQ. 2) THEN
C
C**** TRAY COLUMN
C
            IF (USRCOR .EQ. 1) THEN
C              user subroutine example for tray column: AIChE 58
C
C              AIChE, Bubble Tray Design Manual: Prediction of Fractionation
C                 Efficiency, New York, 1958
C
C              For bubble cap, valve, and sieve trays
C
               IF (IPHASE.EQ.0) THEN
C
C                 Liquid phase
C
                  rhoVms = DENMXV * AVMWVA
                  rhoLms = DENMXL * AVMWLI
                  uV = FRATEV /DENMXV /ARAACT
                  Fs = uV * DSQRT(rhoVms)
                  C = 0.5D0 + 0.438D0 * DEXP(-137.8 * WEIRHT)
                  QL = FRATEL/DENMXL
                  ALPHAE = DEXP(-
12.55D0*(uV*DSQRT(RHOVMS/DABS(RHOLMS-
     1                    RHOVMS)))**0.91D0)
                  hL =ALPHAE*(WEIRHT + C*(QL/WEIRL/ALPHAE)**0.67D0)
                  dTemp = 19700.0D0 *(0.4D0*Fs+0.17D0) * hL
     +                  * ARAACT * DENMXL
C
                  PREK = dTemp
                  EXPKD = 0.5D0
C
               ELSE
C
C                 Vapor phase
C
```

```
                  rhoVms = DENMXV * AVMWVA
                  uV = FRATEV /DENMXV /ARAACT
                  Fs = uV * DSQRT(rhoVms)
                  QL = FRATEL/DENMXL
                  dTemp = 0.776 + 4.57*WEIRHT - 0.238*Fs
     +                  + 104.8*QL/WEIRL
                  dTemp = dTemp * uV * ARAACT * DENMXV
C
C                  COMPOSITION INDEPENDENT PART OF SCHMIDT NUMBER
                  ScVB = VISCMV / rhoVms
C
                  PREK = dTemp /DSQRT(ScVB)
                  EXPKD = 0.5D0
                END IF
C                END OF IF (IPHASE)
C
             END IF
C            END OF IF (USRCOR)
C
          END IF
C         END OF IF (COLTYP)
C
          RETURN
          END
```

A.2 Wetted Area Model

```
          SUBROUTINE area(KSTG,     NCOMPS, IDX,       NBOPST, KPDIAG,
         1                        XCOMPB, FRATEL, YCOMPB, FRATEV, PRESS,
         2                        TLIQ,     TVAP,     AVMWLI, AVMWVA, VISCML,
         3                        DENMXL, SIGMAL, VISCMV, DENMXV, AREAIF,
         4                        COLTYP, USRCOR, TWRARA, COLDIA, HTPACK,
         5                        PACSIZ, SPAREA, CSIGMA, PFACT,    PKPRMS,
         6                        VOIDFR, IPAKAR, IPTYPE, IVENDR, IPMAT,
         7                        IPSIZE, WEIRHT, DCAREA, ARAACT, FLOPTH,
         8                        NPASS,    WEIRL,    IFMETH, SYSFAC, HOLEAR,
         9                        ITTYPE, TRASPC, PITCH,    NINT,     INT,
         A                         NREAL,    REAL)
          IMPLICIT NONE
#include "dms_global.cmn"
#include "dms_maxwrt.cmn"

          INTEGER KSTG, NCOMPS, IDX(NCOMPS), NBOPST(6), KPDIAG,
```

```
     +          COLTYP, USRCOR, IPAKAR, IPTYPE, IVENDR, IPMAT,    IPSIZE,
     +          NPASS, IFMETH, ITTYPE, NINT, INT(NINT), NREAL
      REAL*8   XCOMPB(NCOMPS), FRATEL, YCOMPB(NCOMPS), FRATEV,
     +          PRESS, TLIQ, TVAP, AVMWLI, AVMWVA, VISCML, DENMXL,
     +          SIGMAL, VISCMV, DENMXV, AREAIF, TWRARA, COLDIA,
     +          HTPACK, PACSIZ, SPAREA, CSIGMA, PFACT, PKPRMS(20),
     +          VOIDFR, WEIRHT, DCAREA, ARAACT, FLOPTH, WEIRL,
     +          SYSFAC, HOLEAR, TRASPC, PITCH, REAL(NREAL)
C***********************************************************************
*
C    LICENSED MATERIAL.    PROPERTY OF ASPEN TECHNOLOGY, INC.    TO
BE          *
C    TREATED AS ASPEN TECH PROPRIETARY INFORMATION UNDER THE
TERMS          *
C    OF THE ASPEN PLUS SUBSCRIPTION AGREEMENT.
*
C***********************************************************************
*
C----------------------------------------------------------------------
C               COPYRIGHT (C) 2004
C                ASPEN TECHNOLOGY, INC.
C                CAMBRIDGE, MA
C----------------------------------------------------------------------
C
C        DESCRIPTION: User provided RateSep routine to calculate the
C                           specific interface area AREAIF (see NOTE-1).
C
C        VARIABLES IN ARGUMENT LIST
C
C        VARIABLE I/O    TYPE     DIMENSION     DESCRIPTION AND RANGE
C        -------- ---    ----     ---------     --------------------------------
C        KSTG          I      I             -           SEGMENT NUMBER
C        NCOMPS        I      I             -           NUMBER OF COMPONENTS
C        IDX           I      I           NCOMPS        COMPONENT INDEX VECTOR
C        NBOPST        I      I             6           PHYSICAL PROPERTY OPTION
C                                                       SET BEAD POINTER
C        KPDIAG        I      I             -           PHYSICAL PROPERTY
C                                                       DIAGOSTIC CODE
C        XCOMPB        I      R           NCOMPS        BULK LIQUID MOLE
FRACTION
C        FRATEL        I      R             -           FLOW OF LIQUID (KMOL/SEC)
C        YCOMPB        I      R           NCOMPS        BULK VAPOR MOLE
FRACTION
```

```
C       FRATEV    I     R          -      FLOW OF VAPOR (KMOL/SEC)
C       PRESS     I     R          -      PRESSURE (N/SQ.M)
C       TLIQ      I     R          -      LIQUID TEMPERATURE (K)
C       TVAP      I     R          -      VAPOR TEMPERATURE (K)
C       AVMWLI    I     R          -      AVERAGE MOLECULAR
WEIGHT
C                                         OF LIQUID MIXTURE
C                                         (KG/KMOL)
C       AVMWVA    I     R          -      AVERAGE MOLECULAR
WEIGHT
C                                         OF VAPOR MIXTURE (KG/KMOL)
C       VISCML    I     R          -      VISCOSITY OF LIQUID
C                                         (N-SEC/SQ.M)
C       DENMXL    I     R          -      DENSITY OF LIQUID MIXTURE
C                                         (KMOL/CU.M)
C       SIGMAL    I     R          -      SURFACE TENSION OF LIQUID
C                                         (N/M)
C       VISCMV    I     R          -      VISCOSITY OF VAPOR MIXTURE
C                                         (N-SEC/SQ.M)
C       DENMXV    I     R          -      DENSITY OF VAPOR MIXTURE
C                                         (KMOL/CU.M)
C       AREAIF    O     R          -      INTERFACIAL AREA
C                                         (SEE NOTE-1 BELOW)
C       COLTYP    I     I          -      TYPE OF COLUMN
C                                         1 = PACKED
C                                         2 = TRAY
C       USRCOR    I     I          -      CALCULATION METHOD (I.E.
C                                         CHOICE OF USER CORRELATION)
C                                           1 = USER1
C                                           2 = USER2
C                                           3 = USER3
C                                           4 = USER4
C       TWRARA    I     R          -      CROSS-SECTIONAL AREA OF
C                                         TOWER (SQ.M)
C       COLDIA    I     R          -      COLUMN DIAMETER (M)
C       HTPACK    I     R          -      HEIGHT OF PACKING IN THE
C                                         SEGMENT (M)
C       PACSIZ    I     R          -      SIZE OF PACKING (M)
C       SPAREA    I     R          -      SPECIFIC SURFACE AREA OF
C                                         PACKING (SQ.M/CU.M)
C       CSIGMA    I     R          -      CRITICAL SURFACE TENSION
C                                         OF PACKING MATERIAL (N/M)
C       PFACT     I     R          -      PACKING FACTOR (1/M)
```

```
C       PKPRMS      I       R           20          PACKING PARAMETERS
C                                                   PKPRMS(1) = STICHLMAIR
CONSTANT C1
C                                                   PKPRMS(2) = STICHLMAIR
CONSTANT C2
C                                                   PKPRMS(3) = STICHLMAIR
CONSTANT C3
C                                                   PKPRMS(4) = CL IN BILLET 93
C                                                   PKPRMS(5) = CV IN BILLET 93
C                                                   PKPRMS(6) = B IN BRF 85
C                                                   PKPRMS(7) = S IN BRF 85
C                                                   PKPRMS(8) = H IN BRF 85
C                                                   PKPRMS(9) = Fse IN BRF 92
C                                                   PKPRMS(10) = CE IN BRF 92
C                                                   PKPRMS(11) = THETA IN BRF 92
C       VOIDFR      I       R           -           VOID FRACTION OF PACKING
C       IPAKAR      I       I           -           PACKING ARRANGEMENT
C                                                     1 = RANDOM
C                                                     2 = STRUCTURED
C       IPTYPE      I       I           -           PACKING TYPE
C                                                   See IPTYPE in packsr.f
C       IVENDR      I       I           -           PACKING VENDOR CODE
C       IPMAT       I       I           -           PACKING MATERIAL CODE
C       IPSIZE      I       I           -           PACKING SIZE CODE
C       WEIRHT      I       R           -           AVERAGE WEIR HEIGHT (M)
C       DCAREA      I       R           -           TOTAL AREA OF DOWNCOMER
C                                                   ON TRAY (SQ.M)
C       ARAACT      I       R           -           TOTAL ACTIVE AREA
AVAILABLE
C                                                   ON TRAY (SQ.M)
C       FLOPTH      I       R           -           AVERAGE FLOWPATH LENGTH
(M)
C       NPASS       I       I           -           NUMBER OF TRAY PASSES
C       WEIRL       I       R           -           AVERAGE WEIRH LENGTH (M)
C       IFMETH      I       I           -           FLOODING CALCULATION
C                                                   METHOD; REQUIRED FOR SIEVE
C                                                   TRAY
C       SYSFAC      I       R           -           SYSTEM FACTOR; REQUIRED
FOR
C                                                   SIEVE TRAY
C       HOLEAR      I       R           -           HOLE AREA/ACTIVE AREA;
REQUIRED
C                                                   FOR SIEVE TRAY
```

```
C       ITTYPE      I      I            -          TRAY TYPE
C                                                   1 - BUBBLE CAPS
C                                                   2 - SIEVE
C                                                   3 - GLITSCH BALLAST
C                                                   4 - KOCH FLEXITRAY
C                                                   5 - NUTTER FLOAT VALVE
C       TRASPC      I      R            -          TRAY SPACING (M)
C       PITCH       I      R            -          SIEVE TRAY HOLE PITCH (M)
C       NINT        I      I            -          Size of INT
C       INT        I/O     I          NINT         User correlation INT array
C       NREAL       I      I            -          Size of REAL
C       REAL       I/O     I          NREAL        User correlation REAL array
C
C       NOTE-1:
C       SPECIFIC INTERFACIAL AREA "AREAIF" HAS THE FOLLOWING UNITS.
C       FOR PACKED COLUMNS, THE UNITS IS "SQ.M/CU.M OF PACKING"
C       FOR TRAY COLUMNS, THE UNITS IS "SQ.M/SQ.M ACTIVE TRAY
AREA"
C
C***********************************************************************
*
C       Declare local variables used in the user correlations
C
        REAL*8 ratio,   uV,       rhoVms,
       +           uL,       rhoLms, ReL,
       +           ReV,      d,        Wprime, B, S, H, eta

        eta = REAL(1)
C
C       Compute specific interface area as described above
C       Check COLTYP/USRCOR if providing multiple area correlations
C
        IF (COLTYP .EQ. 1) THEN
C
C       PACKED COLUMN
C
            IF (USRCOR .EQ. 1) THEN
C       Correlation for Packing based on Di
C
                rhoLms = AVMWLI * DENMXL
                uL = FRATEL / TWRARA / DENMXL
C
```

```
C         ratio = 1.16*1*(rhoLms/SIGMAL)**0.138*9.81**0.069*uL**0.138*ap**(-
0.207)

                  ratio = 1.16*eta*(rhoLms/SIGMAL)**0.138 * 9.81**0.069 *
        +                   uL**0.138*SPAREA**(-0.207)

                  AREAIF = (SPAREA*ratio)


               END IF
C              END OF IF (USRCOR)
C
          ELSE IF (COLTYP .EQ. 2) THEN
C
C**** TRAY COLUMN
C
               IF (USRCOR .EQ. 1) THEN
C                   user subroutine example for tray column: Scheffe-Weiland 87
C
C                   Scheffe, R.D. and Weiland, R.H., "Mass Transfer
C                   Characteristics of Valve Trays." Ind. Eng. Chem. Res.
C                   26, (1987) p. 228
C
C                   The original paper only mentioned valve tray.
C                   It is also used for bubble-cap tray and sieve tray.
C
C                   CHARACTERISTIC LENGTH IS ALWAYS 1 METER.
                    d = 1.0D0
                    rhoLms = DENMXL * AVMWLI
                    rhoVms = DENMXV * AVMWVA
                    uL = FRATEL / TWRARA / DENMXL
                    uV = FRATEV / TWRARA / DENMXV
                    ReL = rhoLms * uL * d / VISCML
                    ReV = rhoVms * uV * d / VISCMV
                    Wprime = WEIRHT / d
                    AREAIF = 0.27D0 * ReV**0.375D0 * ReL**0.247D0
                    AREAIF = AREAIF * Wprime**0.515
               END IF
C              END OF IF (USRCOR)
C
          END IF
C         END OF IF (COLTYP)
C
```

```
RETURN
END
```

APPENDIX B: PILOT PLANT DATA PROCESSING CODE IN MATLAB

The pilot plant data were extracted and processed using following code in Matlab.

```
function Summary_Table_Writer_Function()

clc
writefile = 'Summary Table 19 v4.xlsx';
header1 ={'Start Time', 'End Time','T gas in', 'T gas out', ...
    'T solvent in', 'T solvent out', 'T IC in 402 ','T IC out 402',...
    'L IC 402', 'T IC in 401 ','T IC out 401', 'L IC 401'...
    'L_lean', 'L_rich','G in', 'G out',    'O2 in'...
    'CO2 in', 'CO2 out', 'CO2 production', 'Removal',...
    'lean molarity', 'lldg', 'rich molarity', 'rldg', 'mldg',...
    'Calc lean PZ wt%', 'Calc lean CO2 wt%',...
    'Calc rich PZ wt%', 'Calc rich CO2 wt%',...
    'AI lean PZ wt%', 'AI lean CO2 wt%',...
    'AI rich PZ wt%', 'AI rich CO2 wt%',...
    'TI20101', 'TI20117A', 'TI20117B', 'TI20117C',...
    'TI20117D', 'TI20117E', 'TI20119E', 'TI20117F',...
    'TI20119F',     'TI20117G',    'TI20117H',    'TI20117I',...
    'TI20119I', 'TI20117J', 'TI20119J',     'TI20117K',...
    'TI20119K',     'TI20117L',    'TI20119L', 'T WW out',...
    'Cold rich L', 'Warm rich L', 'Warm rich T', 'Warm lean T',...
    'Bypass T', 'Steam T', 'Steam P',...
    'Steam flowrate', 'Sump T', 'Stripper P', 'CO2 flow', 'dP top', 'dP bot'};

header2 = {'','', 'F',     'F',...
    'F', 'F', 'F', 'F',...
    'gpm', 'F', 'F', 'gpm',...
    'lb/hr', 'lb/hr', 'lb/hr', 'lb/hr', '%',...
    '%', '%', 'lb/hr', '%',...
    'm', 'm/m', 'm', 'm/m', 'm/m', '%', '%', '%', '%', '%', '%', '%', '%',...
    'F', 'F', 'F', 'F', 'F', 'F', 'F', 'F', 'F', 'F', 'F', 'F', 'F', 'F', 'F', 'F',...
    'F', 'F', 'F', 'F', 'lb/hr', 'lb/hr', 'F', 'F', 'F', 'F', 'psig', 'pph', 'F', 'psig', 'lb/hr', 'inH2O',
'inH2O'};

xlswrite(writefile, header1, 'sheet1', 'B1')
xlswrite(writefile, header2, 'sheet1', 'B2')
xlswrite(writefile, header1, 'sheet2', 'B1')
xlswrite(writefile, header2, 'sheet2', 'B2')
%{
```

```
filenames = [
    "UT Austin Data 2-14-19 master.xlsx",...
    "UT Austin Data 2-14-19 master.xlsx",...
    "UT Austin Data 2-15-19 master.xlsx",...
    "UT Austin Data 2-16-19 master.xlsx",...
    "UT Austin Data 2-17-19 master.xlsx",...
    "UT Austin Data 2-18-19 master.xlsx",...
    "UT Austin Data 2-18-19 master.xlsx",...
    "UT Austin Data 2-19-19 master.xlsx",...
    "UT Austin Data 2-20-19 master.xlsx",...
    "UT Austin Data 2-21-19 master.xlsx",...%10
    "UT Austin Data 2-22-19 master.xlsx",...
    "UT Austin Data 2-23-19 master.xlsx",...
    "UT Austin Data 2-24-19 master.xlsx",...
    "UT Austin Data 2-25-19 master.xlsx",...
    "UT Austin Data 2-26-19 master.xlsx",...
    "UT Austin Data 2-27-19 master.xlsx",...
    "UT Austin Data 3-4-19 master.xlsx",...
    "UT Austin Data 3-5-19 master.xlsx",...
    "UT Austin Data 3-9-19 master.xlsx",...
    "UT Austin Data 3-10-19 master.xlsx",...%20
    "UT Austin Data 3-11-19 master.xlsx",...
    "UT Austin Data 3-12-19 master.xlsx",...
    "UT Austin Data 3-12-19 master.xlsx",...
    "UT Austin Data 3-13-19 master.xlsx",...
    "UT Austin Data 3-14-19 master.xlsx",...%25
    "UT Austin Data 3-14-19 master.xlsx",...
    "UT Austin Data 3-15-19 master.xlsx",...
    "UT Austin Data 3-15-19 master.xlsx",...
    "UT Austin Data 3-16-19 master.xlsx",...
    "UT Austin Data 3-16-19 master.xlsx",...%30
    "UT Austin Data 3-16-19 master.xlsx",...
    "UT Austin Data 3-17-19 master.xlsx",...
    "UT Austin Data 3-18-19 master.xlsx",...
    "UT Austin Data 3-18-19 master.xlsx",...
    "UT Austin Data 3-18-19 master.xlsx",...
    "UT Austin Data 3-19-19 master.xlsx",...
    "UT Austin Data 3-20-19 master.xlsx",...
    "UT Austin Data 3-21-19 master.xlsx",...
    "UT Austin Data 3-22-19 master.xlsx",...
    "UT Austin Data 4-9-19 master.xlsx",...%40
    "UT Austin Data 4-9-19 master.xlsx",...
    "UT Austin Data 4-10-19 master.xlsx",...
```

"UT Austin Data 4-11-19 master.xlsx",...
"UT Austin Data 4-12-19 master.xlsx",...
"UT Austin Data 4-13-19 master.xlsx",...
"UT Austin Data 4-14-19 master.xlsx",...
"UT Austin Data 4-15-19 master.xlsx",...
"UT Austin Data 4-16-19 master.xlsx",...
"UT Austin Data 4-17-19 master.xlsx",...
"UT Austin Data 4-18-19 master.xlsx",...%50
"UT Austin Data 4-19-19 master.xlsx",...
"UT Austin Data 4-20-19 master.xlsx",...
"UT Austin Data 4-21-19 master.xlsx",...
"UT Austin Data 4-25-19 master.xlsx",...
"UT Austin Data 4-29-19 master.xlsx",...
"UT Austin Data 4-30-19 master.xlsx",...
"UT Austin Data 5-1-19 master.xlsx",...
"UT Austin Data 5-2-19 master.xlsx",...
"UT Austin Data 5-4-19 master.xlsx",...
"UT Austin Data 5-5-19 master.xlsx",...%60
"UT Austin Data 5-6-19 master.xlsx",...
"UT Austin Data 5-7-19 master.xlsx",...
"UT Austin Data 5-8-19 master.xlsx",...
"UT Austin Data 5-9-19 master.xlsx",...
"UT Austin Data 5-10-19 master.xlsx",...
"UT Austin Data 5-11-19 master.xlsx",...
"UT Austin Data 5-12-19 master.xlsx",...
"UT Austin Data 5-13-19 master.xlsx",...
"UT Austin Data 5-14-19 master.xlsx",...
"UT Austin Data 5-15-19 master.xlsx",...%70
"UT Austin Data 5-16-19 master.xlsx",...
"UT Austin Data 5-17-19 master.xlsx",...
"UT Austin Data 5-18-19 master.xlsx",...
"UT Austin Data 5-19-19 master.xlsx",...
"UT Austin Data 5-20-19 master.xlsx",...
"UT Austin Data 5-21-19 master.xlsx",...
"UT Austin Data 5-22-19 master.xlsx",...
"UT Austin Data 5-23-19 master.xlsx",...
"UT Austin Data 5-24-19 master.xlsx",...
"UT Austin Data 5-25-19 master.xlsx",...%80
"UT Austin Data 5-26-19 master.xlsx",...
"UT Austin Data 5-27-19 master.xlsx",...
"UT Austin Data 5-28-19 master.xlsx",...
"UT Austin Data 5-29-19 master.xlsx",...
"UT Austin Data 5-30-19 master.xlsx",...

```
    "UT Austin Data 5-31-19 master.xlsx",...
    "UT Austin Data 6-1-19 master.xlsx",...
    "UT Austin Data 6-2-19 master.xlsx",...
    "UT Austin Data 6-3-19 master.xlsx",...
    "UT Austin Data 6-4-19 master.xlsx",...%90
    "UT Austin Data 6-5-19 master.xlsx",...
   ];

Start_Time = [12, 24, 12, 12, 12, 11, 24, 24, 12, 23,...
                                23, 28, 11, 10, 22, 10.75, 23, 23, 23, 23,...
                                23, 12, 23, 23, 19.5, 23, 7, 24, 7, 11.5,...
                                22, 12, 8, 15, 24, 24, 24, 24, 7, 7,...
                                24, 12, 23, 23, 23, 23, 23, 23, 23, 23,...
                                23, 23, 23, 23, 23, 23, 23, 23, 23, 23,...
                                23, 23, 23, 23, 23, 23, 23, 23, 23, 23,...
                                23, 23, 23, 23, 23, 23, 23, 23, 23, 23,...
                                23, 23, 23, 23, 23, 23, 23, 23, 23, 23,...
                                23];

End_Time =    [13, 25, 13, 13, 13, 12, 25, 25, 13, 24,...
                                24, 29, 12, 11, 23, 11.75, 24, 24, 24, 24,...
                                24, 13, 24, 24, 20.5, 24, 8, 25, 8, 12.5,...
                                23, 13, 9, 16, 25, 25, 25, 25, 8, 8, ...
                                25, 13, 24, 24, 24, 24, 24, 24, 24, 24,...
                                24, 24, 24, 24, 24, 24, 24, 24, 24, 24,...
                                24, 24, 24, 24, 24, 24, 24, 24, 24, 24,...
                                24, 24, 24, 24, 24, 24, 24, 24, 24, 24,...
                                24, 24, 24, 24, 24, 24, 24, 24, 24, 24,...
                                24];
%}
filenames = [
    "UT Austin Data 2-14-19 master.xlsx"];
Start_Time = [12]
End_Time =    [13]
    for i = 1:length(filenames)
        writeposition = ['B' num2str(i+2)];
        readfile = filenames(i);
        T1 = Start_Time(i);
        T2 = End_Time(i);
        Table_Writer(readfile, T1, T2, writefile, writeposition)
    end

end
```

```
function Table_Writer(readfile, T_start, T_end, writefile, writeposition)
N1 = 60*(T_start-7) + 5;
N2 = 60*(T_end-7) + 5;

[~, Time_start] = xlsread(readfile,'Sheet1',['B' num2str(N1)]);
[~, Time_end] =    xlsread(readfile,'Sheet1',['B' num2str(N2)]);
%% Data Extraction
T_WW_loc1 = ['DC' num2str(N1)];
T_WW_loc2 = ['DC' num2str(N2)];
T_WW_loc = strcat(T_WW_loc1, ':', T_WW_loc2);
T_WW = xlsread(readfile,'Sheet1', T_WW_loc);
T_WW_mean = mean(T_WW);
T_WW_std = std(T_WW);

T_gas_in_loc1 = ['Y' num2str(N1)];
T_gas_in_loc2 = ['Y' num2str(N2)];
T_gas_in_loc = strcat(T_gas_in_loc1, ':', T_gas_in_loc2);
T_gas_in = xlsread(readfile,'Sheet1', T_gas_in_loc);
T_gas_in_mean = mean(T_gas_in);
T_gas_in_std = std(T_gas_in);

T_gas_out_loc1 = ['BM' num2str(N1)];
T_gas_out_loc2 = ['BM' num2str(N2)];
T_gas_out_loc = strcat(T_gas_out_loc1, ':', T_gas_out_loc2);
T_gas_out = xlsread(readfile,'Sheet1', T_gas_out_loc);
T_gas_out_mean = mean(T_gas_out);
T_gas_out_std = std(T_gas_out);

G_in_loc1 = ['W' num2str(N1)];
G_in_loc2 = ['W' num2str(N2)];
G_in_loc = strcat(G_in_loc1, ':', G_in_loc2);
G_in = xlsread(readfile,'Sheet1', G_in_loc);
G_in_mean = mean(G_in);
G_in_std = std(G_in);

G_out_loc1 = ['CW' num2str(N1)];
G_out_loc2 = ['CW' num2str(N2)];
G_out_loc = strcat(G_out_loc1, ':', G_out_loc2);
G_out = xlsread(readfile,'Sheet1', G_out_loc);
G_out_mean = mean(G_out);
G_out_std = std(G_out);
```

```
L_in_loc1 = ['BC' num2str(N1)];
L_in_loc2 = ['BC' num2str(N2)];
L_in_loc = strcat(L_in_loc1, ':', L_in_loc2);
L_in = xlsread(readfile,'Sheet1', L_in_loc);
L_in_mean = mean(L_in);
L_in_std = std(L_in);

L_out_loc1 = ['BQ' num2str(N1)];
L_out_loc2 = ['BQ' num2str(N2)];
L_out_loc = strcat(L_out_loc1, ':', L_out_loc2);
L_out = xlsread(readfile,'Sheet1', L_out_loc);
L_out_mean = mean(L_out);
L_out_std = std(L_out);

T_solvent_in_loc1 = ['AZ' num2str(N1)];
T_solvent_in_loc2 = ['AZ' num2str(N2)];
T_solvent_in_loc = strcat(T_solvent_in_loc1, ':', T_solvent_in_loc2);
T_solvent_in= xlsread(readfile,'Sheet1', T_solvent_in_loc);
T_solvent_in_mean = mean(T_solvent_in);
T_solvent_in_std = std(T_solvent_in);

T_solvent_out_loc1 = ['JQ' num2str(N1)];
T_solvent_out_loc2= ['JQ' num2str(N2)];
T_solvent_out_loc = strcat(T_solvent_out_loc1, ':', T_solvent_out_loc2);
T_solvent_out= xlsread(readfile,'Sheet1', T_solvent_out_loc);
T_solvent_out_mean = mean(T_solvent_out);
T_solvent_out_std = std(T_solvent_out);

O2_in_loc1 = ['BH' num2str(N1)];
O2_in_loc2 = ['BH' num2str(N2)];
O2_in_loc = strcat(O2_in_loc1, ':', O2_in_loc2);
O2_in = xlsread(readfile,'Sheet1', O2_in_loc);
O2_in_mean = mean(O2_in);
O2_in_std = std(O2_in);

CO2_in_loc1 = ['BI' num2str(N1)];
CO2_in_loc2 = ['BI' num2str(N2)];
CO2_in_loc = strcat(CO2_in_loc1, ':', CO2_in_loc2);
CO2_in = xlsread(readfile,'Sheet1', CO2_in_loc);
CO2_in_mean = mean(CO2_in);
CO2_in_std = std(CO2_in);

CO2_out_loc1 = ['DE' num2str(N1)];
```

```
CO2_out_loc2 = ['DE' num2str(N2)];
CO2_out_loc = strcat(CO2_out_loc1, ':', CO2_out_loc2);
CO2_out = xlsread(readfile,'Sheet1', CO2_out_loc);
CO2_out_mean = mean(CO2_out);
CO2_out_std = std(CO2_out);

CO2_prod_loc1 = ['FF' num2str(N1)];
CO2_prod_loc2 = ['FF' num2str(N2)];
CO2_prod_loc = strcat(CO2_prod_loc1, ':', CO2_prod_loc2);
CO2_prod = xlsread(readfile,'Sheet1', CO2_prod_loc);
CO2_prod_mean = mean(CO2_prod);
CO2_prod_std = std(CO2_prod);

L_IC1_loc1 = ['CA' num2str(N1)];      % HX20402
L_IC1_loc2 = ['CA' num2str(N2)];
L_IC1_loc = strcat(L_IC1_loc1, ':', L_IC1_loc2);
L_IC1 = xlsread(readfile,'Sheet1', L_IC1_loc);
L_IC1_mean = mean(L_IC1);
L_IC1_std = std(L_IC1);

T_IC1_in_loc1 = ['CE' num2str(N1)];
T_IC1_in_loc2 = ['CE' num2str(N2)];
T_IC1_in_loc = strcat(T_IC1_in_loc1, ':', T_IC1_in_loc2);
T_IC1_in= xlsread(readfile,'Sheet1', T_IC1_in_loc);
T_IC1_in_mean = mean(T_IC1_in);
T_IC1_in_std = std(T_IC1_in);

T_IC1_out_loc1 = ['CG' num2str(N1)];
T_IC1_out_loc2 = ['CG' num2str(N2)];
T_IC1_out_loc = strcat(T_IC1_out_loc1, ':', T_IC1_out_loc2);
T_IC1_out= xlsread(readfile,'Sheet1', T_IC1_out_loc);
T_IC1_out_mean = mean(T_IC1_out);
T_IC1_out_std = std(T_IC1_out);

L_IC2_loc1 = ['CC' num2str(N1)];      % HX20401
L_IC2_loc2 = ['CC' num2str(N2)];
L_IC2_loc = strcat(L_IC2_loc1, ':', L_IC2_loc2);
L_IC2 = xlsread(readfile,'Sheet1', L_IC2_loc);
L_IC2_mean = mean(L_IC2);
L_IC2_std = std(L_IC2);


T_IC2_in_loc1 = ['CF' num2str(N1)];
```

```
T_IC2_in_loc2 = ['CF' num2str(N2)];
T_IC2_in_loc = strcat(T_IC2_in_loc1, ':', T_IC2_in_loc2);
T_IC2_in= xlsread(readfile,'Sheet1', T_IC2_in_loc);
T_IC2_in_mean = mean(T_IC2_in);
T_IC2_in_std = std(T_IC2_in);

T_IC2_out_loc1 = ['CI' num2str(N1)];
T_IC2_out_loc2 = ['CI' num2str(N2)];
T_IC2_out_loc = strcat(T_IC2_out_loc1, ':', T_IC2_out_loc2);
T_IC2_out= xlsread(readfile,'Sheet1', T_IC2_out_loc);
T_IC2_out_mean = mean(T_IC2_out);
T_IC2_out_std = std(T_IC2_out);

Efficiency_loc1 = ['CV' num2str(N1)];
Efficiency_loc2 = ['CV' num2str(N2)];
Efficiency_loc = strcat(Efficiency_loc1, ':', Efficiency_loc2);
Efficiency = xlsread(readfile,'Sheet1', Efficiency_loc);
Efficiency_mean = mean(Efficiency);
Efficiency_std = std(Efficiency);

wt_PZ_lean_loc1 = ['BG' num2str(N1)];
wt_PZ_lean_loc2 = ['BG' num2str(N2)];
wt_PZ_lean_loc = strcat(wt_PZ_lean_loc1, ':', wt_PZ_lean_loc2);
wt_PZ_lean = xlsread(readfile,'Sheet1', wt_PZ_lean_loc);
wt_PZ_lean_mean = mean(wt_PZ_lean);
wt_PZ_lean_std = std(wt_PZ_lean);

wt_CO2_lean_loc1 = ['BF' num2str(N1)];
wt_CO2_lean_loc2 = ['BF' num2str(N2)];
wt_CO2_lean_loc = strcat(wt_CO2_lean_loc1, ':', wt_CO2_lean_loc2);
wt_CO2_lean = xlsread(readfile,'Sheet1', wt_CO2_lean_loc);
wt_CO2_lean_mean = mean(wt_CO2_lean);
wt_CO2_lean_std = std(wt_CO2_lean);

wt_PZ_rich_loc1 = ['BT' num2str(N1)];
wt_PZ_rich_loc2 = ['BT' num2str(N2)];
wt_PZ_rich_loc = strcat(wt_PZ_rich_loc1, ':', wt_PZ_rich_loc2);
wt_PZ_rich = xlsread(readfile,'Sheet1', wt_PZ_rich_loc);
wt_PZ_rich_mean = mean(wt_PZ_rich);
wt_PZ_rich_std = std(wt_PZ_rich);

wt_CO2_rich_loc1 = ['BS' num2str(N1)];
wt_CO2_rich_loc2 = ['BS' num2str(N2)];
```

```
wt_CO2_rich_loc = strcat(wt_CO2_rich_loc1, ':', wt_CO2_rich_loc2);
wt_CO2_rich = xlsread(readfile,'Sheet1', wt_CO2_rich_loc);
wt_CO2_rich_mean = mean(wt_CO2_rich);
wt_CO2_rich_std = std(wt_CO2_rich);

TI20101_loc1 = ['AG' num2str(N1)];
TI20101_loc2 = ['AG' num2str(N2)];
TI20101_loc = strcat(TI20101_loc1, ':', TI20101_loc2);
TI20101 = xlsread(readfile,'Sheet1',TI20101_loc);
TI20101_mean = mean(TI20101);
TI20101_std = std(TI20101);

TI20117A_loc1 = ['AH' num2str(N1)];
TI20117A_loc2 = ['AH' num2str(N2)];
TI20117A_loc = strcat(TI20117A_loc1, ':', TI20117A_loc2);
TI20117A= xlsread(readfile,'Sheet1',TI20117A_loc);
TI20117A_mean = mean(TI20117A);
TI20117A_std = std(TI20117A);

TI20117B_loc1 = ['AI' num2str(N1)];
TI20117B_loc2 = ['AI' num2str(N2)];
TI20117B_loc = strcat(TI20117B_loc1, ':', TI20117B_loc2);
TI20117B= xlsread(readfile,'Sheet1',TI20117B_loc);
TI20117B_mean = mean(TI20117B);
TI20117B_std = std(TI20117B);

TI20117C_loc1 = ['AJ' num2str(N1)];
TI20117C_loc2 = ['AJ' num2str(N2)];
TI20117C_loc = strcat(TI20117C_loc1, ':', TI20117C_loc2);
TI20117C= xlsread(readfile,'Sheet1',TI20117C_loc);
TI20117C_mean = mean(TI20117C);
TI20117C_std = std(TI20117C);

TI20117D_loc1 = ['AK' num2str(N1)];
TI20117D_loc2 = ['AK' num2str(N2)];
TI20117D_loc = strcat(TI20117D_loc1, ':', TI20117D_loc2);
TI20117D= xlsread(readfile,'Sheet1',TI20117D_loc);
TI20117D_mean = mean(TI20117D);
TI20117D_std = std(TI20117D);

TI20117E_loc1 = ['AL' num2str(N1)];
TI20117E_loc2 = ['AL' num2str(N2)];
TI20117E_loc = strcat(TI20117E_loc1, ':', TI20117E_loc2);
```

```
TI20117E= xlsread(readfile,'Sheet1',TI20117E_loc);
TI20117E_mean = mean(TI20117E);
TI20117E_std = std(TI20117E);

TI20119E_loc1 = ['AM' num2str(N1)];
TI20119E_loc2 = ['AM' num2str(N2)];
TI20119E_loc = strcat(TI20119E_loc1, ':', TI20119E_loc2);
TI20119E= xlsread(readfile,'Sheet1',TI20119E_loc);
TI20119E_mean = mean(TI20119E);
TI20119E_std = std(TI20119E);

TI20117F_loc1 = ['AN' num2str(N1)];
TI20117F_loc2 = ['AN' num2str(N2)];
TI20117F_loc = strcat(TI20117F_loc1, ':', TI20117F_loc2);
TI20117F= xlsread(readfile,'Sheet1',TI20117F_loc);
TI20117F_mean = mean(TI20117F);
TI20117F_std = std(TI20117F);

TI20119F_loc1 = ['AO' num2str(N1)];
TI20119F_loc2 = ['AO' num2str(N2)];
TI20119F_loc = strcat(TI20119F_loc1, ':', TI20119F_loc2);
TI20119F= xlsread(readfile,'Sheet1',TI20119F_loc);
TI20119F_mean = mean(TI20119F);
TI20119F_std = std(TI20119F);

TI20117G_loc1 = ['AP' num2str(N1)];
TI20117G_loc2 = ['AP' num2str(N2)];
TI20117G_loc = strcat(TI20117G_loc1, ':', TI20117G_loc2);
TI20117G= xlsread(readfile,'Sheet1',TI20117G_loc);
TI20117G_mean = mean(TI20117G);
TI20117G_std = std(TI20117G);

TI20117H_loc1 = ['AQ' num2str(N1)];
TI20117H_loc2 = ['AQ' num2str(N2)];
TI20117H_loc = strcat(TI20117H_loc1, ':', TI20117H_loc2);
TI20117H= xlsread(readfile,'Sheet1',TI20117H_loc);
TI20117H_mean = mean(TI20117H);
TI20117H_std = std(TI20117H);

TI20117I_loc1 = ['AR' num2str(N1)];
TI20117I_loc2 = ['AR' num2str(N2)];
TI20117I_loc = strcat(TI20117I_loc1, ':', TI20117I_loc2);
TI20117I= xlsread(readfile,'Sheet1',TI20117I_loc);
```

```
TI20117I_mean = mean(TI20117I);
TI20117I_std= std(TI20117I);

TI20119I_loc1 = ['AS' num2str(N1)];
TI20119I_loc2 = ['AS' num2str(N2)];
TI20119I_loc = strcat(TI20119I_loc1, ':', TI20119I_loc2);
TI20119I= xlsread(readfile,'Sheet1',TI20119I_loc);
TI20119I_mean = mean(TI20119I);
TI20119I_std = std(TI20119I);

TI20117J_loc1 = ['AT' num2str(N1)];
TI20117J_loc2 = ['AT' num2str(N2)];
TI20117J_loc = strcat(TI20117J_loc1, ':', TI20117J_loc2);
TI20117J= xlsread(readfile,'Sheet1',TI20117J_loc);
TI20117J_mean = mean(TI20117J);
TI20117J_std= std(TI20117J);

TI20119J_loc1 = ['AU' num2str(N1)];
TI20119J_loc2 = ['AU' num2str(N2)];
TI20119J_loc = strcat(TI20119J_loc1, ':', TI20119J_loc2);
TI20119J= xlsread(readfile,'Sheet1',TI20119J_loc);
TI20119J_mean = mean(TI20119J);
TI20119J_std= std(TI20119J);

TI20117K_loc1 = ['AV' num2str(N1)];
TI20117K_loc2 = ['AV' num2str(N2)];
TI20117K_loc = strcat(TI20117K_loc1, ':', TI20117K_loc2);
TI20117K= xlsread(readfile,'Sheet1',TI20117K_loc);
TI20117K_mean = mean(TI20117K);
TI20117K_std = std(TI20117K);

TI20119K_loc1 = ['AW' num2str(N1)];
TI20119K_loc2 = ['AW' num2str(N2)];
TI20119K_loc = strcat(TI20119K_loc1, ':', TI20119K_loc2);
TI20119K= xlsread(readfile,'Sheet1',TI20119K_loc);
TI20119K_mean = mean(TI20119K);
TI20119K_std = std(TI20119K);

TI20117L_loc1 = ['AX' num2str(N1)];
TI20117L_loc2 = ['AX' num2str(N2)];
TI20117L_loc = strcat(TI20117L_loc1, ':', TI20117L_loc2);
TI20117L= xlsread(readfile,'Sheet1',TI20117L_loc);
TI20117L_mean = mean(TI20117L);
```

```
TI20117L_std = std(TI20117L);

TI20119L_loc1 = ['AY' num2str(N1)];
TI20119L_loc2 = ['AY' num2str(N2)];
TI20119L_loc = strcat(TI20119L_loc1, ':', TI20119L_loc2);
TI20119L= xlsread(readfile,'Sheet1',TI20119L_loc);
TI20119L_mean = mean(TI20119L);
TI20119L_std = std(TI20119L);

Cold_rich_L_loc1 = ['GM' num2str(N1)];
Cold_rich_L_loc2 = ['GM' num2str(N2)];
Cold_rich_L_loc = strcat(Cold_rich_L_loc1, ':', Cold_rich_L_loc2);
Cold_rich_L= xlsread(readfile,'Sheet1',Cold_rich_L_loc);
Cold_rich_L_mean = mean(Cold_rich_L);
Cold_rich_L_std = std(Cold_rich_L);

Warm_rich_L_loc1 = ['GZ' num2str(N1)];
Warm_rich_L_loc2 = ['GZ' num2str(N2)];
Warm_rich_L_loc = strcat(Warm_rich_L_loc1, ':', Warm_rich_L_loc2);
Warm_rich_L= xlsread(readfile,'Sheet1',Warm_rich_L_loc);
Warm_rich_L_mean = mean(Warm_rich_L);
Warm_rich_L_std = std(Warm_rich_L);

Warm_rich_T_loc1 = ['FU' num2str(N1)];
Warm_rich_T_loc2 = ['FU' num2str(N2)];
Warm_rich_T_loc = strcat(Warm_rich_T_loc1, ':', Warm_rich_T_loc2);
Warm_rich_T= xlsread(readfile,'Sheet1',Warm_rich_T_loc);
Warm_rich_T_mean = mean(Warm_rich_T);
Warm_rich_T_std = std(Warm_rich_T);

Warm_lean_T_loc1 = ['FT' num2str(N1)];
Warm_lean_T_loc2 = ['FT' num2str(N2)];
Warm_lean_T_loc = strcat(Warm_lean_T_loc1, ':', Warm_lean_T_loc2);
Warm_lean_T= xlsread(readfile,'Sheet1',Warm_lean_T_loc);
Warm_lean_T_mean = mean(Warm_lean_T);
Warm_lean_T_std = std(Warm_lean_T);

Bypass_T_loc1 = ['ID' num2str(N1)];
Bypass_T_loc2 = ['ID' num2str(N2)];
Bypass_T_loc = strcat(Bypass_T_loc1, ':', Bypass_T_loc2);
Bypass_T= xlsread(readfile,'Sheet1',Bypass_T_loc);
Bypass_T_mean = mean(Bypass_T);
Bypass_T_std = std(Bypass_T);
```

```
Steam_T_loc1 = ['HS' num2str(N1)];
Steam_T_loc2 = ['HS' num2str(N2)];
Steam_T_loc = strcat(Steam_T_loc1, ':', Steam_T_loc2);
Steam_T= xlsread(readfile,'Sheet1',Steam_T_loc);
Steam_T_mean = mean(Steam_T);
Steam_T_std = std(Bypass_T);

Steam_P_loc1 = ['HR' num2str(N1)];
Steam_P_loc2 = ['HR' num2str(N2)];
Steam_P_loc = strcat(Steam_P_loc1, ':', Steam_P_loc2);
Steam_P= xlsread(readfile,'Sheet1',Steam_P_loc);
Steam_P_mean = mean(Steam_P);
Steam_P_std = std(Steam_P);

Steam_F_loc1 = ['HQ' num2str(N1)];
Steam_F_loc2 = ['HQ' num2str(N2)];
Steam_F_loc = strcat(Steam_F_loc1, ':', Steam_F_loc2);
Steam_F= xlsread(readfile,'Sheet1',Steam_F_loc);
Steam_F_mean = mean(Steam_F);
Steam_F_std = std(Steam_F);

Sump_T_loc1 = ['IS' num2str(N1)];
Sump_T_loc2 = ['IS' num2str(N2)];
Sump_T_loc = strcat(Sump_T_loc1, ':', Sump_T_loc2);
Sump_T= xlsread(readfile,'Sheet1',Sump_T_loc);
Sump_T_mean = mean(Sump_T);
Sump_T_std = std(Sump_T);

Stripper_P_loc1 = ['GU' num2str(N1)];
Stripper_P_loc2 = ['GU' num2str(N2)];
Stripper_P_loc = strcat(Stripper_P_loc1, ':', Stripper_P_loc2);
Stripper_P= xlsread(readfile,'Sheet1',Stripper_P_loc);
Stripper_P_mean = mean(Stripper_P);
Stripper_P_std = std(Stripper_P);

CO2_flow_loc1 = ['FF' num2str(N1)];
CO2_flow_loc2 = ['FF' num2str(N2)];
CO2_flow_loc = strcat(CO2_flow_loc1, ':', CO2_flow_loc2);
CO2_flow= xlsread(readfile,'Sheet1',CO2_flow_loc);
CO2_flow_mean = mean(CO2_flow);
CO2_flow_std = std(CO2_flow);
```

```
dP_top_loc1 = ['BW' num2str(N1)];
dP_top_loc2 = ['BW' num2str(N2)];
dP_top_loc = strcat(dP_top_loc1, ':', dP_top_loc2);
dP_top= xlsread(readfile,'Sheet1',dP_top_loc);
dP_top_mean = mean(dP_top);
dP_top_std = std(dP_top);

dP_bot_loc1 = ['BX' num2str(N1)];
dP_bot_loc2 = ['BX' num2str(N2)];
dP_bot_loc = strcat(dP_bot_loc1, ':', dP_bot_loc2);
dP_bot= xlsread(readfile,'Sheet1',dP_bot_loc);
dP_bot_mean = mean(dP_bot);
dP_bot_std = std(dP_bot);
%% Loading Calculation
par = [26.1592, 0.0265, 7.6949, -7.8028, 3.3663]; % Regress by Gao

LT_loc1 = ['FX' num2str(N1)];
LT_loc2 = ['FX' num2str(N2)];
LT_loc = strcat(LT_loc1, ':', LT_loc2);

LD_loc1 = ['JM' num2str(N1)];
LD_loc2 = ['JM' num2str(N2)];
LD_loc = strcat(LD_loc1, ':', LD_loc2);

MT_loc1 = ['CI' num2str(N1)];
MT_loc2 = ['CI' num2str(N2)];
MT_loc = strcat(MT_loc1, ':', MT_loc2);

MD_loc1 = ['JR' num2str(N1)];
MD_loc2 = ['JR' num2str(N2)];
MD_loc = strcat(MD_loc1, ':', MD_loc2);

RT_loc1 = ['JQ' num2str(N1)];
RT_loc2 = ['JQ' num2str(N2)];
RT_loc = strcat(RT_loc1, ':', RT_loc2);

RD_loc1 = ['CS' num2str(N1)];
RD_loc2 = ['CS' num2str(N2)];
RD_loc = strcat(RD_loc1, ':', RD_loc2);

Rmiu_loc1 = ['CT' num2str(N1)];
Rmiu_loc2 = ['CT' num2str(N2)];
Rmiu_loc= strcat(Rmiu_loc1, ':', Rmiu_loc2);
```

```
Lmiu_loc1 = ['CR' num2str(N1)];
Lmiu_loc2 = ['CR' num2str(N2)];
Lmiu_loc= strcat(Lmiu_loc1, ':', Lmiu_loc2);

LTset = xlsread(readfile,'Sheet1', LT_loc);
LDset = xlsread(readfile,'Sheet1', LD_loc);
Lmiuset = xlsread(readfile,'Sheet1', Lmiu_loc);

MTset = xlsread(readfile,'Sheet1', MT_loc);
MDset = xlsread(readfile,'Sheet1', MD_loc);

RTset = xlsread(readfile,'Sheet1', RT_loc);
RDset = xlsread(readfile,'Sheet1', RD_loc);
Rmiuset = xlsread(readfile,'Sheet1', Rmiu_loc);

% Unit conversion
LTset = (LTset+ 459.67) .* 5./9;
RTset = (RTset+ 459.67) .* 5./9;
MTset = (MTset+ 459.67) .* 5./9;

LDset = LDset./0.062427960576145;
RDset = RDset./0.062427960576145;
MDset = MDset./0.062427960576145;

rldgset = zeros(length(RDset), 1);
lldgset = zeros(length(RDset), 1);
mldgset = [];
LMset    = zeros(length(RDset), 1);
RMset    = zeros(length(RDset), 1);
L_PZ_wt_set = zeros(length(RDset), 1);
L_CO2_wt_set = zeros(length(RDset), 1);
R_PZ_wt_set = zeros(length(RDset), 1);
R_CO2_wt_set = zeros(length(RDset), 1);

for i = 1:length(RDset)
      RT = RTset(i);
      RD = RDset(i);
      LT = LTset(i);
      LD = LDset(i);
      MT = MTset(i);
      MD = MDset(i);
      Lmiu = Lmiuset(i);
```

```
        Rmiu = Rmiuset(i);

        [Cpz1, Cco2, rldg, exitflag] = ldg_solver(RT, RD, Rmiu);
        [Cpz2,~,lldg,~] = ldg_solver(LT, LD, Lmiu);
        RM = 1000/(1000/Cpz1 - 86.136 - 88*rldg);
        LM = 1000/(1000/Cpz2 - 86.136 - 88*lldg);
        %lldg = ldg_calc(LT, M, LD);
        mldg = ldg_calc(MT, RM ,MD);

        rldgset(i) = rldg;
        lldgset(i) = lldg;
        if mldg > lldg
                mldgset =    [mldgset, mldg];
        end

        LMset(i) =LM;
        RMset(i) =RM;
        L_PZ_wt = (LM*86.136)/((44*lldg *2*LM)+1000+LM*86.136)*100;
        L_CO2_wt = (44*lldg *2*LM)/((44*lldg *2*LM)+1000+LM*86.136)*100;
        R_PZ_wt = (RM*86.136)/((44*rldg *2*RM)+1000+RM*86.136)*100;
        R_CO2_wt = (44*rldg *2*RM)/((44*rldg *2*RM)+1000+RM*86.136)*100;

        L_PZ_wt_set(i) = L_PZ_wt;
        L_CO2_wt_set(i) = L_CO2_wt;
        R_PZ_wt_set(i) = R_PZ_wt;
        R_CO2_wt_set(i) = R_CO2_wt;
end

rldg_mean = mean(rldgset);
lldg_mean = mean(lldgset);
mldg_mean = mean(mldgset);
LM_mean = mean(LMset);
RM_mean = mean(RMset);
L_PZ_wt_mean = mean(L_PZ_wt_set);
L_CO2_wt_mean = mean(L_CO2_wt_set);
R_PZ_wt_mean = mean(R_PZ_wt_set);
R_CO2_wt_mean = mean(R_CO2_wt_set);

rldg_std = std(rldgset);
lldg_std = std(lldgset);
mldg_std = std(mldgset);
LM_std = std(LMset);
RM_std = std(RMset);
```

```
L_PZ_wt_std= std(L_PZ_wt_set);
L_CO2_wt_std = std(L_CO2_wt_set);
R_PZ_wt_std = std(R_PZ_wt_set);
R_CO2_wt_std = std(R_CO2_wt_set);
%% Data Writing
x = [Time_start, Time_end, T_gas_in_mean, T_gas_out_mean, ...
      T_solvent_in_mean, T_solvent_out_mean,T_IC1_in_mean ,T_IC1_out_mean...
      L_IC1_mean, T_IC2_in_mean, T_IC2_out_mean, L_IC2_mean,...
      L_in_mean, L_out_mean, G_in_mean, G_out_mean,    O2_in_mean,...
      CO2_in_mean, CO2_out_mean, CO2_prod_mean, Efficiency_mean,...
      LM_mean, lldg_mean, RM_mean, rldg_mean, mldg_mean...
      L_PZ_wt_mean, L_CO2_wt_mean,...
      R_PZ_wt_mean, R_CO2_wt_mean,...
      wt_PZ_lean_mean, wt_CO2_lean_mean...
      wt_PZ_rich_mean, wt_CO2_rich_mean,...
      TI20101_mean, TI20117A_mean, TI20117B_mean,...
      TI20117C_mean, TI20117D_mean, TI20117E_mean,...
      TI20119E_mean, TI20117F_mean, TI20119F_mean...
      TI20117G_mean, TI20117H_mean, TI20117I_mean,...
      TI20119I_mean, TI20117J_mean, TI20119J_mean,...
      TI20117K_mean, TI20119K_mean, TI20117L_mean,...
      TI20119L_mean, T_WW_mean,...
      Cold_rich_L_mean, Warm_rich_L_mean,...
      Warm_rich_T_mean, Warm_lean_T_mean,...
      Bypass_T_mean, Steam_T_mean, Steam_P_mean,...
      Steam_F_mean, Sump_T_mean, Stripper_P_mean,...
      CO2_flow_mean, dP_top_mean, dP_bot_mean];

xlswrite(writefile, x, 'sheet1', writeposition)

y = [Time_start, Time_end, T_gas_in_std, T_gas_out_std, ...
      T_solvent_in_std, T_solvent_out_std,T_IC1_in_std ,T_IC1_out_std...
      L_IC1_std, T_IC2_in_std, T_IC2_out_std, L_IC2_std,...
      L_in_std, L_out_std, G_in_std, G_out_std,    O2_in_std,...
      CO2_in_std, CO2_out_std, CO2_prod_std, Efficiency_std,...
      LM_std, lldg_std, RM_std, rldg_std, mldg_std...
      L_PZ_wt_std, L_CO2_wt_std,...
      R_PZ_wt_std, R_CO2_wt_std,...
      wt_PZ_lean_std, wt_CO2_lean_std...
      wt_PZ_rich_std, wt_CO2_rich_std,...
      TI20101_std, TI20117A_std, TI20117B_std,...
      TI20117C_std, TI20117D_std, TI20117E_std,...
      TI20119E_std, TI20117F_std, TI20119F_std...
```

```
        TI20117G_std, TI20117H_std, TI20117I_std,...
        TI20119I_std, TI20117J_std, TI20119J_std,...
        TI20117K_std, TI20119K_std, TI20117L_std,...
        TI20119L_std, T_WW_std,...
        Cold_rich_L_std, Warm_rich_L_std,...
        Warm_rich_T_std, Warm_lean_T_std,...
        Bypass_T_std, Steam_T_std, Steam_P_std,...
        Steam_F_std, Sump_T_std, Stripper_P_std,...
        CO2_flow_std, dP_top_std, dP_bot_std];
xlswrite(writefile, y, 'sheet2', writeposition)
%% Functions
        function [CPZ, CCO2, rldg, exitflag] = ldg_solver(Tk, rho_kg, miu)
        % viscosity and density at given temperature
        v = @(x)(viscosity(x, Tk)-miu);
        d = @(x)(density(x, Tk)-rho_kg);
        guess = [3.21, 1.78];

        fun1 = @(x) [v(x), d(x)];
        options = optimoptions('fsolve','Display','off');
        [x, fval, exitflag, output] = fsolve(fun1, guess,options);
        CPZ = x(1);            % PZ concentration in mol/kg
        CCO2 = x(2);        % CO2 conc in mol/kg
        rldg = CCO2/(2*CPZ);
        end

        function vis = viscosity(C, T)
        %function to calculate solvent viscosity on C&T
                CPZ = C(1);
                CCO2 = C(2);
                v_water = 2.414e-5*10.^(247.8./(T-140))*1000;    % water viscosity
                A = par(1);
                B = par(2);
                C = par(3);
                D = par(4);
                E = par(5);
                vis = v_water * exp((A/T - B)*(C*CPZ + D*CCO2 + E*CPZ.*CCO2));
        end

        function den = density (C, T)
        % function to calculate solvent density on C&T
                CPZ = C(1);
                CCO2 = C(2);
                Tc = T - 273.15;
```

```
        rho_water = 1000*(1-(Tc+288.9414)/(508929.2*(Tc+68.12963))*(Tc-
3.9863)^2);
        rho_solvent = rho_water * (0.0408 * CCO2 + 0.008 * CPZ + 0.991);
        den = rho_solvent;
    end

    function y = lldg_density(x, T, M)
    % function to calculate solvent density at given loading, temperature,
    % and molarity
    pzwt = (M*86.136)/((44*x *2*M)+1000+M*86.136);
    CPZ = pzwt*1000/86.136;
    CCO2 = 2*CPZ*x;

    Tc = T - 273.15;
    rho_water = 1000*(1-(Tc+288.9414)/(508929.2*(Tc+68.12963))*(Tc-3.9863)^2);
    rho_solvent = rho_water * (0.0408 * CCO2 + 0.008 * CPZ + 0.991);
    y = rho_solvent;

    end

    function ldg = ldg_calc( T, M, rho)
    % function to solve solvent loading on given temperature, molarity, and
    % density.
        guess = 0.21;
        fun2 = @(x) lldg_density(x, T, M)- rho;
        options = optimoptions('fsolve','Display','off');
        ldg = fsolve(fun2, guess,options);
    end
end
```

References

Abu-Zahra, M.R.M., Niederer, J.P.M., Feron, P.H.M., Versteeg, G.F., 2007. CO_2 capture from power plants Part II. A parametric study of the economical performance based on mono-ethanolamine. Int. J. Greenh. Gas Con. 1, 135-142.

Awtry, A., Fine, N., Atcheson, J., Dinsdale, B., Kupfer, R., Silverman, T., Staab, G., Tomey, J., Meuleman, E., Brown, A., 2021. Design and Costing of an ION Clean Energy CO_2 Capture Plant Retrofitted to a 700 MW Coal-fired Power Station. Available at SSRN 3816716.

Bhown, A., Dillon, D., Berger, A.H., Du, Y., Haney, K., Carroll, B., Gilmartin, J., Simonson, T., Reddy, S., 2021. Front End Engineering Design Study for Carbon Capture at a Natural Gas Combined Cycle Power Plant in California. Available at SSRN 3812087.

Chen, E., Fulk, S., Sache, D., Lin, Y., Rochelle, G.T., 2014. Pilot Plant Activities with Concentrated Piperazine. Energy Proc 63, 1376-1391.

Clossman, F., Rochelle, G.T., Gao, T., Suresh, A.B., Abreu, M., Drewry, B.J., 2021. FEED for Piperazine withteh Advanced Stripper on NGCC at Denver City, Texas, GHGT-15.

Cullinane, J.T., 2005. Thermodynamics and kinetics of aqueous piperazine with potassium carbonate for carbon dioxide absorption.

Faramarzi, L., Thimsen, D., Hume, S., Maxon, A., Watson, G., Pedersen, S., Gjernes, E., Fostås, B.F., Lombardo, G., Cents, T., Morken, A.K., Shah, M.I., de Cazenove, T., Hamborg, E.S., 2017. Results from MEA Testing at the CO_2 Technology Centre Mongstad: Verification of Baseline Results in 2015. Energy Proc 114, 1128-1145.

Farmer, K., Steen, W., Bernau, M., Sexton, A., Dombrowski, K., Rochelle, G., Chen, E., 2019. Evaluation of Concentrated Piperazine for CO_2 Capture from Coal-Fired Flue Gas. URS Group.

Frailie, P.T., 2014. Modeling of Carbon Dioxide Absorption/Stripping by Aqueous Methyldiethanolamine/Piperazine. The University of Texas at Austin.

Freeman, S.A., 2011. Thermal Degradation and Oxidation of Aqueous Piperazine for Carbon Dioxide Capture. The University of Texas at Austin.

Gao, T., Rochelle, G.T., 2019. CO_2 Absorption from Gas Turbine Flue Gas by Aqueous Piperazine with Intercooling. Industrial & Engineering Chemistry Research.

Gao, T., Selinger, J.L., Rochelle, G.T., 2019. Demonstration of 99% CO_2 removal from coal flue gas by amine scrubbing. Int. J. Greenh. Gas Con. 83, 236-244.

Gjernes, E., Pedersen, S., Cents, T., Watson, G., Fostås, B.F., Shah, M.I., Lombardo, G., Desvignes, C., Flø, N.E., Morken, A.K., de Cazenove, T., Faramarzi, L., Hamborg,

E.S., 2017. Results from 30 wt% MEA Performance Testing at the CO_2 Technology Centre Mongstad. Energy Proc 114, 1146-1157.

Heidel, K., Keith, D., Singh, A., Holmes, G., 2011. Process design and costing of an air-contactor for air-capture. Energy Proc 4, 2861-2868.

Hilliard, M.D., 2008. A predictive thermodynamic model for an aqueous blend of potassium carbonate, piperazine, and monoethanolamine for carbon dioxide capture from flue gas.

Holmes, G., Keith, D.W., 2012. An air–liquid contactor for large-scale capture of CO_2 from air. Philosophical Transactions of the Royal Society A: Mathematical, Physical and Engineering Sciences 370, 4380-4403.

Holmes, G., Nold, K., Walsh, T., Heidel, K., Henderson, M.A., Ritchie, J., Klavins, P., Singh, A., Keith, D.W., 2013. Outdoor prototype results for direct atmospheric capture of carbon dioxide. Energy Proc 37, 6079-6095.

IPCC, 2018. Special Report on Global Warming of 1.5 °C.

Keith, D.W., Holmes, G., Angelo, D.S., Heidel, K., 2018. A process for capturing CO_2 from the atmosphere. Joule 2, 1573-1594.

Kennedy, G., 2020. WA Parish Post-Combustion CO_2 Capture and Sequestration Demonstration Project Final Technical Report. Petra Nova Power Holdings LLC.

Lavalle, G., Lucquiaud, M., Wehrli, M., Valluri, P., 2018. Cross-flow structured packing for the process intensification of post-combustion carbon dioxide capture. Chem. Eng. Sci. 178, 284-296.

Lin, Y.-J., Chen, E., Rochelle, G.T., 2016. Pilot plant test of the advanced flash stripper for CO_2 capture. Faraday Discuss. 192, 37-58.

Masson-Delmotte, V., Zhai, P., Pörtner, H.-O., Roberts, D., Skea, J., Shukla, P., Pirani, A., Moufouma-Okia, W., Péan, C., Pidcock, R., 2018. Global Warming of 1.5 C: An IPCC Special Report on the Impacts of Global Warming of 1.5° C Above Pre-industrial Levels and Related Global Greenhouse Gas Emission Pathways, in the Context of Strengthening the Global Response to the Threat of Climate Change, Sustainable Development, and Efforts to Eradicate Poverty. World Meteorological Organization Geneva, Switzerland.

Minx, J.C., Lamb, W.F., Callaghan, M.W., Fuss, S., Hilaire, J., Creutzig, F., Amann, T., Beringer, T., de Oliveira Garcia, W., Hartmann, J., 2018. Negative emissions—Part 1: Research landscape and synthesis. Environmental Research Letters 13, 063001.

Morgan, J.C., Chinen, A.S., Omell, B., Bhattacharyya, D., Tong, C., Miller, D.C., 2017. Thermodynamic modeling and uncertainty quantification of CO_2 -loaded aqueous MEA solutions. Chem. Eng. Sci. 168, 309-324.

Morgan, J.C., Soares Chinen, A., Omell, B., Bhattacharyya, D., Tong, C., Miller, D.C., Buschle, B., Lucquiaud, M., 2018. Development of a Rigorous Modeling Framework for Solvent-Based CO_2 Capture. Part 2: Steady-State Validation and Uncertainty Quantification with Pilot Plant Data. Industrial & Engineering Chemistry Research 57, 10464-10481.

NETL, 2012. Quality Guideline for Energy System Studies: CO_2 Impurity Design Parameters.

OBrien, K., Lu, Y., Dietsch, J., Zhang, J., Wu, T., Thomas, T., Iwakura, K., Thomas, M., Brown, A., Guletsky, P., 2021. Full-scale FEED Study for Retrofitting the Prairie State Generating Station with an 816 MWe Capture Plant using Mitsubishi Heavy Industries Engineering Post-Combustion CO_2 Capture Technology. Available at SSRN 3815206.

Oddvar Lie, K., Gorset, O., Morten Bade, O., Askestad, I., Nygaard Knudsen, J., Andersson, V., 2021. Technology Qualification to Mitigate Technical Risk in CCS Front End Engineering Design for the HeidelbergCement Norcem Plant.

Plaza, J.M., 2011. Modeling of Carbon Dioxide Absorption using Aqueous Monoethanolamine, Piperazine and Promoted Potassium Carbonate. The University of Texas at Austin.

Preston, C., Bruce, C., Monea, M., 2018. An Update on the Integrated CCS Project at SaskPower's Boundary Dam Power Station, 14th Greenhouse Gas Control Technologies Conference Melbourne, pp. 21-26.

Rao, A.B., Rubin, E.S., 2006. Identifying cost-effective CO_2 control levels for amine-based CO_2 capture systems. Industrial & engineering chemistry research 45, 2421-2429.

Rochelle, G.T., Akinpelumi, K., Gao, T., Liu, C.-T., Suresh, A.B., Wu, Y., 2021. Pilot Plant Results with Piperazine Advanced Stripper at NGCC Conditions, GHGT-15.

Rochelle, G.T., Wu, Y., Chen, E., Akinpelumi, K., Fischer, K.B., Gao, T., Liu, C.-T., Selinger, J.L., 2019. Pilot plant demonstration of piperazine with the advanced flash stripper. Int. J. Greenh. Gas Con. 84, 72-81.

Sachde, D., 2016. Absorber Performance and Configurations for CO_2 Capture using Aqueous Piperazine. The University of Texas at Austin.

Sachde, D., Chen, E., Rochelle, G.T., 2013. Modeling Pilot Plant Performance of an Absorber with Aqueous Piperazine. Energy Proc 37, 1987-2001.

Sachde, D., Rochelle, G.T., 2014. Absorber Intercooling Configurations using Aqueous Piperazine for Capture from Sources with 4 to 27% CO_2. Energy Proc 63, 1637-1656.

Socolow, R., Desmond, M., Aines, R., Blackstock, J., Bolland, O., Kaarsberg, T., Lewis, N., Mazzotti, M., Pfeffer, A., Sawyer, K., 2011. Direct air capture of CO_2 with

chemicals: a technology assessment for the APS Panel on Public Affairs. American Physical Society.

Song, D., 2017. Effect of Liquid Viscosity on Liquid Film Mass Transfer for Packings. The University of Texas at Austin.

Song, D., Seibert, A.F., Rochelle, G.T., 2014. Effect of Liquid Viscosity on the Liquid Phase Mass Transfer Coefficient of Packing. Energy Proc 63, 1268-1286.

Song, D., Seibert, A.F., Rochelle, G.T., 2017. Effect of Liquid Viscosity on Mass Transfer Area and Liquid Film Mass Transfer Coefficient for GT-OPTIMPAK 250Y. Energy Proc 114, 2713-2727.

SPX Cooling Technologies, https://spxcooling.com/.

Wu, Y., Rochelle, G., 2021. Effects of carbon treating on piperazine oxidation in pilot plant testing of PZAS, GHGT-15.

Zeman, F., 2014. Reducing the cost of Ca-based direct air capture of CO_2. Environmental science & technology 48, 11730-11735.

Zhang, Y., 2018. Absorber and Aerosol Modeling in Amine Scrubbing for Carbon Capture. The University of Texas at Austin.

Zhang, Y., Freeman, B., Hao, P., Rochelle, G.T., 2016. Absorber Modeling for NGCC Carbon Capture with Aqueous Piperazine. Faraday Discuss. 192, 459-477.

Zhang, Y., Sachde, D., Chen, E., Rochelle, G., 2017. Modeling of absorber pilot plant performance for CO_2 capture with aqueous piperazine. Int. J. Greenh. Gas Con. 64, 300-313.

Vita

Tianyu Gao was born in Hefei, China on March 18, 1994. He graduated from Hefei 168 high school before attending Dalian University of Technology. He earned a B.S. in Chemical Engineering in 2015 and went to Carnegie Mellon University for a M.S. degree. He joined Dr. John Kitchin's group and worked on DFT simulation and machine learning. Following the completion of the master program, he joined Dr. Gary T. Rochelle's group at UT to pursue his doctoral degree. He has accepted a full-time position at Aramco America in Detroit to continue working on CO_2 capture from mobile source.

Permanent email: gaoty94@gmail.com

This dissertation was typed by the author.